博士学位論文

論文題目 Creation of the Stepless Displacement–Force Converter Mechanism Based on the Internal Force Compensation by Nonlinear Elastic Bodies — Robotic Components Capable of Regulating Large Magnetic Force, Clamping Force, and Tension Force by a Much Smaller Control Force —

提 出 者　東北大学大学院情報科学研究科

応用情報科学専攻

学籍番号　C0ID4004

氏 名　清水 杜織

TOHOKU UNIVERSITY

Graduate School of Information Sciences

Creation of the Stepless Displacement–Force Converter Mechanism Based on the Internal Force Compensation by Nonlinear Elastic Bodies — Robotic Components Capable of Regulating Large Magnetic Force, Clamping Force, and Tension Force by a Much Smaller Control Force —

（非線形弾性要素による内部力補償に基づく無段階変位-力変換機構の創生
－微小操作力で強大な磁気力・把持力・制動力・張力を制御可能とするロボット要素－）

A dissertation submitted for the degree of Doctor of Philosophy
(Information Science)

Department of Applied Information Sciences

by

Tori SHIMIZU

January 10, 2023

Creation of the Stepless Displacement–Force Converter Mechanism Based on the Internal Force Compensation by Nonlinear Elastic Bodies — Robotic Components Capable of Regulating Large Magnetic Force, Clamping Force, and Tension Force by a Much Smaller Control Force —

Tori Shimizu

Abstract

This study proposes a method for gaining a large amplified output force of a robotic component out of a much smaller input force of the actuator, with the aid of an internal force compensation mechanism that steplessly converts the actuation displacement to the force amplification state.

Considering the reduction of the response time, operation duration, and power consumption, one of the desirable features of powerful energy-efficient machines is the ability to shift their force amplification state flawlessly. For example, an actuator of a robotic gripper initially selects a high-speed state until its finger touches the object to execute quick clamping. Subsequently, by enabling the force amplification feature, the actuator switches to a high-torque state to complete clamping and sustain the finger position. Likewise, initially, a variable stiffness gripper in a low-rigidity state, with the jamming media in the fingers free of frictional resistance, is deformable to fit in the shape of the target object in contact. To activate the high-rigidity state, the actuator increases pressure on the jamming media such that its resistance increases, resulting in the fixation of the fingers in the posture they are in when surrounding the object.

To avoid increasing the mechanism volume and mass, the main single actuator of the finger should also take charge of these state transitions without adding degrees of freedom. Conventional grippers use sensors to detect an object and then regulate the current or switch the reduction rate of the decelerator. However, such software approaches are inapplicable to machines without enough computational resources, and they are disadvantageous in situations where circuits get damaged or signal transmissions get interfered with by conditions such as extreme temperatures and radioactive rays. Thus, the study aims to develop a hardware approach that enables a machine to mechanically react to the changes in the operation process and switch its force amplification state. This is important for improving not only the energy–performance efficiency of the robotic components by allowing the selection of a smaller, weaker, and lighter actuator, but also for extending their applicability to extreme environments and conditions such as disaster fields, nuclear decommissioning, and scientific explorations.

Based on this motivation, the study proposes displacement–force converter (DF converter), a mechanism that allows an actuator to regulate a force's intensity in response to its internal components displacement. This device is based on the force compensation principle; it cancels a known, designated, or predictable load (e.g., object with a certain mass) by applying an equal counterpart load (e.g., tension of a spring) in the opposite direction to always maintain their connection point at the equilibrium of the forces regardless of its displacement. An important property is that this compensating relation is symmetrical such that its input and output can be

reversed. In this context, the initially compensated load is called a “reverse spring” because its behavior is opposite to that of a spring. By extracting the state of change of the spring and reverse spring, the DF converter realizes the force amplification corresponding to their deformation regulated by a much smaller control force. The study aims to devise two different reverse springs that exemplify the design methodology of the DF converter: one using a noncircular cam–follower transmission and the other using nonlinearly increasing magnetic attraction. Moreover, to demonstrate the usefulness of the force-amplification feature in robotics, they are applied to three major robotic components: parallel gripper, variable stiffness gripper, and electromagnetic brake.

First, a preliminary proof-of-concept prototype model of the proposed DF converter is introduced to prove its ability to regulate the elastic tension. The model is composed of a pulley–wire system that balances the torques generated by a linear spring connected to a circular pulley and a mass connected to a noncircular pulley as a reverse spring. To overcome the difficulty of maintaining a deviation angle between the pulley tangent and the vertical direction of the radius, which would cause a decrease in the compensation accuracy, a cam–follower system designed through a numerical analysis based on a first-order ordinary differential equation was developed. The prototype successfully showed that the maximum control force required to extend the spring was reduced by 23.2 %, and the difference between the extension and compression shrank decreased from 543. 0 % to 48.7 %. This uniformization allows the selection of an actuator with a smaller maximum output. Moreover, it was incorporated into a variable-stiffness mechanism of a fire-resistant gripper as a wire tensioner to regulate the rigidity of its finger continuously, thus, replacing a conventional massive pneumatic actuator.

Another DF converter that uses a permanent magnet as a reverse spring was also introduced. This converter is based on the internally balanced magnetic unit (IB magnet), an attraction device used to attach it to a ferromagnetic surface, such as a wall or ceiling. Converting the attraction work of the magnet to the potential energy of a compressed spring allows the IB magnet to be easily detached, without using a large external force, by releasing the stored energy. In a parallel gripper equipped with this device, the spontaneously intensifying attraction enhances the clamping; this is the first study aimed at extracting a pressing force, rather than an attractive force, from the IB magnet. This method is novel for its ability to adjust the amplified clamping force from zero to the maximum value continuously by regulating the attraction distance, compared to existing methods that employ load-sensitive grippers with binary toggles and clutches. The development of the prototypes was followed by that of nonlinear springs: parameter optimization, simplification of the design procedure, and downsizing while maintaining precision. The gripper successfully demonstrated that the maximum clamping force increased to 137.5 % while the increase in energy consumption was suppressed, resulting in the force–energy efficiency ratio increasing to 138.7 %. Furthermore, A width-adjustment mechanism using a lever was also devised to achieve a more steady and predictable clamping force independent of the target object width by splitting the actuation of the finger and compensation mechanism. This linearized the width–force characteristic with an inclination of 0.15 N/mm, which was an insignificant influence of 0.3 % on the major output of approximately 50 N.

Furthermore, as another configuration of the gripper, an electromagnetic brake was developed by equipping the fingers of the gripper with brake pads. To solve the problem of the pad having to be actuated for a long compensation stroke to fully disable braking, a novel multistage spring, comprising two linear springs connected in series, was devised. In addition to decreasing its spring constant for compensation, the multistage spring detaches the pad with a small displacement. The developed prototype was superior to the contrasted EM brake when braking for longer than 0.43 s while keeping the responsiveness comparable; for example, the output dynamic friction torque–input energy ratio increased to 451.1% when braking for 1.0 s.

In these ways, the research outcomes validated both the effectiveness of the proposed DF converter for stepless force amplification and its applicability to robotic components. With more application instances, such as the variable stiffness gripper using a magnetorheological fluid and an electropermanent-magnetic jumping mechanism, the study proved an impactful contribution of the DF converter to the performance improvement of machines in extreme environments with design and operation restrictions.

TABLE OF CONTENTS

LIST OF FIGURES

LIST OF TABLES

Part I

Introduction

Part I Introduction

Chapter I.1 Research background: attempts to achieve efficient actuation through state transition

A machine works against a large load using its actuator. Considering the reduction of the response time, operation duration, and power consumption, one of the desirable features of powerful energy-efficient robotic components is the ability to shift its force amplification state flawlessly.

For example, as illustrated in Fig. 1 (a), an actuator employed in a robotic gripper initially selects a high-speed state until the finger touches the object to quickly execute clamping. Then, by enabling the force amplification feature, the actuator switches to a high-torque state to complete clamping firmly and sustain the finger position [1], [2]. Likewise, as depicted in Fig. 1 (b), a variable stiffness gripper that is initially in a low-rigidity state, with the jamming media in the fingers free of frictional resistance, is deformable to fit the shape of the target object in contact. By transitioning to a high-rigidity state, the actuator increases pressure on the jamming media such that the resistance increases, resulting in the fixation of the fingers in the posture they are in when surrounding the object [3]–[5].

To avoid increasing the mechanism volume and mass, the main single actuator used to actuate the finger should also take charge of these state transitions without adding other degrees of freedom.

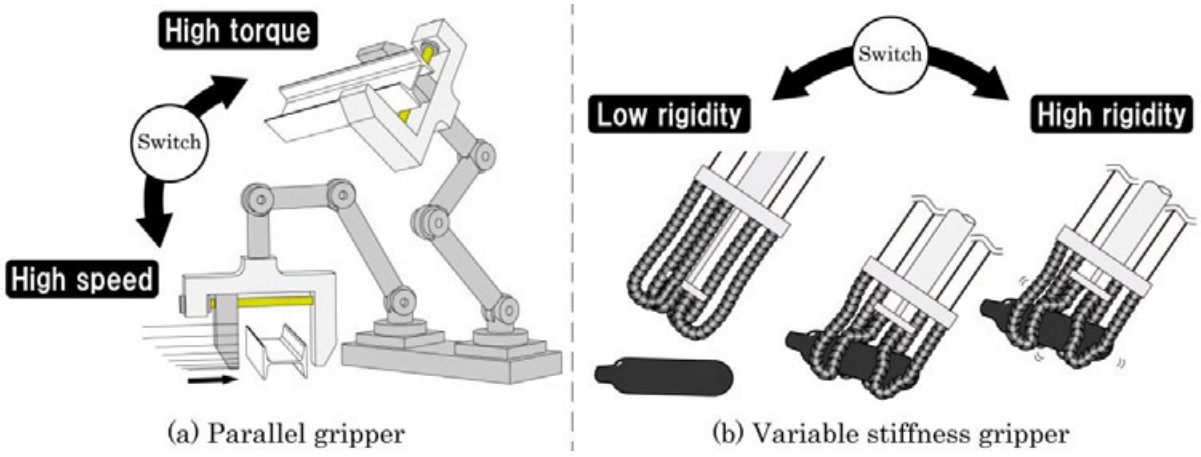

Fig. 1 Examples of robotic grippers that switch their states when handling their target objects.

Most conventionally, a clamping system integrated as a gripper uses sensors to gather information to recognize the object between the fingers and then regulates the current supplied to the actuator once the object is detected. However, such software approaches require a certain load on the calculation processing for control; therefore, inapplicable to machines without enough computational resources (including human tools). These approaches are disadvantageous in situations where electronic circuits such as processors and memory elements get damaged or signal transmissions of sensor values and actuation controls get interfered with, such as by extreme temperatures and radioactive rays [6]–[8].

For this reason, this study develops hardware approaches that mechanically (and thus spontaneously) react to changes in the operation process and switch its force amplification state, which is important for extending their applicability to extreme environments such as disaster field, nuclear decommissioning, and scientific explorations in addition to improving the energy–performance efficiency of the robotic components by allowing the selection of a smaller, weaker, and lighter actuator.

Chapter I.2 Previous research: compensation mechanisms

The simplest way to make a machine capable of working against a large load is using powerful actuators. The larger the target load is, the higher the required performance and thus the energy consumption of the actuators. Therefore, there lies a vicious cycle to be avoided when designing a machine, in which the required power is further increased due to an increase in the mass and volume of the entire system by selecting more powerful but heavier and bulkier actuators [9]–[11].

To reduce the maximum output force required by the load, force amplification mechanisms such as levers, wedges, and gears have been applied to most machines. These mechanisms typically convert the input with a small force F_{in} and a long distance d_{in} to an output with a large force F_{out} and a short distance d_{out}, providing the machine with a mechanical advantage (MA) [12]. The force amplification ratio is defined as

$$\mathrm{MA} = \frac{F_{\mathrm{out}}}{F_{\mathrm{in}}} = \frac{d_{\mathrm{in}}}{d_{\mathrm{out}}} = \frac{N_{\mathrm{out}}}{N_{\mathrm{in}}} \tag{1}$$

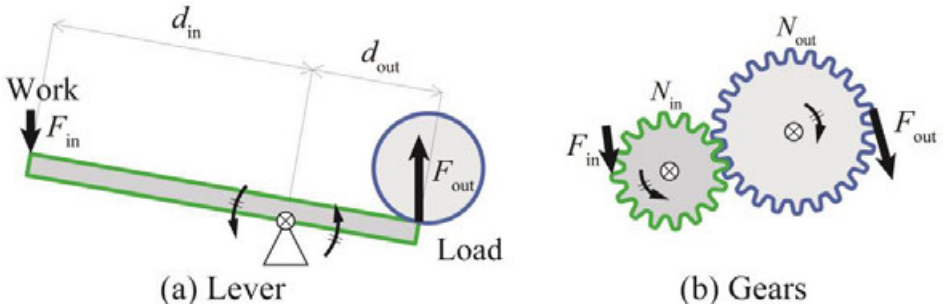

Fig. 2 Conceptual diagram of force amplification performed by simple machines that achieve MA that is greater than one.

While sufficiently providing MA, major amplification mechanisms are inconvenient in terms of responsiveness because the extension of the actuation distance affects the duration of operation (resulting in the cumulative energy consumption after all), reflecting that they are more popularly called “reduction mechanisms” or “decelerators.” Therefore, this research regards a force amplification that can achieve both high MA performance and energy efficiency without “reduction” as ideal.

Force amplification without reduction is possible when the load of a target object is fixed, known, or predictable; applying an equal load in its opposite direction can relieve the control force of a load without affecting the actuation distance, as illustrated in Fig. 3. This is called “force compensation” or “force balancing”, which represents the cancellation of the control force by always maintaining the driven part at the equilibrium point of the forces regardless of its displacement or orientation angle [13], [14]. For better clarification, the following sections enumerate the representative examples of the compensation mechanisms.

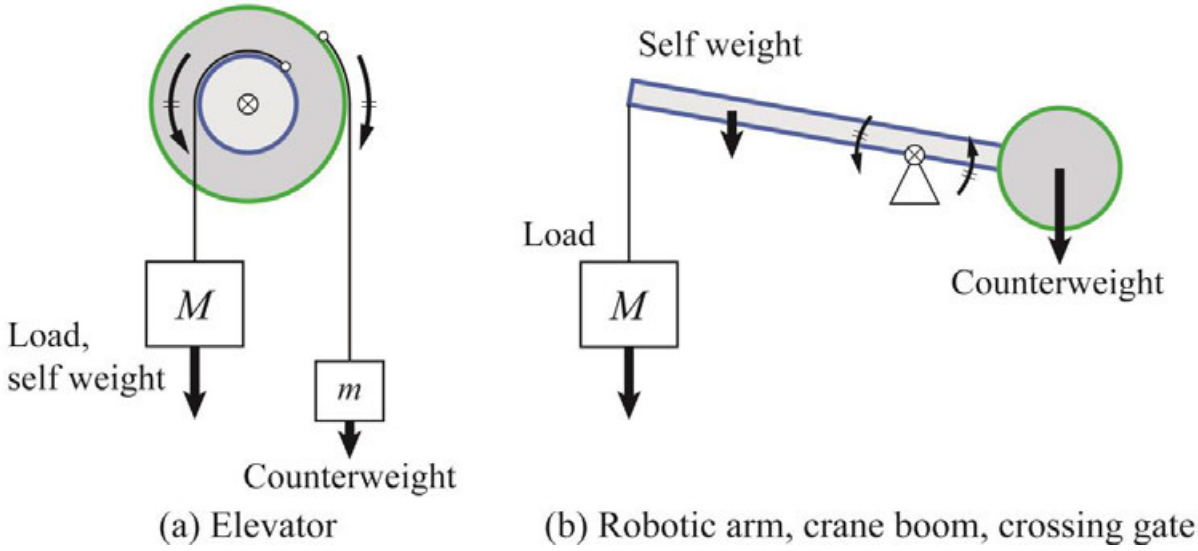

Fig. 3 Conceptual diagram of the weight compensation mechanism.

Section I.2.1 Self-weight compensation for mechanisms working for internal loads

The most typical target load to be compensated is the self-weight, because most machines are installed under the influence of gravity. For example, light stands [15] and railroad crossing gates [16] have long arms that bear both the concentrated load on the tip and the distributed load on themselves. To relieve the input torque exerted by the actuator or power required to raise their arms, these machines tend to extend their arms in the opposite direction around the pivot to mount counterweights such that the compensation torque of these "tails" balances the load torque of the arms by following the principle of leverage. Ideally, the control torque can be reduced to zero, while the compensation error, which results from the difference between the torque to be compensated and the compensating torque, remains.

Weight compensation is the conversion of the potential energy generated by the driven part (here, light bulb and stop bar) to the energy consumed by the compensating part (counterweight), or vice versa. This internal energy conservation system virtually allows the mechanism to produce a larger output on the load, compared to the input of the actuator without changing the required actuation distance, resulting in a high MA, if the system carries an equal load and does not exert force externally like a seesaw.

Section I.2.2 Weight compensation for mechanisms working for external loads

Like the self-weight compensation for mechanisms working for internal loads, elevators, crane booms, and robotic arms [9], [17] have counterweights used to balance their self-weight such that their actuators only have to deal with the increased load applied by the target luggage. Some of these mechanisms can adjust the compensating torque in accordance with this change in the load by increasing either the mass of the counterweight [18] or the length of the counter arm [19]–[21], resulting in a less load torque required from the actuator.

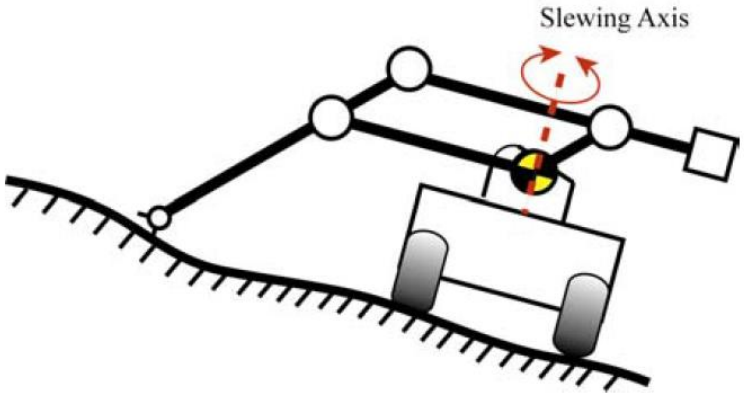

Fig. 4 Robotic arm with a weight compensation mechanism that uses a counterweight [22].

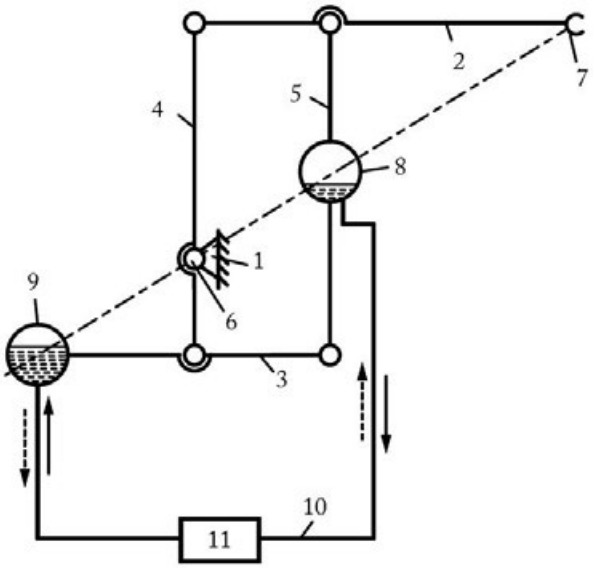

Fig. 5 Actively adjustable weight compensation mechanism realized by moving the weight fluid between tanks (8, 9) using a pump (11) [11][18].

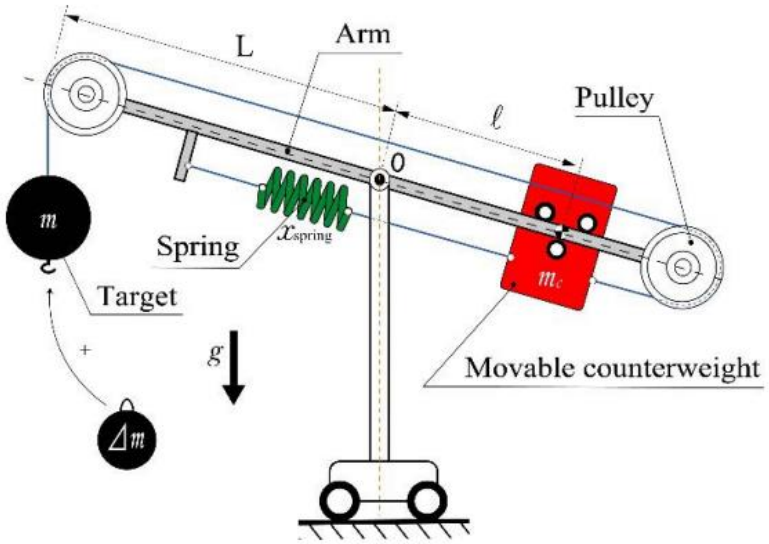

Fig. 6 Passively adjustable weight compensation mechanism realized by a movable counterweight [21].

Section I.2.3 Compensation mechanisms without counterweights

While adding weight is a simple design method, it causes problems to emerge; the total mass of a machine increases not only due to the weight but also due to the structural reinforcement for ensuring tensile strength; responsiveness declines due to the increased inertia. The overweight is especially problematic when the machine is installed at unstable and fragile scaffolding. Therefore, various self-weight compensation mechanisms for robotic arms [10], [23], [24] and light stands [15] using tension springs instead of weights have been proposed. The translational displacement or rotational angle of the load is converted to the deformation of springs via links, pulley–wire, or cam–follower systems that are designed to follow the displacement–force characteristics of the load.

Unlike powered suits that augment human body movement by providing additional muscle forces using articular actuators such as motors and pneumatics, some assistive suits use mechanical and unpowered compensation mechanisms such that they can operate without electricity, independent of the battery capacity. For example, highly elastic rubbers are embedded in the back and buttock parts of an assistive harness [25], and they stretch when the user bends forward to grab an object on the ground and then shrink when they stand, generating an assistive force to pull the body and object upwards.

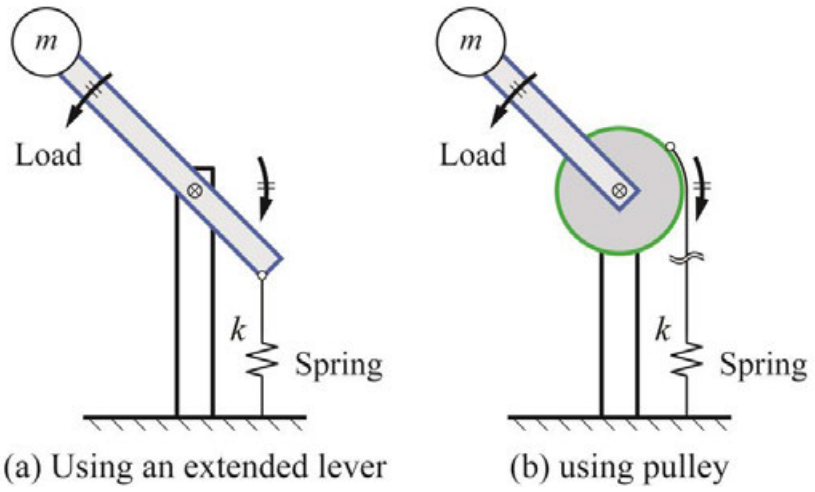

Fig. 7 Conceptual diagram of compensation mechanisms using springs instead of weights.

Fig. 8 Anglepoise lamp with a weight compensation mechanism using springs [15].

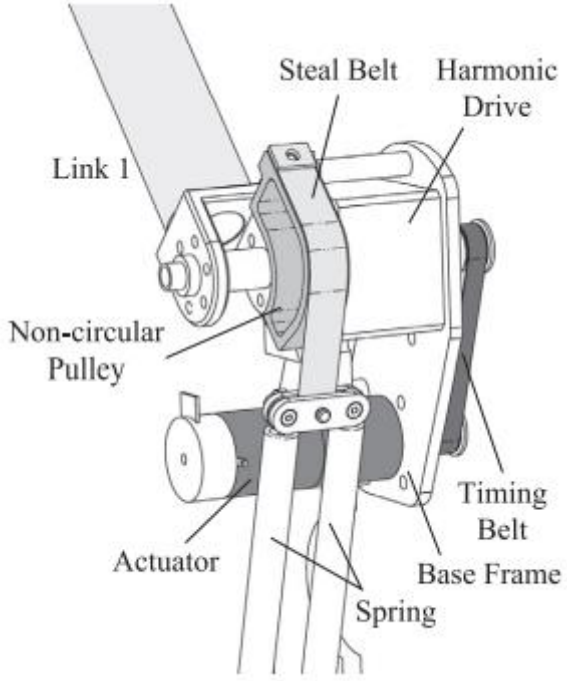

Fig. 9 Weight compensation mechanism for a robotic arm with a noncircular pulley connected to springs [10].

Fig. 10 Assistive function of an unpowered assistive suit, whose elastic rubber on the buttocks generates a tension force to the support user to life a heavy load [26].

Section I.2.4 Compensation mechanisms for the magnetic attraction force

The internally-balanced magnetic unit (IB magnet) is a mechanism that compensates for the magnetic attractive force, and it is used for attraction devices that enable robots to climb ferromagnetic surfaces [27], [28].

During the attaching process, its attractive force increases nonlinearly in close proximity to the target attraction surface. Simultaneously, a nonlinear spring gets compressed, increasing its repulsive force with a displacement–force characteristic identical but opposite in sign to that of the magnetic attraction, resulting in the cancellation of the control force of the magnet. By converting the attraction work of the magnet to a potential energy stored in the compressed spring, the IB magnet allows itself to be detached easily without requiring a large external force, by releasing the compressed spring.

In this way, the IB magnet allows robots to use attraction devices efficiently, and thus, it has been incorporated into various structures such as magnetic wheels [29] and magnetic crawlers [30]. Further details of the IB magnet will be discussed in Subsection III.2.7.1.

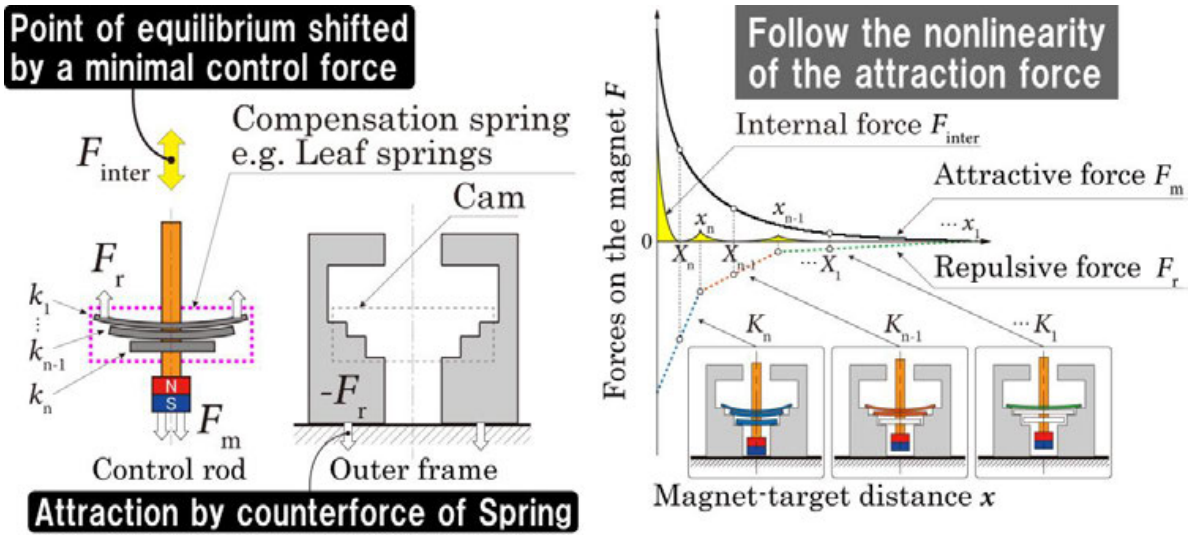

Fig. 11 Conceptual diagram of the internally balanced magnetic unit (IB magnet).

Chapter I.3 Proposed principle: conceptual expansion from the “compensation mechanism” to the “displacement–force converter (DF converter)”

Balancing the internal forces in a mechanism, a load element (e. g., a weight) with a certain displacement–force characteristic, and a counter-element (e. g., a counterweight or a spring) with the characteristics that are identical but opposite in sign, makes their coupling part the point of equilibrium of forces, whose position can be altered by a minimal external force.

The important characteristic is that, as this compensation relation is symmetrical, the compensation mechanism can be generalized as a mechanism that also allows the force produced by the compensating counter-element, such as the spring, to be controlled efficiently, when regarding its input and output elements reversely, as depicted in Fig. 12 and more schematized in Fig. 13. In this context, the initially compensated load element is called a “reverse spring,” an irregularly behaving spring whose elastic force is exerted in the opposite direction to assist with its further deformation when displacement is applied, in contrast to the usual spring that resists its deformation when displacement.

This point of view is noble in that there have seldom been applications of compensation mechanisms that are mainly aimed at adjusting the internal force generated within the mechanism, as most mechanisms are expected to exert forces outside themselves. However, if a metrology of extracting the change in the internal force of a mechanism to interact with external objects and circumstance (at the expense of some energy loss to overcome the antinomy of “outputting the internal force”) can be established, machines and robots receive a great profit of becoming capable of working against a large load with small, lightweight, and weak (less energy-consuming) actuators. Mobile robots with strict limitations on mass, size, and power source can efficiently perform tasks for a longer time, robotic equipment in a factory can reduce their cumulative electricity cost, and electric cars can expand their mileage. Human tools without electricity can also be operated with a smaller force with the aid of a DF converter. In these ways, the DF converter is expected to widely contribute to universal technological solutions that will realize a society with sustainable development.

Based on this motivation, this research proposes the internally balanced displacement–force converter (DF converter) and systemizes the application methods on robotic components to introduce its practicality.

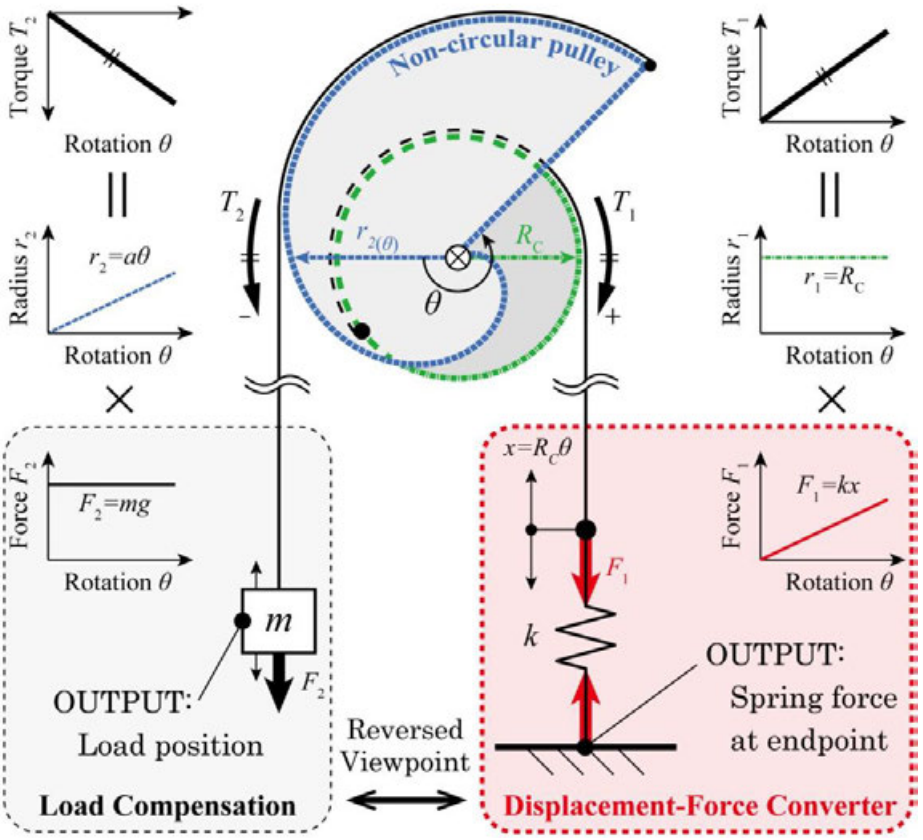

Fig. 12 Symmetrical relationship between the weight compensation mechanism and displacement–force converter (DF converter) using a spring and a noncircular pulley.

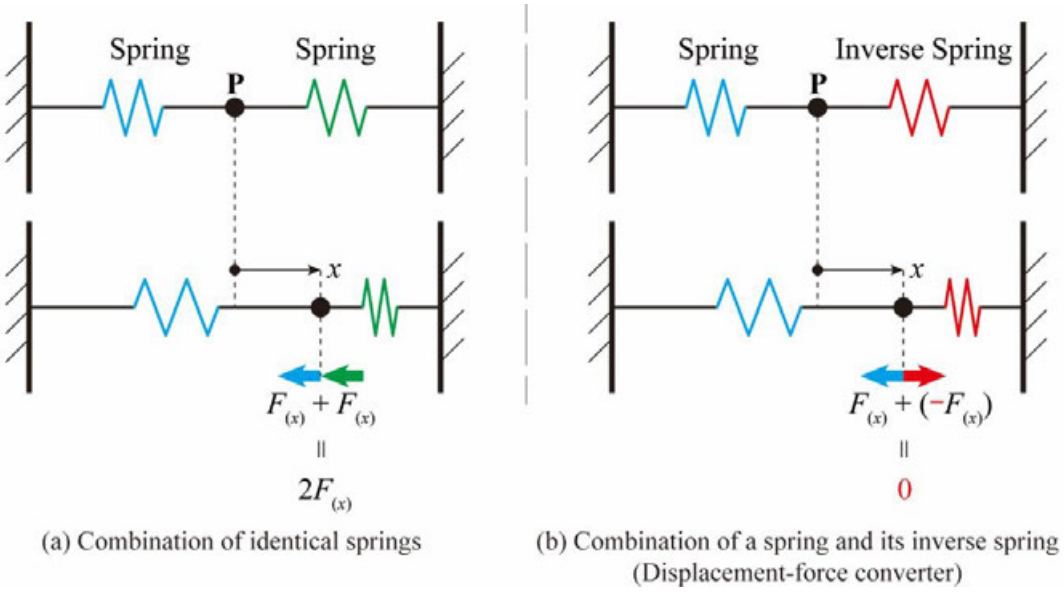

Fig. 13 Conceptual diagram of the reverse spring of the proposed DF converter.

Chapter I.4 Research purpose: proposal of the DF converter, establishment of the design method of its reverse springs, and verification of its usefulness through applications

In the preliminary research summarized in Chapter II.3, the conceptual principle of the DF converter was verified to be effective for force amplification. However, as described, it posed some issues for application to robotic components: using a weight increases the mass and limits the usable posture of the mechanism: a pulley is unsuitable for generating zero compensation torque, and the direction of the compensating force from the wire tension does not coincide with that of the tangency of the pulley, resulting in compensation imprecision.

Solving these problems, this study aims to achieve three objectives.

First, by developing new reverse springs that generate a compensating force or torque using mechanical components other than weight and a pulley, a solution to the mentioned design challenges of the proposed DF converter is provided. Specifically, the property of a cam–follower system, instead of the pulley–wire system, is featured, whose torque depends on its rate of change, in addition to the cam radius, which results in a variable pressure angle between the cam and follower. Moreover, the characteristic of a permanent magnet whose attractive force increases to pull itself even closer to the target object is also expected to be useful to create a reverse spring with less components.

Second, by identifying issues of the DF converter and seeking mechanical solutions to realize concrete examples of robotics applications, the study aims to demonstrate the usefulness of the idea of the proposed principle that makes robotic components exerting large loads drivable by smaller, lighter, and weaker actuators through force amplification without reduction. Prototype models of a wire tension regulator for a variable stiffness mechanism in a fire-resistant soft gripper, parallel gripper with an arbitrarily adjustable clamping force, and an energy efficient electropermanent-magnetic brake using the proposed converter are developed. Subsequently, evaluations are made on the changes in the energy consumption of the actuator, output force, and responsiveness of these mechanisms, compared to those driven solely by the actuator without compensation.

Third, primarily, these sophisticated design methods of the proposed DF converter and its application examples are conducted to widely publicize the practicability of the idea of compensation for force amplification, which effectively minimalizes the power consumption for controlling robotic components.

Chapter I.5 Structure of the thesis

Fig. 14 schematizes the structure of this thesis.

In Part II, a preliminary proof-of-concept (POC) prototype model of the proposed DF converter was introduced first and proved its ability to regulate the elastic tension. To overcome the compensation imprecision due to the deviation angle between the pulley tangent and vertical direction of the radius, its pulley–wire compensation system, a reverse spring using a cam–follower system, and its cam radius calculation process based on a simplified numerical analysis of a first-order ordinary differential equation were developed. The POC prototype model was built to conduct experiments to verify its effectiveness. As an application example, the converter is embedded in a continuous wire tensioner for a variable stiffness mechanism in a fire-resistant soft gripper to replace a massive and bulky pneumatic actuator.

Next, in Part III, another DF converter was introduced that uses a permanent magnet as a reverse spring, which generates a spontaneously increasing attractive force with the proximity to the target surface. For developing a robotic gripper whose clamping force is amplified by this proposed DF converter, existing attraction devices that allow the distance between a pair of magnets (and thus the attraction force between them) to be easily regulated were explored. Then, the principle and design procedure of the selected method employing an IB magnet (introduced briefly in Section I.2.4 in advance) were described in detail to clarify its advantages to adopt it to the gripper. The IBM gripper was developed to achieve coexistence of spontaneousness and steplessness on force amplification by continuously regulating the attraction distance of the magnet, which has not been accomplished by existing load-sensitive grippers using binary toggles and clutches.

In Chapter III.3, to realize the basic POC model of the IBM gripper, a one-sided (single-parting) gripper that has an active finger with an IB magnet embedded in it and another fixed finger with a target attraction surface was developed. The performance of the proposed gripper was examined through simple man-powered experiments, and the validity of the spontaneous force amplification achieved by attaching the magnet was inspected. To simplify the design procedure of the nonlinear spring of the IB magnet, a new compensation method using a pair of magnets facing like poles as a magnetic spring was invented.

In Chapter III.4, a bi-parting gripper that has two active fingers with an IB magnet embedded in each, to enhance dexterity, was developed. Because the magnetic spring was unsuitable for this configuration, as there was a mismatch of the approach speed of the magnets and compression speed of the springs, the focus shifted to the nonlinear property of the conical coil compression spring. A continuous regulation of the displacement of the magnets and fingers by a DC motor connected to a bidirectional screw revealed the validity of the steplessly adjustable force amplification feature of the IBM gripper. The performance evaluation experiment visualized the conditions in which the efficiency of the output clamping force relative to the power consumption maximizes.

In Chapter III.5, to solve the problem discovered in Chapter III.4 (the clamping force is nonlinearly affected by the width of the target object), a clamping-width adjustment mechanism was newly developed and implemented in the IB magnet bi-parting gripper to enhance its versatility. To make the clamping force more arbitrarily adjustable and predictable, the active finger and the IB magnet embedded in it must be actuated by a single actuator, but their displacements must be independent of each other such that the compensation does not get disturbed by the existence of an external object that mismatches the actuations of the magnet and spring. To mechanically suspend them while loosely connecting them when there is no external load, a lever–follower system was chosen to realize a clutch mechanism with a low transmission loss. The experiments showed that the clutch successfully minimalized and linearized the influence of the object width on the clamping force while sustaining the steplessly adjustable spontaneous force-amplification effect of the DF converter.

Furthermore, in Part IV, the structure of the one-sided gripper with a fixed width, designed in Chapter III.3, was turned into a brake mechanism by equipping the fingers with brake pads to introduce an application example of the IBM gripper, in which the target object has a known clamping width. To solve the problem of the pad having to be actuated for a long compensation stroke to fully disable braking, a novel multistage spring comprising two linear springs in series was devised. The multistage spring not only decreases its spring constant for compensation but also detaches the pad in accordance with a small displacement. By realizing an electropermanent configuration, the DF converter made the brake capable of exerting larger and more energy-efficient braking torques for both short- and long-span braking while sustaining the responsiveness comparable to it, compared to an existing electromagnetic brake.

In Part V, based on these research outcomes, common features of the DF converter observed throughout the study, problems left unsettled, and their possible solutions are discussed. Furthermore, other applications of the DF converter such as a variable stiffness gripper using a magnetorheological fluid and electropermanent-magnetic jumping mechanism are briefly introduced. These symbolize a further versatility of the idea of the DF converter for regulating not only elastic tension, magnetic attraction, and pressing but also magnetic repulsion and magnetic flux strength by a minimal external force. The expected significance and impactful contribution of the DF converter implied in the study, which include value creation on enhancement of energy efficiency in robotics and performance improvement of machines in extreme environments with design and operation restrictions, are discussed.

Finally, Part VI presents the conclusion and future aspects of the study.

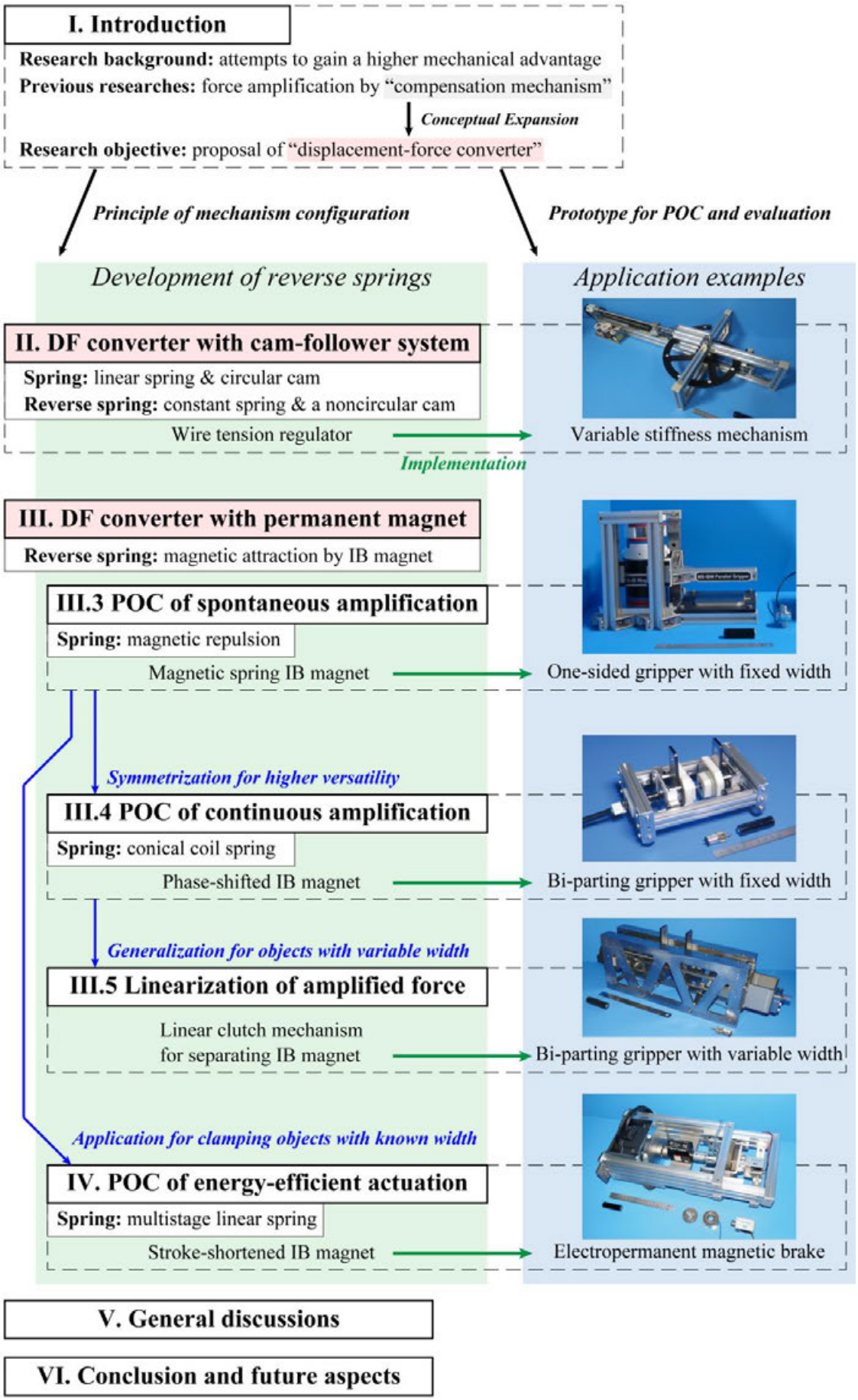

Fig. 14 Structure of this thesis.

Part II

Development of the DF converter with a reverse spring comprising a cam–follower system, and its application to a variable stiffness gripper

Part II Development of the DF converter with a reverse spring comprising a cam–follower system, and its application to a variable stiffness gripper

Chapter II.1 Abstract of Part II

In this part, a new compensation method for the DF converter, which uses a noncircular cam as a reverse spring, is introduced.

First, a preliminary POC prototype model of the DF converter using a pulley–wire system was developed, and its ability to regulate the elastic tension was proven. This model balances the torques generated by a linear spring connected to a circular pulley and a mass connected to a noncircular pulley as a reverse spring.

To overcome the compensation inaccuracy due to the deviation angle between the pulley tangent and the vertical direction of the radius, a cam–follower system designed through a simplified numerical analysis on a first-order ordinary differential equation was developed. This generates a compensation torque by the contact force of the follower, which is split in the tangential direction of the cam by the pressure angle varying in accordance with the rotation.

The prototype demonstrated that the compensation decreased the maximum control force required to extend the spring by 23.2 % and the difference of the control force between extension and compression from 543 % to 49 % . This uniformization allows the selection of an actuator with a smaller maximum output. Moreover, it was incorporated into a variable stiffness mechanism of a fire-resistant soft robotic gripper as a wire tensioner to regulate the rigidity of its finger continuously, thus, replacing a conventional massive pneumatic actuator.

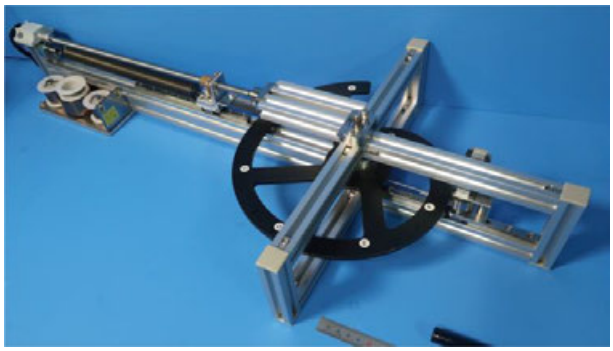

Fig. 15 Appearance of the POC model of the proposed displacement–force converter using the pressure angle method.

Chapter II.2 Application of the DF converter #1: wire tension regulator for a fire-resistant variable stiffness robotic gripper

This chapter proposes the first specific example of the practical use of the DF converter, and thus, it clarifies how the stepless and energy-efficient control of deformation of a spring is useful in robotic components.

Fig. 17 illustrates a variable stiffness structure named the line jamming mechanism, a series of beads that changes its stiffness state due to the frictional force between neighboring beads according to the tension of the wire penetrating them. The cup-shaped beads in Fig. 17 (b) are used in a heart stabilizer during surgery, as shown in Fig. 18 [31], and in the fingers of a cut- and fire-resistant soft robotic gripper, as shown in Fig. 19. The latter is developed by the author's research team to grasp burning, sharp, and unshaped debris in a disaster field, as demonstrated in Fig. 20. Its jamming media, the beads and wire, can be made of durable materials such as metal. This characteristic is highly advantageous to existing variable-stiffness grippers composed of a soft membrane filled with powder (more specifically described in Section V.2.2) that cannot sustain its functionality once the membrane is damaged.

Conventionally, the line-jamming mechanisms have been regulated by a hand-driven toggle or a pneumatics to switch the wire tension in a binary manner. Inserting the DF converter between the mechanism and a weak actuator would enable the mechanism to change its stiffness arbitrarily, steplessly, and efficiently.

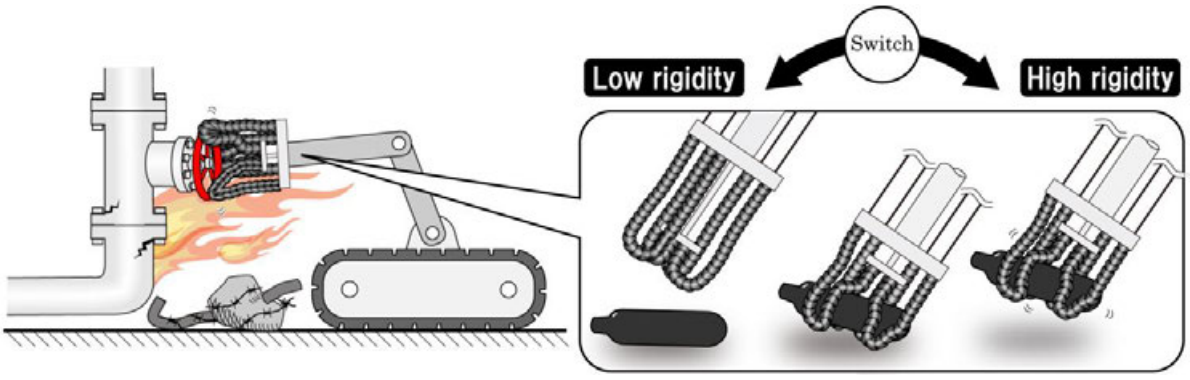

Fig. 16 A conceptual diagram of a variable stiffness gripper that switches its operational state between low-rigidity and high-rigidity states.

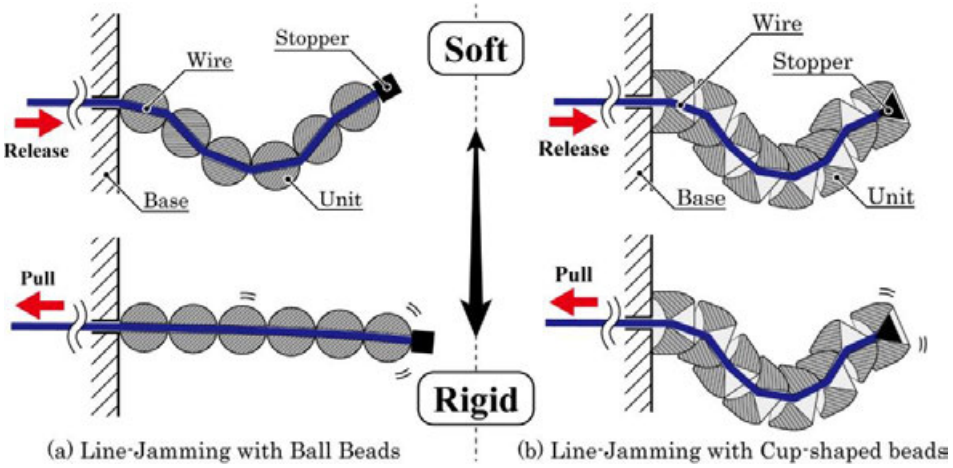

Fig. 17 Principle of the line-jamming mechanism. By optimizing the shape of the bead units and the wire path, the application of tension (a) restores or (b) maintains the relative posture between beads in contact.

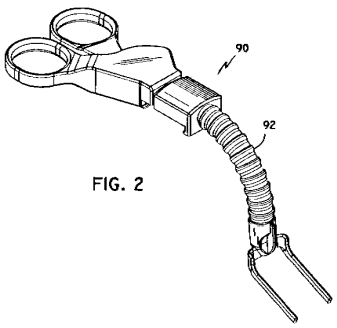

FIG. 2

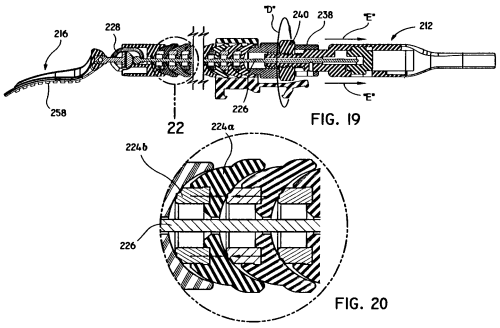

FIG. 19

FIG. 20

Fig. 18 Surgical instrument with the line-jamming mechanism that is used to fix the relative position of the heart-stabilizing tool relative to the surgical site [31].

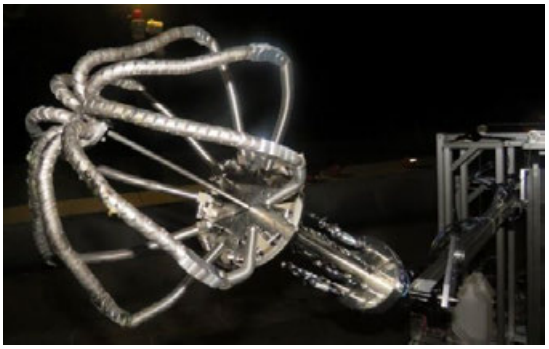

Fig. 19 Fire-resistant soft robotic gripper using the line-jamming mechanism.

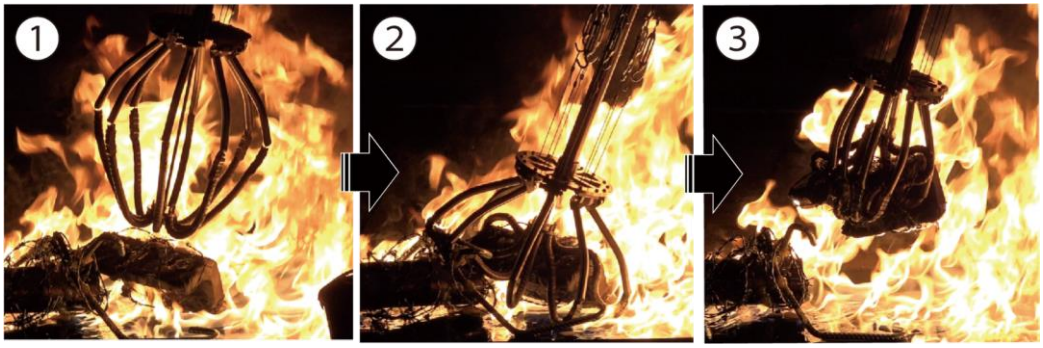

Fig. 20 The fire-resistant soft robotic gripper grasping debris on fire.

Chapter II.3 Preliminary study: development of the first prototype POC model of the DF converter

Fig. 21 shows the appearance of the preliminary conceptual prototype model of the proposed DF converter, whose structure is illustrated in Fig. 12. As the most representative example of the reverse spring, a weight connected to a noncircular pulley is balanced to a linear spring connected to a circular pulley such that both loads possess linear displacement–torque characteristics.

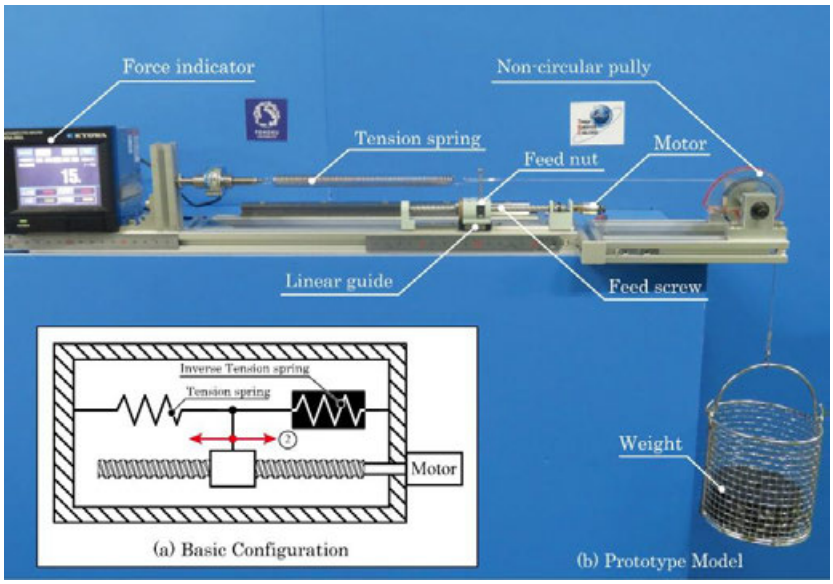

Fig. 21 Preliminary prototype model of the DF converter for proof of principle.

Section II.3.1 Design procedure of the noncircular pulley of the DF converter

Here, the torque $\boldsymbol{T_1}$ to be compensated, generated by a linear spring (as the simplest example) with a spring constant k, connected to a circular pulley of constant radius $|\boldsymbol{R_1}| = R_C$, is designed to be balanced with the torque $\boldsymbol{T_2}$. $\boldsymbol{T_2}$ is generated by a constant load of a weight m under gravity g connected to a noncircular pulley of variable radius $|\boldsymbol{R_2}| = r_{(\theta)}$. r is derived as follows: First, the torque applied to a circular pulley $\boldsymbol{T_1}$ is expressed as

$$\boldsymbol{T_1} = \boldsymbol{F_1} \times \boldsymbol{R_1} = (kR_C\theta)(R_C)\boldsymbol{e_z} \tag{2}$$

as the elastic force $\boldsymbol{F_1}$ increases proportionally with the rotation angle θ of the pulley. Note that $\boldsymbol{e_z}$ is the unit vector facing toward the front of the paper.

Next, the torque $\boldsymbol{T_2}$ applied to the noncircular pulley by a constant load mg is determined by the pulley diameter $\boldsymbol{R_2}$ as

$$\boldsymbol{T_2} = \boldsymbol{F_2} \times \boldsymbol{R_2} = -(mg)(r)\boldsymbol{e_z} \tag{3}$$

as the load $\boldsymbol{F_2}$ is constant, regardless of the rotation angle. Substituting (2) and (3) in $\boldsymbol{T_1} + \boldsymbol{T_2} = 0$ generates (4), thereby showing that r is an Archimedes' spiral that increases proportionally to the rotation angle, as plotted in Fig. 22.

$$r_{(\theta)} = \frac{kR_C^2}{mg}\theta \tag{4}$$

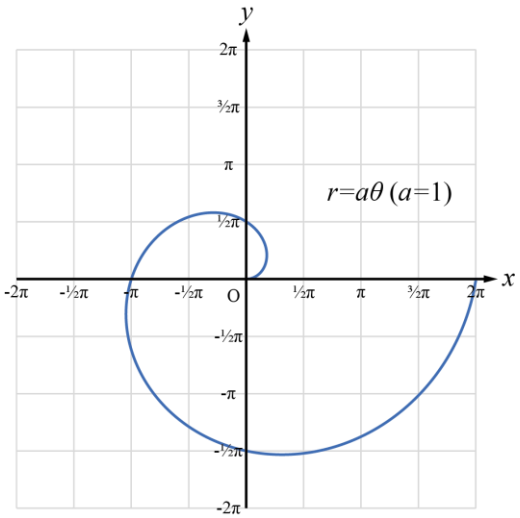

Fig. 22 Archimedes' spiral representing the pulley radius profile.

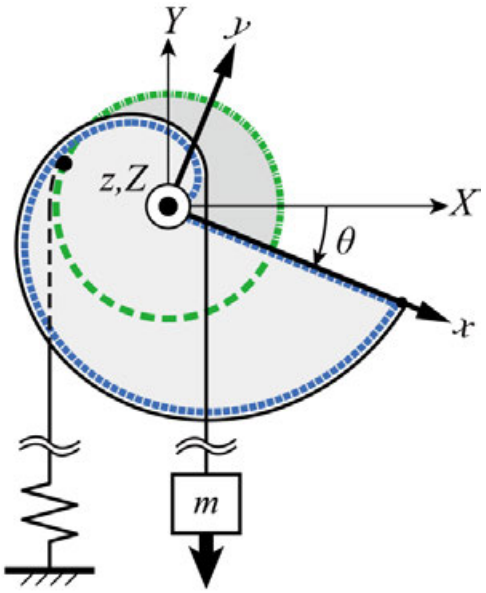

Fig. 23 The definition of the coordinate systems. The curve on the xy-plane is rotated from the XY-plane of the mechanism by angle θ around the Z-axis.

Section II.3.2 Basic operation experiment of the DF converter

To demonstrate the effectiveness of the DF converter, an experiment was conducted using the prototype, as shown in Fig. 24. A hand-powered input was applied on the point of equilibrium using the tip of a mechanical pencil, and the output was expressed as the tension force of the spring measured by a loadcell (Kyowa Electronics, LUR-A-2KNSA). As shown in the figure, the point of equilibrium can be shifted to the right and left directions, resulting in an increase and decrease in the internal force generated by the spring, with a control force reasonably smaller than the output force such that the fragile pencil lead does not break.

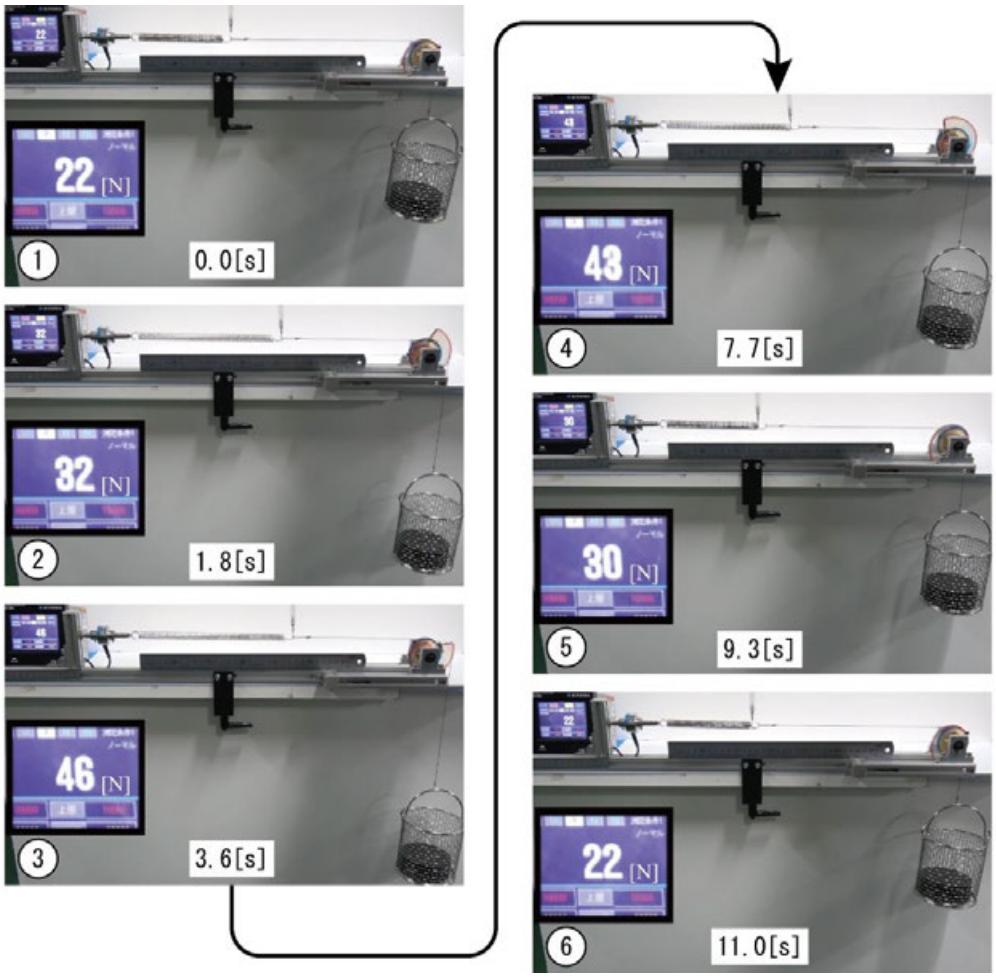

Fig. 24 Basic operation experiment of the DF converter. (1)–(3) The point of equilibrium was first shifted rightward, during which the spring stretched and the pulley radius increased, resulting in an increase in the output force. (4)–(6) The point was then shifted leftward, during which the spring got compressed and the pulley radius decreased, resulting in a reduction in the output force.

Section II.3.3 Performance evaluation experiment of the DF converter

By powering the DC motor as the input actuator, the properties of the output and input forces were inspected according to the change in displacement. In addition to the loadcell attached to the spring, a force gauge was connected to the point of equilibrium to measure the operation force. Offset stroke b was inserted between the spring and pulley to observe the effect of compensation accuracy.

The results are shown in Fig. 25. When $b = 0$, the spring deformation was successfully controlled with an input force of 0.3 % of the output force in average, both linearly increasing as the spring further extended. In addition, when $b = 10$ and 20 mm, an extra force was required for the operation, but the control force remained at 5 % and 8 % of the output, respectively. Because the force required to control the input point has an approximately constant displacement–force characteristic on a macroscopic view, it can be concluded that the DF converter can be driven by an actuator with a stable and weak output force, verifying the proposed principle.

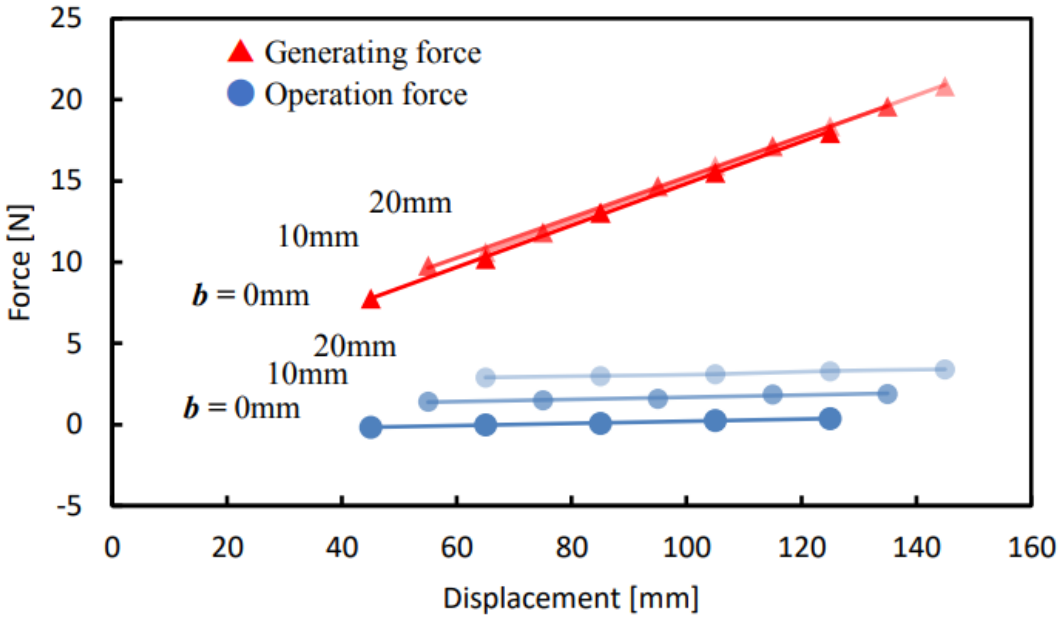

Fig. 25 Result of the performance evaluation experiment of the DF converter.

Chapter II.4 Disadvantages of the DF converter

In the preliminary study [32], the conceptual principle of the DF converter was verified. However, it posed some issues: the use of a weight increases the mass and limits the usable posture of the mechanism; the direction of the compensating force from the wire tension does not coincide with that of the tangency of the pulley.

Section II.4.1 Deviation of the tangency of the noncircular pulley from the tension direction of the wire

In case of a circular pulley, the wire is stretched perpendicularly to the radius at any rotation angle as long as a tension is applied in a certain direction. However, as illustrated in Fig. 26, achieving strict compensation with a noncircular pulley having a radius simply proportional to the rotation angle is difficult. This is because the vertical direction of the radius $r_{(\theta)}$ at the rotation angle θ (the segment $\overline{\mathrm{OR}}$) is diverted from the tangential at **R** by a deviation angle ϕ. This indicates that the wire cannot extend perpendicularly to the radius from **R** for an accurate generation of compensation force because the tension force stretches the wire along the tangential direction of the pulley.

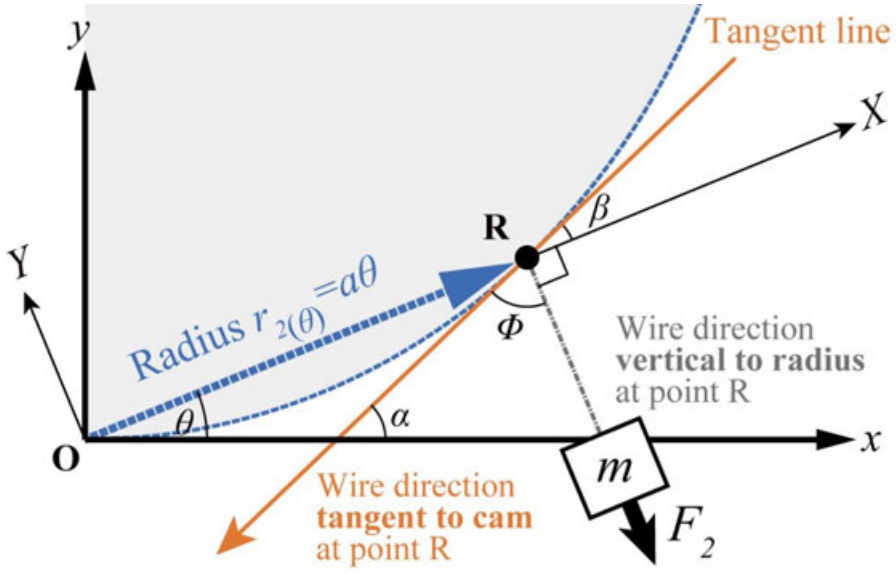

Fig. 26 Deviation angle ϕ between a vertical line to the radius and a tangential line at point R in the noncircular pulley–wire system.

The equational analysis of the deviation angle is as follows. First, considering $r' = \mathrm{d}r/\mathrm{d}\theta$, the slope of the tangent α at a certain $r_{(\theta)}$ on the pulley curve is expressed as

$$\tan\alpha = \frac{\mathrm{d}y}{\mathrm{d}x} = \frac{r + r'\tan\theta}{r' - r\tan\theta} \tag{5}$$

Since ϕ is the residual of the deviation angle between the radius and the tangent angle $\beta(=\alpha-\theta)$, (6) and (7) are obtained from (5) as follows:

$$\begin{aligned}\tan\beta = \tan(\alpha-\theta) &= \frac{\tan\alpha - \tan\theta}{1+\tan\alpha\tan\theta} \\ &= \frac{r}{r'} = \tan(90^\circ - \phi)\end{aligned} \tag{6}$$

$$\Leftrightarrow \cot\phi = \frac{r}{r'} \tag{7}$$

Equation (7) plotted in Fig. 27 shows how the deviation angle increases as θ decreases; ϕ even reaches 90° at $\theta = 0$. This deviation of direction leads to a misalignment of the departing point of the wire from the pulley, which is ununiform beyond the current radius, as illustrated in Fig. 27. Thus, it is ineffective to make the radius proportional to the rotation angle especially in a small range of rotation angle θ.

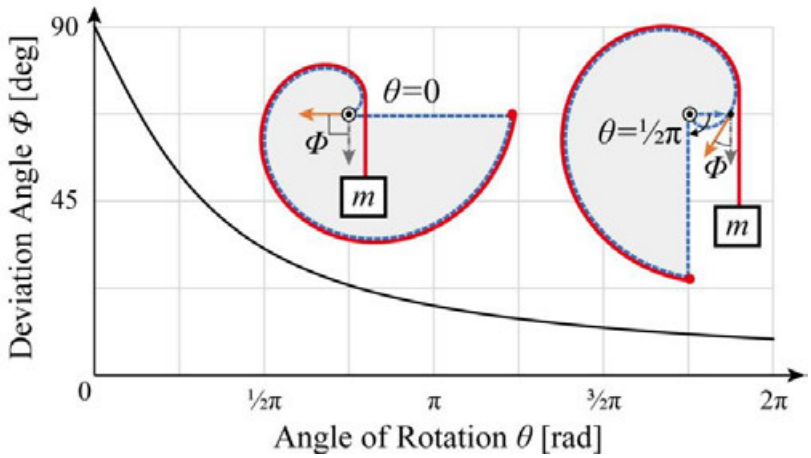

Fig. 27 Deviation angle between a line perpendicular to the radius and a tangential line. The actual direction of the wire is also illustrated in red.

Therefore, in some studies on weight compensation for robotic arms [10], [23], [24] and a variable-force pantograph for inner-pipe locomotion [33], numerical analysis methods for determining the pulley radius were proposed by modeling the geometric relationship of this misalignment. However, since severe and complex constraints on establishing the assumptions of the analysis were used, iterations are required for the optimization of the design variables, as exemplified in Fig. 28.

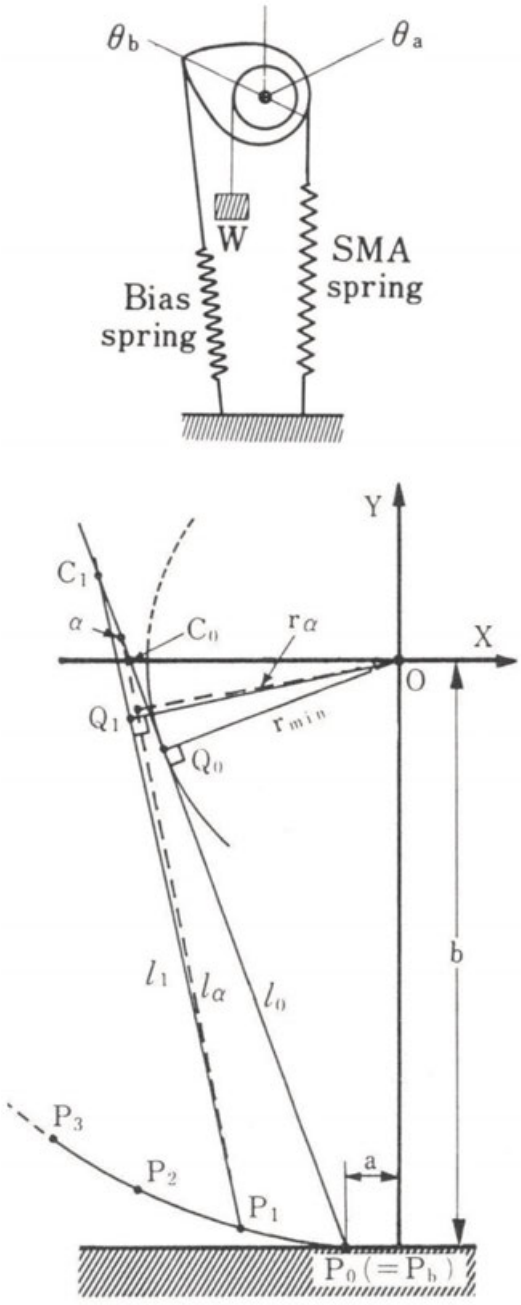

1. Set structural design parameters a, b in Fig. 3, as well as initial arm angle θ_0 and desired torque profile $\tau(\theta)$.
2. Set spring stiffness k, natural length x_0, initial tension F_0. In case of an ordinary linear spring, spring force F_s can be expressed as $F_s = kx + F_0$, where x is displacement.
3. Numerical design starts with maximum displacement x_{max} of the spring, where initial pulley radius is $r_0 = \tau(\theta_0)/F_{max}$.
4. Draw a tangent line of a circle l_0 to intersect the fixed point of the spring P_0 in Fig. 3, where the center of the circle is O and its radius is r_0. Define C_0 which is intersection of l_0 and X axis.
5. Draw a circle with radius of $\overline{OP_0}$ and define points $P_1, P_2, \ldots, P_n$ with constant incremental angle $\Delta\theta$ in the motion range ($\theta_0 \le \theta \le \theta_{max}$). This is because an analytical procedure is to be taken in which the pulley curve is drawn around the rotating center O by inversely rotating the spring supporting point P_i (instead of rotating the pulley) and unwinding the flexible part at the spring end from the pulley side.
6. Choose a random point α on the tangent line l_0. Obtain the displacement x_α of the spring stretched between the segment $\overline{\alpha P_1}$ and distance r_α of the straight line αP_1 from the origin O. The variation of the displacement of the spring stretched from the point α is $(\overline{\alpha P_0} - \overline{\alpha P_1})$ because the flexible part wound around the pulley is supposed to be non-ductile. Consequently, the displacement is $x_\alpha = x_{max} - (\overline{\alpha P_0} - \overline{\alpha P_1})$, where spring force is $F_{s\alpha} = k \cdot x_\alpha + F_0$.
7. Perform the operation in which the position of the point α is shifted until it agrees with the desired torque profile $\tau(\theta)$ by $F_{s\alpha} \cdot r_\alpha$ by means of a convergent calculation.
8. Make the position of α the point C_1, which is the first vertex of the pulley configuration to be polygonally approximated.
9. Assume a new point α on the straight line $\overline{C_1 P_1}$ and repeat the calculations of 6.- 8. for the points α and P_2 to obtain C_2.
10. Repeat the above-mentioned procedure until the displacement becomes zero or $\theta = \theta_{max}$.

Fig. 28 An example of the iterative calculation process of designing a weight compensation mechanism using a pulley–wire system for assisting a shape memory alloy actuator [10].

Section II.4.2 Design restrictions due to the use of a weight and pulley for the reverse spring

As described in Chapter I.2, the reverse spring using weight obviously become heavy, resulting in the increase in the total mass of the machine, while the purpose of DF converter is to amplify the output force of the machine without using large actuator, contractively. Additionally, because the load of the weight is applied only vertically downward, the installable posture of the machine is limited, in which the room for the weight to move up and down is available.

Furthermore, as the weight generates a constant load, the pulley radius has to become $r_{(\theta=0)} = 0$ instead when the spring deformation and the torque to be compensated is zero. Making the radius zero precisely is impracticable not only because of its design inconvenience but also because there is a large deviation angle between the pulley tangency and wire direction, as analyzed in Section II.4.1.

To resolve these problems, new kinds of reverse springs that do not include weights are required.

Chapter II.5 Proposed principle: Variable pressure-angle method of the cam–follower system

This chapter is aimed at developing a new cam compensation system for a DF converter that generates compensating torque using not only the variable cam radius but also its rate of change which results in a variable pressure angle between the cam and follower. The proposed method admits and makes use of the existence of the deviation angle ϕ, which is inevitable if the radius changes, even if adopting a cam–follower system defined in Fig. 29 instead of the pulley–wire system.

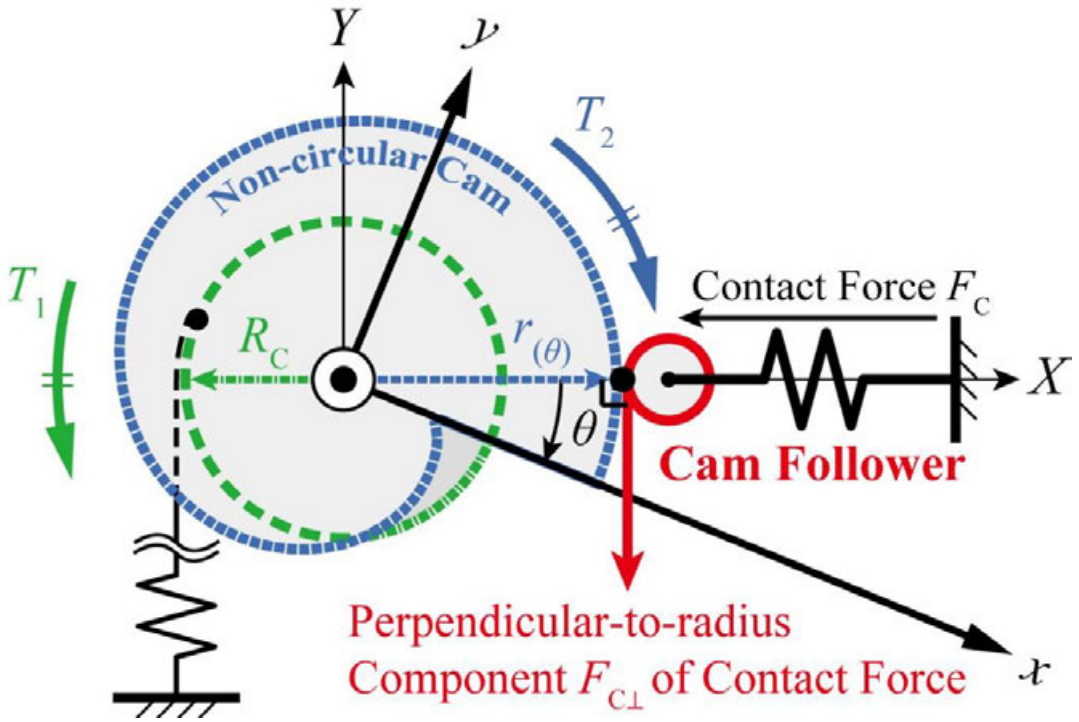

Fig. 29 Definition of the coordinate systems of the proposed compensation method for a DF converter using the pressure angle between the cam and the follower.

Fig. 30 illustrates how a follower is in contact or is pressed against a noncircular cam and generates a force component $F_{C\perp}$ perpendicular to the radius. Equation (7) provides the pressure angle ϕ between the cam and follower, by which the force applied by the follower is divided into directions perpendicular and parallel to the tangential first, and then into directions perpendicular and parallel to the radius. Once the pressure angle is designed to produce an appropriate compensating torque over the range of angles to be used, the total cam profile can be calculated using integration.

This method also allows the initial cam radius $r_{(0)} = r_0$ to be more than zero by setting the pressure angle to zero instead, while the previously mentioned pulley had to consider $r_{(0)} = 0$ to generate zero-compensation torque, which is impractical. This characteristic of the cam–follower system significantly improves the flexibility in design of the axis of rotation.

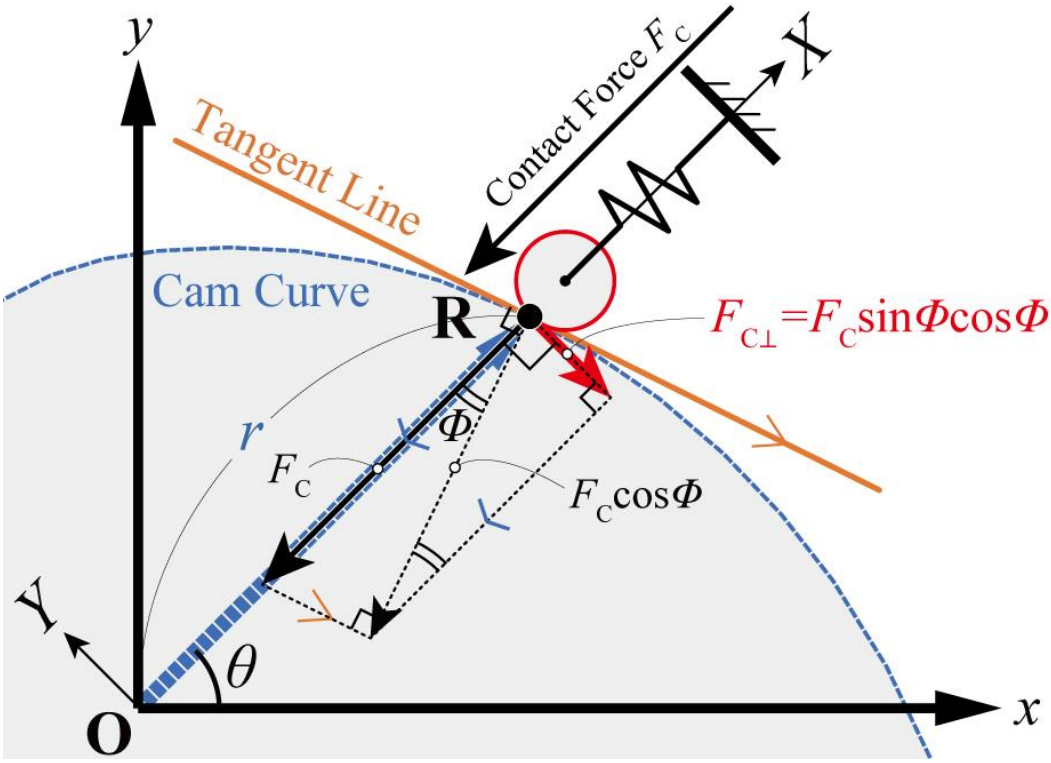

Fig. 30 Definition of component forces applied to the cam by the follower.

Similar studies using the contact force between the cam and follower for weight compensation of robotic arms have been conducted, but as these arms behave in a their torques were limited to a sine function [11], [34]–[36]. This study differs from them in that its purpose is to generalize the compensation to any displacement–force characteristic for deforming an elastic element by reversing the relationship between input and output components.

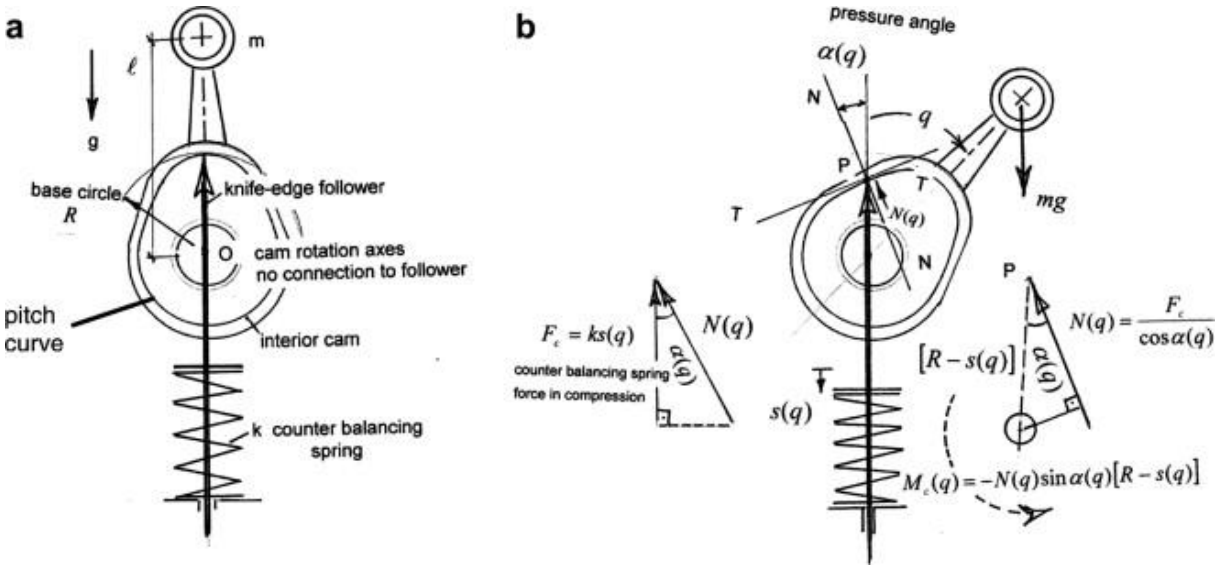

Fig. 31 Weight compensation mechanism using an interior cam–follower system for a robotic arm [34].

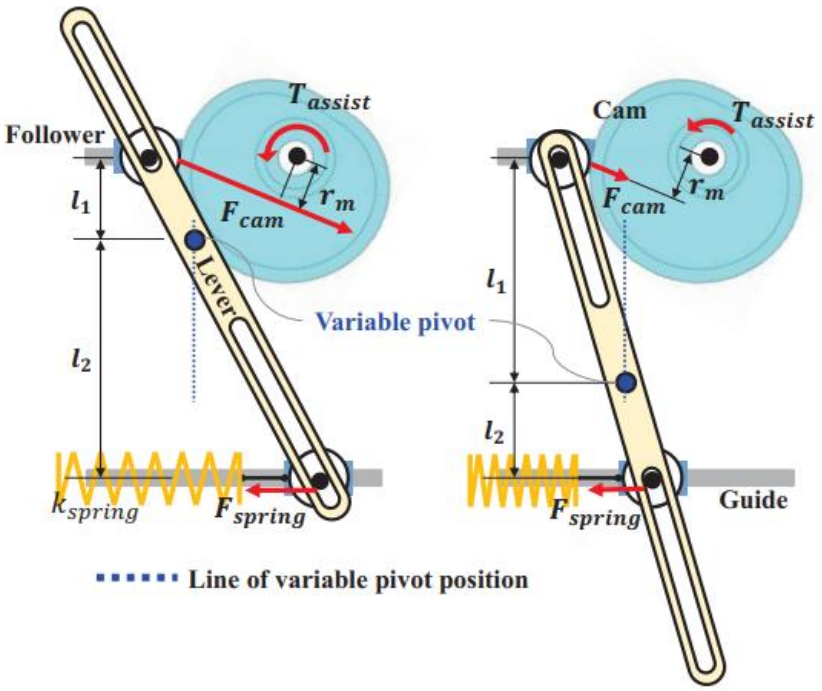

Fig. 32 Weight compensation mechanism using an interior cam–follower system for a robotic arm, with a variable pivot of a lever [35].

Based on the concept, the characteristic equation representing the cam radius for compensating a linear spring is derived from the following process. First, the torque $\boldsymbol{T_1}$ applied to the circular pulley is equated to (2), which gives:

$$\boldsymbol{T_1} = \boldsymbol{F_1} \times \boldsymbol{R_1} = (kR_C\theta)(R_C)\boldsymbol{e_z} \tag{8}$$

If the follower diameter is zero (point contact), the torque $\boldsymbol{T_2}$ applied to the noncircular cam is expressed as

$$\boldsymbol{T_2} = \boldsymbol{F_2} \times \boldsymbol{R_2} = -(F_C \cos\phi)(r)\sin\phi\, \boldsymbol{e_z} \tag{9}$$

as the partial force component $F_2 = F_C \cos\phi$ in the tangential perpendicular direction of the pushing force F_C (assumed to be constant here) is applied to the dynamic diameter of the cam by the follower. Moreover, the tangential deviation of the tangent angle is taken further along the direction of the rotation angle. From (6) and the definition of the trigonometric functions, the following transformation holds.

$$\begin{aligned}\sin\phi\cos\phi &= \cos(90° - \phi)\sin(90° - \phi) \\ &= \frac{r'}{\sqrt{r^2 + r'^2}} \cdot \frac{r}{\sqrt{r^2 + r'^2}}\end{aligned} \tag{10}$$

As in the conventional method of Chapter II.3, (11) is obtained by substituting (8)–(10) in $\boldsymbol{T_1} + \boldsymbol{T_2} = 0$.

$$kR_C^2\theta = \frac{r^2 r'}{r^2 + r'^2} F_C \tag{11}$$

As $r^2 + r'^2 \neq 0$ for any θ, multiplying both sides of (11) by $r^2 + r'^2$ yields the following equation:

$$(kR_C^2\theta)r'^2 + (-F_C r^2)r' \quad + (kR_C^2\theta r^2) = 0 \tag{12}$$

Solving (12) by setting $r_{(\theta=0)} = r_0 > 0$ gives $r'_{(\theta=0)} = 0$ and dividing both sides by $kR_C^2\theta$ for $\theta \neq 0$ gives a quadratic:

$$r'^2 + \left(-\frac{F_C r^2}{kR_C^2\theta}\right)r' + (r^2) = 0 \tag{13}$$

With a constant $C = F_C/kR_C^2$, (14) is obtained as the quadratic formula of r' as follows:

$$r' = -\frac{Cr^2}{2\theta} \pm \frac{1}{2}\sqrt{\left(\frac{Cr^2}{\theta}\right)^2 - 4r^2} \tag{14}$$

Hence, once the mechanical parameters included in the constant C are determined according to the design requirement of the converter mechanism, the cam profile $r_{(\theta)}$ can be calculated numerically by solving (15) as a first-order ordinary differential equation. The monotonically decreasing characteristic of $r_{(\theta)}$ is illustrated in Fig. 33.

$$r'_{(\theta)} = \begin{cases} 0 & (\theta = 0) \\ -\dfrac{Cr^2}{2\theta} \pm \sqrt{\left(\dfrac{Cr^2}{2\theta}\right)^2 - r^2} & (\theta > 0) \end{cases} \tag{15}$$

Compared to the existing cam–follower self-weight compensation mechanisms [11], [34]–[36], a numerical analysis is still required for the proposed method. However, its only initial parameter to be optimized is r_0, and its condition for the radius to always have a real value within the range of θ is already clear as $r_0 > 2\theta_{\max}/C$. Therefore, the restrictions of the proposed method are much fewer than those of the conventional pulley–wire methods used in previous self-weight compensation and DF converters, whose convergence conditions of parameters for recursive numerical analysis are not found symbolically.

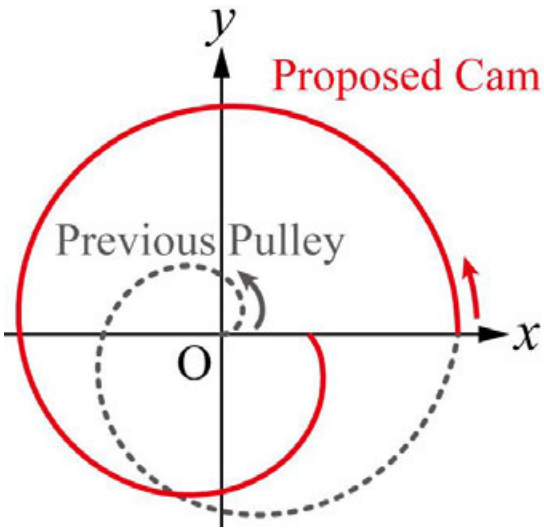

Fig. 33 Comparison of the monotonously increasing pulley radius of the conventional method (dashed line) and the monotonously decreasing cam radius of the proposed method (solid line).

Since the actual follower diameter is always greater than zero, the cam and follower placed at a rotation angle θ are in contact with each other at an angle slightly less than θ. To avoid this error resulting in the compensation, using an offset curve $r_{\mathrm{P}(\theta)}$ containing a set of points **P** shifted from the points **R** on the curve $r_{(\theta)}$ in the perpendicular direction by the length of the follower radius R_{f}, as depicted in Fig. 34, is necessary.

It is verified in this section that a change between the compensation torques generated before and after applying the offset does not ideally exist. Analyses of the effects of offsetting have been done, but they assume a more general use of the cam–follower mechanism, in which the cam as the driving component transfers force to the follower for lifting it up and down (e.g., [37]). However, these analyses are mainly used to confirm that the pressure angle is within its proper range, and none of them have considered the transferred torque in detail so far. Therefore, it is stated here as follows.

Once the corrected radius $\overline{\mathrm{OP}}$ is obtained as (16) by applying the cosine theorem to ΔORP, the angle of deviation of the contact point ∠ROP (correction angle λ) at each θ is uniquely determined using (7) and another geometric relationship in ΔORP is expressed as (17). Note that $\angle\mathrm{ORP} = \phi$ from the definition of the offset curve.

$$\begin{aligned}\overline{\mathrm{OP}}^2 &= \overline{\mathrm{OR}}^2 + \overline{\mathrm{PR}}^2 - 2\overline{\mathrm{OR}}\,\overline{\mathrm{PR}}\cos\phi \\ &= r^2 + R_{\mathrm{f}}^2 - 2rR_{\mathrm{f}}\cos\phi\end{aligned} \tag{16}$$

$$r = R_{\mathrm{f}}\cos\phi + \overline{\mathrm{OP}}\cos\lambda \tag{17}$$

The corrected torque $\boldsymbol{T}_{\boldsymbol{2}}'$ is obtained from (18) using (17), as the component force of the follower in the rotational direction of the corrected follower force is inclined by an angle λ.

$$\begin{aligned}&\boldsymbol{T}_{\boldsymbol{2}}' = \boldsymbol{F}_{\boldsymbol{2}} \times \boldsymbol{r}_{\mathbf{P}} = (F_{\mathrm{C}}\cos\phi)(\overline{\mathrm{OP}})\sin(\phi+\lambda)\,\boldsymbol{e}_{\mathbf{z}} \\ &= F_{\mathrm{C}}\cos\phi\,\frac{r - R_{\mathrm{f}}\cos\phi}{\cos\lambda}(\sin\phi\cos\lambda + \cos\phi\sin\lambda)\boldsymbol{e}_{\mathbf{z}} \\ &= F_{\mathrm{C}} r\sin\phi\cos\phi\,\boldsymbol{e}_{\mathbf{z}} + F_{\mathrm{C}}\cos^2\phi\,\{(r - R_{\mathrm{f}}\cos\phi)\tan\lambda - R_{\mathrm{f}}\sin\phi\}\boldsymbol{e}_{\mathbf{z}}\end{aligned} \tag{18}$$

The first term equals $\boldsymbol{T_2}$ in (9) and another geometric relationship in ΔORP expressed as (19) transforms (18) into (20). Hence, the compensating torques before and after offsetting are ideally equal, allowing an arbitrary diameter of the follower with an appropriate load-bearing capacity.

$$(r - R_{\mathrm{f}} \cos \phi) \tan \lambda = R_{\mathrm{f}} \sin \phi \tag{19}$$

$$\boldsymbol{T}_2' = \boldsymbol{T_2} + F_{\mathrm{C}} \cos^2 \phi \, (0) \boldsymbol{e_z} = \boldsymbol{T_2} \tag{20}$$

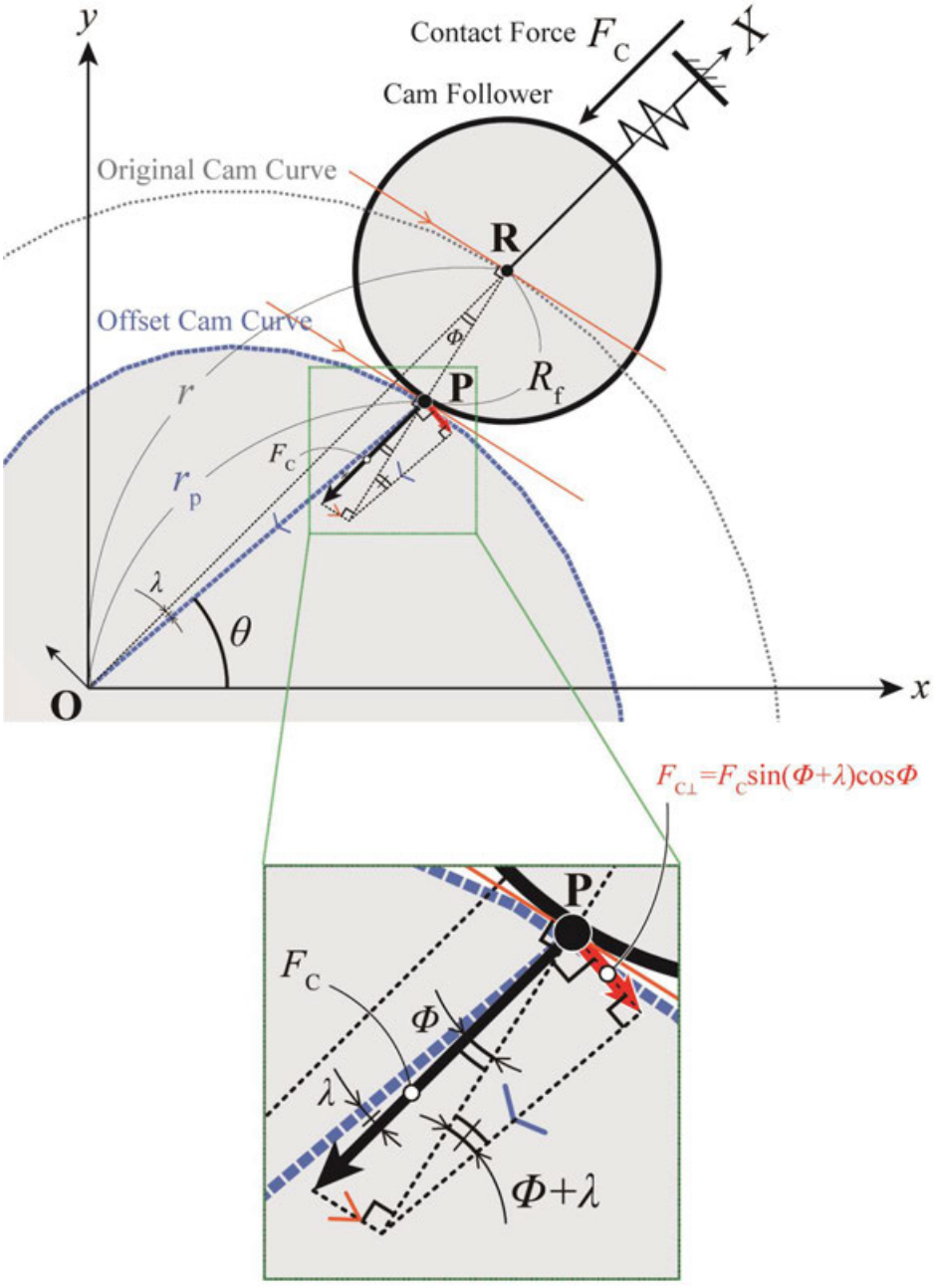

Fig. 34 Definition of component forces applied by the follower to the cam with an offset curve.

Chapter II.6 Embodiment of the DF converter using the cam–follower system

Section II.6.1 Design and development of the DF converter using the cam–follower system

Fig. 35 shows the image and dimensions of the prototype of the proposed DF converter for the POC of the pressure angle method. Its specifications, listed in TABLE I, were designed following the procedure mentioned below.

First, a constant-load spring was adopted in the POC model here for generating a pressing force of the follower. In the preliminary study [32], a weight was used as the compensating element for easily generating a constant force, but this limited the posture of the mechanism strictly horizontally. Not only can the constant spring extend in an arbitrary direction, but it can also sustain a load much greater than its own weight (10.7 times in this case). Thus, a pair of a linear spring to be compensated and a corresponding constant spring for compensation was selected such that the maximum elastic force of the former was approximately twice that of the latter.

Second, the transmitting medium of the spring force to be compensated was changed from a conventional pair of a wire and a circular pulley to a pair of a rack and a pinion in this POC model after considering the durability and elongation fatigue of the wire. The gear transmission is also selected as it translates the displacement of the spring to the rotation of the cam even when extending the spring in which a wire would sag after losing its tension. A 40-mm pitch diameter of pinion was chosen as the reasonable size, and then it was confirmed that the maximum operating distance of $2\pi R_{\mathrm{C}} \cong 125.7$ mm, the circumference of the pinion with a rotation range of $0 \leq \theta \leq 2\pi$ (can be set beyond 2π if needed), fits within the maximum permissible extension of the linear spring from its free length.

Substituting the constants determined as stated before in (15), whose double sign was substituted to + to prevent the excessive steepness of the curve, the cam profile was calculated and is plotted in Fig. 36. The transition of the pressure angle was also obtained from (7). The minimum integer value under these conditions was determined as the initial radius r_0.

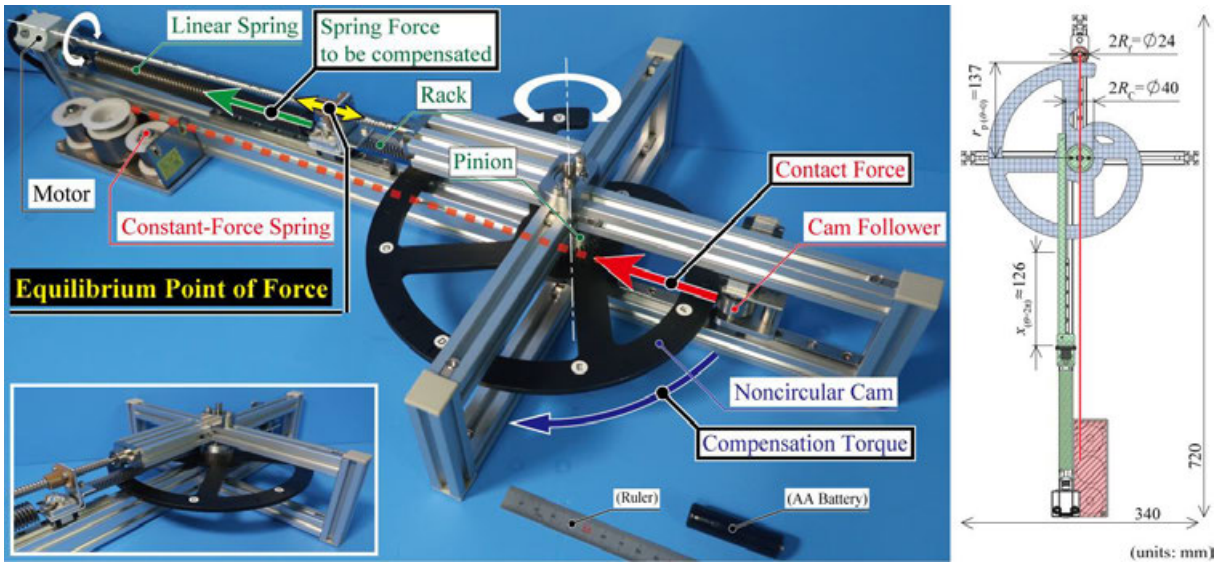

Fig. 35 Appearance and design sketch of the POC model of the proposed displacement–force converter using the pressure angle method. The wire of the constant spring penetrates the cam axis through its side hole. The cam made of stainless steel is coated with electroless nickel-phosphorus plating for better visibility.

TABLE I

MECHANICAL COMPONENT VALUES USED FOR CAM PROFILE CALCULATION

Linear spring to be compensated **AWY20-175**	Spring Constant	k 0.39 N/mm
	Max. Spring Force	$F_{1(\theta=2\pi)}$ 60 N
	Pinion Radius	R_C 20 mm
Constant spring for compensation **NWT3.0-1-R**	Const. Spring Force	F_C 35.6 N
	Max. Cam Radius	r_0 149 mm
	Follower Radius	R_f 12 mm

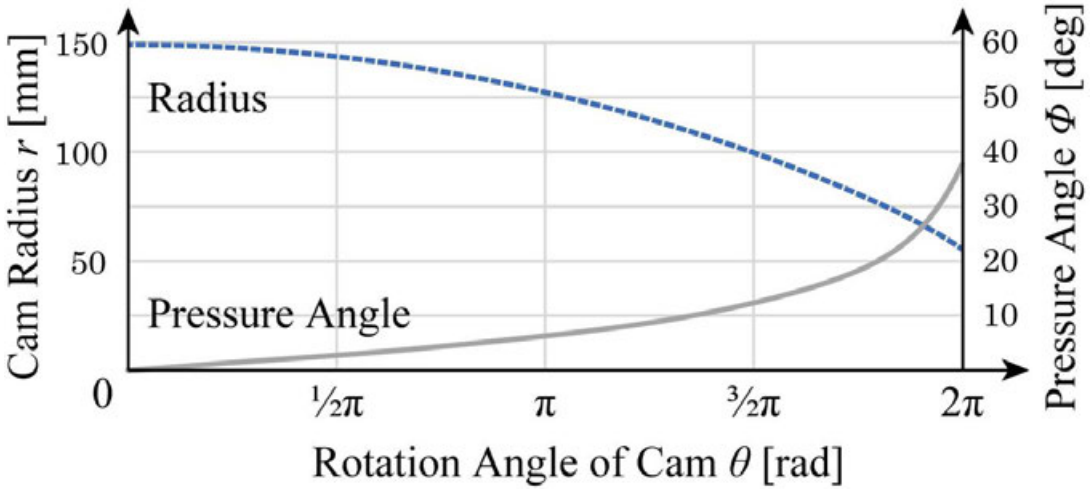

Fig. 36 Transition of the radius and pressure angle of the POC model of the proposed displacement–force converter using the pressure angle method.

Section II.6.2 Performance evaluation experiment of the DF converter using the cam–follower system

First, a basic operation of the proposed DF converter was conducted to verify its principle. It was evaluated based on whether the control force required to extend and compress the spring, represented by the power consumption of an actuator, is reduced due to the compensation by the cam.

The system constituents and the experiment procedure are shown in Fig. 37, in which a load cell (Kyowa Electric, LUR-A-2KNSA) is mounted on the fixed end of the spring to indicate the tension applied by the spring, and an encoder (Omron, E6A2-CW3C 360P/R 0.5M) is attached to the rotation axis of the cam. The other end of the spring is connected to a nut of the feed screw, where the spring force is coupled to and balanced with the compensation force via the rack. A DC motor (Pololu, 3057) drives the screw with a constant power supply of 12 V.

The processes of spring extension and subsequent compression were repeated five times for each contrasted configuration—with and without the follower in contact with the cam generating the compensating force so that the motor actuated the screw only with its own driving force.

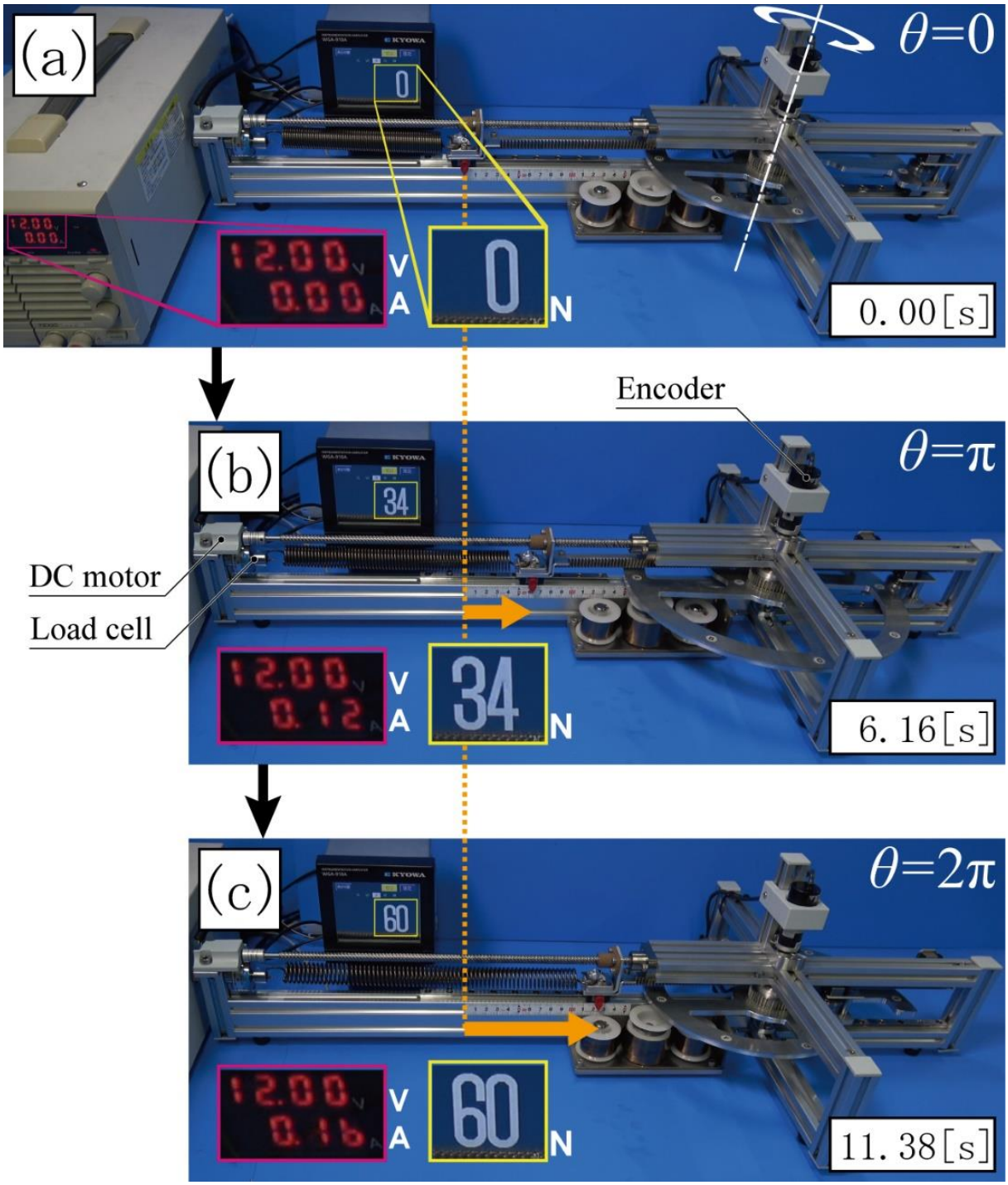

Fig. 37 Operation process and current consumption of the POC model. (a) The initial tension measured by the linear spring was 0 N. (b) The spring tension and cam rotation angle increased with the extension of the feed screw, and (c) the spring force reached its maximum at a displacement of $x = 2\pi R_C$.

Fig. 38 displays the results of the measured power consumption during the processes. When compensation was used, the power consumption reproducibly changed suddenly in the range $x \gtrsim 28/15\pi$ (discussed in Chapter II.7) in addition to fluctuations due to inrush and stall currents around $x = 0$ and $x = 2\pi R_{\mathrm{C}}$. As the displacement x_{S} is now regarded as the farthest point for the stable compensation in this prototype, a comparison of the performance with and without compensation was conducted in a range $0 < x < x_{\mathrm{S}}$ for further analysis.

In the extension processes plotted in Fig. 38, the power consumption is seen to increase monotonously with the displacement of the spring as well as with its elastic force when the nut connected to the spring had to be moved by the motor thrust alone without compensation. By contrast, using compensation, the increase in power consumption became moderate, while the same elastic force was generated. The energy consumed during one cam rotation was reduced by 4.1 J (23.2 %) using compensation, indicating that the operating force is successfully reduced using the proposed mechanism.

In the compression processes without compensation, the power consumption was almost constant (close to the ideal value at no load operation) because the spring tension was exerted in the helping direction of the thrust of the screw. By contrast, the energy consumption increased by 1.8 J (25.4 %) per rotation with compensation because the compensating force suppressed the abovementioned assistance of the spring.

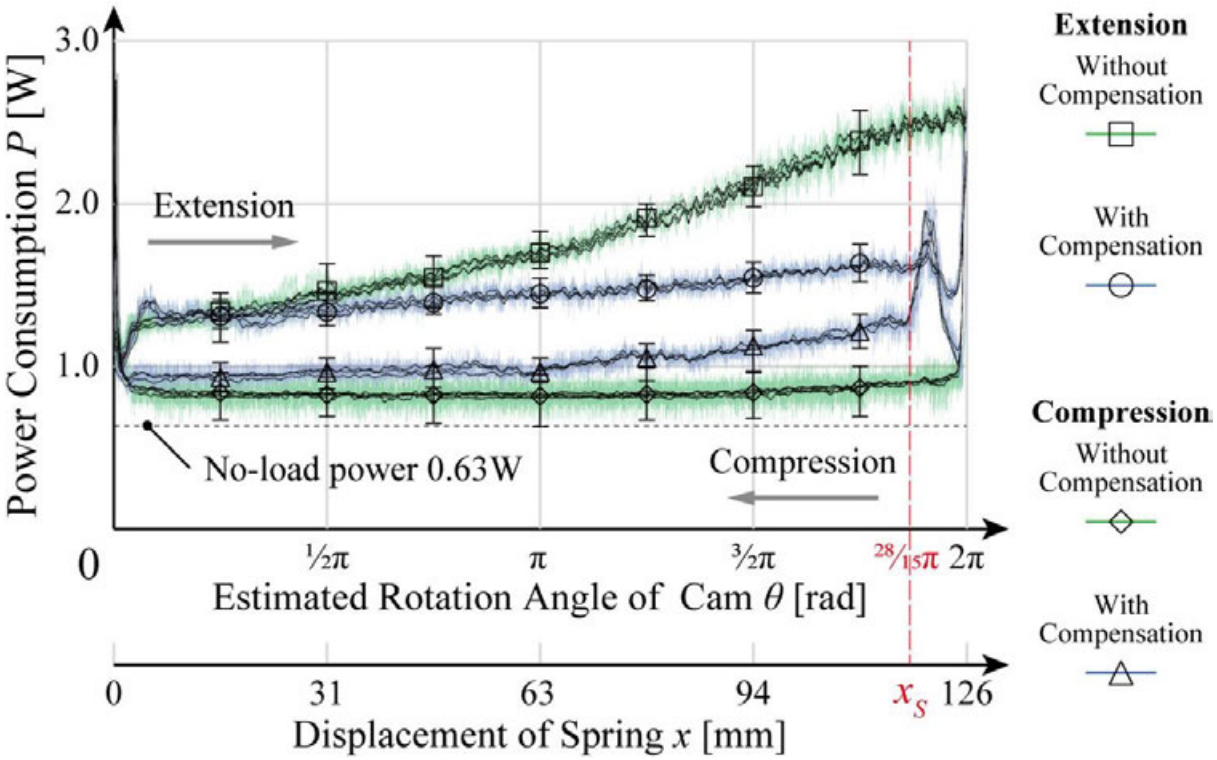

Fig. 38 Transition in power consumption with respect to displacement x of the spring (equals the counts of the encoder multiplied by the gear ratio and the lead of the screw). The estimated cam rotation angle θ was calculated by dividing x by the pinion radius R_C. Solid black lines represent the moving averages of the interval at 36, which is three times the counts per rotation of the motor.

The maximum control force exerted by the lead screw and the entire energy consumption per operation were then calculated in this range and are plotted in Fig. 39. The compensation reduced the total energy consumption by 2.3 J (9.3 %) per operation of extension and then compression in the range $0 < x < x_S$ (Fig. 13 (a)). The operating force at position x_S, where the largest energy is required, was reduced by 46.2 % in the extension process and increased by 132.7 % in the compression process (Fig. 13 (b)). Thus, the difference of the maximum operating forces between extension and compression shrank significantly from 543.0 % to 48.7 % relative to compression force. This uniformity enables the spring to be controlled by an actuator with smaller maximum output and current fluctuations.

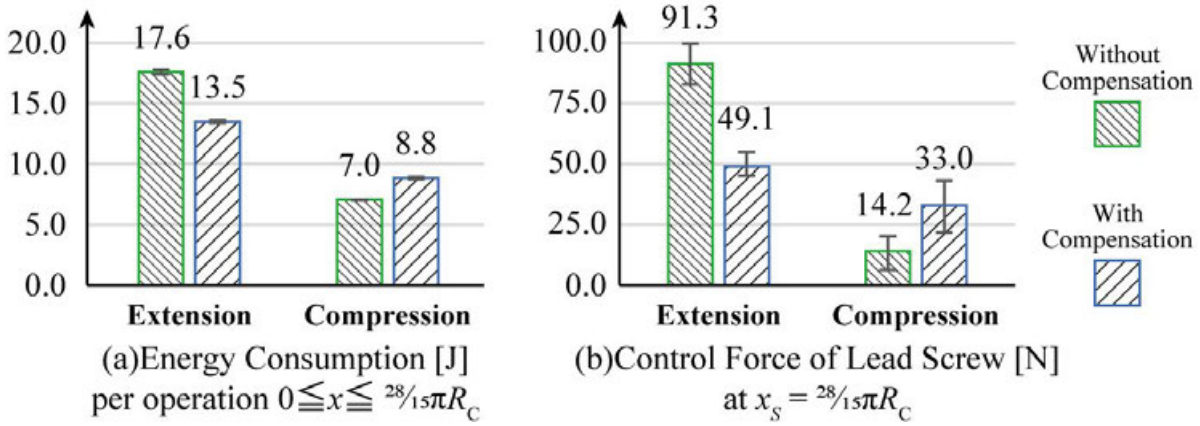

Fig. 39 (a) Energy consumption in the range $0 < x < x_S$. (b) Thrust force of the feed screw at x_S calculated from the motor performance table [38].

Also, as observed in Fig. 40, the actual cam rotation angle θ was monitored by the encoder. The angle was found to deviate by approximately 4– 5° (1.1– 1.4 % of one rotation) from the value assumed as the spring displacement x, regardless of whether compensation was used.

The delay in the rotation angle with respect to the feed amount first emerged at the origin for each outward route of extension and lasted till the end of a rotation. Without compensation, the return route of compression went through practically the same transition. With compensation, however, the rotation angle delayed at the beginning of the return route in the same way as extension and then returned to the origin like a hysteresis loop.

The occurrence of these phenomena depends on the direction of the internal force on the nut to be actuated that remains even after compensation due to its inaccuracy and friction. This force bias made the feed screw to actuate the nut more than expected to fill the gap of the alignment. The gap here is a backlash that occurs in two stages: one between the screw and the nut, and the other between the rack fastened to the nut and the pinion.

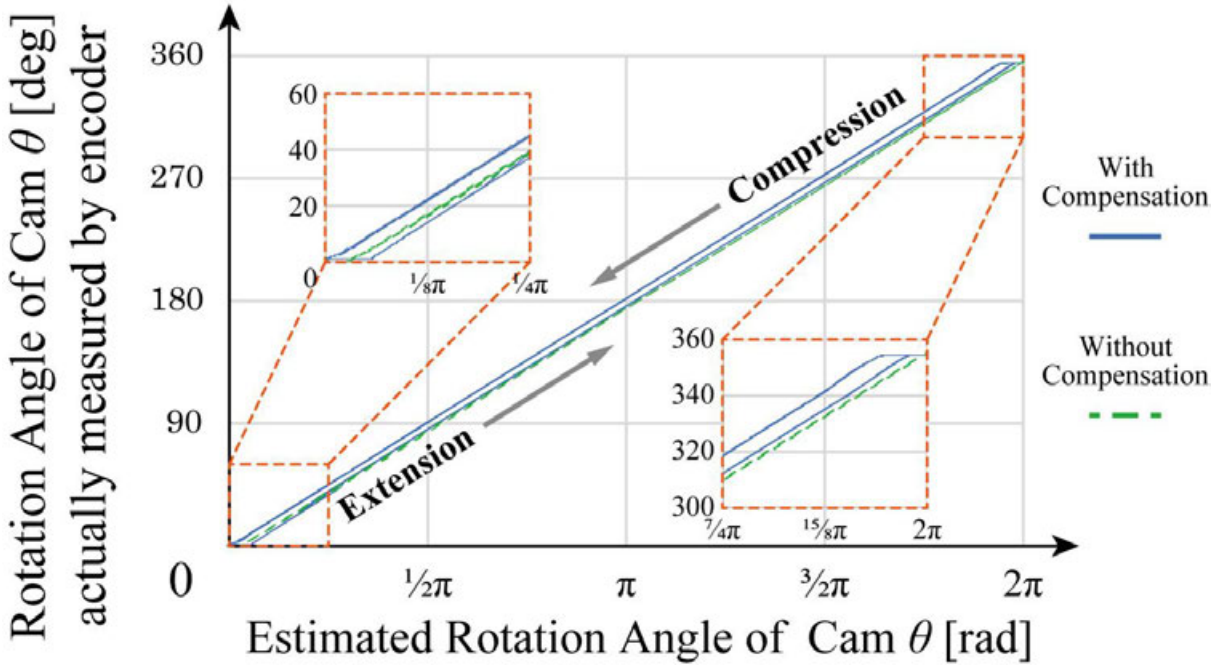

Fig. 40 Difference between the rotation angles of the cam calculated from the displacement and as measured by an encoder.

Furthermore, to investigate whether its constitution has overcome the gravitational effect on operation, the same procedure was repeated for systems in which the POC model was placed vertically. For the conventional self-weight compensation mechanisms and DF converter used in the previous study [32] with a counterweight, tilting to an arbitrary posture was impossible because the wire extending to a weight would drop out of the pulley if the cam plane does not remain horizontal. Since the proposed method abolishes the pulley and the weight, the POC model should be able to operate at any posture.

The image on the left in Fig. 41 shows the POC model installed in two ways: cruciformly (spring extends upward) and inverse-cruciformly (downward). The results of the measured power consumption are shown on the right-hand side.

It is seen that the power consumption slightly increased by 1.4 – 22.7 % in each process compared to Fig. 38 when placed inverse-cruciformly (Fig. 41 (b)). When placed cruciformly, the power consumption increased more significantly by 38.3 – 123.0 %, however, the compression process with compensation decreased by 4.7 % (Fig. 41 (a)).

While the force required to extend the spring was reduced by compensation as intended even when placed vertically, gravity was found to disturb the force equilibrium on the actuated nut by including the weight of components (especially the stainless rack) in the balancing. The position of the center of gravity of the rotating cam also must be centered for minimizing the effect of its gravitational torque as a future task on optimization. Even without these factors, improvements on the guide elements receiving the load from the spring and the pinion connected to the screw nut are obviously required for a higher performance.

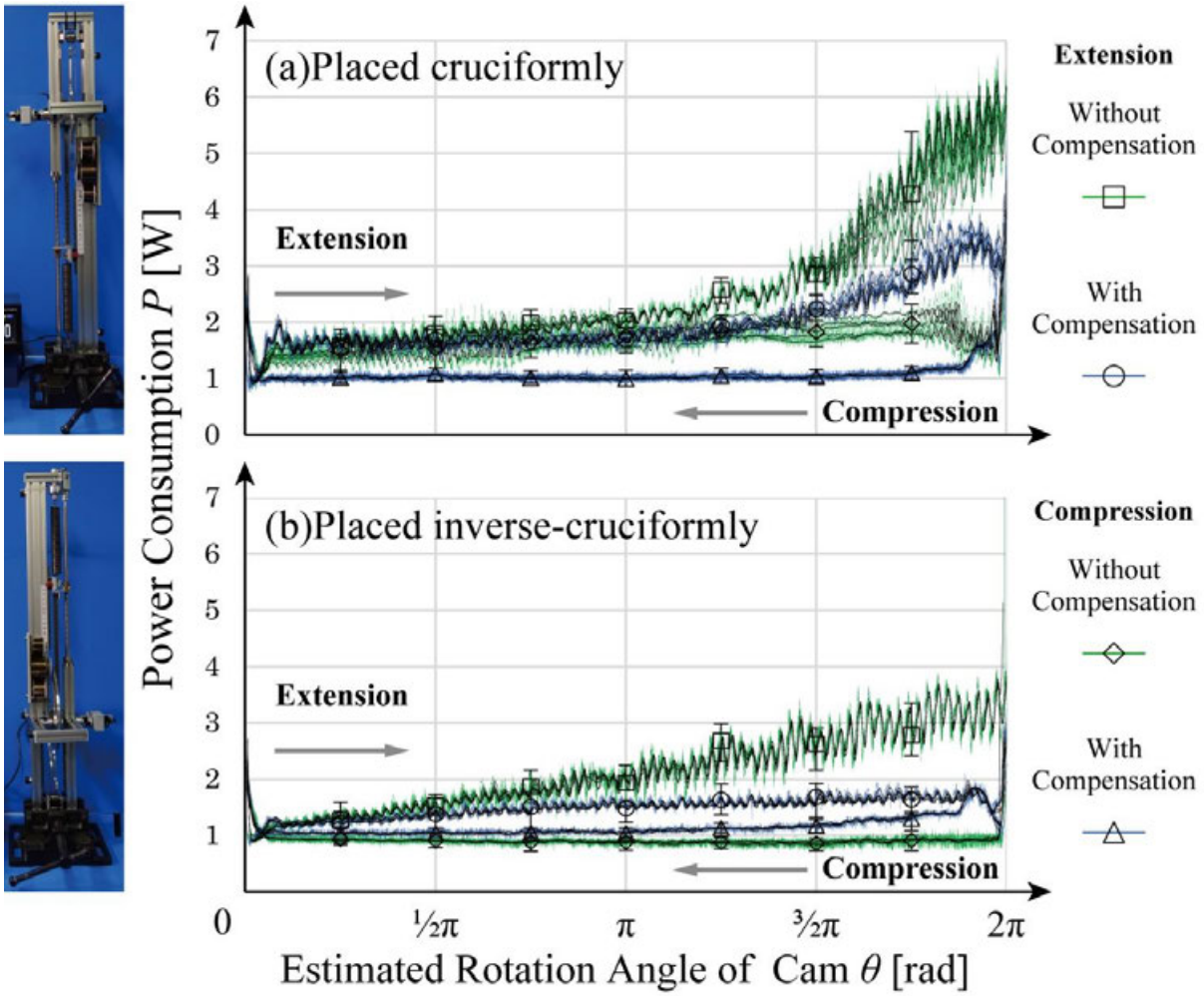

Fig. 41 Transition in power consumption on the system placed vertically.

Section II.6.3 Application experiment of the DF converter using the cam–follower system in the line-jamming mechanism

As an example of application, the developed DF converter was implemented to the line jamming mechanism as its wire tensioner, as illustrated in Fig. 42. The fixed end of the spring that used to be pinned on the mechanism structure was now connected to a wire of the line jamming mechanism, so that the converter can adjust the wire tension by the elastic deformation of the spring arbitrarily. It resulted in the behavior of the finger that could (a)—(b) deform passively in the low-stiffness mode, (c)—(d) maintained its own posture but was unable to hold an extra weight on the tip in the medium-stiffness mode, (e)—(f) and supported the weight in the high-stiffness mode.

The experimental results successfully verified that implementing the POC model of the converter allows line jamming to switch its mode of stiffness steplessly and with a low power consumption due to the compensation effect of the cam follower. By miniaturizing, as discussed in the next chapter, the proposed DF converter has the potential to replace conventional actuators, such as pneumatics that require large external devices for generating tension or pressure.

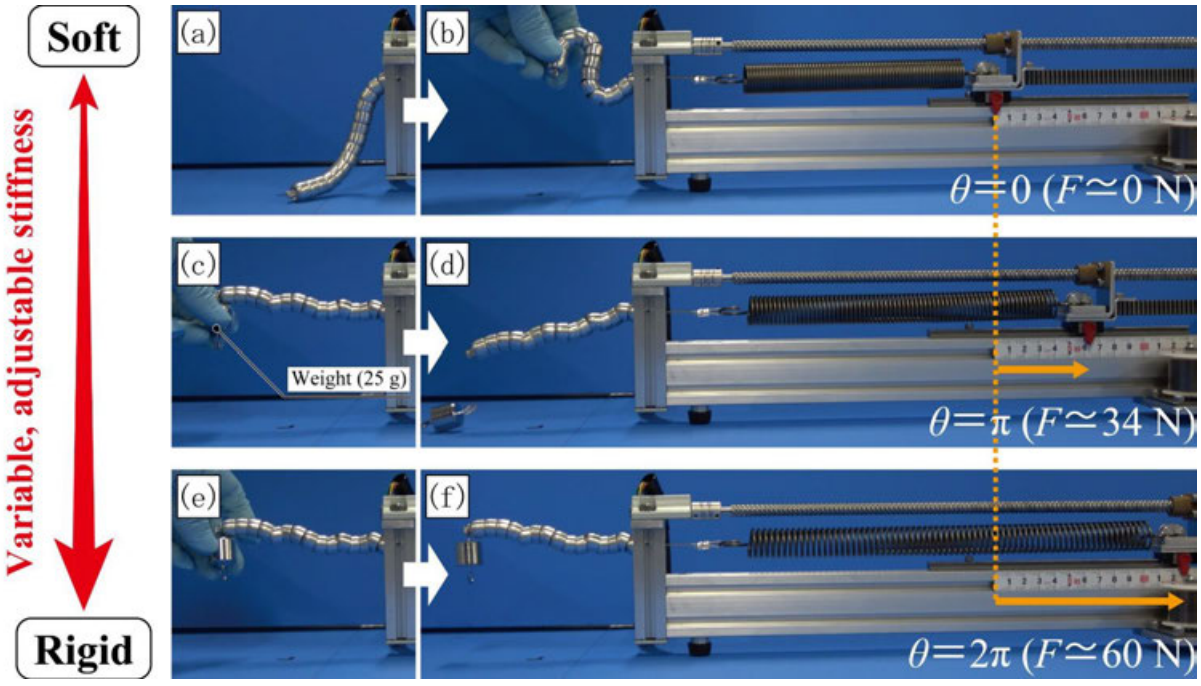

Fig. 42 Line jamming mechanism with ϕ12 beads of aluminum alloy whose wire tension is controlled by the proposed displacement–force converter.

Chapter II.7 Discussion of the characteristics of the DF converter using the cam–follower system

If an ideal compensation could have been achieved, the increase in power consumption from the no-load state would have been minimal and equal for both the compression and extension processes. The possible factors that affected the accuracy of compensation are discussed below, in addition to the gap of the angle originating in the backlash at screw–nut and rack–pinion transmissions.

Section II.7.1 Effect of an excessive increase in the pressure angle

First, the nonuniform and sharp increase in the consumption power in the range $x > x_S$, as observed in Fig. 38, can be attributed to an excessive increase in the pressure angle ϕ. As plotted with the cam characteristics in Fig. 36, the pressure angle at the end of rotation exceeds 30°, which is a standard practical design limit for converting the radius of the cam to the lift amount of the follower [37], [39]. In this study, it was found that pressure angles less than $\phi_{(\theta=x_S/R_C)} \approx 23°$ are desirable when the purpose is to transmit torque to the cam from the follower. Increasing the initial radius r_0 is effective in replacing the increase required in ϕ to satisfy this condition.

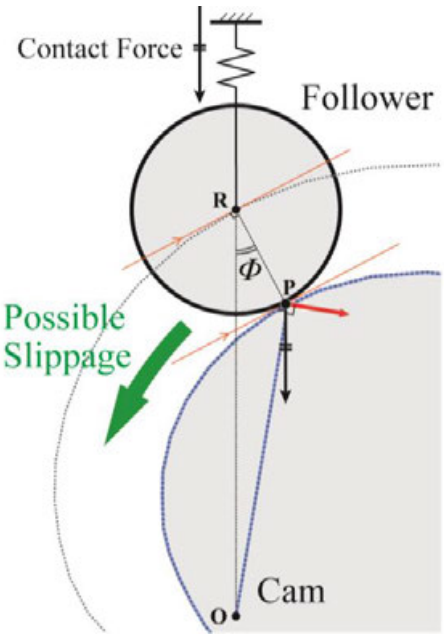

Fig. 43 Slippage of the cam–follower system at a large pressure angle ϕ.

Section II.7.2 Efficiency of the torque transmission between the rack and pinion

Second, the loss in efficiency of the torque transmission between the rack and pinion was underestimated. While the force component generated by the pressure angle between the cam and follower was used for compensation, the generated compensating torque was not properly applied to the coupling point of the spring and rack. This is possibly because the force transmitted between the rack and pinion is split into component forces due to the existence of a pressure angle of 20° at the teeth. Furthermore, the component force perpendicular to the linear motion of the spring was assumed to be ineffective but is possibly disadvantageous because it can increase the frictional resistance on the slider guide, thereby amplifying the resistive effect of the assembly error on the movement. An improvement can be achieved by substituting F_C in (14) with eF_C, where e represents an efficiency factor.

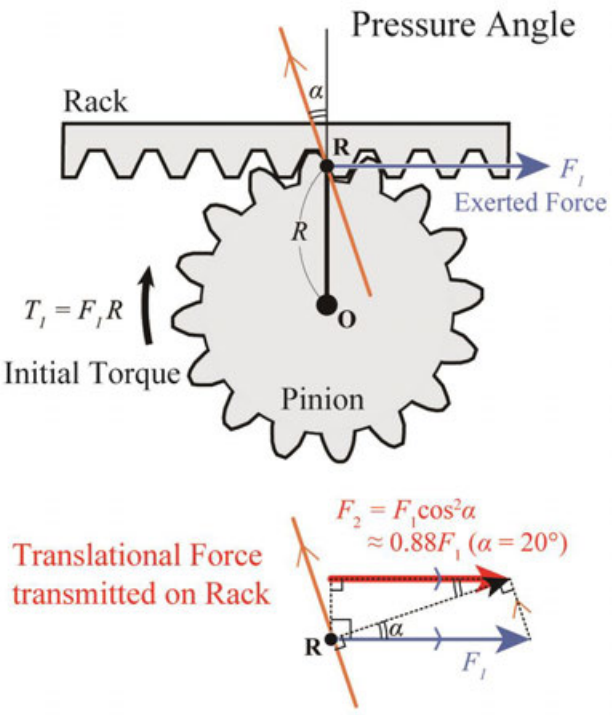

Fig. 44 Loss of force transmission efficiency between the rack and pinion.

Section II.7.3 Constancy of the constant spring

Third, in the numerical analysis of the cam profile, the force of the constant spring F_C was strictly defined to be constant and that of the linear spring F_1 proportional to the displacement without an intercept. However, as shown in Fig. 46, the characteristic of the constant spring fluctuates (a) and that of the linear spring results in a smaller displacement until the external force exceeds the initial internal tension of its elasticity (b). The latter results in the steep initial rise of force lasting till the end as an average excess of 11.3 N from the supposed value to be compensated, corresponding to the initial rise of the power consumption in the extension process and the final fall in the compression process, as observed in Fig. 38. Therefore, for a higher accuracy, F_1 and F_2 should be corrected to functions of θ following their actual nonlinear, possibly hysteretic properties. This generalization also allows configurations other than the pair of springs in the POC model, thus, increasing the flexibility of design. The follower may be pressed to the cam by a linear spring, for example, so that the contact force increases according to the rotation and replaces the increase in the pressure angle, thus, miniaturizing the cam.

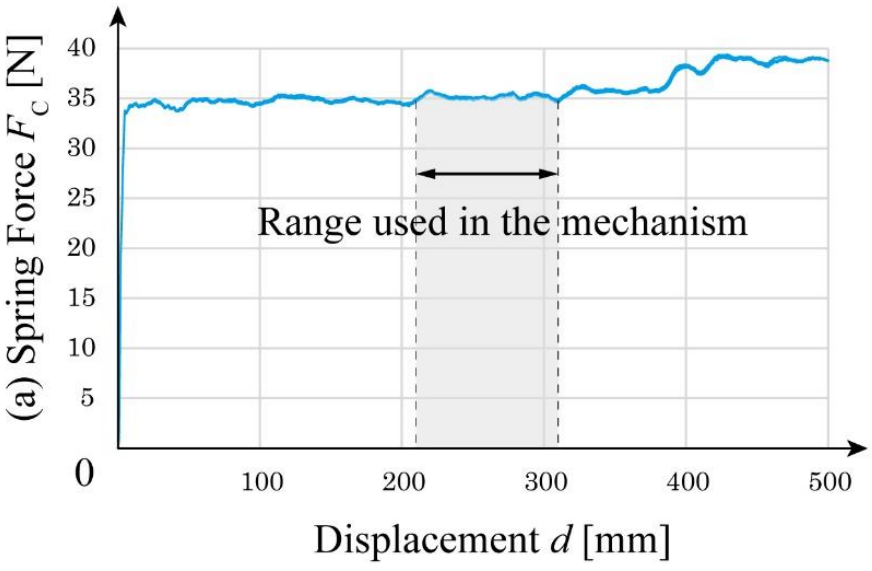

Fig. 45 Force of constant load spring measured by a material testing machine (Instron, 3343). F_C was defined by the average of the highlighted section, whose range corresponds to the displacement of the follower.

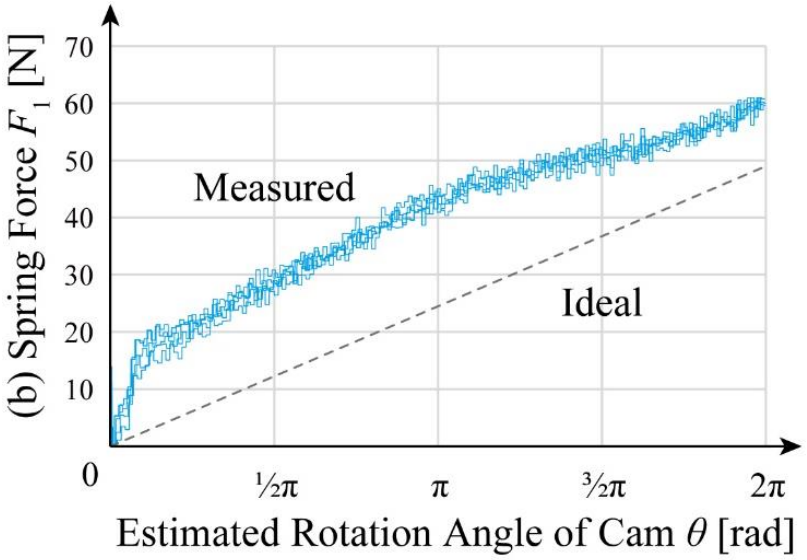

Fig. 46 Force of the linear spring measured in Experiment 1 by the load cell.

Chapter II.8 Conclusion of Part II

In this part, the preliminary prototype model of a DF converter using a pulley–wire system was introduced and its difficulties on maintaining the deviation angle were analyzed. To overcome the difficulties, an entirely new iterative numerical calculation theory was developed for a cam–follower system; it can generate a compensation torque with a contact force split by the pressure angle between the cam and the follower.

The prototype POC model demonstrated that the devised DF converter successfully decreased both the energy consumption and control force required to extend the spring. Thereby, uniformization of force such that the difference of the maximum control force between extension and compression allows the selection of an actuator with a smaller output. This also indicated that the proposed cam–follower system is valid for generating a compensation torque with a simplified calculation process of the cam radius, replacing the conventional pulley–wire system with a design method that uses a complicated numerical analysis, contributing not only to the development of the DF converter but also to the improvement of existing compensation mechanisms.

Moreover, this was incorporated into the variable stiffness mechanism of a fire-resistant soft robotic gripper, as its stepless wire tensioner, to regulate the rigidity of its finger continuously, implying the applicability of the DF converter in replacing conventional massive and powerful actuators such as pneumatics and hydraulics. This resulted in a performance enhancement of robots equipped with them.

For further development, an efficient structure for achieving a higher compensation performance by directly driving the cam and making the compensating force adjustable, i.e. using a variable pivot [35], can be designed. In addition to replacing fluid-driven actuators for the variable stiffness mechanism, the application will be expanded to the study of robotic components, such as a load-sensitive joint structures with a passive compliance.

Part III

Development of the DF converter with a reverse spring comprising permanent magnets, and its application to a parallel robotic gripper

Part III Development of the DF converter with a reverse spring comprising permanent magnets, and its application to a parallel robotic gripper

Chapter III.1 Abstract of Part III

In this part, another new compensation method for the DF converter is introduced. This method uses a permanent magnet as a reverse spring. In a parallel robotic gripper using the IB magnet as a DF converter, the attraction movement of the magnet generates an assistive pressing force that increases the clamping force. Reflecting the research process, this part is composed of three major chapters.

In Chapter III.3, to improve the design procedure and the trade-off relationship between compensation precision and the mechanism volume of the IB magnet, a magnetic spring was invented, and its reduction rate of 13.0 % was found to be comparable to those of conventional IB magnets. Subsequently, it was modified to a one-sided IBM gripper with a fixed clamping width. The experiment revealed that applying magnetic attraction spontaneously amplified the direct the input into an output equal to the control force of the magnet by 2.0.

In Chapter III.4, a new conical spring was developed to manage both compactness and followability to the nonlinear characteristic of the magnet suited to a bi-parting constitution for a higher dexterity. The prototype of the gripper successfully amplified its clamping force continuously from zero to at most 292.2 % by the magnetic assistance, while suppressing the increase in power consumption of a DC motor to 11.8 % through compensation, resulting in the multiplication of the force–energy efficiency by 2.6.

In Chapter III.5, a new stepless width-adjustment mechanism using a lever toggle was featured to achieve a more steady and predictable clamping force independent of the target object width. The developed gripper recorded a force–energy efficiency ratio multiplied by 1.39 in average. Furthermore, it realized the linearization of the width–force characteristic with an inclination of 0.15 N/mm, which was an insignificant influence of 0.3 % on the major output that was approximately 50 N.

Chapter III.2 Application of the DF converter #2: spontaneous force amplifier for a parallel robotic gripper

Section III.2.1 Abstract of Chapter III.2

This chapter proposes the principle of a parallel robotic gripper as an application mechanism that lets the DF converter exert a clamping force on an external object. To compensate the force to grasp an object, a clamping mechanism that can spontaneously and steplessly generate an attractive force to assist clamping movement using a pair of permanent magnets was invented. Comparisons are made among the proposed gripper and other existing grippers that have passive force amplification mechanisms.

For realization, various methods used to detach a permanent magnet using a control force much smaller than its original attractive force were explored, and the internally-balanced magnetic unit (IB magnet) was found to be the best for this application. This mechanism has been applied to magnetic attraction devices such as wall-climbing robots, ceiling-dangling drones, and modular swarm robots. Its fundamental principle, design procedure, and optimization process are analyzed.

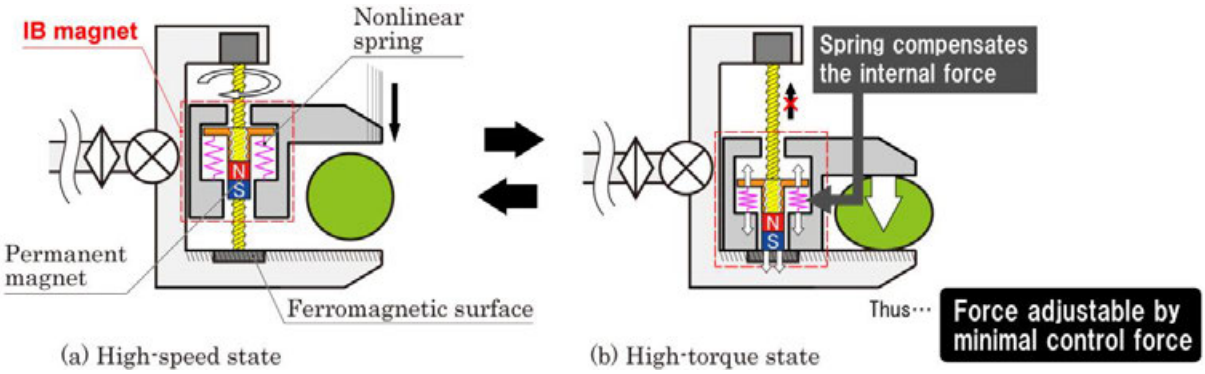

Fig. 47 Principle diagram of the proposed gripper with a force amplification mechanism using the IB magnet (IBM gripper).

Section III.2.2 Research background: Realization of an energy-efficient clamping operation of a robotic gripper through force amplification

A parallel robotic gripper can be raised as another representative example of a mechanism that can derive a benefit from the implementation of the proposed DF converter. Robotic grippers with less power consumption are effective for reducing the cumulative electricity cost of a factory line, as they are repetitively used for long periods. They also help to extend the operation time of robots and mileage of mobilities with a limited power supply, such as battery and solar cells.

Considering the reduction of the response time, operation duration, and power consumption, one of the desirable features of robotic grippers (i.e., actuator-driven clamps or vises) is the ability to switch its actuation states, between a high-speed state, until the finger touches the object to complete the clamping and a high-torque state after the finger touches the object to firmly sustain the clamping position [1], as illustrated in Fig. 48.

To avoid increasing the mechanism volume and mass, this state transition should be achieved by the main actuator that drives the finger without adding another degree of freedom. Most conventionally, sensors have been used to provide information regarding the existence of the object to be clamped between the fingers and by regulating the current for the actuator. However, such software approaches require a certain load on the calculation processing for control and are especially disadvantageous in situations where signal transmissions of sensors and control may be interfered with, such as by radioactive rays.

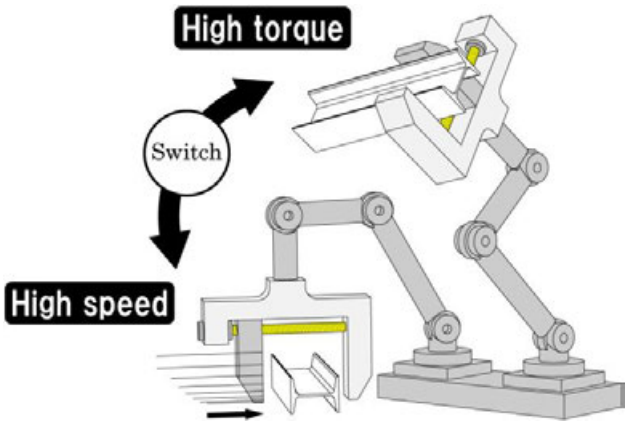

Fig. 48 A conceptual diagram of a robotic gripper that switches its operational state.

Section III.2.3 Previous research: spontaneous force amplification by load-sensitive mechanisms

To reduce the complexity of the control, grippers with assistive mechanisms that activate reduction spontaneously (independent of the electric control of the actuator) have been proposed. They can be driven passively by a small low-power actuator of the gripper, ideally without increasing the actuation load at any displacement. Then, they begin force amplification when they mechanically detect that the gripper has touched or reached the target object to be clamped. Most of them are categorized as load-sensitive mechanisms, as they decide the timing for changing the state by sensing the increase in the load, not by displacement. This section enumerates the representative examples of the compensation mechanisms.

Subsection III.2.3.1 Toggle mechanism using a lever

The mechanism [2] shown in Fig. 49 employs two pairs of feed screws and nuts along a single shaft. (1) The motor first actuates the active finger ("output jaw") via gear 1–gear 2 transmission, as the latter is fastened on Feed-screw 2. Feed-screw 1, with a larger pitch, enables a quick motion of the finger. (2) After the finger touches the target object, the load on the finger (that equals the clamping force) increases and stops the rotation of the shaft. (3) By further driving Gear 1, Gear 2 becomes loosened and begins to move along Screw 2. (4) The freed Gear 2 shifts the toggle lever to push in the entire shaft system to the direction of the fixed finger, which generates a large clamping force.

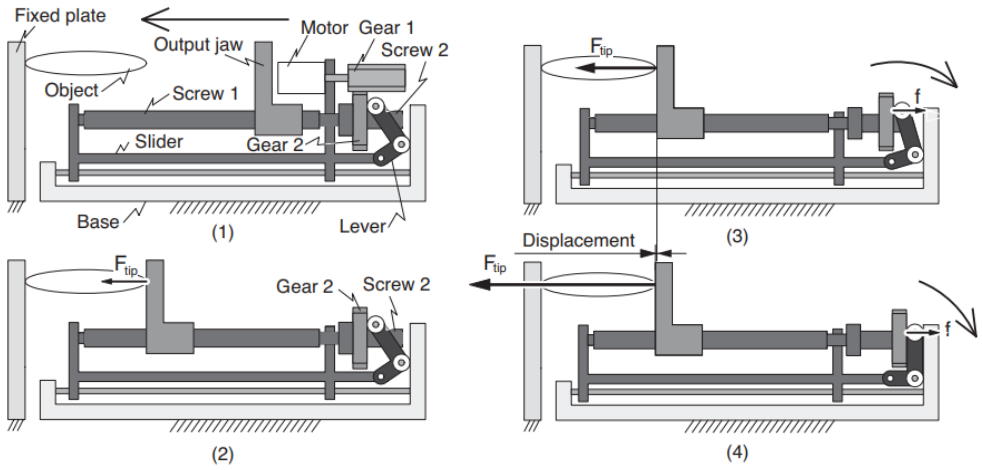

Fig. 49 Force amplification mechanism using a toggle lever [2].

Subsection III.2.3.2 Worm drive used as a rack and pinion

The mechanism shown in Fig. 50 switches the usage of a worm drive according to the actuation state [1]. (a) In a high-speed state, the input worm screw and output worm gear pair is regarded as a rack and pinion pair. The translational extension of the screw pushes out the tread of the gear, resulting in its faster rotation than its original reduction rate. (b) When the output load exceeds the designed threshold, the connection between the actuator and screw gets separated, and the mechanism turns into a high-torque state; the rotation of the screw drives the gear with the initial large reduction rate.

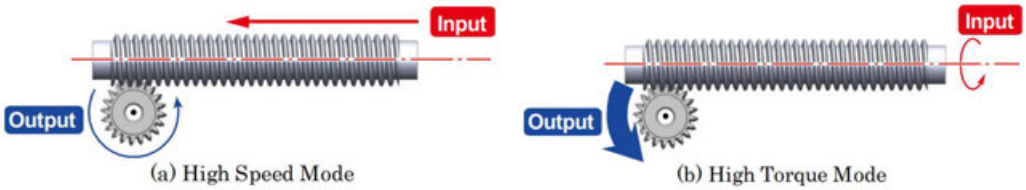

Fig. 50 Force amplification mechanism using a worm drive [1].

Subsection III.2.3.3 Toggle using a lever and worm drive

The gripper [40] in Fig. 51 can be regarded as a combination of those in Subsection III.2.3.1 and Subsection III.2.3.2. This gripper has two actuators, one for the worm drive connected to the finger and the other for the "three-dimensional toggle," and for assembling tension rods that are initially twisted. (a) In a high-speed state, the worm drive actuates the finger normally. (b) Once the load exerted on the target object is detected, the toggle stretches and forcibly pushes the worm screw in its axial direction as a rack, resulting in a further rotation of the worm gear as a pinion.

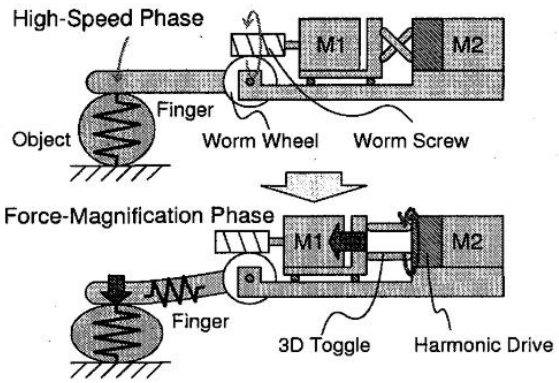

Fig. 51 Force amplification mechanism using a toggle lever and worm drive [40].

Subsection III.2.3.4 Toggle using a linkage

The transformable linkage [41] in Fig. 52 has a folding link with a torsion spring inserted. (a, b) In the high-speed state, the load is small enough, such that this folding link is extended to its maximum length, resulting in a fast actuation of the finger by a four-bar linkage. (c, d) In the high-torque state, when the finger touches the target object, the counter torque of the load exerts the resistive force of the torsion spring and shortens the folding link, resulting in a rigid fixation to a three-bar linkage. The mechanism is applied not only to grippers but also to a knee joint of a leg mechanism such that it can switch between the swing and stance phases smoothly [42].

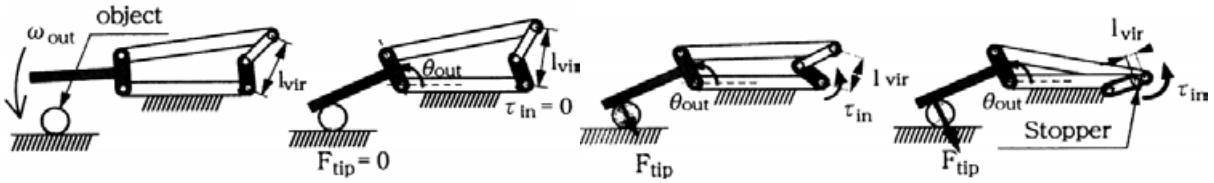

Fig. 52 Force amplification mechanism using a linkage [41].

Subsection III.2.3.5 Screw using oblique and decentered feed

The oblique screw [43], [44], as illustrated in Fig. 53, is combined with a nut that has a larger inner diameter than that of the screw such that the nut becomes oblique and decentered to the rotation axis. (1) In the high-speed state, the nut has a small effective diameter resulting in an actuation with a small reduction rate. (2) In the high-torque state, the load causes the nut and screw to align coaxially such that they engage at the original reduction rate.

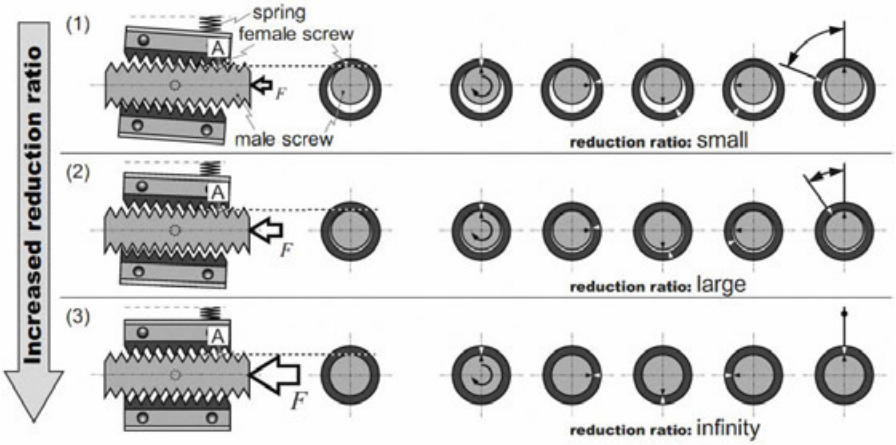

Fig. 53 Force amplification mechanism using an oblique screw [43].

Section III.2.4 Disadvantages of the previous spontaneous force amplification: binarity of the state switching

As generalized in Fig. 54, the load-sensitive mechanisms for passive force amplification listed in Section III.2.3 typically use mechanical joints, such as toggles and clutches, to restrict a further movement of the actuated position by placing them to the dead center when the finger touches the object. In other words, the detection of the load or displacement triggers a switch in the reduction state by increasing the internal rigidity of the mechanism to infinity in the direction of movement.

These mechanisms do not require an additional operation energy to sustain the clamping position and force. However, they cannot adjust the clamping force because they tend to allow only a binary state of clamping (either zero or maximum force), even if another actuator is added (which is against the development policy of force amplification and state switching by a single actuator) to adjust the clamping width or a sensor is used to detect the load. This is problematic when the robotic system must handle heavy or fragile objects: a lack in force leads to dropping the object, and an excessive force leads to crushing or damage.

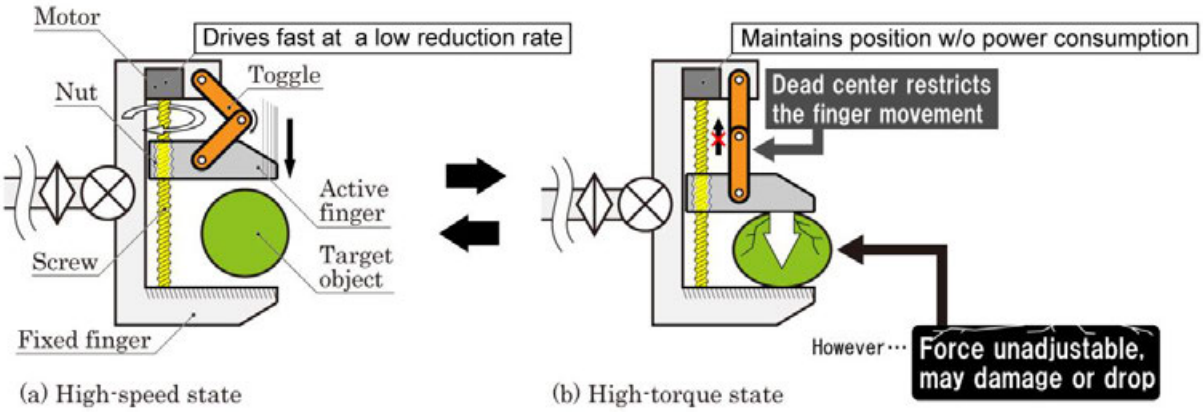

Fig. 54 Generalized principle diagram of a conventional gripper with a force amplification mechanism.

Section III.2.5 Proposed principle: Spontaneous force amplification using magnetic attraction, and its application to a robotic gripper

To solve these problems, a robotic gripper with a force amplification mechanism is proposed. This uses a permanent magnet embedded in the active finger to enhance the clamping action through an attraction to the ferromagnetic body embedded in the fixed finger, as shown in Fig. 55. Unlike binary toggles and levers, a magnet gradually and spontaneously increases its attractive force in proximity to the ferromagnetic surface, allowing the output clamping force to be adjusted continuously and arbitrarily by shifting the implemented magnet in and out. As the magnetic attractive force follows a nonlinear but pre-measurable function of the distance between the magnet and target surface, the encoder of the actuator ideally becomes the only sensor required to control the output clamping force.

To enable the control force to withstand the strong attractive force of the magnet when close to the ferromagnetic surface, the gripper requires an actuator with a minimal backlash and a large stiffness, such that it can control its own displacement precisely, or a mechanism that allows the actuator to easily detach the magnet against its permanently exerted load.

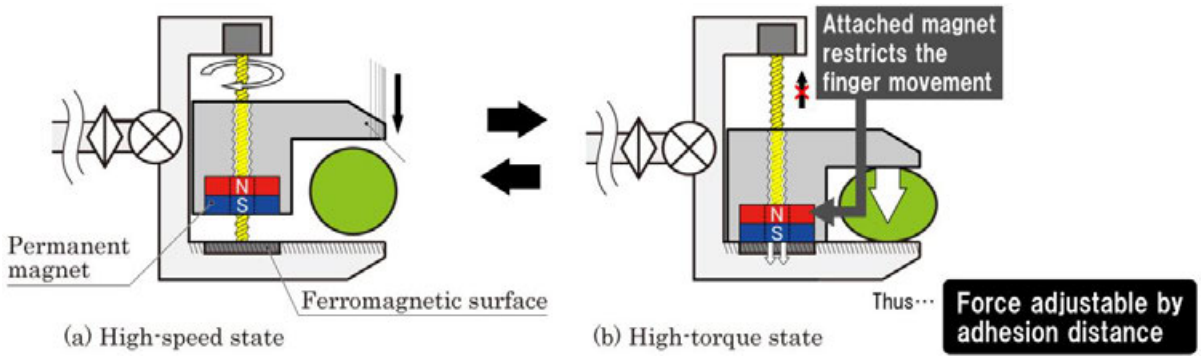

Fig. 55 Principle diagram of the proposed gripper with a force amplification mechanism using a permanent magnet.

Section III.2.6 Previous research: detaching mechanisms of a permanent magnet

In this section, the representative examples of the mechanisms that allow a permanent magnet to be detached with a force that is much smaller than its original attractive force are enumerated.

Magnetic attraction is one of the most widely used attraction methods alongside vacuum adsorption, static cling, and van der Waals adhesion [45]. It has been applied to various machines, such as robots that run on walls and ceilings for cleaning and inspections [46]–[53], grippers and chucks that clamp ferromagnetic objects [54], [55], jamming soft grippers and powder brakes that change their internal stiffness by applying magnetic flux on a magnetorheological fluid [56], and machines that sort equipment to screen ferromagnetic contamination [57], [58]. Compared to other attraction methods, the magnetic force acts at a certain distance; thus, it can generate a large force even if the contact is partial or incomplete. Therefore, it is suitable for use in the proposed gripper. Because a magnet cannot choose non-ferromagnetic objects as its attraction target, the application of magnets has been limited to mechanisms that enable a direct attraction to artificial objects and environments that contain iron, as listed above. By employing a mechanism that involves the attraction target, the proposed gripper removes this restriction.

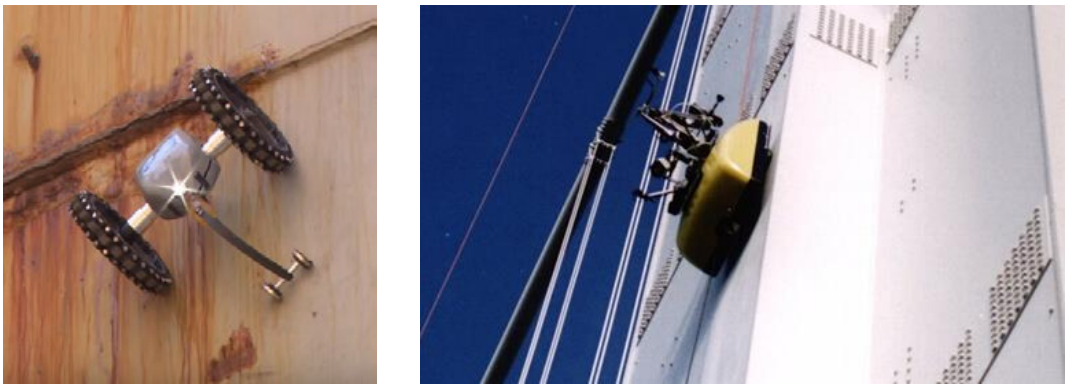

Fig. 56 Inspection robots for body of vessels using magnetic wheels [52], [53].

There are two types of major magnetic attraction devices: permanent magnet and electromagnet, as illustrated in Fig. 57. The former is better when considering the battery capacity of the machine, as it retains its magnetization without external energy and thus heat generation unlike the latter. This characteristic also works as a failsafe system for a sudden cut from the power source.

The permanent magnet has two problems: its magnetic flux per volume and mass tends to be smaller than that of the electromagnet; it continuously requires a large external force to be detached and then pulled away from the target object, as it permanently exerts a magnetic force once it gets magnetized. If a bare magnet is directly attached to an actuator, the attractive load becomes large such that controlling the displacement precisely becomes difficult for a weak actuator. Moreover, selecting a strong actuator is against the objective of this study. Therefore, to solve the second problem for implementing the permanent magnet in the proposed gripper, this section lists and compares existing conventional methods for switching the attraction state of the magnet with a small external control force.

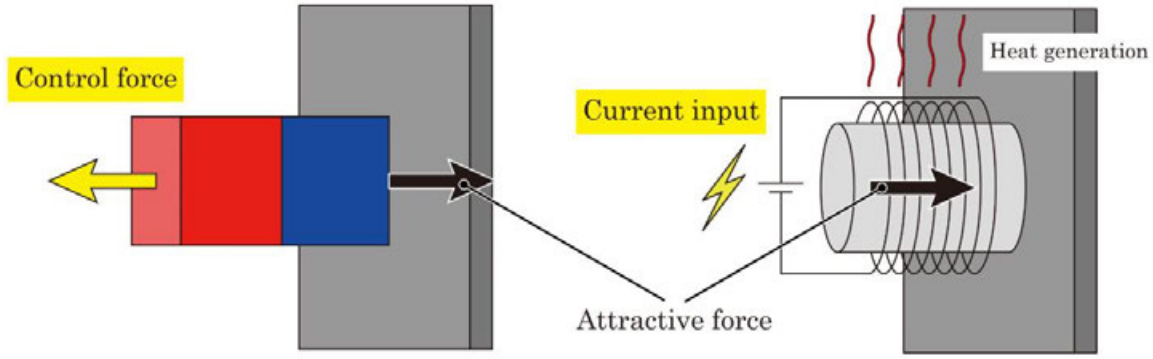

Fig. 57 Magnetic attraction methods.

Subsection III.2.6.1 Detaching using the law of the lever

The simplest method is to use of the law of the lever. As mentioned in Chapter I.1, levers and wedges with mechanical advantages of more than one can convert the detachment process of the magnet consisting of the product of a large control force and short control distance to the work, consisting of the product of a small force and long distance. Simple objects such as screws [59] and cam [60] are widely used in magnetic devices of hand-power tools but tend to require long strokes and thus long switching time to decrease the magnetic attractive force enough for detachment.

Fig. 58 A pair of window-cleaning robots with a magnetic distance adjustable by a screw [61].

Subsection III.2.6.2 Electropermanent magnet

The combination of a permanent magnet used for attraction and an electromagnet for cancelling out the magnetic flux of the permanent magnet is called an electropermanent magnet. As it requires electric current only when disabling magnetic attraction, the electropermanent magnet is suited for long-time continuous attraction. There are various mechanisms using electropermanent magnets such as a ceil-tangling anchor for drones [62], expandable actuator for position control [63], magnetorheological fluid jamming gripper [56], slip moving mechanism using vibration [64], magnetically floating table [65], and an electromagnetic brake with a fail-safe ability [66].

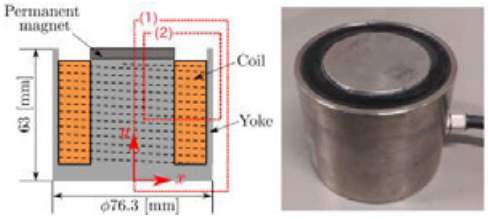

Fig. 59 Magnetic flux supplier of the MR fluid jamming gripper [56].

Subsection III.2.6.3 Yoke switching

There is a method of switching the flow of the magnetic flux of the permanent magnet by changing its relative position to the yoke such that the flux, which usually flows into the target object, gets disconnected (or circumvents the object), resulting in the loss of the attractive force. Here, a yoke is piece of soft magnetic material with a higher magnetic permeability than surrounding objects. Originally, the yoke is used to form a magnetic circuit, in which the magnetic flux of the magnet flows into the target object without leakage.

As shown in Fig. 60, there is a magnetic wheel with this yoke-switching mechanism, which switches (a) a fully attractive state with a flux flowing into the yoke for a complete stop on the wall and (b) a partially attractive state with a flux flowing into the roller for moving on the wall by rotating the magnet to change the orientation of the poles [67]. Moreover, magnetic chucks for fixing ferromagnetic processes [68], [69] and magnetorheological fluid-jamming grippers [70] using this method also exist.

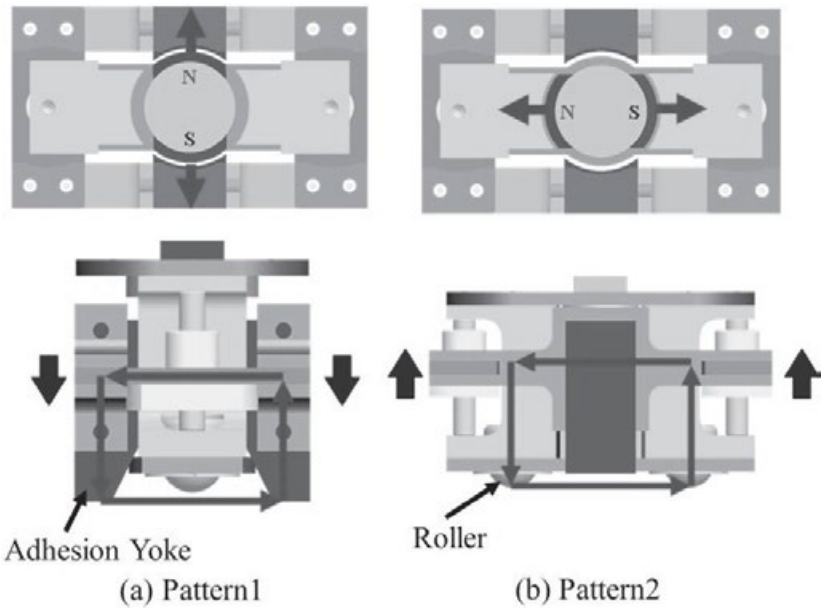

Fig. 60 Magnetic circuit switching mechanism of a wall climbing robot [67].

Subsection III.2.6.4 Active shunting

Similar to yoke switching, the method illustrated in Fig. 61, called active shunting [71], combines a pair of magnets in the direction (a) in which their like poles align to externally exert magnetic flux as a single large magnet, and by rotating one side, in the direction (b) in which their unlike poles align to close the flux inside them. The magnetic chucks, clamps, wheels, and grippers that apply this mechanism have been developed.

Likewise, there is an electropermanent magnet that combines a permanent magnet and a weakly magnetized permanent magnet aligned in the direction in which their like poles align. By applying momentary electric current and thus magnetic flux to the latter, the magnetization rotates, resulting in the internally closed magnetic circuit [72].

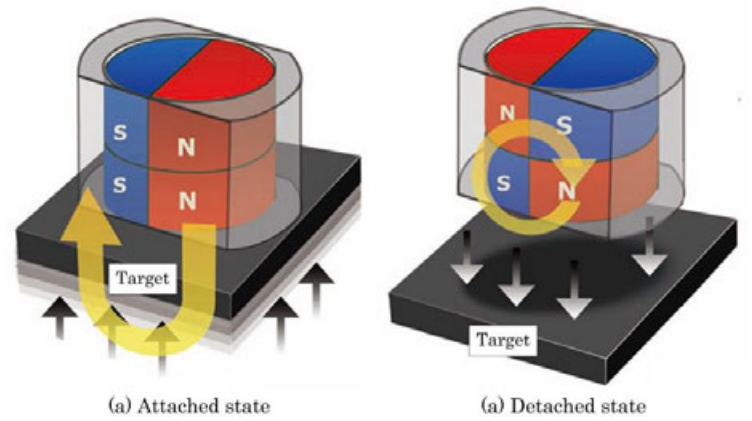

Fig. 61 Principle diagram of active shunting [73] (translated in English).

In these ways, various methods for detaching a magnet have been developed. They momentarily require a large current consumption for electromagnets or large external force for actuators to switch from the attraction state to detaching state, resisting the existing magnetic attractive force. Relieving this loss of energy would lead to a further power saving, downsizing, and lightening of the actuator and power source such that the cumulative electricity cost of numbers of robotic arms in a factory production line that is working continuously can be reduced, and the operation time of mobile robots operated in outdoors and disaster fields without enough power supply can be extended. Therefore, developing a mechanism that allows magnets to be detached at a minimal external force plays an important role in improving the usability of any magnetic devices for machines.

Section III.2.7 Selected detaching mechanism: Internally-balanced magnetic unit (IB magnet)

Subsection III.2.7.1 Principle of the IB magnet and the IBM gripper

Comparing the mechanisms of detaching a permanent magnet as listed in TABLE II, the internally-balanced magnetic unit (IB magnet) [27] shown in Fig. 63 was regarded as the most suitable object to use for the proposed gripper, with a magnetic force amplification mechanism "IBM gripper" in a way illustrated in Fig. 64.

TABLE II
MECHANICAL COMPONENT VALUES USED FOR CAM PROFILE CALCULATION

	Actuation	Control force	Control distance	Characteristic
Permanent magnet	translation	Large	-	Requires large control force
Permanent magnet with lever or wedge	rotation	Small	Longer	Requires large control distance
Permanent magnet with switchable yoke or active shunting	rotation	Large	90° or 180°	Extra iron or magnet components increase mass
IB magnet	translation	Small	As is	Become multi-component
Electromagnet	electrification	None	-	Requires a large electricity for continuous magnetization
Electropermanent magnet	electrification	None	-	Requires a large electricity for continuous demagnetization

The IB magnet is composed of a permanent magnet used for attraction held by the control rod and a nonlinear spring for internal balancing, which is held by a control rod and the mechanism frame. The spring is designed such that it has a displacement–force repulsion characteristic $F_{\mathrm{r}(x)}$ identical, but opposite in sign, to the displacement–force attraction characteristic of the magnet, as expressed in Eq. (21). Consequently, the sum of these displacement–force characteristics, which is the internal force exerted on the control rod, calculated as (22), is zero. Because the control rod is at the equilibrium point of force at any displacement x from the target object, ideally zero control force is required for shifting the control rod to attach and detach the magnet. Meanwhile, the entire system is still attracted to the target object by the counterforce exerted on the frame by the spring.

$$F_{\mathrm{r}(x)} = -F_{\mathrm{m}(x)} \tag{21}$$

$$F_{\mathrm{inter}(x)} = F_{\mathrm{m}(x)} + F_{\mathrm{r}(x)} = 0 \tag{22}$$

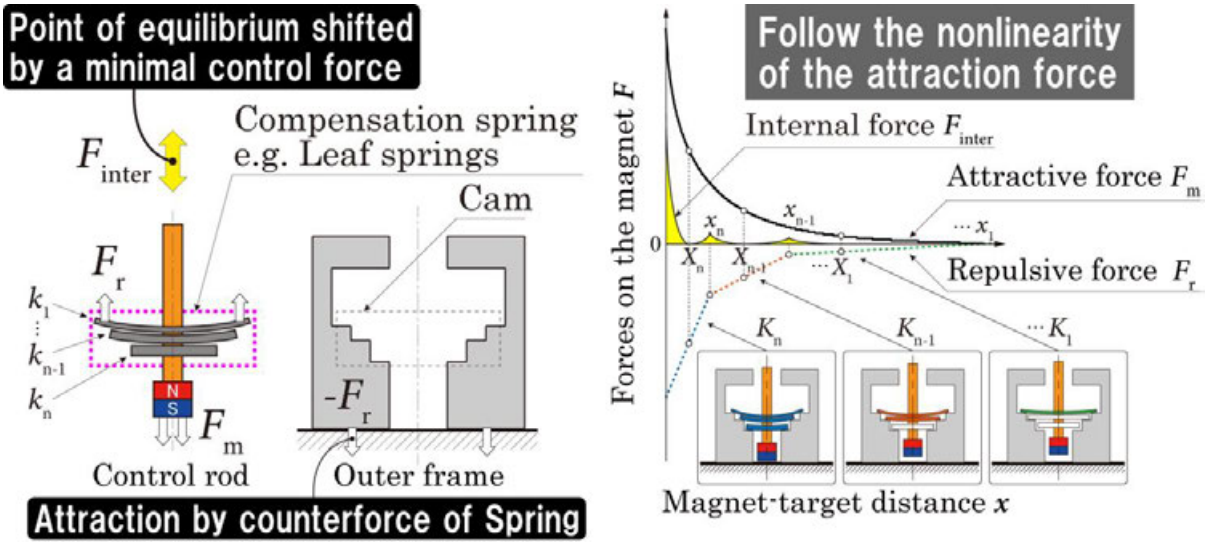

Fig. 62 Conceptual diagram of the IB magnet (repost of Fig. 11).

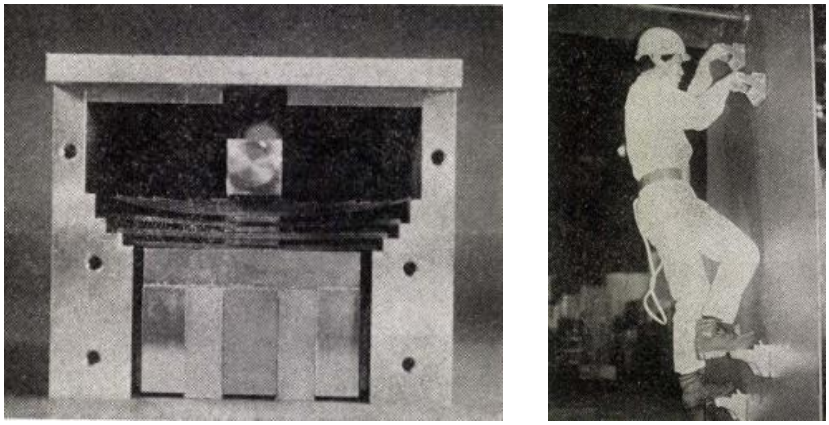

Fig. 63 Appearance of the original IB magnet and walking experiment on a wall [27].

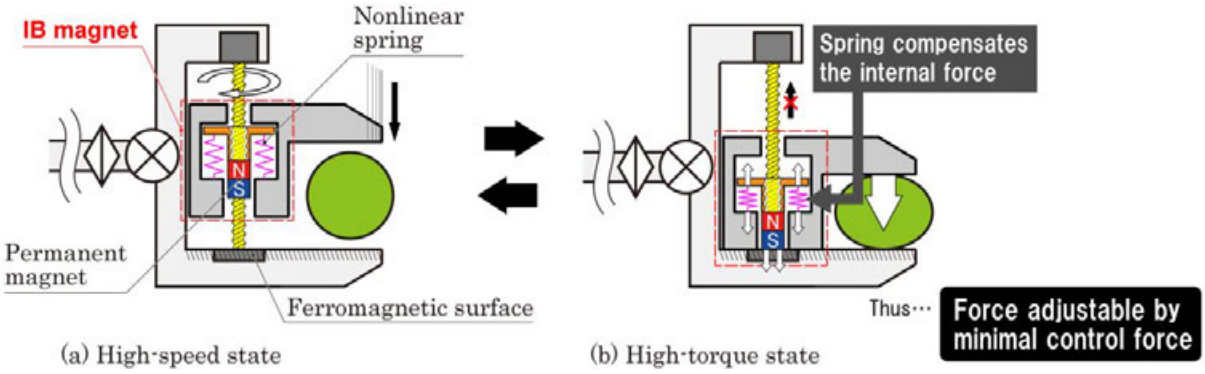

Fig. 64 Principle diagram of the proposed gripper with a force amplification mechanism using the IB magnet (Repost of Fig. 47).

Subsection III.2.7.2 Design methodology of the conventional IB magnet

As illustrated in Fig. 62, the conventional nonlinear spring for IB magnets is composed of multiple linear springs (leaf springs, for example). Its state transition is controlled by the displacement x of the control rod. To trace the displacement–force characteristics of the magnet increasing nonlinearly in close proximity to the attracted object, the cam on the frame is designed to be a multistage object, which increases the number of activated linear springs stepwise as the rod gets pushed in further as exemplified in Eq. (23) (e.g., with $n = 3$ springs). This compensates the control force required to shift in and out the control rod, while the counterforce of the spring applied on the outer frame F_{a}, following (24), pushes the entire system to the target surface, resulting in an attraction with the ideally identical force of the magnet.

$$k_{(x)} = \begin{cases} k_1 + k_2 + k_3 & (0 \le x \le x_3) \\ k_1 + k_2 & (x_3 < x \le x_2) \\ k_1 & (x_2 < x \le x_1) \end{cases} \tag{23}$$

$$F_{\mathrm{a}(x)} = -F_{\mathrm{m}(x)} = F_{\mathrm{r}(x)} \tag{24}$$

In a statics perspective, the spring can be regarded as a mean of storing attraction work as elastic energy, which gets released as repulsion work when the control rod is pulled out to detach the magnet from the target object. Therefore, (25) holds in an ideal situation in which self-weight, friction, and plastic deformation of the spring can be ignored, meaning that the law of conservation of mechanical energy stands in a process of actuating the control rods from complete desolated state $x = \infty$ to complete attached state $x = 0$ and also in one in the reverse direction.

$$\begin{aligned} W_{\infty\to 0} &= W_{0\to\infty} \\ &= \int_0^\infty F_{\mathrm{inter}(x)}\,\mathrm{d}x = \int_0^\infty \left\{F_{\mathrm{m}(x)} + F_{\mathrm{r}(x)}\right\}\mathrm{d}x \\ &= \int_0^\infty 0\,\mathrm{d}x = 0 \end{aligned} \tag{25}$$

Fig. 65 shows a basic example of an IB magnet used for demonstrations with a nonlinear spring composed of compression springs. The chosen springs do not only have different spring constants k_n and compression timings x_n but also free lengths, such that their ditches on the frame have a different depth to true up the extruded lengths of the springs. The ditches on the control rod also determine their compression timing. For the springs to exert a force on the center of the mechanism, each k_n is divided by an integer and springs of that number are arranged concentrically.

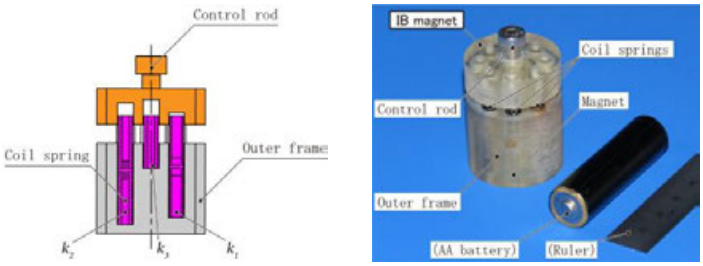

Fig. 65 Example design sketch and appearance of the IB magnet using compression springs.

Subsection III.2.7.3 Novelty of the proposed IBM gripper

Because it drastically reduces the external force to switch the attracted state of a strong permanent magnet, the IB magnet has been applied to various robotic devices such as a magnetic handle and wheels for locomotion on walls [74], [75], an anchor for a drone to dangle on a ceiling [76], and a connection joint for modular robots [77], [78]. The research team the author belongs to also has developed an IB magnet wheel that allows its operator to easily remove the body of the robot from the surface it is attracted to and an IB magnet crawler that suppresses the locomotion resistance and vibration of each magnetic track pad at the contact surface [19].

While validating the practicability of the IB magnet, these existing applications have been limited to attraction mechanisms. No research has ever realized the nature of an IB magnet that can also control a repulsive propping force or indirect pressing force generated by the compensation spring. Therefore, this study is different and unique in that it generalizes the application of the IB magnet to any robotic component that exerts an adjustable mechanical force by regulating the displacement of the control rod.

Chapter III.3 Proof of principle of the spontaneous amplification effect of the IBM gripper

Section III.3.1 Abstract of Chapter III.3

In this chapter, to realize the first POC model of the gripper using the IB magnet depicted in Fig. 55, a one-sided, single-parting gripper that has an active finger with an IB magnet embedded in and another fixed finger with a target attraction surface was developed. The performance of the proposed gripper was examined through simple man-powered experiments, and the validity of the spontaneous force amplification effect by the magnet was examined through an observation in which the net clamping force achieved with the magnet was found to be 2.0 times larger than the original clamping force exerted by the actuator.

In contrast to its significant reduction rate regarding the control force, during the development, it was found during that the nonlinear spring of the IB magnet, which serves the purpose of cancelling out the internal force on the magnet, has two major problems. These problems include the complicated design procedure and the trade-off relationship between balancing the precision and the volume of the mechanism. To simplify the design procedure of the nonlinear spring of the IB magnet, a new compensation method using a pair of magnets with like-poles facing each other as a magnetic spring is proposed. The repulsive force of the magnetic spring should equal the attractive force of an unlike-pole pair. To verify the proposed principle, a prototype of the IB magnet was designed using a magnetic spring and verified through experiments such that its reduction rate 13.0 % is comparable to those of conventional IB magnets.

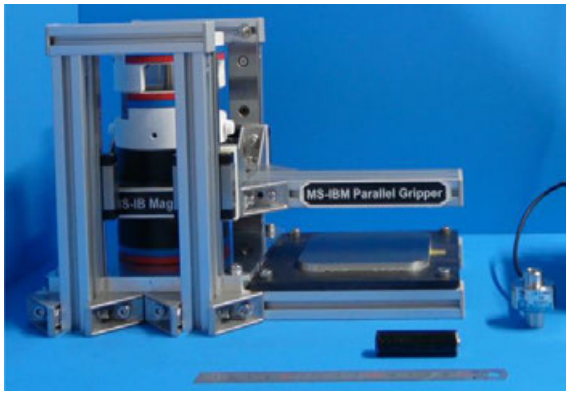

Fig. 66 Appearance of the POC model of the IBM gripper using a magnetic spring.

Section III.3.2 Elemental technology: Simplification of the design procedure of the nonlinear spring of the IB magnet

First, the problems of the IB magnet observed during the development of its demonstration model in Fig. 65 and their solution are introduced in this section.

Subsection III.3.2.1 Problems of the conventional nonlinear springs of the IB magnet: complicatedness of the design procedure

While the IB magnet enables a significant reduction of the control force of magnetic mechanism, its applications have not been widespread. One of the reasons is the difficulty to design a nonlinear spring that is both compact and precisely balanced because of the trade-off relationship between the compensation precision and the volume of the mechanism. More kinds of linear springs are required to let the spring characteristic reproduce the nonlinearity more smoothly.

Another reason is that the nonlinear spring has a complicated design procedure. As seen in , the conventional nonlinear spring for the IB magnet is composed of multiple linear springs. This requires an optimization process that cannot be achieved via a hand calculation. Referring to the previous research [27], [28], the design procedure of the spring can be described as follows:

i. Measure the displacement–force characteristic of the attractive force exerted between the magnet and the target object.
ii. Define the stroke of the mechanism and the number of linear springs n to use. The more springs that are used, the higher the balancing precision (smaller control force and thus smaller energy loss ΔE) that will be achieved.
iii. Draw the displacement–force characteristic graph of the spring by placing n tangent lines to the characteristic of the magnet at x_n and calculate their inclination equivalent to K_n.
iv. Determine the linear springs with spring constants that are close to k_n and measure their free length.
v. Using k_n, provide feedback to the graph to determine the starting positions x_n of the springs and calculate the depth X_n of the cam on the frame.

To improve the balancing precision, an optimization method using the following equations was developed. First, the loss of energy ΔE at conversion from attraction work to elastic energy is calculated by the attraction work as following Eq. (26).

$$\Delta E = \int_0^{\infty} \left\{ F_{\mathrm{r}}(x) - \sum_n k_n x \ (x \le x_n) \right\} \mathrm{d}x \tag{26}$$

This integrates the out-of-balance force at every unit of displacement dx from the target surface $x = 0$ to the maximum stroke of the rod, $x = x_{\mathrm{MAX}}$. Next, this optimization minimizes the ΔE by choosing spring constants K_n ($K_0 = 0$) at tangent points X_n ($X_n < X_{n-1}, X_0 = 0$) for the characteristics of the magnet and solves Eq. (27) to find x_{n}. This is the intersection where the tangent lines meet with the spring constants K_n and K_{n-1}.

$$x_n = \frac{(K_n X_n - K_{n-1} X_{n-1}) + \left(F_{\mathrm{r}(X_n)} - F_{\mathrm{r}(X_{n-1})} \right)}{K_n - K_{n-1}} \tag{27}$$

Finally, the range $(0, x_{\mathrm{n}})$ defines the stroke of a single linear spring with a spring constant k_n that is calculated by using Eq. (28) and (29).

$$K_n = \left. \frac{\mathrm{d}F_{\mathrm{r}}(x)}{\mathrm{d}x} \right|_{X_n} = \sum_n k_n \tag{28}$$

$$k_n = K_n - K_{n-1} \tag{29}$$

For an example of the unsophisticatedness of the multistage spring, the bi-parting gripper in Fig. 67 and Fig. 68 with $n = 6$ built for structure consideration became unreasonably larger and heavier than the magnets. This occurred because six pairs of springs were placed point-symmetrically around the screw for each finger, requiring 24 springs in total.

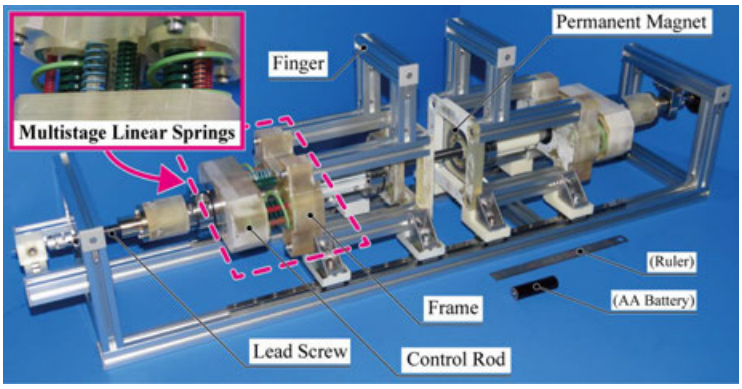

Fig. 67 Appearance of the preliminary prototype of the bi-parting IBM gripper using multistage linear springs.

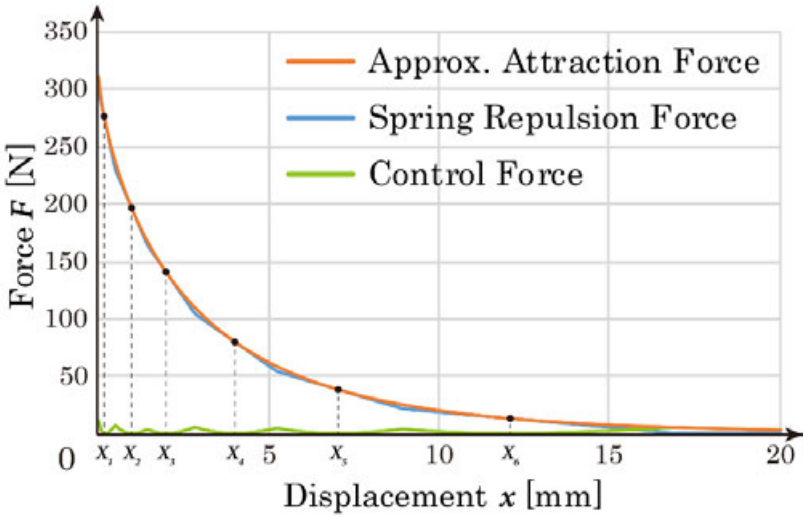

Fig. 68 Displacement–force characteristics of the spring and the pair of the magnets of the preliminary prototype of the bi-parting IBM gripper using multistage linear springs.

Subsection III.3.2.2 Proposed principle: IB magnet using the magnetic spring

To solve the abovementioned problems, a new internal balancing method using a magnetic spring was invented as depicted in Fig. 69. It focuses properties of a pair of magnets: the repulsive displacement–force characteristic of a like-pole pair, which is called a magnetic spring, is ideally identical, but opposite in sign, to that of the attractive force of an unlike-pole pair. This happens because both the attractive and repulsive force interacting between magnetic poles m_1 and m_2 ($m_1 m_2 > 0$ for repulsion, $m_1 m_2 < 0$ for attraction) at a distance x with a magnetic permeability μ follow the Coulomb's law of force formula (30).

$$F_{\mathrm{r}}(x) = -F_{\mathrm{m}}(x) = \frac{1}{4\pi\mu}\frac{m_1 m_2}{x^2} \tag{30}$$

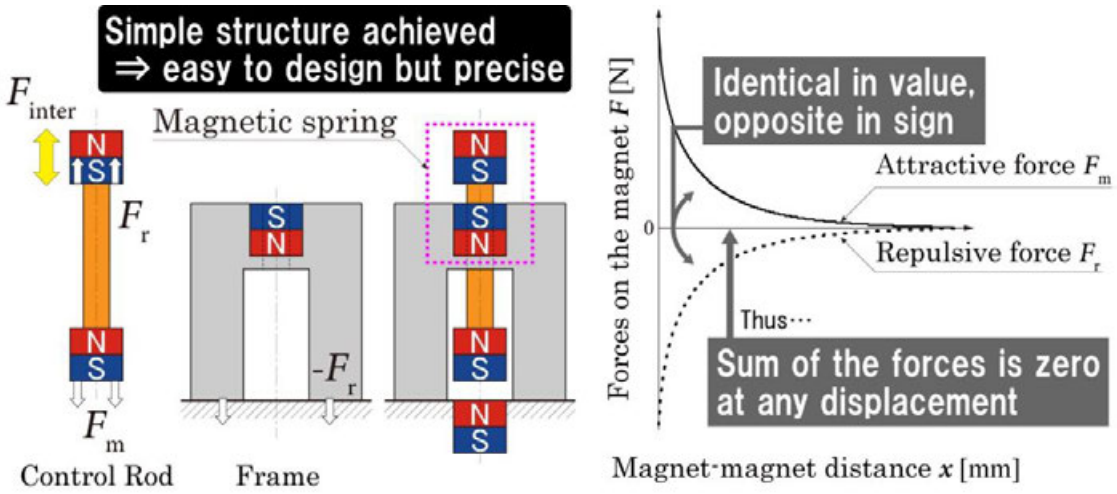

Fig. 69 Conceptual diagram of the IB magnet using the magnetic spring.

Because the sum of their force always equals zero for any displacement, just aligning two pairs of magnets each in the same distance establish the compensation. Therefore, the proposed magnetic spring drastically simplifies the design procedure compared to the conventional multistage spring, which can be even ignored if the stroke can be determined by an abstract physical sense of the designer, especially for human tools, showing the high degree of design flexibility of the IB magnet using the magnetic spring:

i. Measure the displacement–force characteristic of the attractive force exerted between the pair of magnets.
ii. Define the stroke of the mechanism, which is equal to the maximum displacement of the magnetic spring.

The IB magnet using a magnetic spring is innovative in that it is composed of only four identical magnets while expected to keep or even improve the compensation precision. Because the magnetic spring acts remotely, its contactless and thus frictionless force transmission restrains the material fatigue of the mechanism structure that causes malfunction, unlike conventional springs that require contact to both the control rod and outer frame to generate repulsive force. Furthermore, point-symmetric feature of the magnetic springs made of disc or ring magnets gives the IB magnet applicability to endlessly rotating mechanisms that need compensation independent of the angle of the control rod relative to the frame.

As this study intends to utilize the IB magnet using the magnetic spring in a gripper, an embedded magnet in the fixed finger is specified as the attraction target. On the other hand, if attaching to any ferromagnetic objects other than the identical magnet used in the IB magnet, the repulsive force of the magnetic spring always exceeds the attractive force. A similar phenomenon happens to any IB magnet, in which the spring exerts too large or too weak repulsive force, as its displacement–force characteristic is designed to follow that of the attractive force between the magnet and a specifically designated target object. The excess of compensation force leads to sudden unexpected detachment of the control rod due to vibration or shock, while the lack leaves the control force unaffordable by the selected weak actuator.

To adjust the control force, an offset on the distance between the magnetic spring can be added so that its repulsive force decreases, admitting some loss of control work, as illustrated in Fig. 70. In that sense, the merit of the magnetic spring can be summarized as the coexistence of simplicity and the balancing precision, especially for applications that can embed a magnet inside as a target.

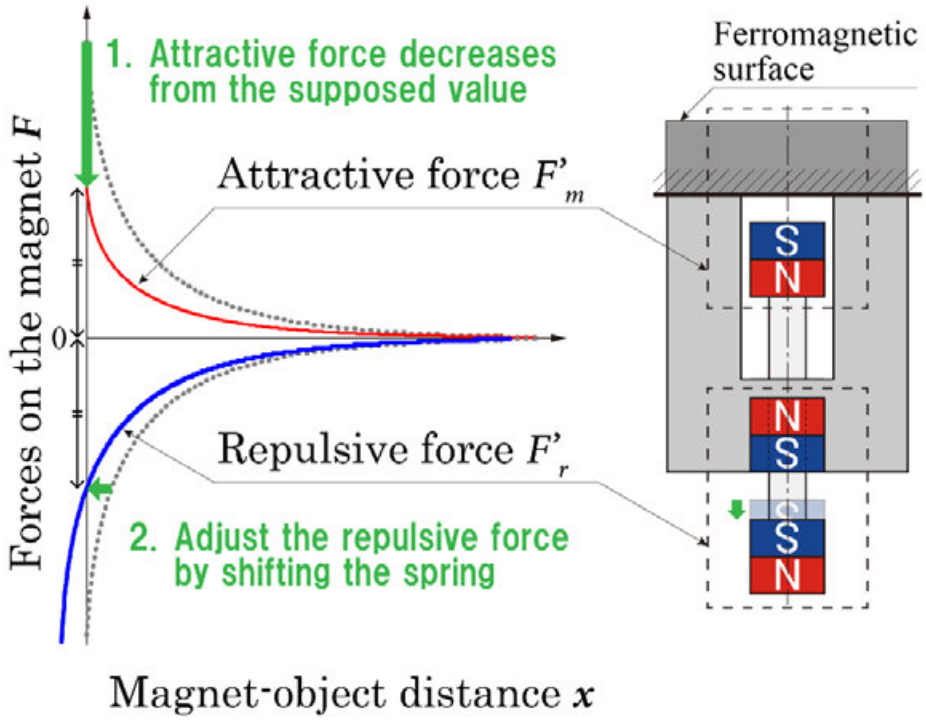

Fig. 70 Force adjustment of the IB magnet using the magnetic spring.

Subsection III.3.2.3 Verification of the effectiveness of the IB magnet using the magnetic spring

III.3.2.3.1 Design and development of the prototype model of the IB magnet using the magnetic spring

Based on the proposed principle, a POC prototype of the IB magnet using a magnetic spring in Fig. 71 was developed and its specification is listed in TABLE III. Ring magnets were selected so that a tube-like rod and dry bearings can be placed through the holes for lubrication and future expandability. The latter includes, but is not limited to, controlling the rod by the side of the attraction magnet, rotating the control rod relative to the frame and/or target surface, and ducting fluids. Their exposed surface is shielded by a cover with a thickness of 1 mm to avoid ferromagnetic sand. The stroke was defined as 7.5 mm, where a material testing machine (Instron, 3343) measured the attractive force between the magnets 0.5 N, reasonably small enough.

Fig. 1 displays the embodied proof-of-concept prototype of the proposed IB magnet using a magnetic spring. A 3D-printed acrylic material (Keyence, AR-M2) is used for the structure for the sake of rapid prototyping. Materials with a higher stiffness such as polycarbonate and aluminum can be used for better durability.

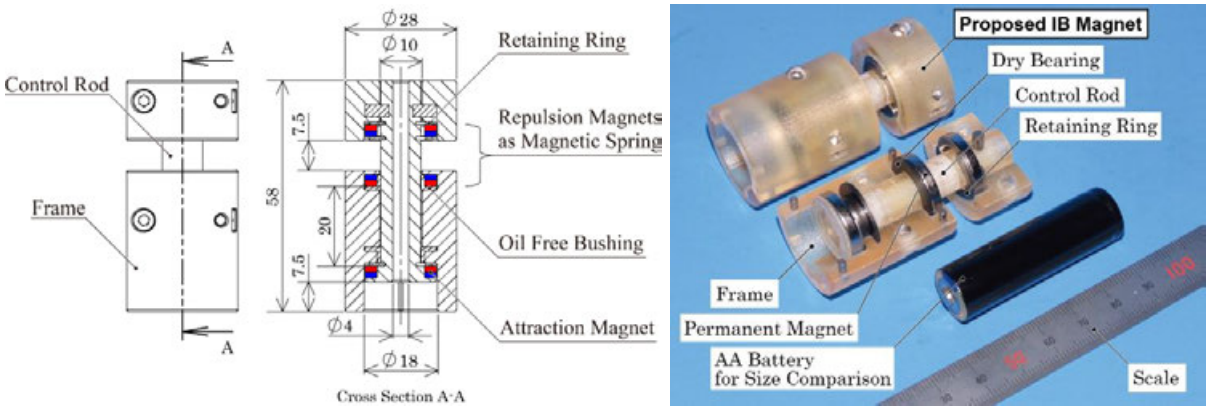

Fig. 71 Design and appearance of the prototype of the IB magnet using the magnetic spring.

TABLE III

SPECIFICATION OF THE PROTOTYPE OF THE IB MAGNET USING THE MAGNETIC SPRING

Magnet	Type Number	HXCW18-12-3		
	Outer Diameter	18 mm	Diameter	28.0 mm
	Inner Diameter	12 mm	Maximum Length	58 mm
	Thickness	3 mm	Stroke	7.5 mm
	Weight	2.9 g	Weight	44.3 g

III.3.2.3.2 Basic operation experiment of the prototype model of the IB magnet using the magnetic spring

A basic attraction operation of the IB magnet using the magnetic spring was conducted to demonstrate its usability as recorded in Fig. 72. The IB magnet lifts up an object in a following process. (a)–(b) First, the IB magnet is placed on the target object, an iron cuboid block with a mass of 491 g (4.82 N in weight). (c)–(d) The control rod was pushed down so that the attraction magnet on the rod approaches the target object, during which the magnets of the magnetic spring also get closer and increases repulsive force for compensation. (e)–(f) Once the control rod is fully pushed in, pulling up the outer frame results in the lifting up of the target object attracted to it. (g)–(k) The attractive force was found to be strong enough to keep the attached state against the shaking movement. (l)–(o) Without applying detaching force between the outer frame and the target object, pulling out the control rod led to loss of the attractive force, resulting in the drop of the object.

The process of the experiment qualitatively revealed that the prototype successfully behaved as an IB magnet.

Fig. 72 Basic operation of the prototype of the IB magnet using the magnetic spring.

III.3.2.3.3 Performance evaluation experiment of the prototype model of the IB magnet using the magnetic spring

To evaluate the internal force compensation effect of the proposed magnetic spring, this study conducted an examination using the material testing machine as illustrated in Fig. 73. The IB magnet was placed on and attached to a target acrylic plate with the target magnet buried 1 mm deep. A T-shape hook was attached to the testing machine to pull up the jig connected either to the frame or to the control rod at the rate of 0.5 mm/sec and to the maximum displacement of 15 mm (twice the stroke). Thus, the values of the control force required to detach the IB magnet by pulling its frame and its control rod were measured.

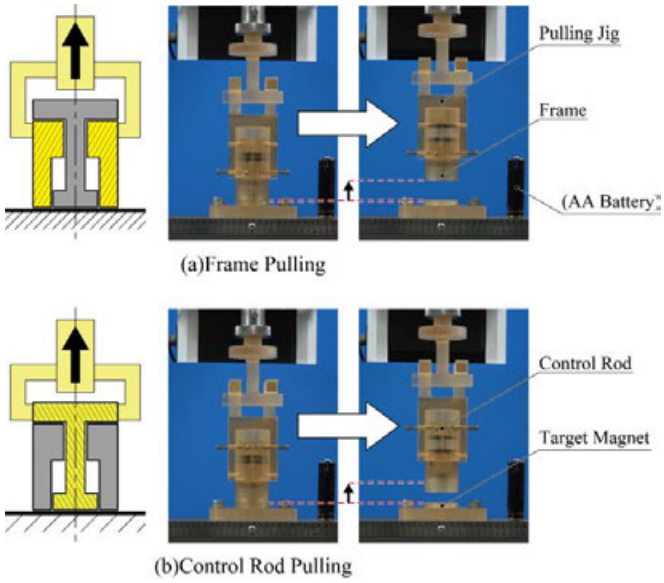

Fig. 73 System constituents of the performance evaluation experiment of the prototype of the IB magnet using the magnetic spring.

Fig. 74 shows the typical transition of the measurements and Fig. 75 shows the five-time average net maximum control force. (a) When the ascending T-shape hook touches the jig that is connected to the frame, the control force suddenly reaches the highest net value of 8.4 N. This is identical to the maximum attractive force of the original magnet. Afterwards, the detached magnets gradually decrease the control force, so it matches the weight of the whole mechanism and the jig. (b) When the jig is connected to the control rod, the control force likely increases; however, the highest net value 1.1 N is apparently reduced to 13.0 % of the value during frame pulling. The control force then decreases to the total weight with one rising edge when the rod touches the frame at its maximum stroke.

Ideally, the maximum control force is expected to be recorded at the origin where the magnets are in contact and thus their attractive force becomes the largest. The reason the actual peaks were with displacement is thought to be that the tension force applied on the mechanism and the jigs was large enough to deform them. For a more precise evaluation, replacement to nonferromagnetic materials is suggested.

The interference between the magnet for attraction and the one for the frame was not strictly considered but was regarded as weak enough since the shortest distance of 20 mm between them results in a magnetic force of less than 2.0×10^{-3} N, which is 2.3×10^{-2} % of the maximum attractive force. It is expected that the interference can be effectively eliminated by magnetically isolating them from each other using magnetic shields.

The reduction ratios of the control force of conventional IB magnets are reported to be 11.8 % for a multistage spring comprising six kinds of coil springs and 15.4 % for a rubber ring spring with a nonlinear cam [14], which are the values comparable to that of the proposed magnetic spring. In these ways, this experiment successfully validated the effectiveness of the proposed magnetic spring and likely reduced the ratio with a simpler structure and an easier design procedure.

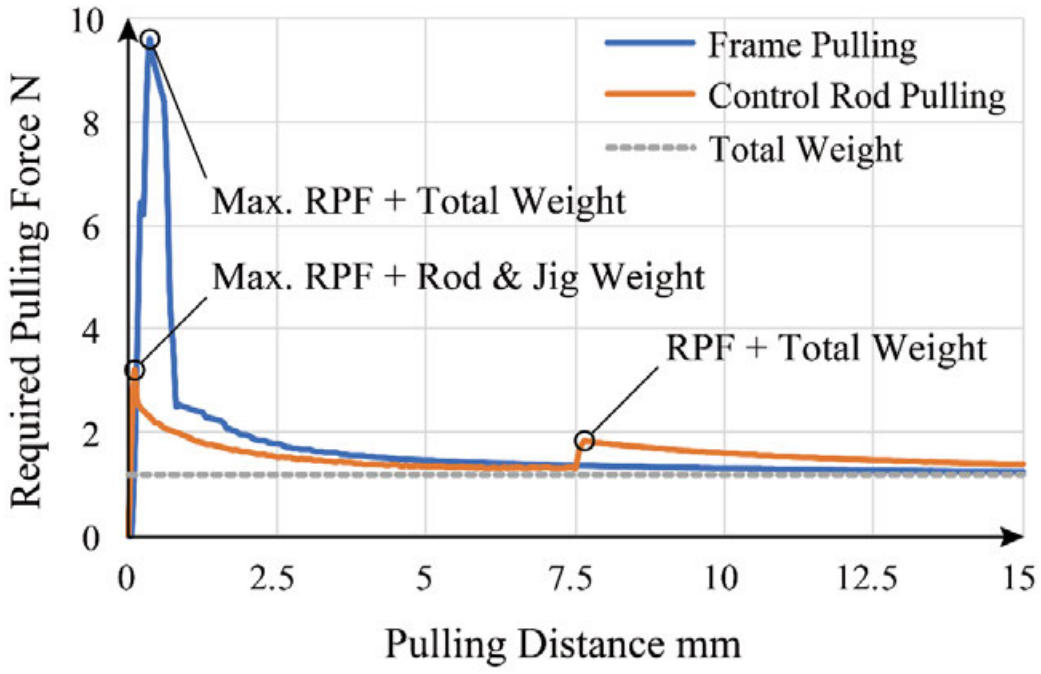

Fig. 74 Transition of the control forces for pulling out the outer frame and control rod of the proposed IB magnet using the magnetic spring.

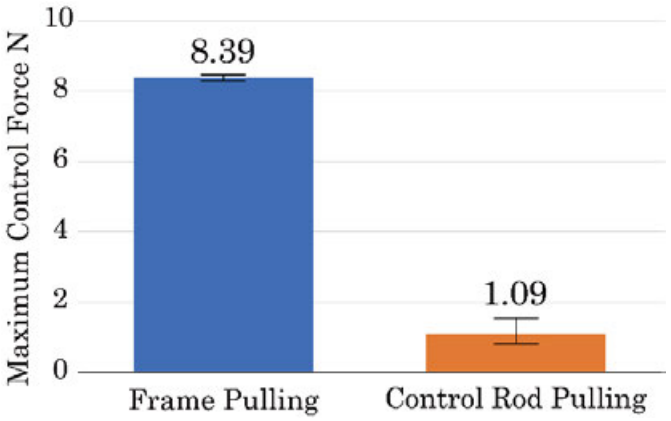

Fig. 75 Direct comparison of the net maximum control forces for pulling out the outer frame and control rod of the proposed IB magnet using the magnetic spring.

Subsection III.3.2.4 Elemental technology: rescaling of the IB magnet using the magnetic spring for reinforcement

While small magnets are chosen for a rapid proof of concept, larger magnets with stronger force more suit to embed in a gripper. So, also to evaluate the scalability of the magnetic spring, a reinforced IB magnet using larger magnets was developed.

III.3.2.4.1 Design and development of the reinforced IB magnet using the magnetic spring

As displayed in Fig. 76 and TABLE IV, the prototype of the reinforced IB magnet using the magnetic spring is composed of 3D-printed polymer (Stratasys, ABS-P430) and non-magnetic steel (SUS304). To maximize the attractive force, the attraction magnet is press-fitted to expose its surface. the interfering force between the magnet on the frame for the spring and the attraction magnet was measured to be 3.4×10^{-3} N, which is 1.1×10^{-3} % of the maximum attractive force.

To avoid the sudden and unintended release of the control rod by a shake or vibration that results in the forced separation from the target object, which occasionally happens as the internal force is too balanced, a twisting lock mechanism was installed. This ensures not only the complete attraction state, but also the complete detached state of the magnet to and from the target object.

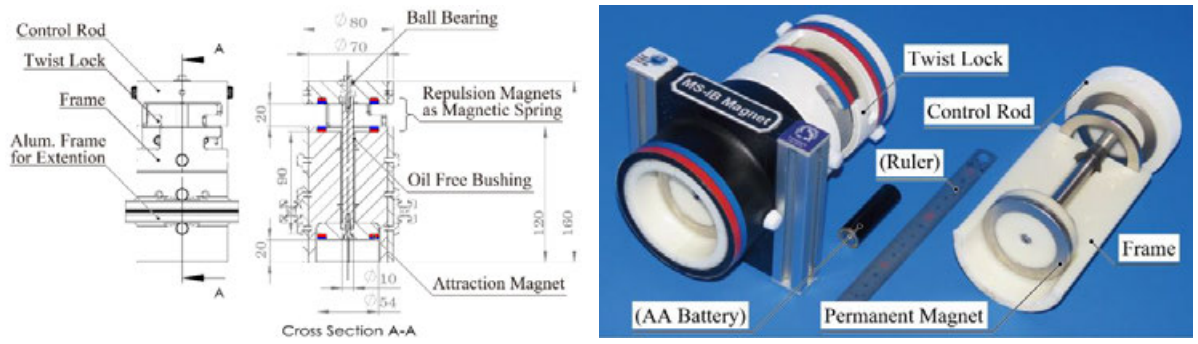

Fig. 76 Design and appearance of the reinforced IB magnet using the magnetic spring.

TABLE IV

SPECIFICATION OF THE REINFORCED IB MAGNET USING THE MAGNETIC SPRING.

Magnet	Type Number	NOR391
	Outer Diameter	54 mm
	Inner Diameter	38 mm
	Thickness	5 mm
	Weight	40.8 g

Diameter	80 mm
Maximum Length	160 mm
Stroke	20 mm
Weight	683.4 g

III.3.2.4.2 Basic operation experiment of the reinforced IB magnet using the magnetic spring

A basic operation of the reinforced IB magnet using the magnetic spring was conducted as recorded in Fig. 77. (a)–(b) First, the IB magnet is placed on an iron plate of 15.4 kg. (c)–(d) The control rod was pushed down and then twisted to lock. (e)–(f) Pulling up the outer frame results in the lifting of the target object.

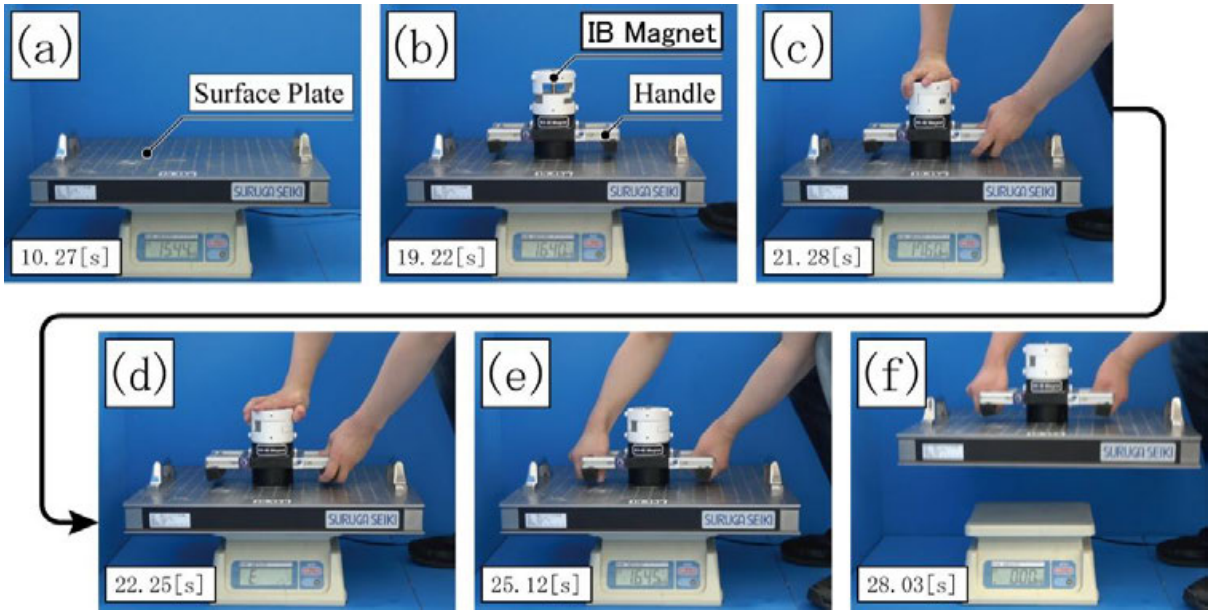

Fig. 77 Basic operation of the reinforced IB magnet using the magnetic spring.

III.3.2.4.3 Performance evaluation experiment of the reinforced IB magnet using the magnetic spring

The measurement depicted in Fig. 78 was conducted under the same condition as III.3.2.3.3 The result in Fig. 79 showed that the magnetic spring is even valid for a larger scale but with a lower compensation precision of 31.7 %.

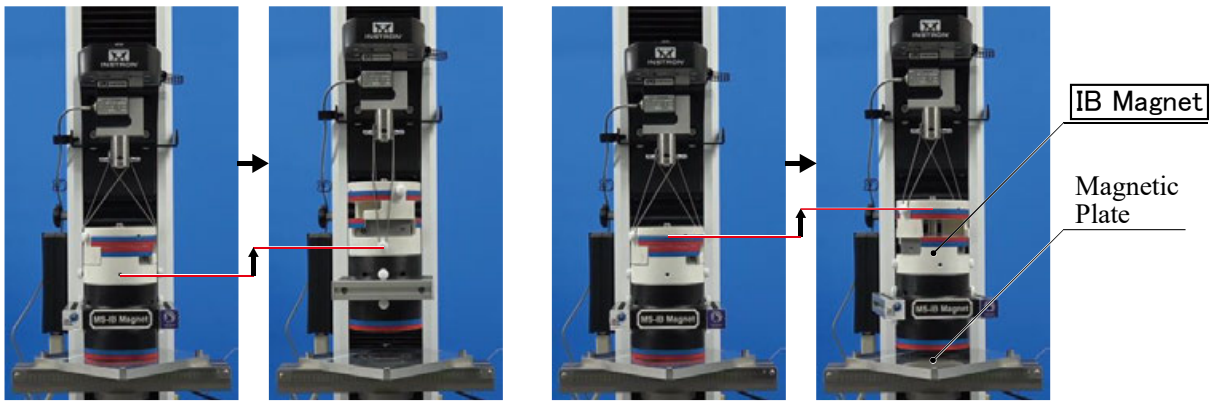

Fig. 78 System constituents of the performance evaluation experiment of the reinforced IB magnet using the magnetic spring.

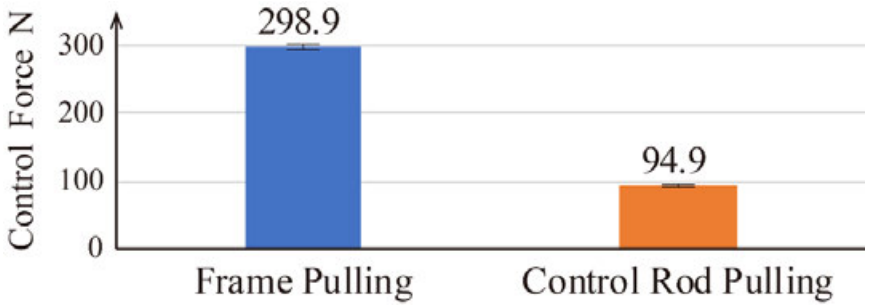

Fig. 79 Direct comparison of the net maximum control forces for pulling out the outer frame and control rod of the reinforced IB magnet using the magnetic spring.

Subsection III.3.2.5 Discussion on the characteristics of the IB magnet using the magnetic spring

The experiments of the prototype of the proposed IB magnet using the magnetic spring showed a measurable compensation impreciseness that results in a non-zero control force. The causes are expected as followings, in addition to the individual difference in the magnetization of the magnets. Analyses on the static magnetic field would be effective to comprehend these phenomena.

III.3.2.5.1 Property of the magnetic circuits

It is hypothesized that the cause of this phenomenon could be the difference between the shape of the magnetic circuits of the like-pole pair and unlike-pole pair of magnets. As a result, the deviation between the attraction and repulsion characteristics around the origin (where the facing magnets meet) may have become larger and more apparent as the volume and the magnetic flux became larger for the enlarged version of the IB magnet using the magnetic spring.

III.3.2.5.2 Magnetic interference

Also, the magnets for attraction and repulsion would have been placed too closely to each other such that their magnetic circuits interfered, resulting in the loss of balancing precision. In the prototype model for POC, the attraction magnet on the control rod and repulsion magnet on the outer frame were facing their like poles. To avoid the effect of their repulsive force on the control force, the IB prototype was designed such that approach 20 mm at the closest, in which they exert force less than 0.01 N. In observation of the realized prototype, however, a bias of the control force was found such that the attractive force exceeded the repulsive force. The cause is a leak in the magnetic circuits via the structure of the mechanism that unintendedly interfere with each other. Therefore, locating the magnets apart in a further distance or inserting a magnetic shield would become solutions.

III.3.2.5.3 Magnetization of the target object

As stated in Subsection III.3.2.2, if attaching to any ferromagnetic objects other than the identical magnet used in the IB magnet, the repulsive force of the magnetic spring always exceeds the attractive force. The excess of compensation force requires a continuous external force on the control rod to sustain the attached state or leads to sudden unexpected detachment of the control rod due to vibration or shock.

This phenomenon is caused by the fact that a ferromagnetic object first exerts attraction force when it gets magnetized by an external magnetic field (in this case, that of the attraction magnet on the control rod), aligning the magnetic moment of its constituent elements so that the whole object behaves as a single magnet. As a ferromagnetic object has a smaller magnetic susceptibility than magnetic materials, the induced magnet made of it cannot be stronger than the original attraction magnet which is the source of the magnetic field. This results in the lack of the attraction force between a magnet and a ferromagnetic object compared to the repulsive force between a pair of magnets.

According to the previous research that intendedly designs a spring weaker than the magnetic attraction [27], this bias is useful for preventing the sudden unintended release of the control rod due to shock or vibration, which happens as the balanced control rod is weak to external disturbance. In another research, an adjustment mechanism of the compensation force was developed to deal with the decrease in the attraction force due to nonmagnetic paint coating or rust on the surface of the attraction target [79]. Its linear springs that compose the nonlinear springs can be shifted on the control rod to make an offset that corresponds to the thickness of the coating, likely to the way introduced in Fig. 70.

For any causes of the compensation disturbance, implementation of an adjustment system that mechanically detects the change in the attraction force and then relieves the repulsive force would be effective for generalization of the IB magnet applicable to any unknown target objects with various shape, susceptibility, and permeability.

Section III.3.3 Embodiment of the one-sided IBM gripper with a fixed clamping width

Subsection III.3.3.1 Design and development of the one-sided IBM gripper with a fixed clamping width

Based on the proposed principle illustrated in Fig. 64, a hand-powered prototype of the proposed IBM gripper was designed as depicted in Fig. 81. The clamping width between fingers is fixed to 35 mm, adjustable by inserting shim plates. Indicating the ease of embedding the IB magnet using the magnetic spring in an application mechanism, the mechanism is designed simply by containing the IB magnet of Fig. 76, whose outer frame is extended as the active finger, while its attraction target magnet is embedded in the fixed finger. The IB magnet can be shifted upward for more than its stroke to fit to objects that are wider than the designed clamping width.

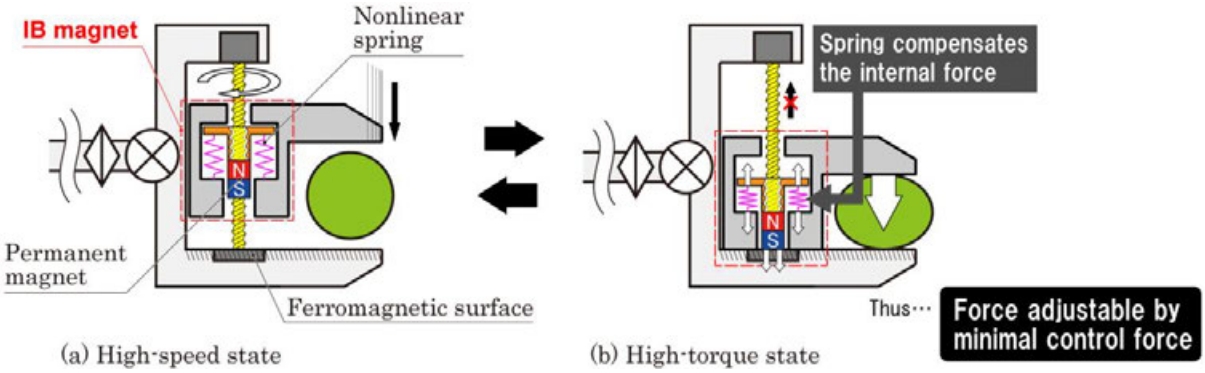

Fig. 80 Principle diagram of the proposed gripper with force amplification mechanism using the IB magnet (repost of Fig. 64).

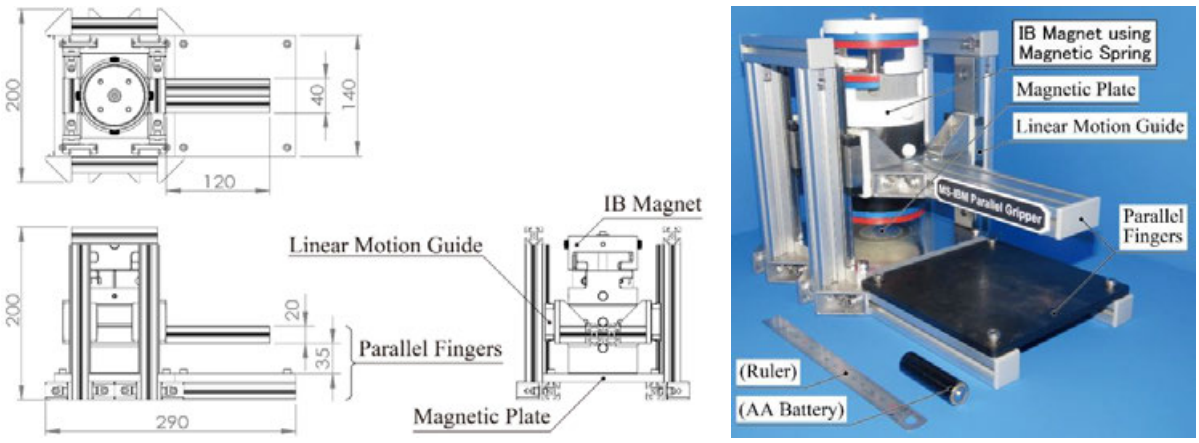

Fig. 81 Design and appearance of the reinforced IB magnet using the magnetic spring.

III.3.3.1.1 Basic operation experiment of the one-sided IBM gripper with a fixed clamping width

A basic operation of the one-sided IBM gripper with a clamping width of 39 mm was demonstrated as recorded in Fig. 82. (b)–(c) First, a tape of 40 mm width as a target object was placed between fingers. (d) Clamping just by the self-weight of the active finger is not strong enough such that the tape can be moved by an external force. (e)–(f) Attaching the magnet by shifting down the control rod activates the force amplification, resulting in a clamping strong enough to hold the object firmly. The process of the experiment qualitatively revealed that the IBM gripper has an ability to spontaneously increase the clamping force.

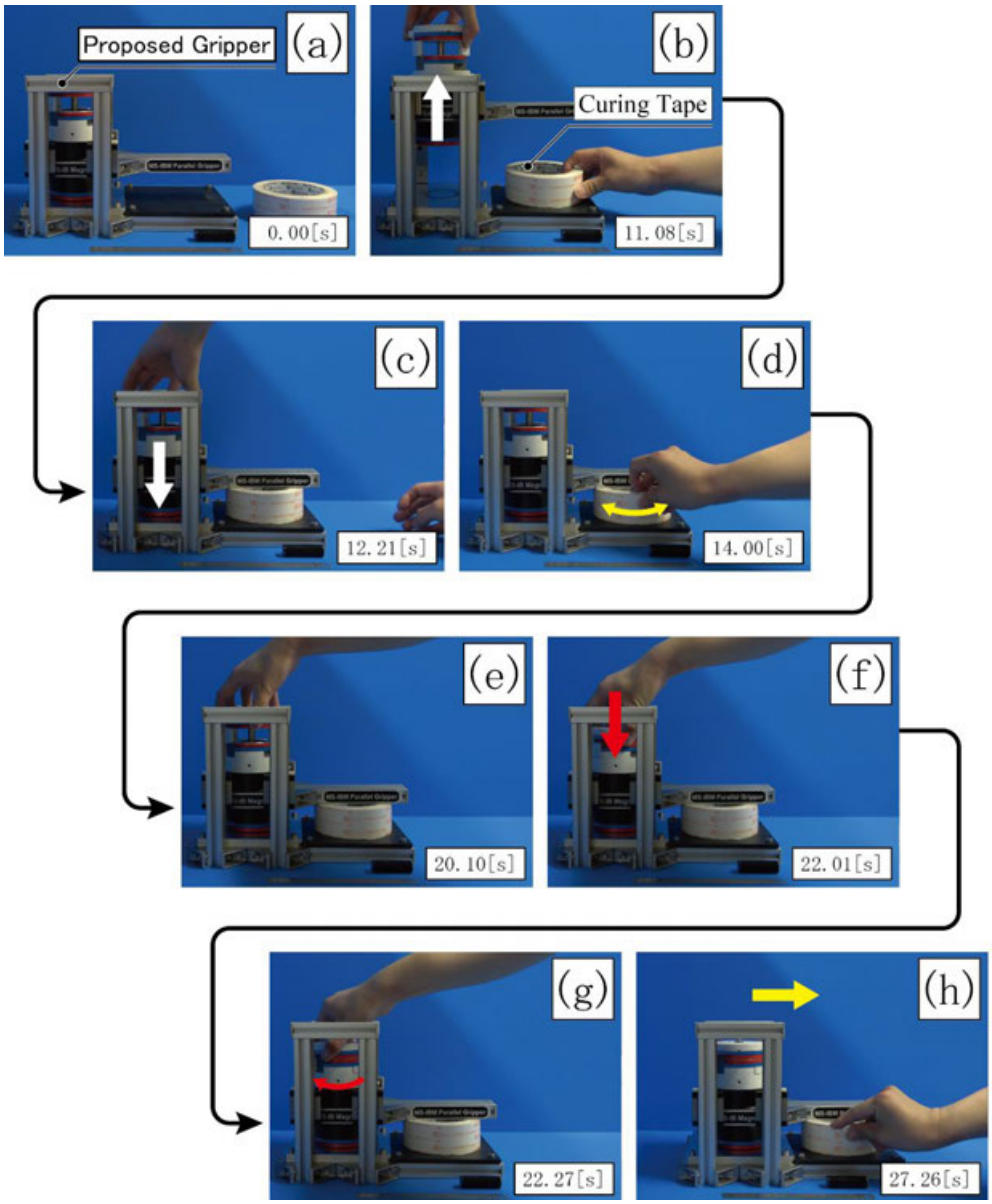

Fig. 82 Basic operation of the one-sided IBM gripper with a fixed clamping width.

III.3.3.1.2 Performance evaluation experiment of the one-sided IBM gripper with a fixed clamping width

To evaluate the spontaneous amplification of the proposed IBM gripper with a clamping width of 34 mm, an examination was conducted as featured in Fig. 83 and the results are presented in Fig. 84. This experiment occurred as follows: (b) The loadcell (Kyowa Sangyo, LUR-A-2KNSA) with a width of 34 mm was inserted between the parallel fingers. (c) The initial load on the loadcell exerted by the weight of the active finger was measured to be 12.9 N, which is the gravity bias of the clamping force. (d) The maximum control force 94.9 N (represented as a mass of 9.68 kg) was required to shift the control rod up and down. When it was applied on the rod in the fully pulled-out state, the net clamping force without the spontaneous reduction was measured to be 18.5 N. (e) The control rod was shifted down by hand. (f) The net clamping force with the spontaneous reduction by the magnet was measured to be 36.9 N, which is 2.0 times the original clamping force (d). The experiment successfully validated the effectiveness of spontaneous amplification effect of the proposed IBM gripper quantitatively.

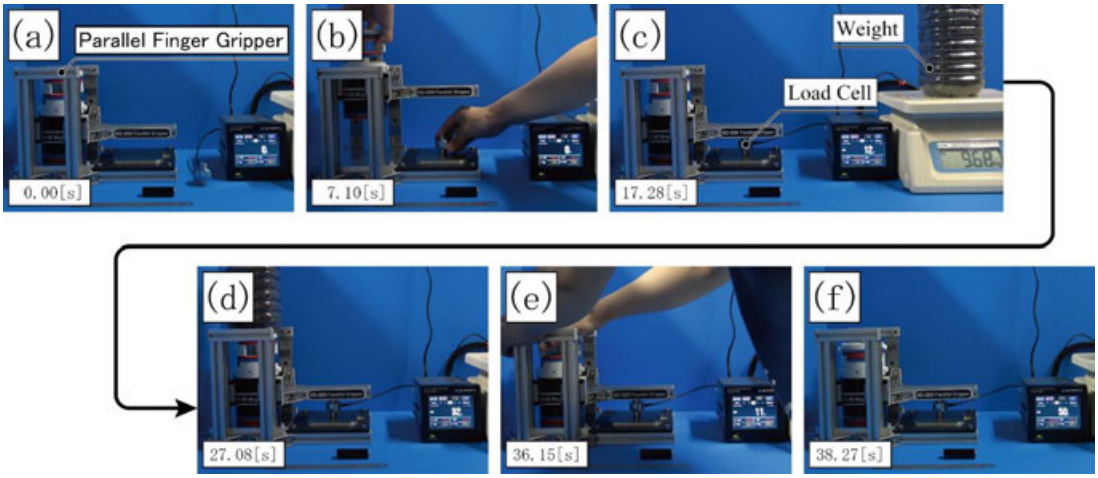

Fig. 83 Performance evaluation of the one-sided IBM gripper with a fixed clamping width.

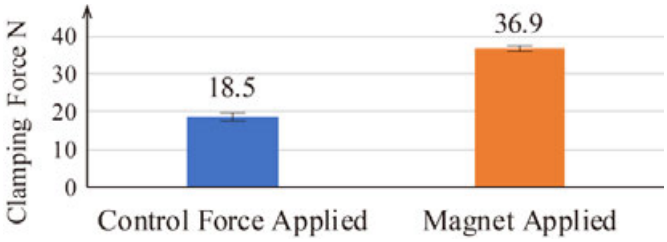

Fig. 84 Direct comparison of the net maximum clamping forces of the one-sided IBM gripper with a fixed clamping width.

Subsection III.3.3.2 Discussion on the characteristics of the one-sided IBM gripper with a fixed clamping width

III.3.3.2.1 Observation on the actual behavior

The observation on the behavior of the realized prototype model of the gripper revealed that the clamping procedure is more complicated than expected in Fig. 64, as illustrated in Fig. 85. The larger the deviation of the object width and the designed clamping width between the fingers, the earlier the active finger meets the object before the frame approaches the target surface. Therefore, the compensation is disturbed by this gap and the linear actuator has to supply a larger control force to shift in the magnet than expected at the design step. As the control rod is pushed in, the attraction magnets increase the attractive force and so as the deformation of the target object and the finger, resulting in the requirement of further actuation of the finger by the actuator control force and magnetic assistive force to exceed the elastic force of the relating bodies. The control rod continues the process of clamping through this nonlinear interaction. Therefore, modelling and its analysis of the relationship among the control force, attractive force and clamping force are expected to be complicated and too specified unsuitable for general use, as long as adopting the current structure.

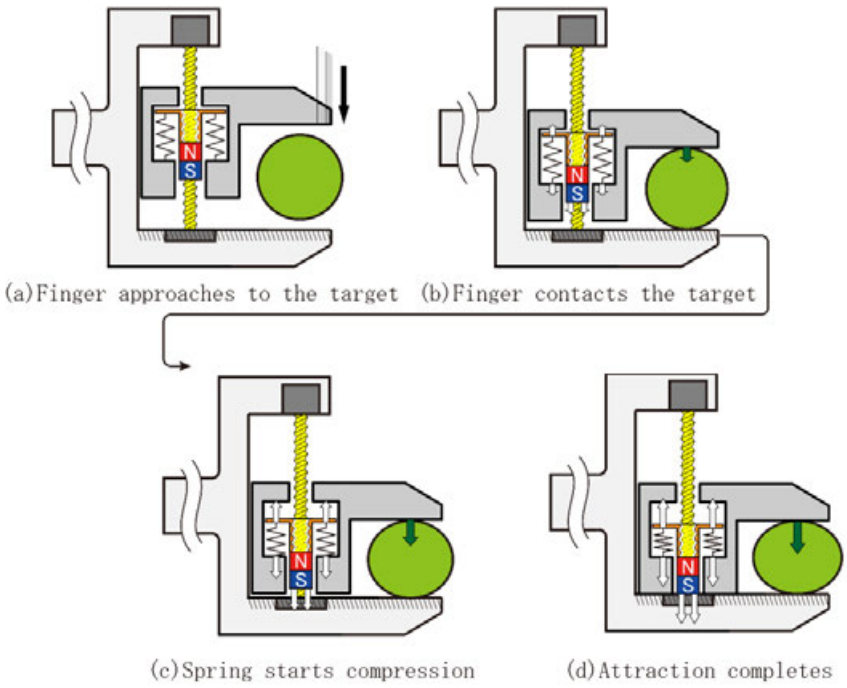

Fig. 85 Actual clamping process of the one-sided IBM gripper with a fixed clamping width.

The compensation precision is decayed because the situation is against the premise of the IB magnet that the magnet–target surface distance and the spring compression distance are strictly synchronized. However, the assistance of clamping an object by spontaneous magnetic attraction and the keeping the state of clamping without continuous external force supply is successfully accomplished.

Section III.3.4 Conclusion of Chapter III.3

In this chapter, to prove the concept of the proposed IBM gripper, a one-sided prototype model with a fixed clamping width was developed.

To solve the problems of the conventional nonlinear spring used for the IB magnet, including its complicated design procedure and trade-off relationship between volume and compensation precision, the principle for a new balancing method that uses a magnetic spring was also proposed. An experiment was conducted to show that the reduction rate of the magnetic spring 13.0 % is comparable to those of conventional IB magnets while its structure became much simpler.

Then, a reinforced version of the IB magnet that uses the magnetic spring was introduced in the gripper, and an evaluation experiment revealed that the net clamping force achieved with the spontaneous amplification by the magnetic assistance was measured to be double the original clamping force generated by the single input of the actuator. In this way, the effectiveness of a spontaneous force amplification by the IB magnet as a DF converter was verified.

To further improve compensation precision, an electromagnetic field analysis on the magnetic spring and the mechanism structure can be conducted to establish magnetic circuits with a less leakage and interference.

Chapter III.4 Proof of principle of the continuous amplification effect of the IBM gripper

Section III.4.1 Abstract of Chapter III.4

In this chapter, a bi-parting gripper that has two active fingers with an IB magnet embedded in each, to enhance dexterity, was developed. The magnetic spring was unsuitable for this configuration, as there was a mismatch between the approach speed of the magnets and compression speed of the springs; therefore, the focus shifted to the nonlinear property of the conical coil compression spring to ensure both precision and miniaturization.

By actuating the gripper with a DC motor connected to a bidirectional screw, the basic operation experiment revealed the validity of the steplessly adjustable force amplification feature of the IBM gripper. The performance evaluation experiment visualized the conditions in which the efficiency of the output clamping force relative to the power consumption maximizes. Relative to the constitution with a motored screw only, the prototype successfully amplified the grasping force to at most 292.2 %, assisted by the magnetic attraction, while achieving an increase in power consumption of the DC motor only by 11.8 %, making the force–energy efficiency 2.6 times larger. Thus, it was verified that the proposed gripper enables the use of actuators and current supplies that require less power.

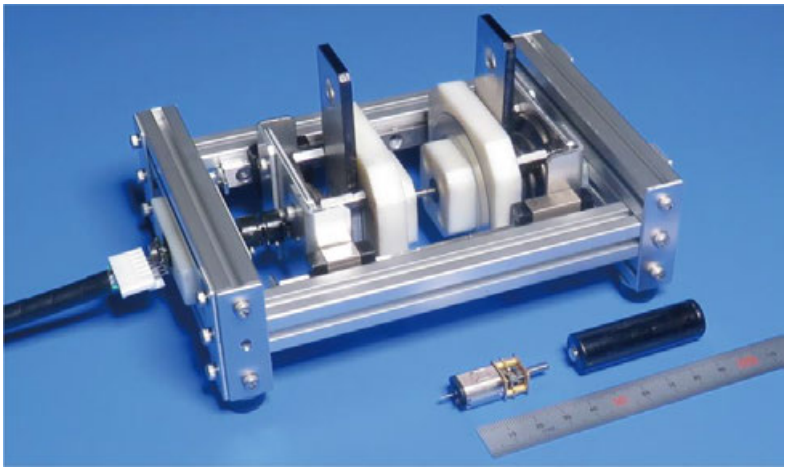

Fig. 86 Appearance of the prototype of the bi-parting IB magnet using the magnetic spring with a fixed clamping width.

Section III.4.2 Elemental technology: further miniaturization of the compensation spring

Subsection III.4.2.1 Disadvantages of the IB magnet inherent in bi-parting constitution: mismatch of approaching speeds

While simplifying the design procedure and reducing the number of components, a magnetic spring was found to be improper when applied to a bi-parting constitution because of the mismatch of approaching speeds of the pairs of magnets for magnetic springs and the pair of magnets for attraction. As depicted in Fig. 87, the distances between the magnets for attraction and repulsion are both x_{MAX} when the frames first come into contact and stop their movement. However, the control rods and magnets on them are pushed in by the screw into the center plane of the symmetry at a certain speed, while the magnets for attraction also approach each other at a relative double speed.

Desynchronizing these approaching speeds by splitting the attraction and repulsion parts of the control rod may solve this issue. However, adding reduction mechanisms such as reduction levers or gears would increases design complexity and energy loss, which is against the study purpose.

Developing a nonlinear spring with a re-scaled displacement–force characteristic that achieves $F_{\mathrm{r}(x)} = -F_{\mathrm{m}(2x)}$ is also effective to solve this problem. However, as the preliminary prototype assembled for design consideration appears in Fig. 67, the conventional multistage spring unignorably increases the mass and volume of the entire mechanism compared to the output clamping force.

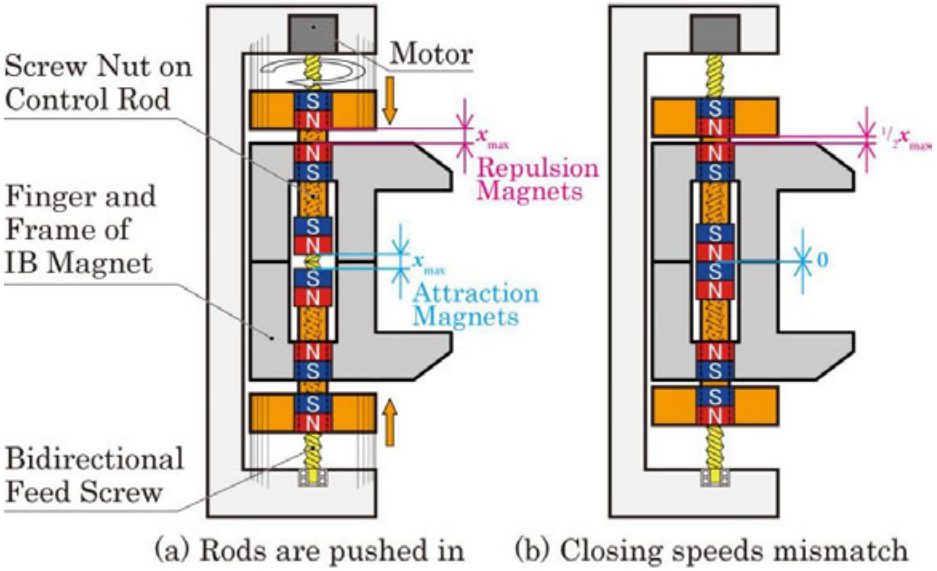

Fig. 87 Mismatch of approaching speeds of magnets in the proposed bi-parting IBM gripper using magnetic spring.

Subsection III.4.2.2 Proposed principle: conical coil spring

To attain both the miniaturization and re-scaling of the displacement–force characteristic to achieve $F_{\mathrm{r}(x)} = -F_{\mathrm{m}(2x)}$, the nature of a conical coil spring was focused on. It has either a varying diameter or pitch or both, such that its part with a smaller spring constant becomes compressed first, followed by the part with a larger spring constant, thereby nonlinearly increasing the displacement–force characteristic by only a single elastic body. In addition, its conical structure allows each spiral to fit inside the neighboring spiral, making the fully compressed volume smaller than those of the other compression springs. Using these features effectively, the repulsive characteristic of the conical spring for the IBM gripper was adjusted to follow $-F_{\mathrm{m}(2x)}$ on every millimeter of the compression length by rectifying the pitch and diameter as recorded in Fig. 88, in contrast to an usual compression coil spring whose spring constant is monitored at only two compression length. Still, the tolerable tracking error of the force must be set to ± 10 % due to production constraints, resulting in an integrated absolute deviation of forces of 11.4 %, which equals the loss of control energy. Therefore, the major problem of the adopting a conical coil spring to the IB magnet would be its productivity.

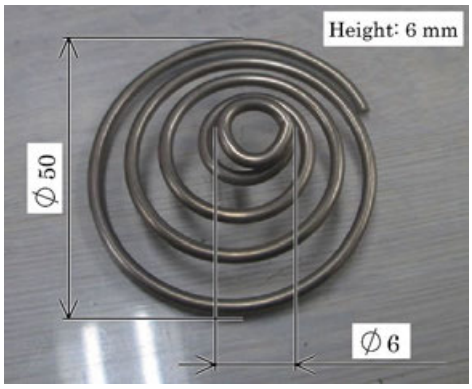

Fig. 88 Appearance of the conical coil spring.

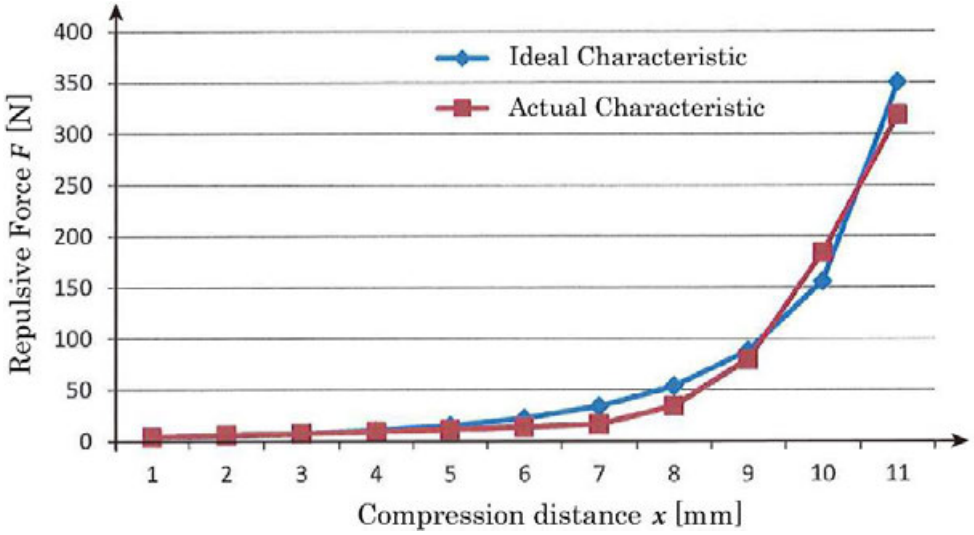

Fig. 89 Displacement–force characteristics of the conical coil spring and the attraction magnets to be compensated (data provided by the manufacture, Yamato Spring Corporation).

Section III.4.3 Embodiment of the bi-parting IBM gripper with a fixed clamping width

Subsection III.4.3.1 Design and development of the bi-parting IBM gripper with a fixed clamping width

Fig. 90 shows the design sketch and dimensions of the prototype of the proposed bi-parting IBM gripper. The structure was designed in the following process under a policy of miniaturization. First, a ring magnet was chosen such that a bidirectional feed screw could penetrate the entire mechanism, and the frame of the IB magnet could fit inside the control rod. Next, a conical spring was produced to fit the characteristics of the chosen magnet, and then the M3 screw was selected as a reasonable size smaller than the minimum inner diameter $\phi 6$ mm of the spring. The minimum clamping width was designed to be 40 mm, as it was sufficiently large to clamp a loadcell for later experiments. The stroke of the control rod x_{MAX} was designed to be 10 mm, in which the magnet decreased its attractive force the necessary to be pulled out by the actuator without compensation.

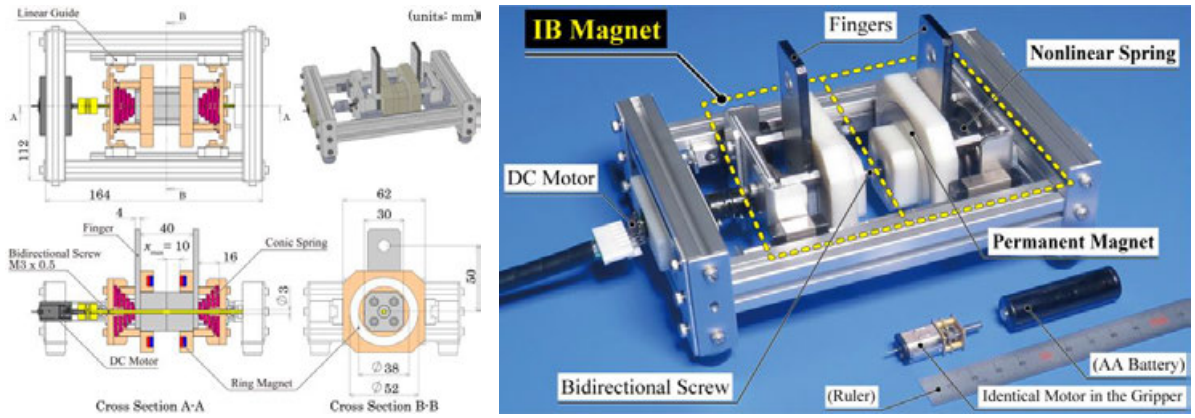

Fig. 90 Design and appearance of the prototype of the bi-parting IB magnet using the magnetic spring with a fixed clamping width.

TABLE V

SPECIFICATION OF THE PROTOTYPE OF THE BI-PARTING IB MAGNET USING THE MAGNETIC SPRING WITH A FIXED CLAMPING WIDTH.

Ring Magnet **NOR391**	*Outer Diameter*	54 [mm]	*Min. Clamping Width*	40 [mm]
	Inner Diameter	38 [mm]	*Max. Frame-Frame Distance*	35 [mm]
	Thickness	5 [mm]	*Stroke of the Control Rod*	10 [mm]
	Mass	40.8 [g]	*Total Mass*	860 [g]
DC Motor **Pololu-3053**	*No-Load Performance*	220 [RPM], 60 [mA] (at 12 [V])		
	Stall Extrapolation	176 [Nmm], 750 [mA] (at 12 [V])		
	Feed Speed	Approx. 5 [mm/s]		

Subsection III.4.3.2 Basic operation experiment of the bi-parting IBM gripper with a fixed clamping width

First, a basic operation of the proposed IBM gripper was conducted to demonstrate how it grasps an object, as shown in Fig. 91. A 4kg plastic bottle stuffed with lead beads was chosen as the target object to be lifted, and a pad made of ABS polymer was attached to each finger to adjust the clamping width. (a) Fingers on the frames were set apart. (b) The screw drove the fingers to the center until the frames met. (c)–(d) The control rods started to shift to x_{MAX} while increasing the clamping force by the magnetic attraction. (e) The clamping force achieved the maximum when the motor was stalled. (f) The gripper successfully lifted the target object without a power supply. The fundamental utility of the IBM gripper was successfully validated experimentally.

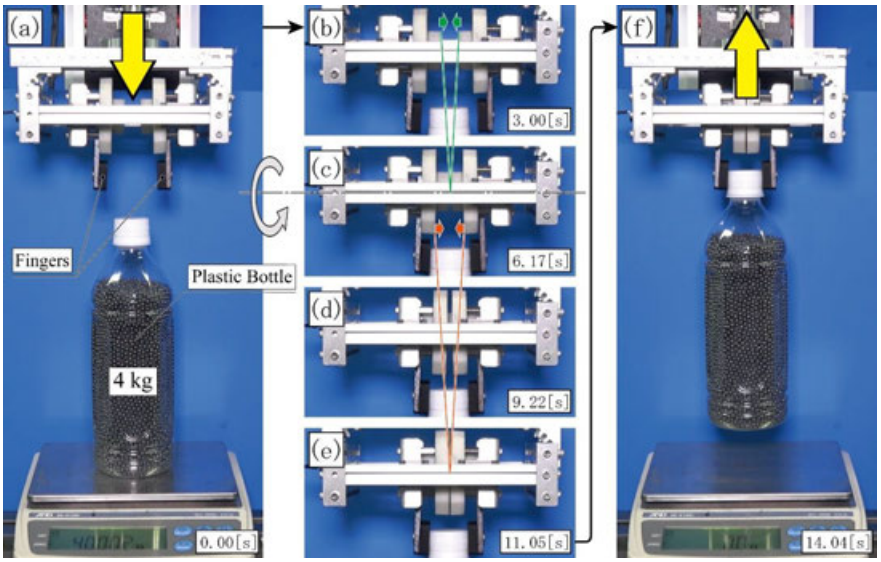

Fig. 91 Basic operation of the one-sided IBM gripper with a fixed clamping width.

Subsection III.4.3.3 Performance evaluation experiment of the bi-parting IBM gripper with a fixed clamping width

Next, the clamping force and power consumption were measured to evaluate the effects of force amplification and internal force compensation. The processes of grasping objects with variable widths were repeated ten times for each contrasted configuration listed in TABLE VI. Under configurations [C] and [D], the control rod was directly fixed on the frame and the finger without inserting spring. The motor actuated the screw only with its own driving force under [D].

TABLE VI

MECHANISM CONFIGURATIONS IN THE PERFORMANCE EVALUATION EXPERIMENT

		Magnet	
		with	*without*
Spring	*with*	[A] IB Magnet Gripper	[B] Variable Stiffness Gripper adjustable by spring
	without	[C] Screw Clamp assisted by magnet	[D] Screw Clamp

Fig. 92 shows the system constituents and the experimental procedure, in which a load cell (Kyowa Electric, LUR-A-100NSA) was mounted on one of the fingers to measure the compressive load applied by the gripper. The DC motor was driven by a constant power supply of 12 V, such that the current was proportional to the measured power consumption. (a) The fingers (bordered with white lines for better visibility) were 5 mm × 2 apart from each other. (b) The compressive load was slight when the frames met. (c) The control rods started to push in for x_{MAX}. (d) The clamping force gradually increased until the motor stalled. (e) The maximum clamping force at x_{MAX} was calculated as the average value in the timespan from 0.5 to 1.0 s after the current cutoff, waiting for stable values.

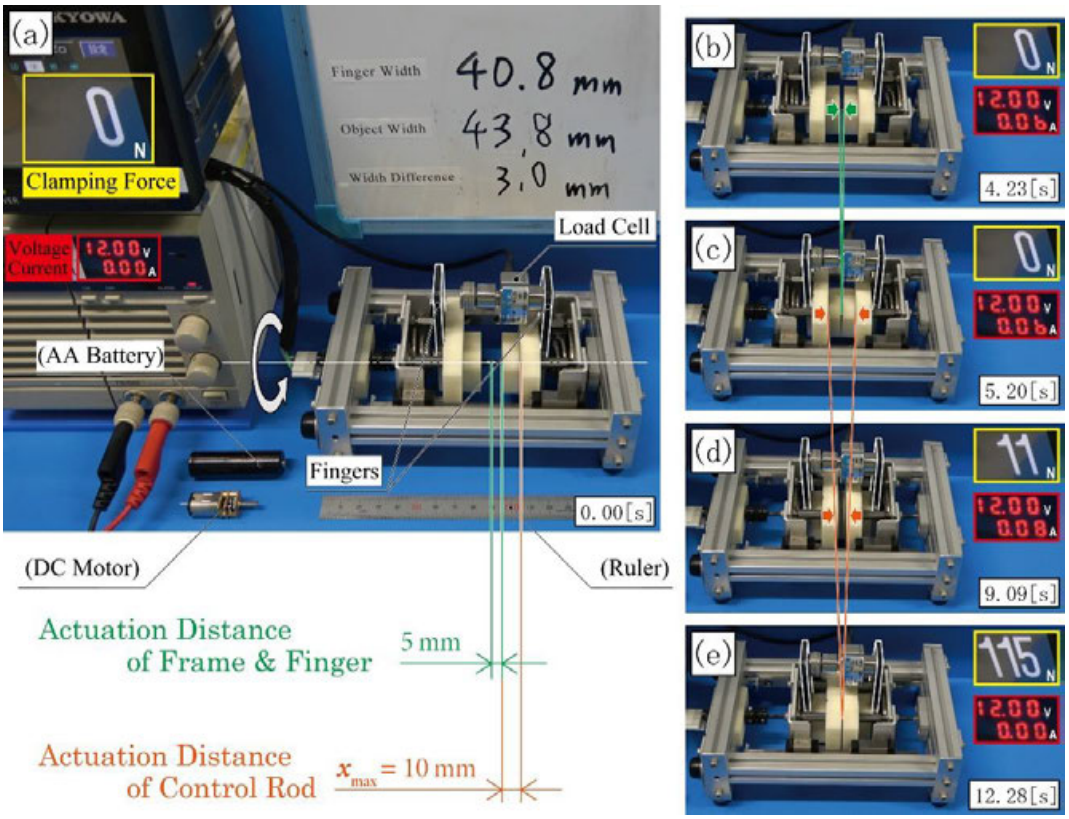

Fig. 92 System constituents of the performance evaluation experiment of the bi-parting IBM gripper with a fixed clamping width.

Fig. 93 displays the results of the measured clamping force and power consumption during the clamping operation under configurations [A] and [D], with a load cell 3 mm wider than the minimum clamping width.

Although the motor was controlled such that the finger was always actuated for 15 mm (shifting out the control rod for $x_{\mathrm{MAX}} = 10$ mm first and then out of the frame for 5 mm) when opening the gripper, the actuation distance of the closing finger exceeded it by approximately 0.4 mm. This seemingly overrun occurred because of the backlash of the motor gears and flexibility of the coupling connecting the motor and screw.

The maximum current corresponding to the stall current of the motor was stable at 0.84 ± 0.03 A regardless of the gripper configuration and object width. This indicates that the IBM gripper may replace the conventional screw clamps without upgrading the actuator with a higher rated current.

While closing the finger without the IB magnet [D], both the clamping force and the power consumption remained constant (the former at 0 N and the latter close to the ideal value of 0.7 W at no load operation [80]) in most part of the range of the actuation distance of the screw $y \lesssim 14$ mm. In sequence, they steeply increased as the control rods contacted each other and until the motor stalled, leaving less time to stop the screw for controlling the clamping force at an arbitrary value between zero and the maximum. The tendencies of the transitions of the clamping force and power consumption were similar in the opening (or releasing) operations.

In contrast, when clamping with the help of the IB magnet [A], the clamping force started increasing immediately after $y > 5$ mm when the frames of the IB magnets contacted each other (which also occurred with the power consumption). As the slope of the displacement–force characteristic became gentler, the IBM gripper could adjust its clamping force at a larger time allowance for control. The power consumption of opening operations generally exceeded that of closing operations because the spring force for compensation was designed to be no larger than the magnetic force that resists the thrust of the screw.

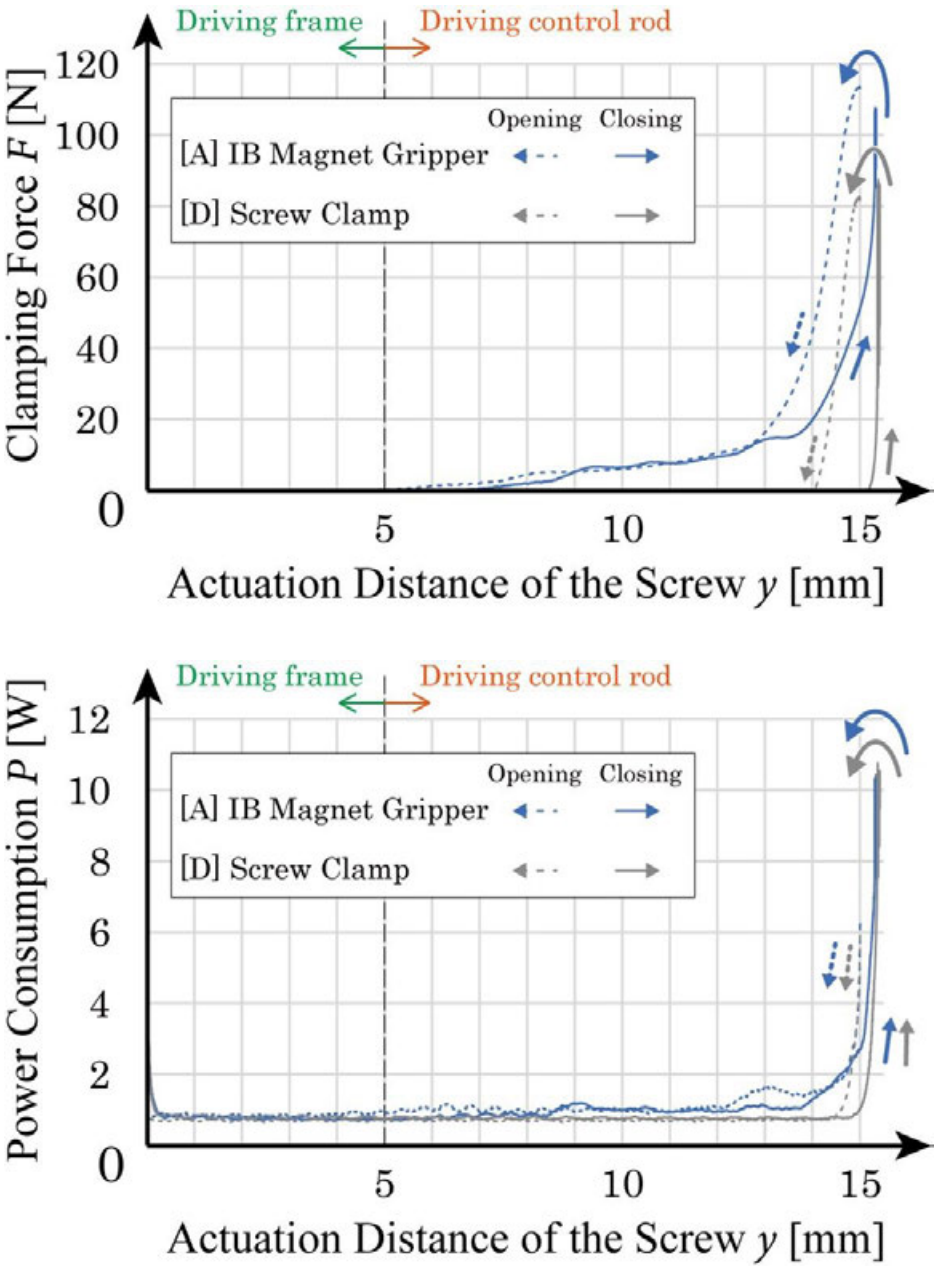

Fig. 93 Ten-times average transition in the clamping force and power consumption with respect to the displacement of the screw (which equals the counts of the encoder multiplied by the gear ratio and the lead of the screw).

Fig. 94 shows the results of the measured maximum clamping force during the clamping operation under configurations [A]–[D] with a load cell of variable widths. To a higher or lesser extent, the clamping force first linearly increased with the deviation of the object width from the minimum clamping width between the fingers δ, remained constant, and then gradually decreased for any configuration. The use of spring [B] reduced the minimum width deviation δ which provided the first measurable clamping force, whereas the use of magnet [C] resulted in an increase in the maximum clamping force compared to the values of the screw clamp [D]. Therefore, the IBM gripper [A] exhibited an intermediate property between [B] and [C]. The magnetic assistance on grasping was so strong that the motor could not re-open the finger and burned out once the magnets fully stuck to each other under configuration [C] (clamping supported by the magnet but not compensated by the spring) for any δ. This fact emphasizes the necessity of compensation when using permanent magnets.

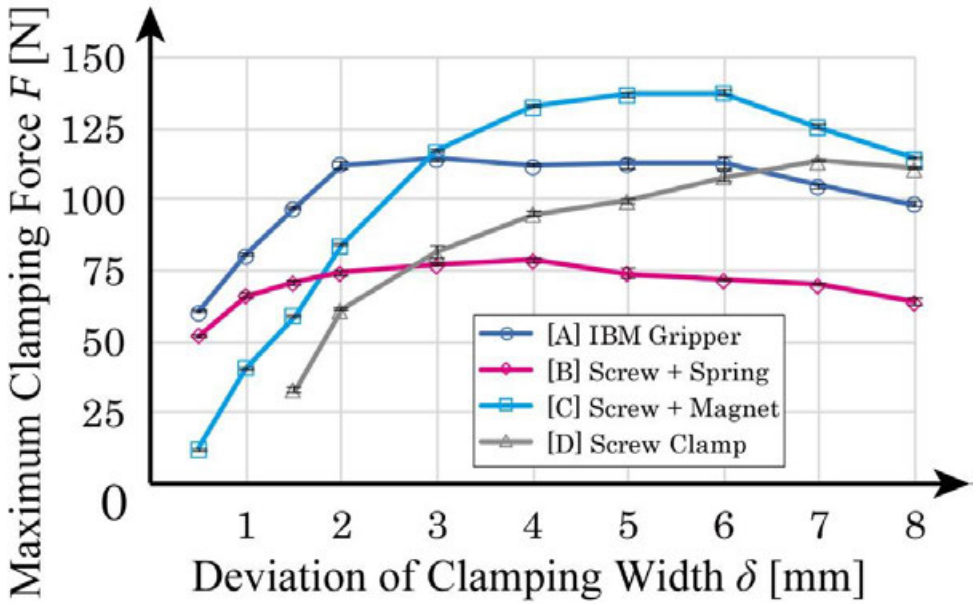

Fig. 94 Ten-times average maximum clamping force based on the deviation of the object width from the minimum clamping width of the fingers δ.

Likewise, the total energies as integrated power consumption of configurations except [C] (whose opening procedure could not be measured) are contrasted in Fig. 95. Without magnetic amplification under [B] and [D], the energy consumption roughly stabilized even when the width deviation δ increased. The energy consumption of the IBM gripper [A] first exhibited a likely value to [D] and then gradually increased in accordance with δ, indicating that the property of the IBM gripper became like that of the variable stiffness gripper aided by spring.

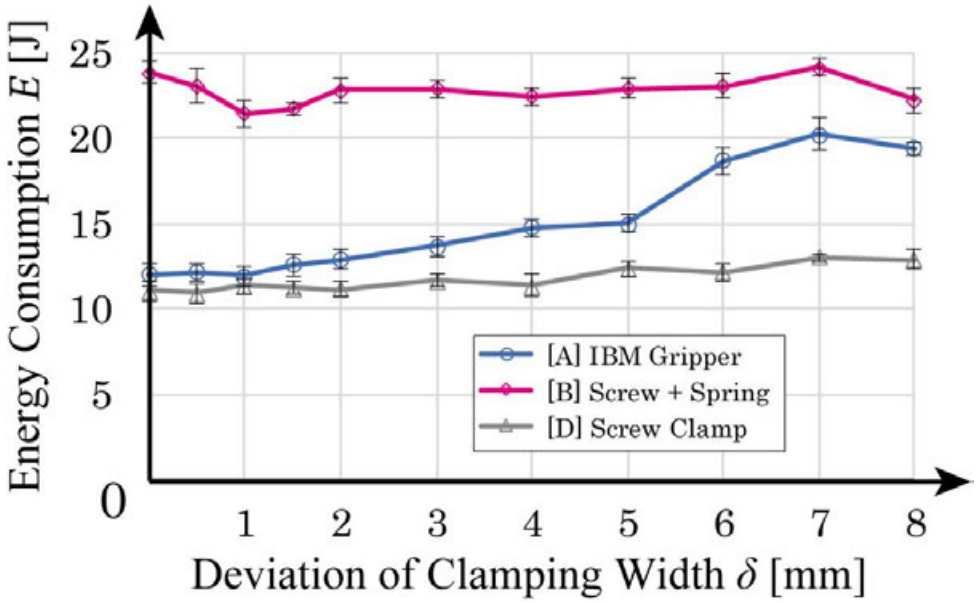

Fig. 95 Ten-times average energy consumption according to the deviation of the object width from the minimum clamping width of the fingers δ.

Fig. 96 shows the clamping efficiency of the gripper under configurations (except [C]), which is an evaluation index calculated by dividing the average maximum clamping force by the average power consumption. The efficiency of the IBM gripper first increased linearly to δ and then gradually decreased with a pinnacle at $\delta = 2$ mm, surpassing the value of the screw clamp in the range $\delta \lesssim 3.5$ mm.

The calculated ratio of efficiency [A] to [D] is the largest, with a value of 2.61 at $\delta = 1.5$ mm, in which the maximum clamping force is amplified by 292.2 %, Fig. 94, while keeping the increase in power consumption at 11.8 %, as shown in Fig. 95. If extrapolated, the ratio would have been even larger at $\delta \approx 1$ mm. This coexistence of force amplification by the magnet and compensation by the spring realizes a gripper to clamp an object with an arbitrary value of force controlled by an actuator with a smaller maximum output.

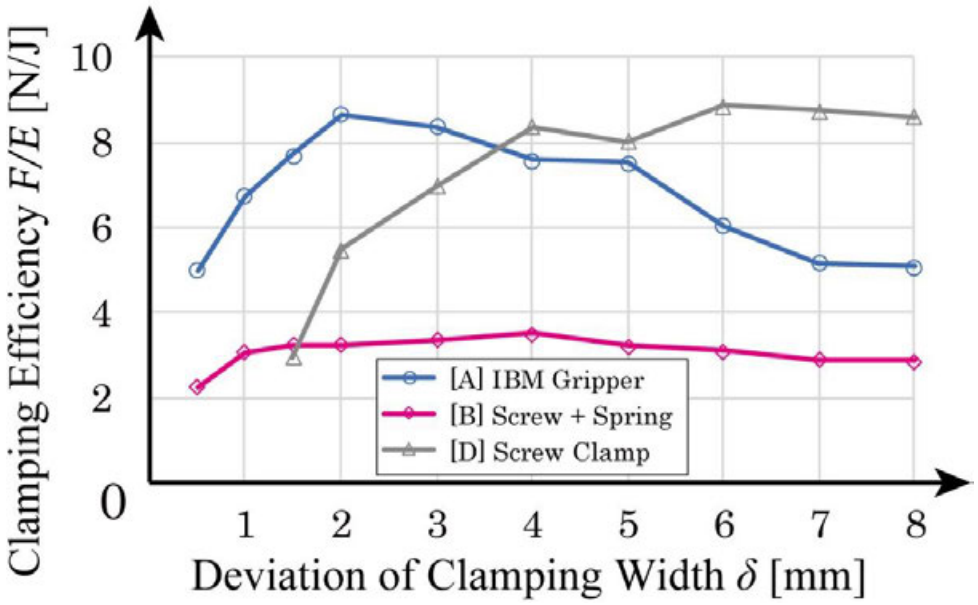

Fig. 96 Clamping efficiency according to the deviation of the object width from the minimum clamping width of the fingers δ.

In these ways, the results indicate that the effectiveness of the proposed principle and mechanism constitution of the IBM gripper was successfully validated.

Section III.4.4 Discussion on the characteristics of the bi-parting IBM gripper with the fixed clamping width

Subsection III.4.4.1 Feature of the proposed gripper

The result of the measurements suggests that the assistive pressing of the magnet by its attraction movement is especially effective in a situation in which the deviation width is small. In other words, the clamping force of the gripper under configuration [D] exceeded that of [A] when clamping an object with a large clamping width. The cause of this phenomenon can be regarded as the decrease in magnetic attraction when the deviation width is too large and thus the initial distance between the magnets when the fingers first touch the target object become too wide such that the actuator cannot receive enough assist to overcome the sum of the repulsive force of the compensation spring and the elastic force of the target object. The disturbed compensation of force resulted in the incomplete actuation of the control rods, whose magnets cannot get in contact even when the motor stalled. In that situation, the simple screw clamp [D] without springs that inhibit the clamping exhibits a better performance. In that sense, the aptitude of this version of the proposed IBM gripper is for a target object with a known width that has a high rigidity and thus allows only a small amount of elastic deformation.

Subsection III.4.4.2 Disturbance on compensation

As the spring is to cancel out the additional load on the actuator produced by the application of the magnet, the increase in power consumption from screw clamping would have been minimal if an ideal compensation could have been achieved. The possible factors that affected the compensation accuracy are as follows.

First, in the design procedure of the conical spring, the target characteristic of the attraction force of a pair of sampled magnets F_m was defined to be strictly constant as an ideal model. However, the characteristics of a hand-made spring, and those of a mass-produced magnet may fluctuate. Therefore, the compensation error of 11.4 % as an integrated deviation of the absolute force may have become larger owing to the individual differences.

Second, because the object has to be wider than the fixed minimum clamping width as long as the current design is used, the fingers first contacted the target object before the contact of frames was completed, as shown in Fig. 91 (c) and Fig. 92 (b). Then the magnets on the control rods started to shift in, resulting in a slight gap between the magnets at the end, as observed in Fig. 91 (e) and Fig. 92 (e). This gap made the magnetic attraction less than expected and caused the loss of power consumption as the excessive compensation by the spring disturbed the actuation. This is the major reason the range of δ was limited, in which the IBM gripper outperformed the screw clamp in terms of force–energy efficiency.

Subsection III.4.4.3 The potential for further development

As previously mentioned, the POC model in this study was not intended to grasp an object thinner than the fixed minimum grasping width. To acquire versatility while maintaining the force amplification and compensation effects, additional mechanical components are needed for the gripper to be used without minimum width restrictions, so that it can grasp any object. However, the current constitution is already applicable and beneficial in power conservation to factory lines and braking devices, in which the shape and material properties of target objects to be clamped are known or controlled. The latter is realized in Part IV.

Similar to the jumping mechanism [81] and the MR fluid gripper [82] proposed in the other studies by the author introduced in Chapter V.2 that incorporate the IB magnet as their magnetic flux supplier, the gripper showed a technological novelty in making use of the IB magnet as a built-in force amplifier. It was achieved by including the target object of attraction inside the structure, and by regarding the spring as a variable stiffness material that can arbitrarily adjust the internal rigidity of the mechanism and thus the transmittable maximum output force, unlike toggles and clutches that work only digitally. Likewise, it can be regarded as an adjustable passive compliance body applicable to a mechanism structure such as link of a robotic arm, as the stroke of the control rod works as deformable length of a damper. This property is profitable for gripper too as the compliance of the spring buffers the shock of the contact of rapidly actuated fingers with unignorable inertia that may break the object to be clamped.

These unprecedented applications of the IB magnet other than as an attraction device will contribute to the development of new academic area of magnetic mechanisms, in which permanent magnets are used for energy conservation of actuators by workload reduction.

Section III.4.5 Conclusion of Chapter III.4

In this chapter, to overcome the difficulties of previously used compensation methods when applied to a bi-parting constitution, a new conical spring was developed to manage both compactness and followability to the nonlinear characteristic of the magnet. The advanced prototype for POC successfully showed that its clamping force was amplified by the magnetic assistance by at most 292.2 % relative to the constitution with a single motored screw, while the power consumption of the DC motor increased by 11.8 %. The multiplication of the force–energy efficiency by 2.6 verified that the proposed gripper enables the use of actuators and current supplies that require less power.

For further development, a more efficient structure can be designed to achieve a higher compensation performance and miniaturization. In addition, a numerical model for estimating the exerted clamping force according to the object width and elasticity is established to develop a control law. Not restricted by a linear actuator in a parallel gripper, the applications of the variable stiffness mechanism achieved by internal compensation will be generalized as and expanded to the studies of labor-saving tools and robotic components such as a joint structure with passive compliance.

Chapter III.5 Linearization of the amplified clamping force of the IBM gripper relative to the object width through a clamping-width adjustment mechanism

Section III.5.1 Abstract of Chapter III.5

In this chapter, a new width adjuster using a lever to overcome the difficulty discussed in Chapter III.4 is discussed. To make the clamping force arbitrarily controllable and predictable, the adjuster eliminated the nonlinear influence of the object width on the clamping force by temporarily separating the interlocked movement of fingers, and they compensated magnets driven by a single actuator, while sustaining the spontaneous force amplification feature of the IBM gripper.

The prototype POC gripper revealed that the adjuster successfully linearized the width–force characteristic with an inclination of 0.15 N/mm, which is sufficiently insignificant, compared to the major output force of approximately 50 N. The force amplification effect coexisted with this phenomenon, such that the clamping force was amplified to 137.5 % while maintaining the energy consumption of the DC motor, and the force–energy efficiency was multiplied by 1.39. Thus, being drivable by a weaker, smaller, and lighter actuator, the gripper contributes to the extension of the operation time of robots with limited power supply.

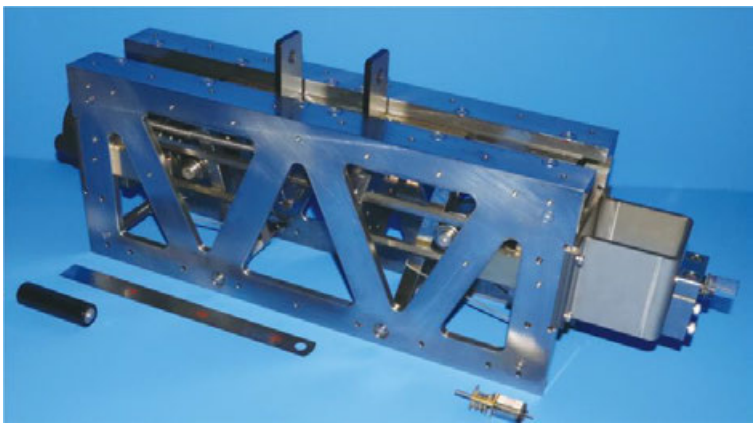

Fig. 97 Appearance of the prototype of the bi-parting IB magnet using the magnetic spring with the adjustable clamping width.

Section III.5.2 Elemental technology: clamping width adjustment mechanism

Subsection III.5.2.1 Problems of the IBM gripper without the clamping width adjustment mechanism

In the studies reported in Chapter III.3 and Chapter III.4, there were some challenges in the constitutions wherein the IB magnet is simply inserted between the finger and the actuator; the finger is simply fixed on the outer frame of the IB magnet. First, as depicted in Fig. 98 (a), the initial distance between the fingers defines the minimum clamping width of the gripper. If the object is even slightly thinner than the clamping width, the outer frames meet each other first before the fingers touch the object, resulting in a failure to clamp. Contrarily, if the object is extremely wider by ε than the clamping width, the initial distance of the magnet is insufficiently close to exert its attractive force, as described in Fig. 98 (b). Therefore, the actuator has to push in the control rods of the IB magnets without sufficient assistance, resulting in an increase in energy consumption. If the elastic restoring force of the target object exceeds the thrust force of the actuator, the shift-in of the control rods may stop before attraction is attained.

These problems occur because the compensation of the IB magnet works under the major premise that the approaching displacement of the magnet is always equal to the compression distance of the spring. Although the magnet and spring have the origin of the stroke on the outer frame, the rod begins to be pushed in depending on the finger contact to the object rather than the outer frame contact to the attracted surface as the magnet and spring are fixed on the identical rod. Furthermore, interactive deformation of the spring and target object occurs closely linked to the progression of the actuator, making it difficult to predict the nonlinear clamping force characteristics according to the input force, actuation displacement, object width, and elasticity.

The previous gripper had a strict limitation on clampable object width and a complexity of nonlinear characteristics. If the width of the target object is known and fixed, e.g., the products in a factory line and the wheel to be braked [13], these inconveniences can be ignored. However, even then, their clamping width should be able to realign to handle a variety of products and brake pad wear. Therefore, a new mechanism must be introduced so that the actuation of the compensation mechanism and the finger can be mechanically suspended when the fingers adjust the clamping width.

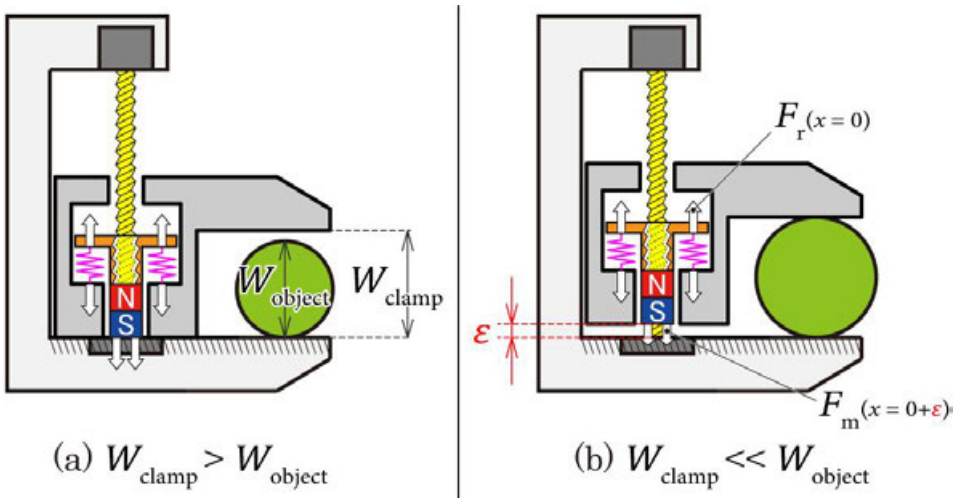

Fig. 98 Problems in the previous one-sided structure of the IBM gripper.

Subsection III.5.2.2 Previous research: classification of clutch mechanisms

Because the IB magnet itself does not have a load-sensitive feature, another degree of freedom would be required to adjust the clamping width to realign with an object. As illustrated in Fig. 99, the simplest configuration has a coarse movement lead screw with a larger pitch than a fine movement lead screw so that the finger can be actuated quickly until it meets the target object. To restrict the back drive due to the low reduction rate of the large lead, a kind of clutch mechanism such as torque diode that inhibits the reverse rotation is needed to resist to the force that works in the direction opening the gripper. However, as the motivation to develop the gripper with an IB magnet as a spontaneous reduction mechanism includes reducing the complexity of control, adding two actuators for coarse actuation and for releasing the clutch shall be avoided.

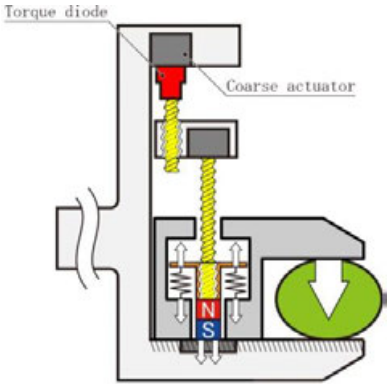

Fig. 99 Active clamping width adjustment by an additional actuator.

For the proposed gripper to be versatile for any application by solving the abovementioned problems, adding a new passive interlocking clutch mechanism is required that mechanically splits the IB magnet and the finger until the finger meets the object and then locks their relative position firmly when clamping is complete, so that the compensation of the magnet is independent of the absolute displacement of the finger. That is, the finger should be loosely connected to the IB magnet during its closing actuation, and the contact force of the target object must not be transmitted to the IB magnet. A linear one-way freewheel clutch, continuously activatable at any displacement and arbitrarily lockable by actuation, must be installed to realize such a separation of force transmission.

TABLE VII categorizes the features of major existing clutches and similar mechanisms. Spring-tensioned rollers or sprags were used to transmit either rotational or translational movement by jamming between the input and output surfaces. In the table, "forward" is defined as force or displacement transmission from input to output, and "inverse" as from output to input, generally called a back drive. Furthermore, "positive direction" means one direction of the input rotation or translation (e.g., clockwise) and "negative" in the reverse direction (e.g., counterclockwise). Observing the table, the mechanism that fulfills features required by the IBM gripper is unique in that it allows both forward and inverse transmission in the positive direction only when the outer frame detects its origin on the fixed finger. The wire gripper [83] illustrated in Fig. 101, a metal bracket to hang canvas art on a wire, has a feature to release the jamming state but is not applicable to the proposed gripper as it requires a feature to activate jamming.

TABLE VII
CATEGORIZATION OF CLUTCH MECHANISMS

	One direction only	Both positive & negative direction
Forward transmission only	Linear clutch (one-sided) [84] Force diode (one-sided) [85]	Linear clutch [86] Force diode [85] Torque diode [87]
Forward and inverse transmission	Sprag clutch Wire gripper [83]	(Rigid coupling)

As depicted in Fig. 100, the wedge was found to be unsuitable as its follower invaded the gap between the wedge and the active finger rolled along the wedge, feeding the finger in the reverse direction of the clamping motion. Furthermore, the sprag cannot be pinned at an arbitrary point as the pressing force from the IB magnet partially circumvents the finger via the positioning pin. This clutch can be used not only with the IB magnet, but also with other compensation mechanisms, such as those that balance a weight to a spring and output its repulsive force as a tension load.

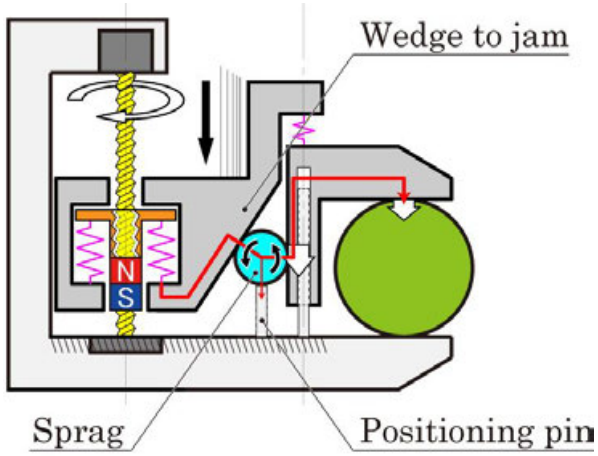

Fig. 100 Width adjustment mechanism composed of a sprag and wedge.

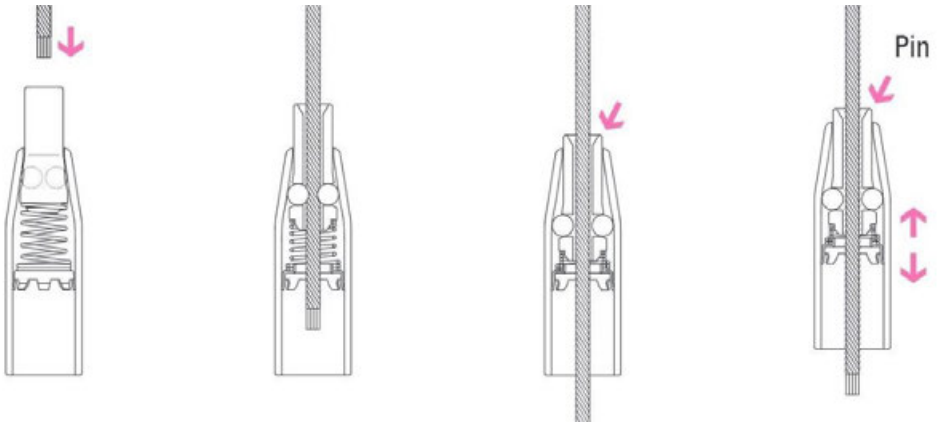

Fig. 101 Wire gripper that fixes its position on the inserted wire. It can actively release the lock when the pin is pushed [88].

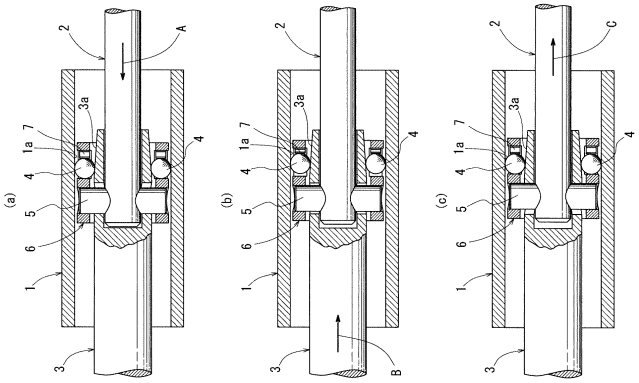

Fig. 102 Linear clutch that hinders a reverse input, but only in one way [84].

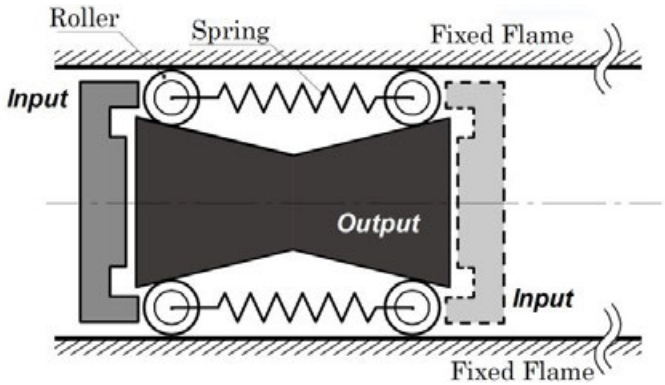

Fig. 103 Force diode that prevents inverse bidirectional input [85].

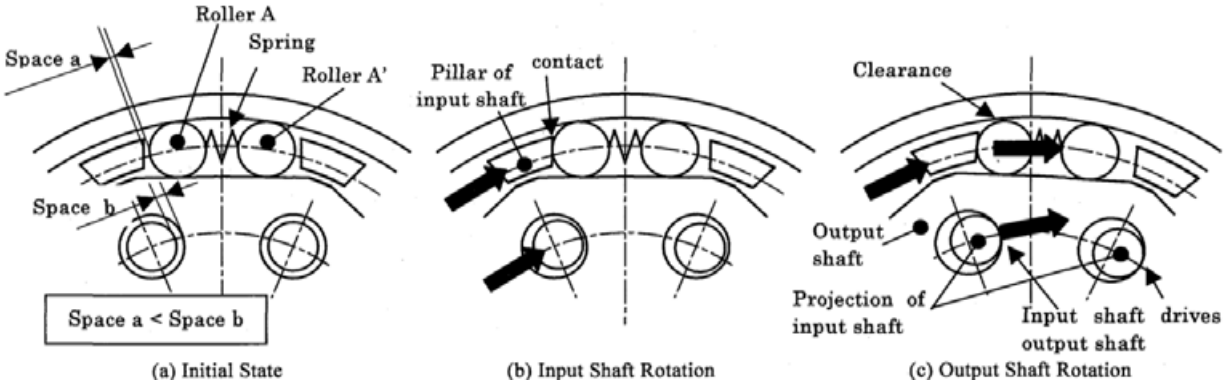

Fig. 104 Torque diode that transmits rotation only in one direction [87].

Subsection III.5.2.3 Proposed principle: width-adjustment mechanism using a lock lever

Unlike existing clutches in TABLE VII that use wedges and sprags to jam, herein, a pair of lever and follower were selected. Fig. 105 depicts the IBM gripper with a newly devised width adjustment mechanism in which a lock lever and a circular lever follower are inserted between the outer frame of the IB magnet and the active finger. If they are rigid bodies, the lever and follower stay at a certain point, independent of the object width and pressing force. Therefore, the spring of the control rod can begin to get compressed at the identical displacement of the IB magnet in all instances. In this manner, this clutch enables the IB magnet to extract a pressing force from its fixed end of the spring, which was impossible as the spring had to be pinned in a designated position to sustain compensation.

The mechanism operates as follows. (a) Starting from the initial position, both the IB magnet and the active finger, loosely connected to the IB magnet via an adequately weak buffer spring, approach the target object. The lever is now disengaged by a separation spring and does not inhibit the actuation of the finger as the lever follower is still free. (b) Once the finger is in contact with the object, it stops further progress, resulting in the single actuation of the IB magnet. The buffer spring continues to get compressed to comply with the object width. (c) Next, when the outer frame of the IB magnet comes in contact with the lever follower, it starts to stretch the lever to lock the position of the finger relative to the outer frame of the IB magnet. The magnet approaches its attraction target with its designed actuation distance to be compensated. (d) Finally, the control rod of the IB magnet starts to move relative to the outer frame, increasing both the attractive force of the magnet and the repulsive force of the spring, resulting in the continuous increase of the force on the lever follower and thus the output clamping force.

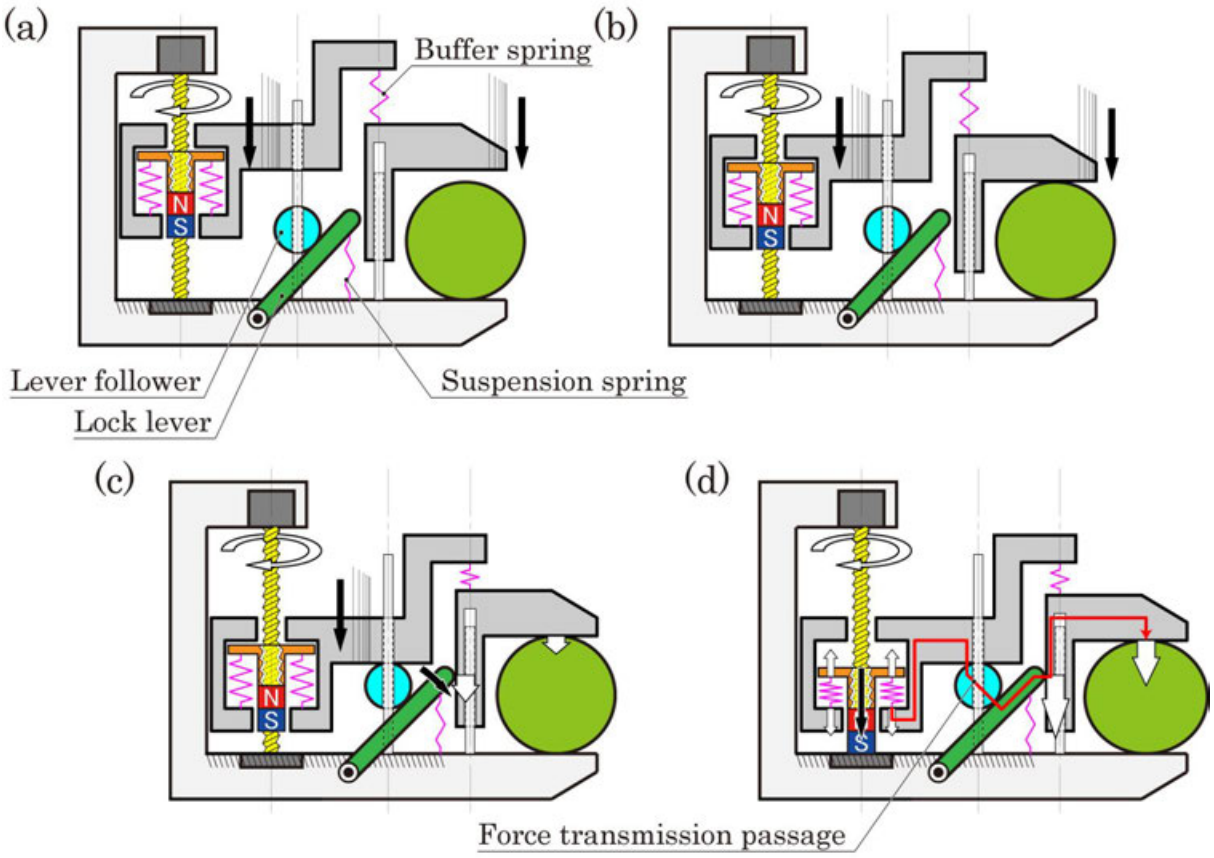

Fig. 105 Principle diagram of the IBM gripper with the width adjustment mechanism comprising a lock lever and a follower to push it down.

Section III.5.3 Embodiment of the bi-parting IBM gripper with the adjustable clamping width

Subsection III.5.3.1 Design and development of the bi-parting IBM gripper with the adjustable clamping width

Fig. 107 shows the dimensions of the prototype model of the proposed IB magnet, whose specifications are listed in TABLE VIII. To prevent the increase in the mechanism volume, the axes of linear constraints, the bidirectional screw of the IB magnet, and the linear guide of the lever follower are arranged to coincide. Further miniaturization will be held in future to obtain a practical size and mass for integration to a robotic system. The distance between the contact surface of the finger and the axis of the lever is adjusted by inserting shims into the gap δ. Furthermore, the single conical coil spring with a varying diameter, and the pitch was customized to reproduce the nonlinearity of the magnetic attraction, unlike a bulky compensation spring in a conventional IB magnet comprising multiple linear springs that are activated stepwise to follow the nonlinearity approximately.

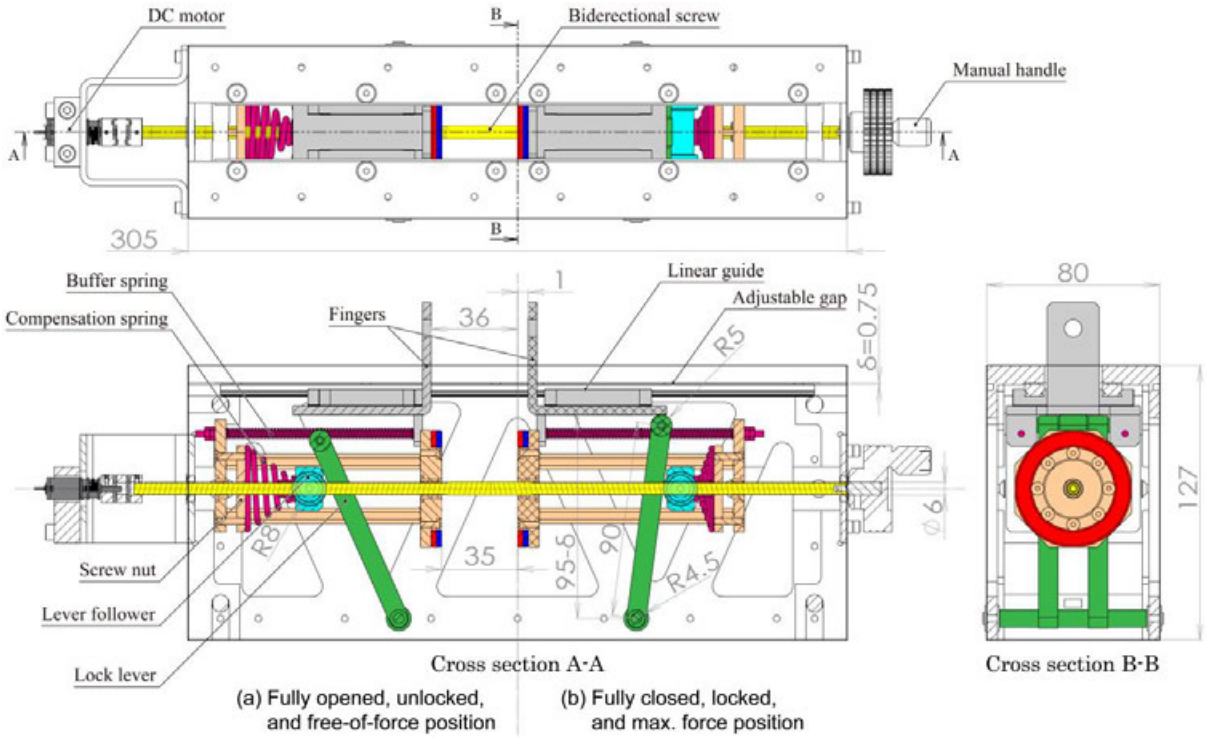

Fig. 106 Design of the prototype of the bi-parting IB magnet using the magnetic spring with the adjustable clamping width.

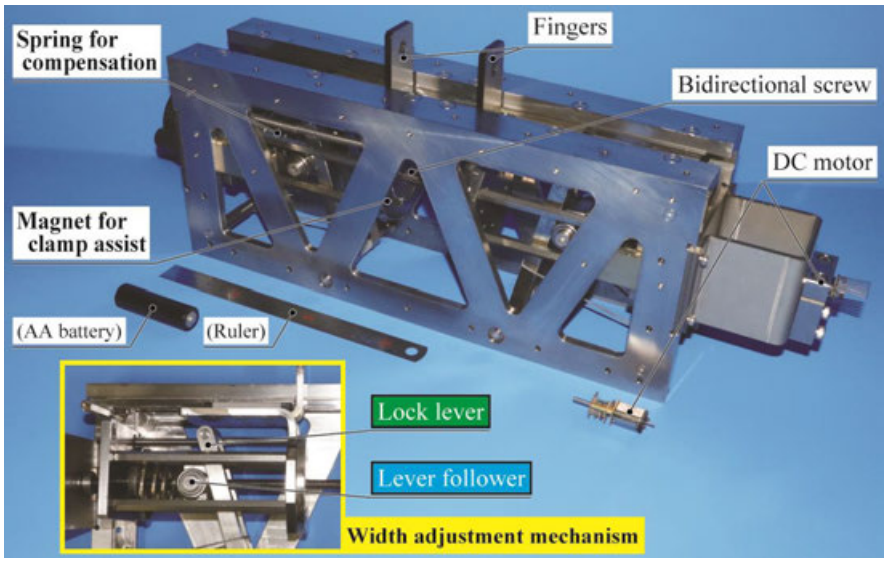

Fig. 107 Appearance of the prototype of the bi-parting IB magnet using the magnetic spring with the adjustable clamping width.

TABLE VIII

SPECIFICATION OF THE PROTOTYPE OF THE BI-PARTING IB MAGNET USING THE MAGNETIC SPRING WITH THE ADJUSTABLE CLAMPING WIDTH

Ring Magnet **NOR391**	*Outer Diameter*	54 [mm]	*Min. Clamping Width*	2 [mm]
	Inner Diameter	38 [mm]	*Max. Clamping Width*	72 [mm]
	Thickness	5 [mm]	*Stroke of the Control Rod*	35 [mm]
	Mass	40.8 [g]	*Total Mass*	5.7 [kg]
DC Motor **Pololu-3057**	*No-Load Performance*	35 [RPM], 80 [mA]		at 12 [V]
	Stall Extrapolation	176 [N·mm], 750 [mA]		
	Feed Speed	Approx. 1.0 [mm/s] with M6 screw		

Subsection III.5.3.2 Performance evaluation experiment of the bi-parting IBM gripper with the adjustable clamping width

First, a basic operation experiment was conducted using the prototype of the proposed IBM gripper. Fig. 108 shows the system constituents and the experimental procedure, in which a load cell (Kyowa Electric, LUR-A-100NSA) was mounted on one of the active fingers to measure the compressive load to evaluate the effects of force amplification and internal force compensation. The DC motor was driven by a constant power supply of 12 V so that the current was proportional to the power consumption. The processes of clamping objects with widths $38.5 \leqq W_{\mathrm{obj}} \leqq 63.5$ mm, incremented by 5 mm by replacing stainless screws with corresponding lengths, were repeated five times for each contrasted configuration with and without magnetic attraction. Each IB magnet was initially arranged $x_{\max} = 35$ mm apart from the center, resulting in the initial distance between fingers $W_{\max} = 72$ mm.

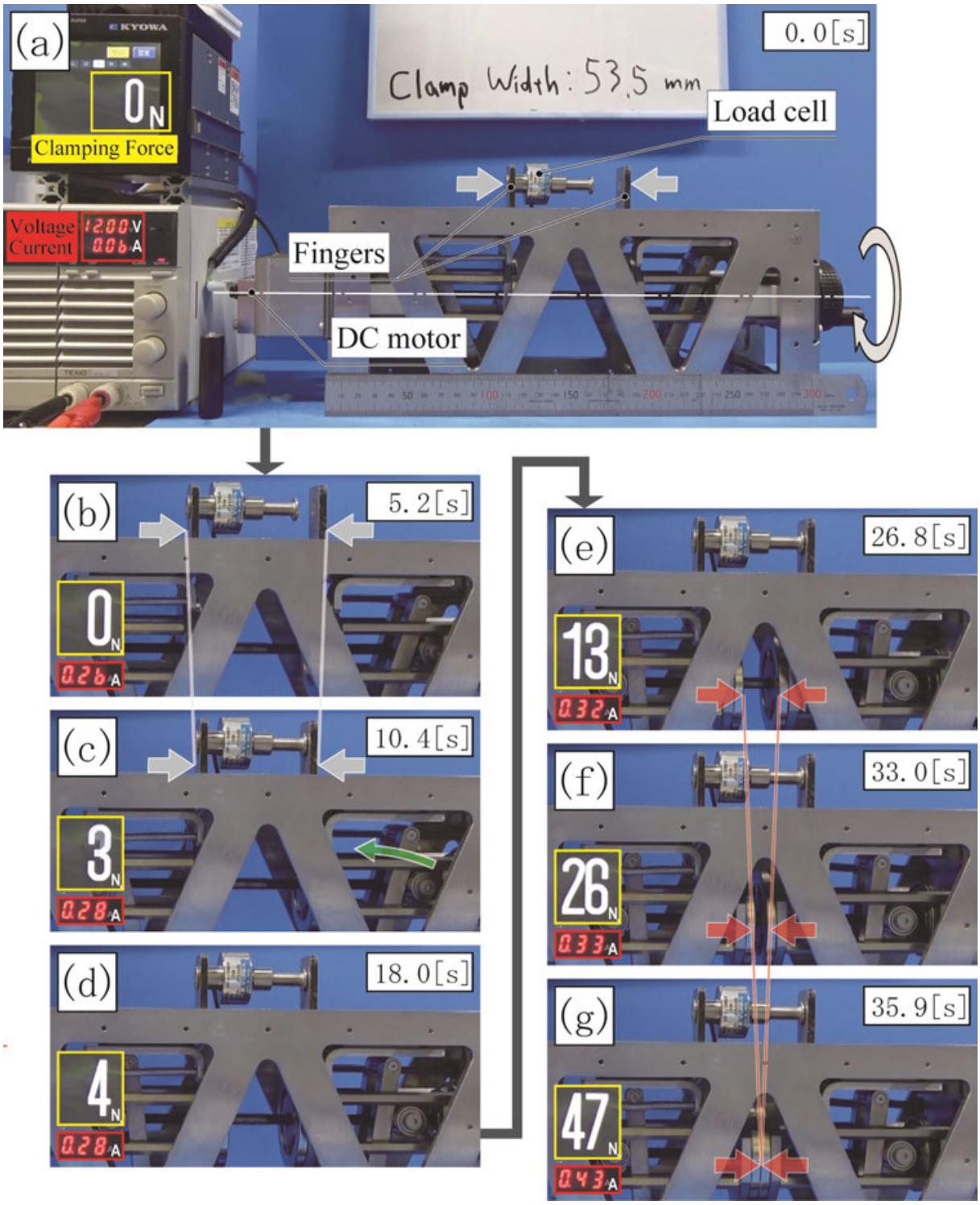

Fig. 108 Experimental system and the operation process of the prototype model of the IBM gripper. (a) The fingers were set 72 mm apart. (b) The screw began driving the control rods and fingers connected to them to the center. (c) The fingers stopped further actuation once they met the object. Instead, the buffer springs began to get compressed and the lock levers to lean against the fingers. (d) As the lock levers contacted the fingers, the control rods were ready to transmit force via the compensation springs. (e)–(f) As the magnets approached each other, both the magnetic attractive force and the spring repulsive force increased, resulting in a stepless, gradual increase of the clamping force.

Fig. 109 and Fig. 110 display the typical transitions of the clamping force and power consumption measured with and without magnetic assistance when (a) closing and (b) opening the fingers to clamp the load cell with $W_{\mathrm{obj}} = 53.5$ mm.

During closing, the clamping force first increased to an almost constant value, approximately 5 N, when the fingers contacted the load cell at the displacement $x = x_{\max} - (W_{\max} - W_{\mathrm{obj}})/2 = 25.75$ mm. It kept slightly increasing in linearly, until the width adjustment by the buffer spring was completed. When the lever was first pushed onto the finger by the control rod via the compensation spring at $x = x_{\max} - X_{\mathrm{f}}$ (discussed in Subsection III.5.4.1), the lever locked the position of the finger on the IB magnet. Then, as the spring further compressed, it transmitted the counter force to the lever follower, gradually increasing the clamping force. As the actuator can stop the position at an arbitrary displacement, the gripper can exert any desired value of the clamping force from zero to the maximum in an analog (or stepless) manner, as intended. With the aid of the magnets, the clamping force after the compensation spring was compressed became larger, while the power consumption remained almost unchanged from that of the constitution without magnets. This can be regarded as even slightly less due to the deviation of imperfect compensation, in which the internal force of the IB magnet that assists the actuation is oriented to the center of the gripper.

During opening, the clamping force is relieved gradually by releasing the compensation spring. After decreasing to zero, the clamping force is increased again as the lever releases the finger that clamps the object loosely with its buffer spring. The power consumption after inrush current at the beginning drops and then increases because the compensation is adjusted to be most precise at the origin where the attraction is originally the largest. The internal force after then inhibits actuation to some extent, contrary to the property observed during closing.

With the IB magnet, a 1 mm-periodic fluctuation of the power consumption was observed. It corresponds to the actuation by a lead screw with a pitch of 1 mm, whose thread stuck the edge of the dry bush of the magnet holder inclined due to gravity. To suppress this phenomenon, the bush shall be replaced with a longer one or one with a stricter fitting.

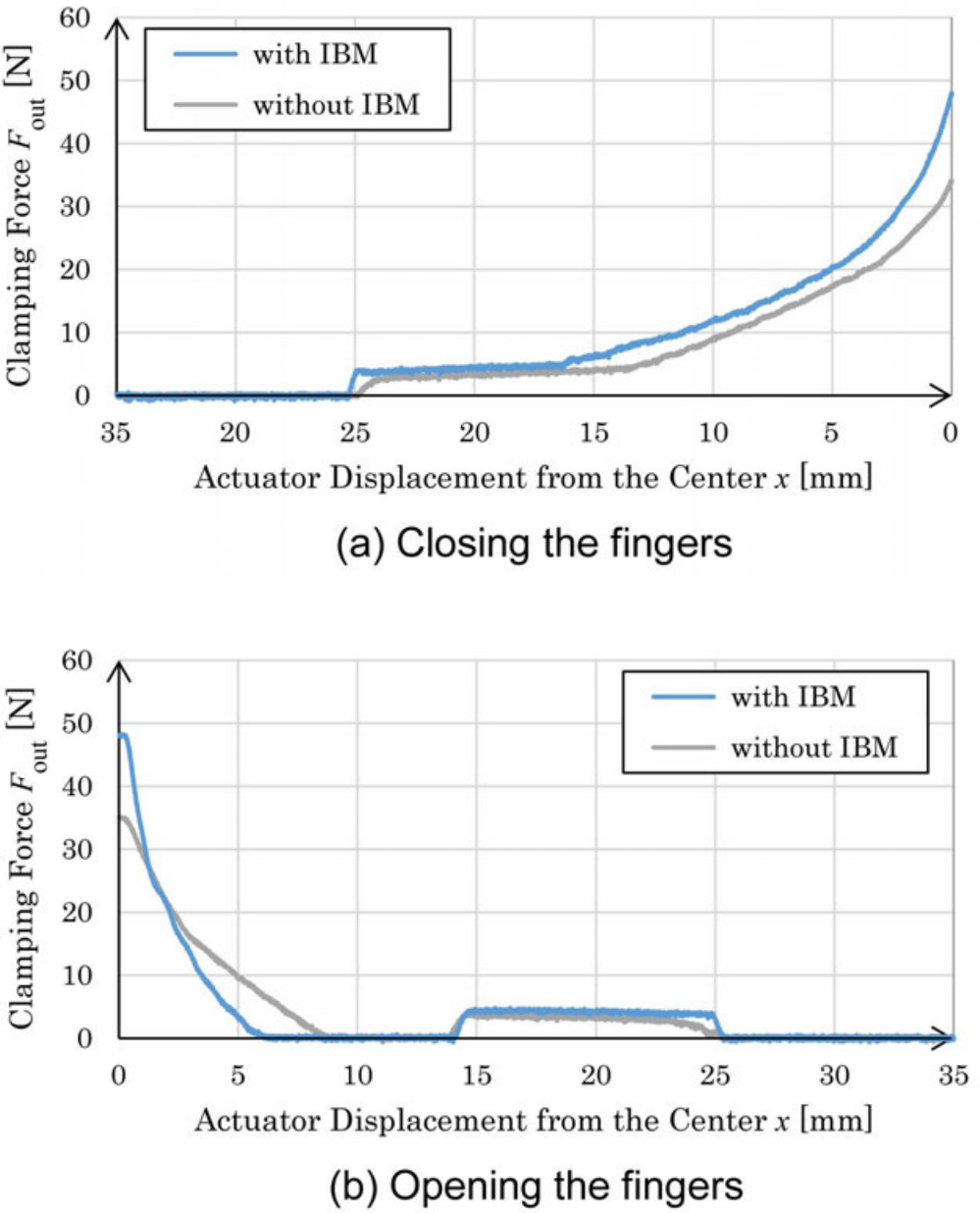

Fig. 109 A typical transition in the clamping force F_{out} of the IBM gripper with respect to the displacement x of the control rod of the IB magnet.

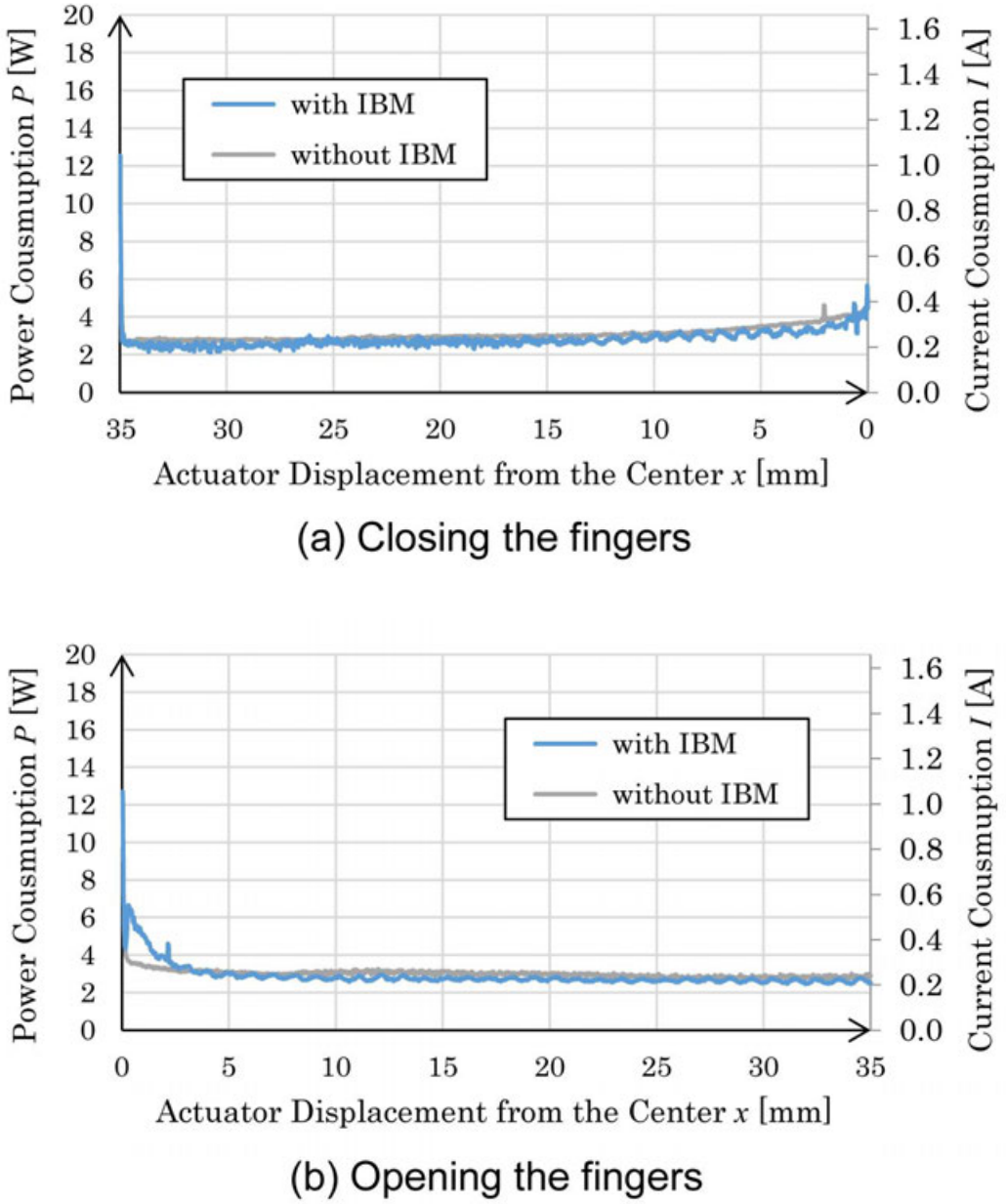

Fig. 110 A typical transition in the power consumption P of the IBM gripper with respect to the displacement x of the control rod of the IB magnet.

Fig. 111 illustrates the characteristic of the maximum clamping force characteristic with respect to the object width with and without magnetic assistance. F_{ave} is defined as the average value of the force measured for 1.0 s in a static state after the closing and the current cut off, while F_{max} is the maximum value recorded during the closing operation.

Both F_{ave} and F_{max} show similar increasing transitions for each constitution, while the former exceeds the latter by less than 1.9 % for any condition (Let F_{ave} represent the maximum clamping force hereafter). The existence of the magnet increased F_{ave} to 137.5 % in average, verifying the effectiveness of the magnetic assistance in generating clamping force by its attraction movement.

Notably, F_{ave} and F_{max} show linear characteristics with inclinations around 0.15 N/mm, 0.3 % of the major clamping force 50 N and corresponding to the nominal theoretical range 0.131-0.160 N/mm of the spring constant of the buffer spring for width adjustment. By selecting an even weaker buffer spring, the dependence on the clamping width can be reduced further. This property of consistency is important for a gripper to be easily predictable and thus controllable.

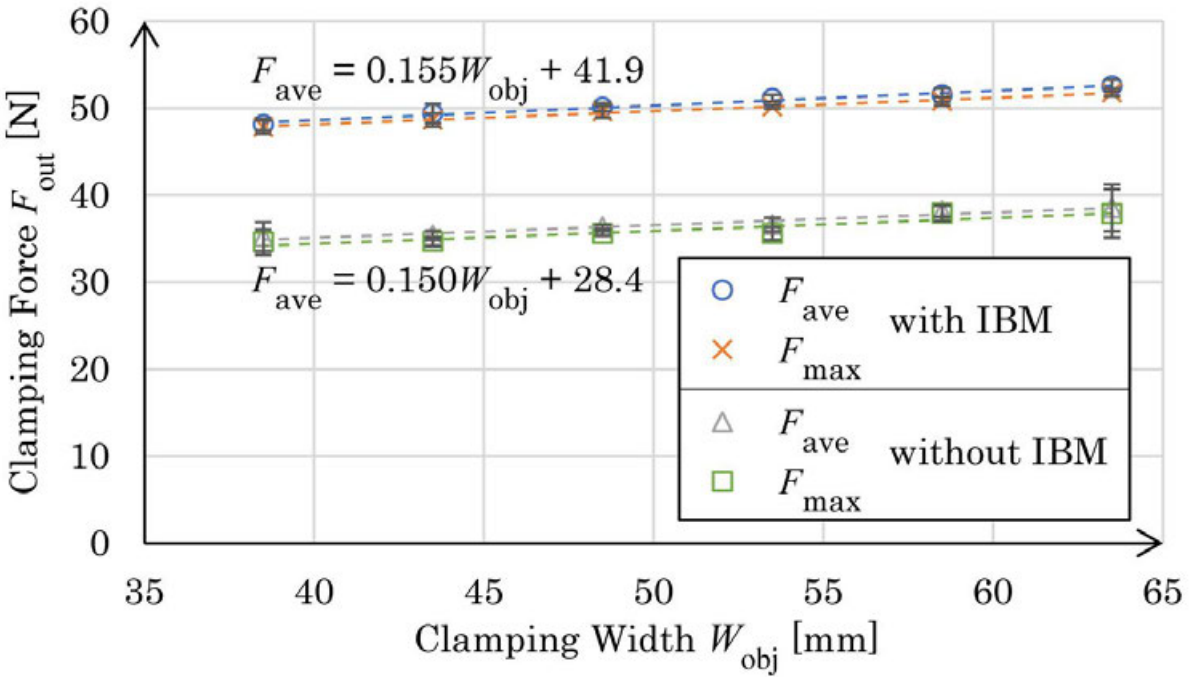

Fig. 111 Five-time average maximum clamping force max(F_{out}) exerted by the IBM gripper with respect to the clamping width W_{obj}.

Fig. 112 contrasts the graphs of Fig. 111 (F_{ave}) and Fig. 94 ([A] and [B]). The IBM gripper discussed in Chapter III.4 with a fixed minimum clamping width of 40.3 mm had a width–force characteristic with a nonlinearly convex property in a tolerable clamping width range of 8 mm. Conversely, the figure emphasizes that the newly developed IBM gripper with the adjustable clamping width acquired the obviously steady characteristic in a much wider tolerable clamping width range.

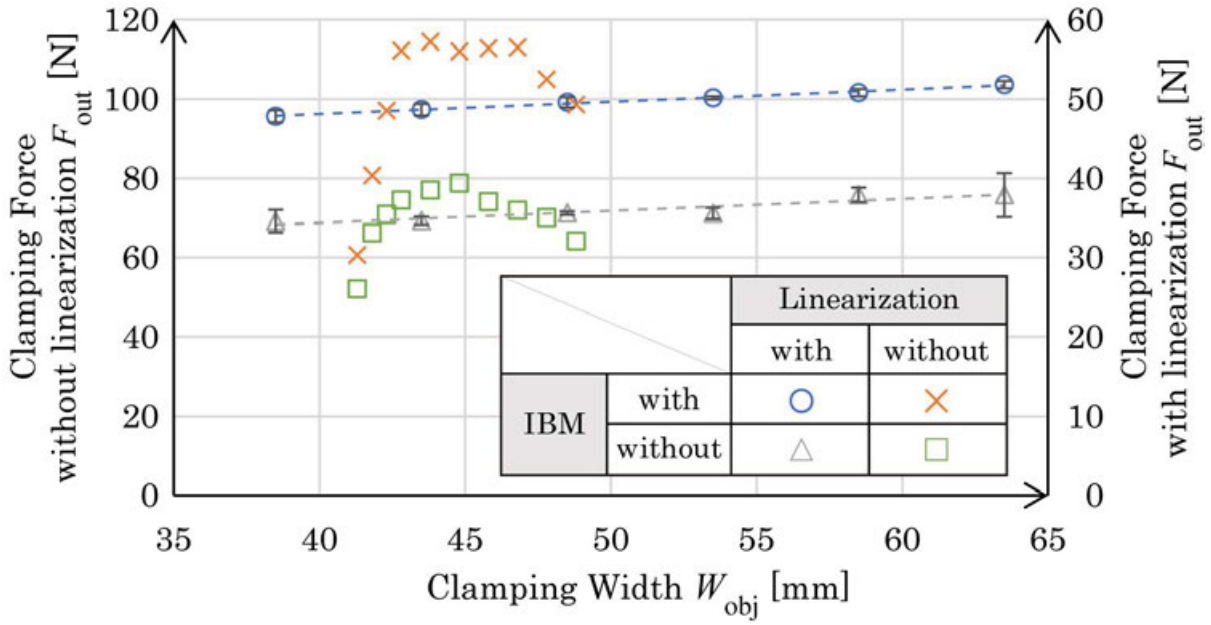

Fig. 112 Average maximum clamping force by the IBM grippers with and without the adjustable clamping width, with respect to the clamping width W_{obj}. Here, $W_{obj} = \delta + 40.3$ mm for the graphs from Fig. 94.

Fig. 113 shows the (a) energy consumption as an integration of the power consumption and (b) duration, measured separately during closing, opening, and the entire process. As visually observed in Fig. 10, the compensation mechanism slightly decreased E_{close} and increased E_{open} so that their sum E_{total} was barely affected: it just decreased by 0.8%.

Contrary to the clamping force, both energy and duration showed unsteady but similar transitions, fluctuating with deviation less than 4.5% for energy and 1.7% for duration. This observation implies that these characteristics are affected by other environmental factors such as lubrication and motor heating rather than the clamping width. The reason why these characteristics resemble each other is simple: the longer the duration, the more the power consumption.

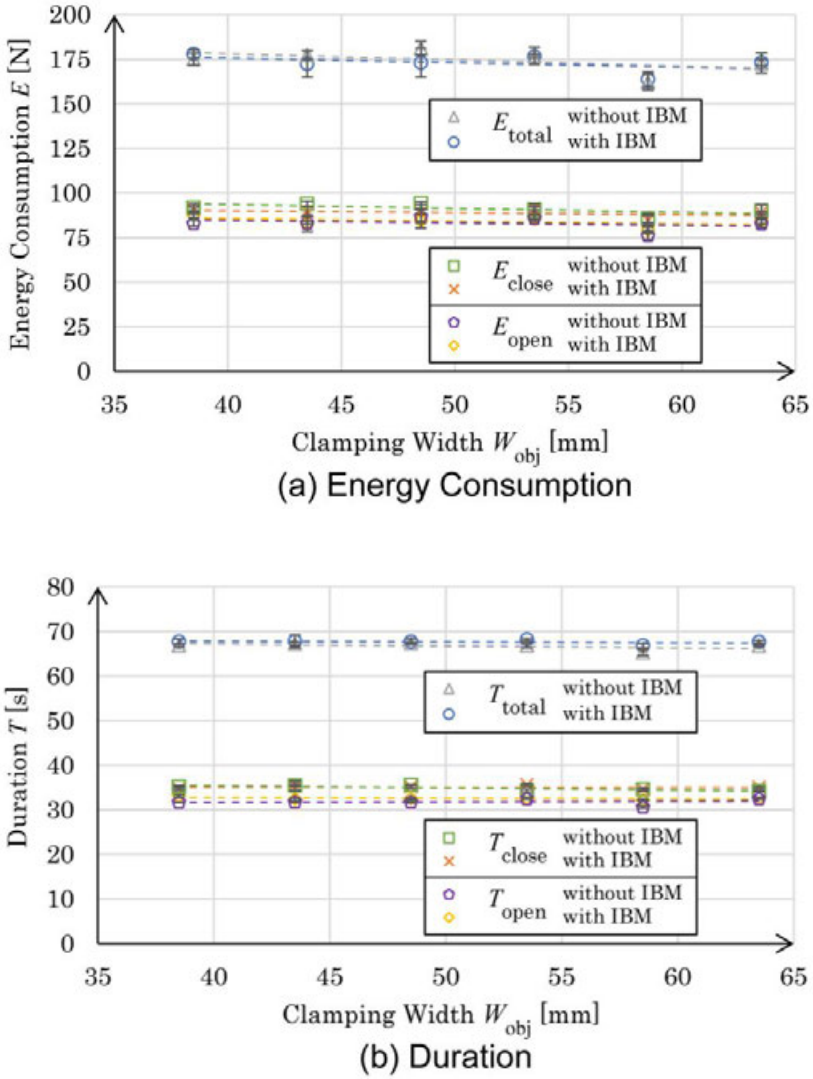

Fig. 113 Five-time average energy consumption E and duration T recorded on the IBM gripper with respect to the clamping width W_{obj}.

Fig. 114 depicts the performance efficiency of the gripper, an index defined by the maximum clamping force F_{ave} divided by the total energy consumption E_{total}. As the F_{ave} was linear to W_{obj} and the E_{total} was independent of W_{obj}, the graphs of their quotient also show linear characteristics. For a better intuitive understanding, average results of F_{ave} and E_{total} in the range of W_{obj} are compared in Fig. 115. While the clamping force was amplified by the magnetic attraction, an additional external force required by the control rod to the actuator to push in and pull out the magnet against the attractive force was cancelled out by the repulsive force of the compensation spring, resulting in multiplication of the force–energy efficiency by 1.39 in the mean.

In these ways, the experiment successfully validated the principle of the proposed gripper by demonstrating characteristic-steady, force-amplified, and energy-efficient clamping ability against objects of various widths.

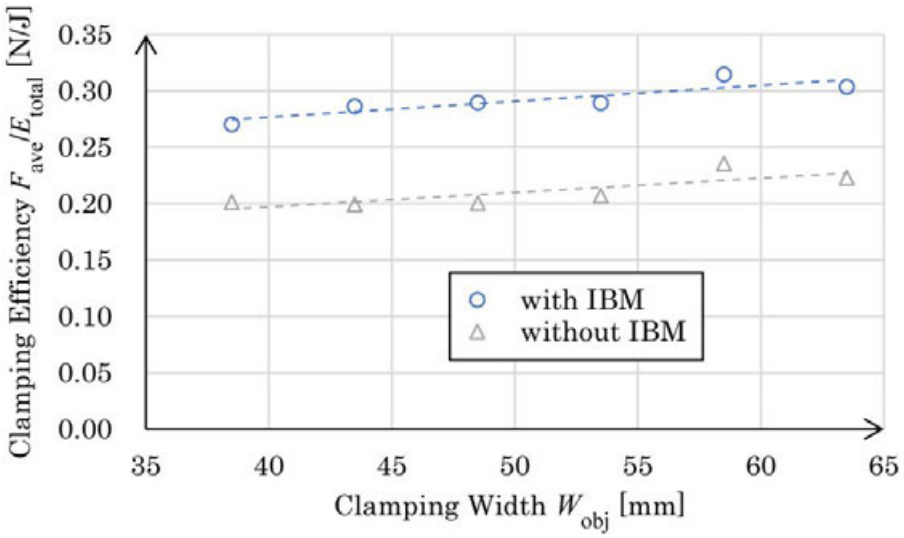

Fig. 114 Clamping efficiency of the IBM gripper defined as the average maximum clamping force F_{ave} divided by the average energy consumption E_{total} with respect to the clamping width W_{obj}.

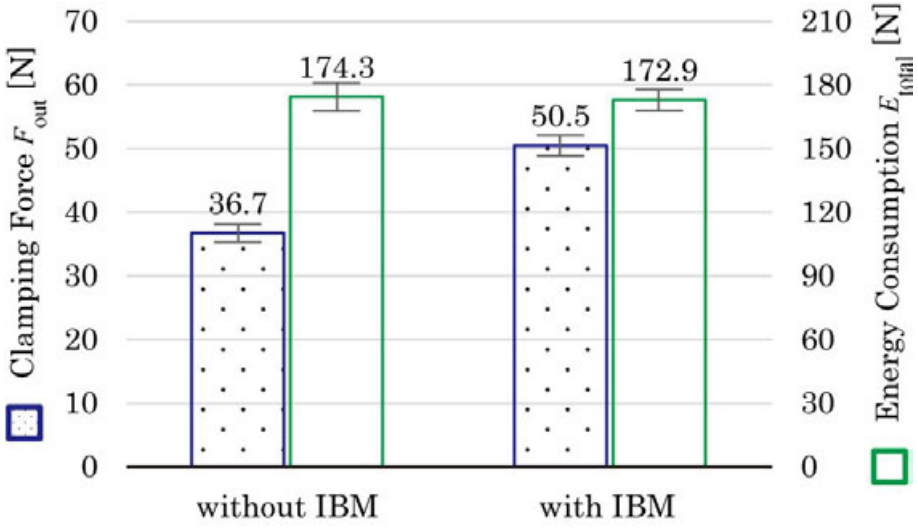

Fig. 115 Comparison of the results of measuring the maximum clamping force F_{ave} and energy consumption E_{total} under constitutions with and without IB magnet.

Subsection III.5.3.3 Transmission Efficiency of the Lever–follower system

The output clamping force was measured in relation to the input pressing force applied to the lever follower to derive the transmission efficiency of the width adjustment mechanism. The system constituents are shown in Fig. 116, wherein the gripper is installed vertically in the material testing machine (Instron, 3343). The finger below is fixed at the center of the system, and the finger above is free of mechanical restraints except the linear guides. The moving part of the material testing machine is equipped with a force transducer (Instron, 2516-104) with the capacity of 500 N to regulate the constant input force $25 \leqq F_{in} \leqq 300$ N incremented by 25 N, and a cylindrical rod to push down the lever follower. The gripper clamped the load cell with W_{obj} = 38.5, 43.5, and 48.5 mm five times for each configuration. Furthermore, for evaluating the effect of friction on the transmission, a friction-improved version of the lever–follower system was inspected. As contrasted in Fig. 117, its contact surface of the finger to the lever was matt-finished by rough electrical discharge machining, and the tip shaft of the lever that contacts the finger was substituted with one with straight knurling.

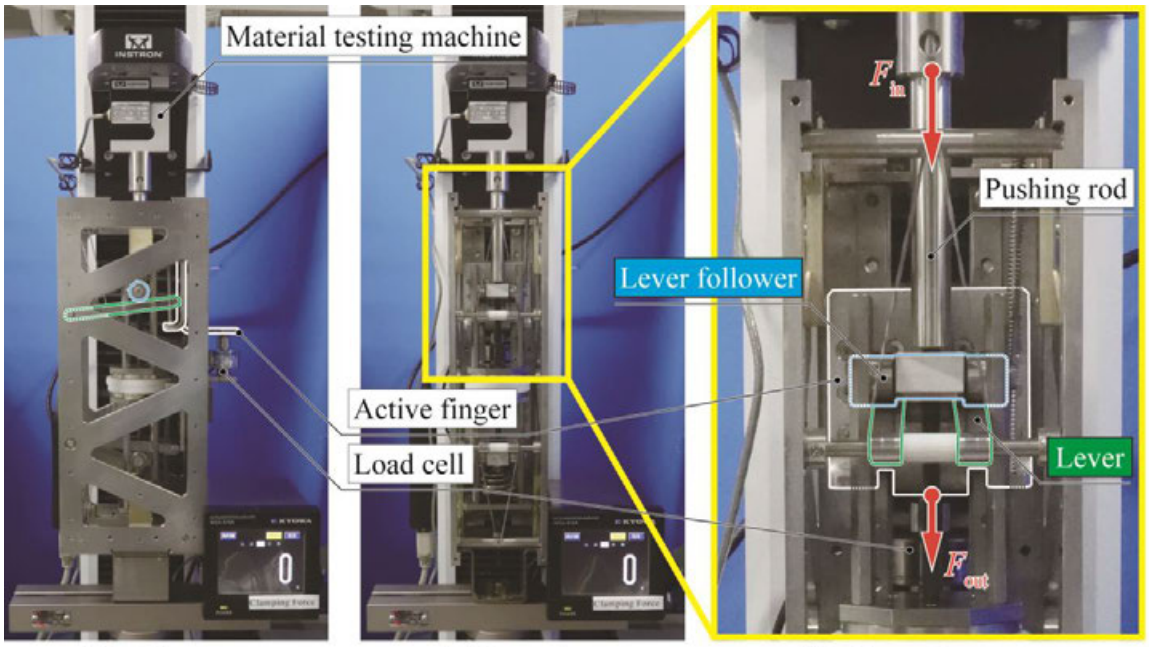

Fig. 116 Experimental system of the IBM gripper for measuring the transmission efficiency of its lever–follower clutch system.

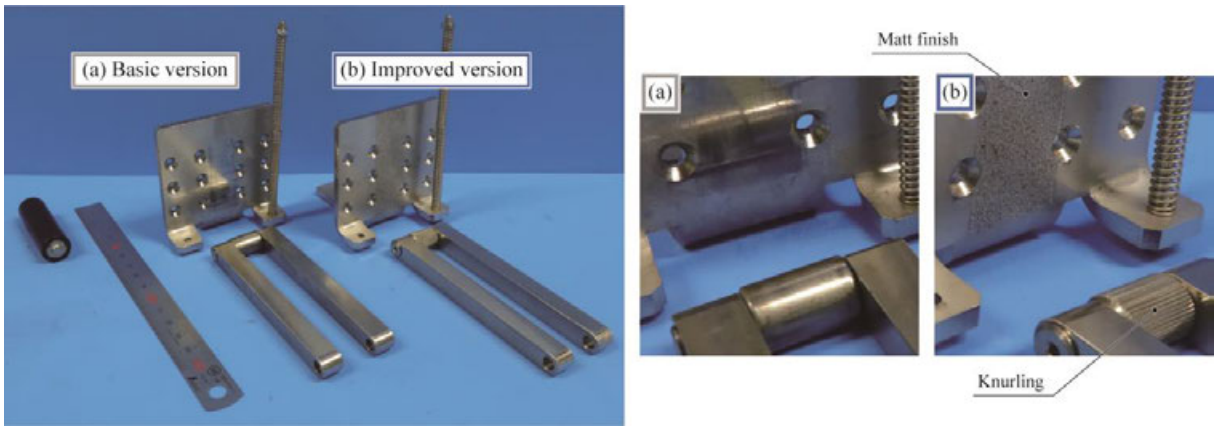

Fig. 117 Appearance of the (a) basic version and (b) friction-improved version of the lever and the contact surface of the finger.

Fig. 118 compares the results of the measurements of the input–output force characteristics and the average transmission efficiencies are listed in Fig. 119. Due to the deformation, the lever broke through its leaning position against the contact surface of the finger with an input force larger than 175 N for the basic version, resulting in “unlocking” of the finger and thus no further records. This implies that the rigidity of the mechanism, especially the lever, should be increased to avoid this phenomenon without improving friction.

As the graphs show constant inclinations, the average transmission efficiency was stable around 0.29 independent of the clamping width for the basic version

and increased to 0.47 for the friction-improved version, indicating that enhanced friction would multiply the clamping force and thus the force–energy efficiency of the gripper by 1.62. However, the result of the measurement under the condition $W_{obj} = 43.5$ mm for the improved version was notably inconsistent with other results. The cause of this outlier would be the difference in the engagement position of the knurling of the lever tip in contact with the finger. By replacing the lever tip with a continuously rough surface similar to the finger, the fluctuation could be avoided and the transmission efficiency could be further increased.

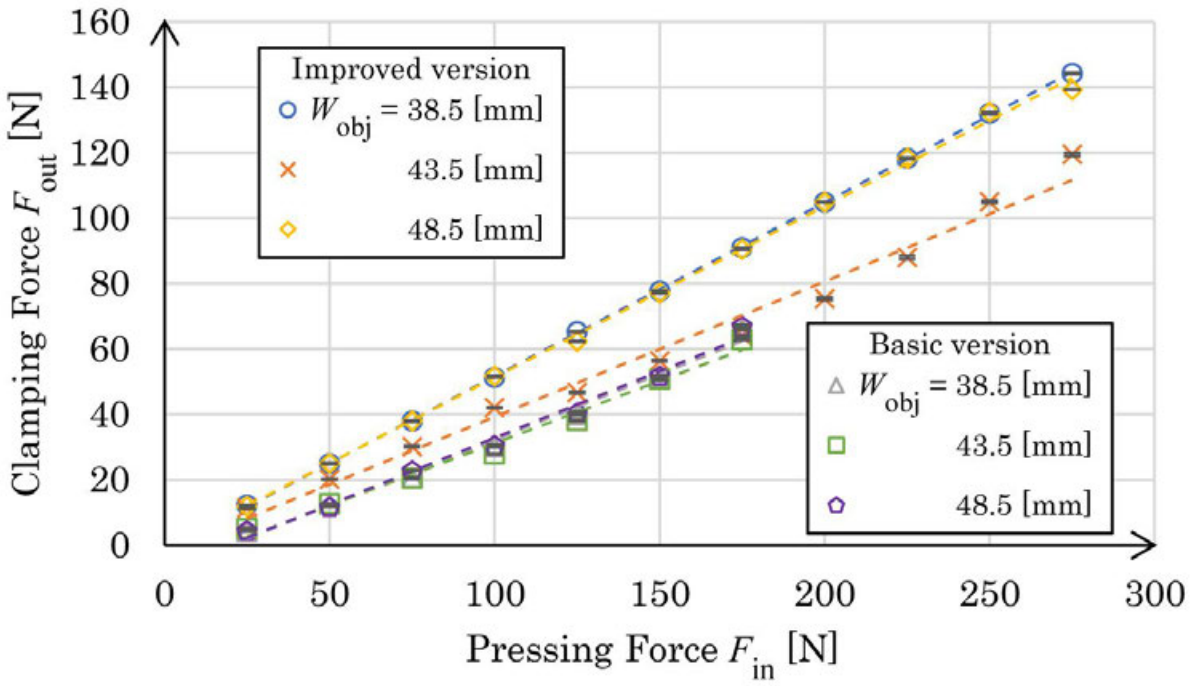

Fig. 118 Five-time average output clamping force F_{out} exerted by the lever–follower transmission mechanism with respect to the input pressing force F_{in}.

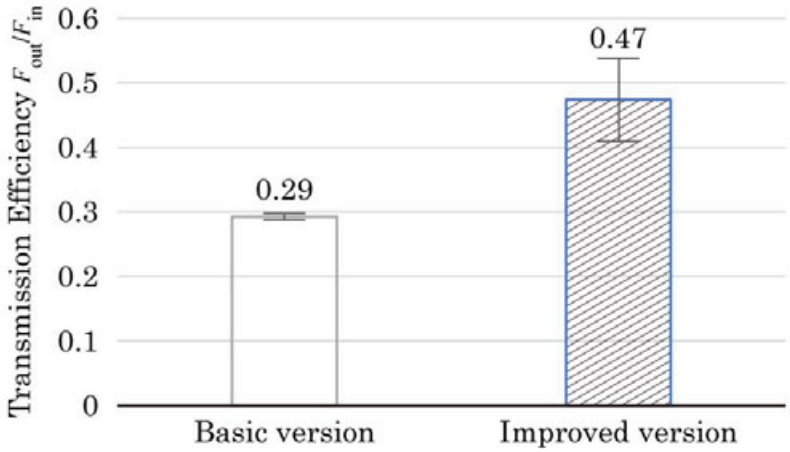

Fig. 119 Comparison of the transmission efficiency defined as the average output clamping force F_{out} divided by the average input pressing force F_{in}.

Section III.5.4 Discussion on the characteristics of the bi-parting IBM gripper with the adjustable clamping width

Subsection III.5.4.1 Transmission Efficiency

Referring to the dimensions in Fig. 107, the transmission efficiency of the lever–follower system in the width adjustment mechanism can be estimated as follows:

Fig. 120 illustrates how a follower is in contact and pressed against the lever with F_{in} at point **P** by the pressure angle α. The force applied by the follower is partitioned into those perpendicular and parallel to the surface of the lever, and then into directions perpendicular and parallel to the actual moment arm **OP** with elevation β, resulting in the effective force component F'_{in} expressed as follows:

$$F'_{\text{in}} = F_{\text{in}} \cos\alpha \cos(\beta - \alpha) \tag{31}$$

Here, the elevation angle α of the lever tangent to the finger at **Q** equals the pressure angle of the lever follower, which is expressed by design constants as:

$$\alpha = \cos^{-1} \frac{Y_{\max} - (R_{\text{tip}} + \delta)}{L_{\text{lever}}} = 7.4° \tag{32}$$

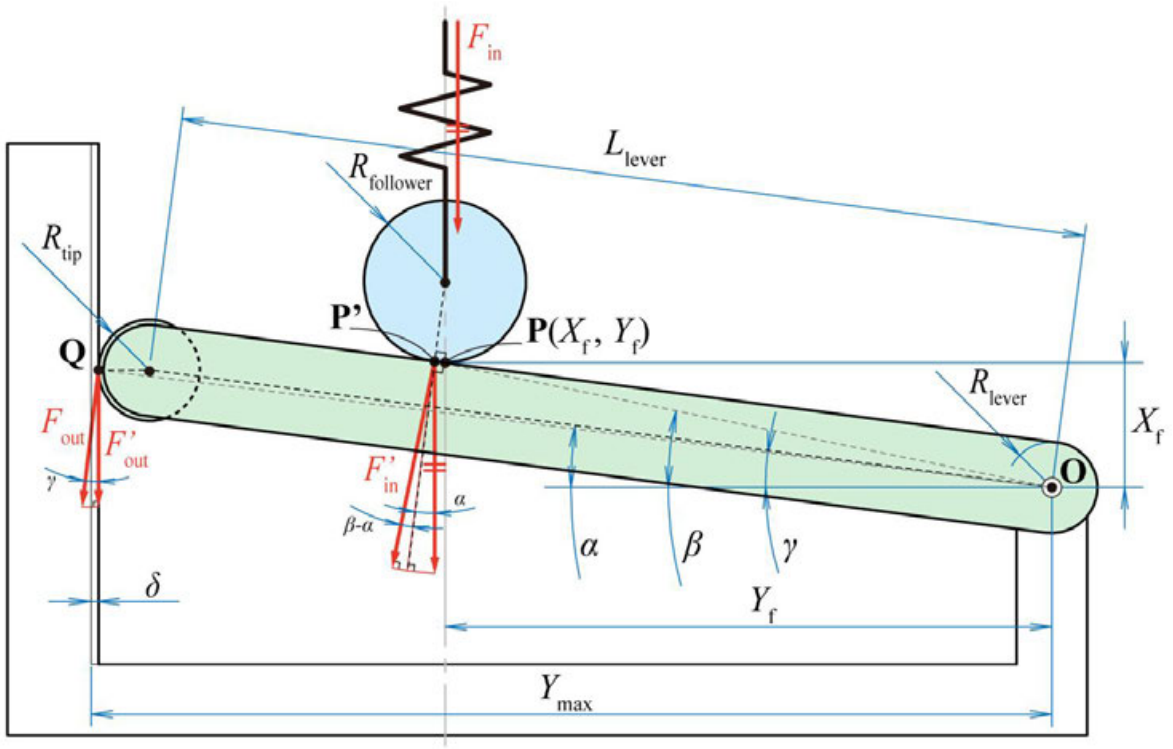

Fig. 120 Definition of the coordinate systems, variables, and forces of the lever–follower transmission.

The torque T_{out} applied to the finger by the tip of the lever is the that generated by the follower $T_{\mathrm{in}} = F'_{\mathrm{in}} L_{\mathrm{OP}'}$. $L_{\mathrm{OP}'}$ is the length of the actual moment arm of the actual contact point of the follower $\mathbf{P}'(X'_{\mathrm{f}}, Y'_{\mathrm{f}})$ to the lever axis **O**, expressed by the coordinate of the apparent contact point $\mathbf{P}(X_{\mathrm{f}}, Y_{\mathrm{f}})$ on the constraint axis of the follower, where

$$Y'_{\mathrm{f}} = Y_{\mathrm{f}} + R_{\mathrm{follower}} \sin\alpha = 61.0 \text{ mm} \tag{33}$$

$$X'_{\mathrm{f}} = \frac{Y_{\mathrm{f}} \sin\alpha + R_{\mathrm{lever}} + R_{\mathrm{follower}} \sin^2\alpha}{\cos\alpha} = 12.5 \text{ mm} \tag{34}$$

$$L_{\mathrm{OP}'} = \sqrt{{X'_f}^2 + {Y'_f}^2} = 62.3 \text{ mm} \tag{35}$$

$$\beta = \tan^{-1}\frac{X'_{\mathrm{f}}}{Y'_f} = 11.5° \tag{36}$$

The actual moment arm L_{OQ} of T_{out} with elevation angle γ are also calculated by geometric relationships as follows:

$$\gamma = \tan^{-1}\frac{L_{\mathrm{lever}} \sin\alpha}{Y_{\max} - \delta} = 7.0° \tag{37}$$

$$L_{\mathrm{OQ}} = \frac{L_{\mathrm{lever}} \sin\alpha}{\sin\gamma} = 95.0 \text{ mm} \tag{38}$$

By balancing the torques $T_{\mathrm{in}} = T_{\mathrm{out}}$ along **O**, the force applied on **Q** perpendicular to the moment arm is derived as $F_{\mathrm{out}} = T_{\mathrm{in}}/L_{\mathrm{OQ}}$, and its effective component parallel to the translational direction of the finger as follows:

$$F'_{\mathrm{out}} = F_{\mathrm{out}} \cos\gamma = \frac{L_{\mathrm{OP}'}}{L_{\mathrm{OQ}}} F'_{\mathrm{in}} \cos\gamma \tag{39}$$

Substituting the equations (2) and (6) in (1) yields $F'_{\mathrm{in}} = 0.98\, F_{\mathrm{in}}$, and then (1), (5), (7), and (8) in (9) gives $F'_{\mathrm{out}} = 0.64\, F_{\mathrm{in}}$. This result indicates that the theoretical maximum transmission efficiency is 0.64, while the prototype model satisfies only 45.4 % of this value with the basic structure but achieves 73.5 % with the friction-improved version. In reality, the friction resistance proportional to the normal force $F_{\mathrm{out}} \sin\gamma$, the counterforce of the ineffective component of F_{out}, should

have decayed the clamping force by less than 1/8 of F'_{out}. Furthermore, mechanism deformations, such as bending of the lever and widening of the distance between the finger and the lever axis, result in the gradual decrease of the contact angle and thereby the inclination of the lever, as the F_{in} increases during clamping.

Subsection III.5.4.2 Disturbance on Compensation

The increase in power consumption from screw clamping was minimal because the spring cancelled out the additional load on the actuator caused by the magnet. The point to be considered is that the input force on the lever follower must have been approximately 150 N to exert the recorded output clamping force of 50 N on an average, according to Fig. 118, while the displacement–force characteristic of the pair of sampled magnets to which the spring was customized to follow, demonstrated a maximum value of 300 N.

The factors that may have affected the decrease in the input force are listed as follows. First, although mass-produced, the attraction force of magnets is known empirically to vary 250–300 N by individual difference. Second, the characteristic of each hand-made spring is designed to be less than the magnetic force for any displacement with feasible production conditions of error within 10 %. Furthermore, the mechanism deformation leads to a subduction of the contact position X_{f} of the follower to the lever, which also results in the compressed length of the spring being less than designed.

Overall, the observation suggested that preparing a more precise one-to-one spring specifically corresponding to the pair of magnets actually implemented in each gripper and reinforcing its mechanical rigidity would yield more energy-efficient and highly amplified clamping performance.

Subsection III.5.4.3 Selection of Actuators

For prototyping, a simple bidirectional screw driven by a DC motor was selected as an actuator, as it provides both sufficient torque and detailed positioning to conduct evaluation experiments. However, the way the IB magnet is used in the proposed gripper is categorized as a reduction mechanism, which does not restrict the actuator; any other actuator with even weaker output, such as artificial muscles made of shape-memory alloys, can be selected if the compensation spring is designed with higher precision. Moreover, if the clamping state has to be only on and off, two-state actuators without positioning ability, such as solenoids and pneumatics, can be selected.

Subsection III.5.4.4 Technological Value of the Outcome

In conjunction with the jumping mechanism [19] and the MR fluid gripper [20] proposed in other studies by the author that incorporate the IB magnet as their magnetic flux supplier, the gripper in this study possesses a technological novelty in the idea of embedding the IB magnet as a built-in force amplifier, contrary to conventional applications of the IB magnets limited to attraction mechanisms. The amplifier can be easily implemented by including both the IB magnet and its attraction target inside the mechanism structure. Adjusting its magnitude of attraction by shifting the equilibrium point of compensation, the control rod, indirectly regulates the output force.

For the gripper, the difficulty of extracting a pressing force instead of non-contact magnetic force is that the output destination to be utilized is not the magnet but the fixed end of the spring, which is the outer frame of the IB magnet. As it is "fixed," its position has to be maintained at a certain position in the mechanism to establish a precise compensation, or its misalignment leads to the unsteady nonlinear output force with insufficient compensation, as observed in the previous design in Fig. 98 (b). The desired application of the magnetic compensation mechanism as a gripper was finally achieved in this study by implementing the adjustment mechanism that made the position of the fixed end independent of the finger and the actual output destination.

These unprecedented applications of the IB magnet other than as attraction devices will contribute to the development of a new academic area of magnetic mechanisms, in which permanent magnets are used for reinforcement and energy conservation of robotic components that require large forces. Furthermore, as the IB magnet can be activated even without electricity, the gripper can be powered by human power as a tool or by an external mechanical force as a passive mechanism.

Section III.5.5 Conclusion of Chapter III.5

To achieve a more steady and predictable clamping force independent of the target object width, this chapter features a new width-adjustment mechanism using a lever toggle, which allows the mechanical separation of the fixed end of the compensation that generates the pressing force and the finger that exerts it on the object.

Experiments using the embodied prototype model were conducted to verify the amplification feature of its magnets on the clamping force and the compensation feature of its spring on the input control force. The gripper demonstrated that the magnetic assistance increased the maximum clamping force while the spring compensation prevented the energy consumed by the actuator from increasing, resulting in the force–energy efficiency ratio multiplied by 1.39 in average, compared to the constitution without magnets. Furthermore, the width adjustment mechanism realized a linear width–force characteristic with a weak inclination, and its lever–follower locking system exhibited a stable transmission efficiency, drastically making the clamping force more predictable and controllable than the gripper with the previous design.

In this manner, the proposed principle of the IBM gripper was successfully validated, implying that conventional grippers can be replaced with a more energy efficient, force-amplified, and control-free gripper with the aid of the DF converter.

Future studies will aim to adopt a more accurate compensation, enhanced friction, and rigid structure to achieve a higher amplification rate and transmission efficiency will be using the discussed methods. A design with a more practical size and mass will be investigated for integration in robotic systems. In addition, a numerical model for precisely estimating the exerted clamping force according to the elasticity of the mechanism and clamped object will be established to develop a control law.

Chapter III.6 Conclusion of Part III

In this part, the DF converter using a permanent magnet as a reverse spring was introduced. As its application example, a clamping mechanism implementing a pair of permanent magnets to spontaneously and steplessly generate an attractive force to assist with clamping movement was proposed. For realization, various methods for detaching a permanent magnet using a control force much smaller than its original attractive force were sought, and results revealed that the mechanism employing an IB magnet was the best.

In Chapter III.3, to verify the effectiveness of spontaneous force amplification, a one-sided IBM gripper was developed using a magnetic spring, which is the solution to the complicated design procedure and trade-off relationship between compensation precision and mechanism volume of the conventional springs of the IB magnet.

In Chapter III.4, to verify the effectiveness of continuous force amplification, a bi-parting IBM gripper was developed using a conical coil spring that manages both compactness and followability to the nonlinear characteristic of the magnet suited to a bi-parting constitution.

In Chapter III.5, to decrease and linearize the effect of the clamping width on the amplified clamping force, a bi-parting IBM gripper with a stepless width-adjustment mechanism using a lever toggle was developed to achieve a more steady and predictable clamping force independent of the target object width. The width adjustment mechanism enabled the gripper both to acquire the enhanced force–energy efficiency due to the spontaneous and continuous force amplification by the DF converter and to linearize the width–force characteristic with a small enough inclination.

In these ways, the prototype models showed the applicability of the IB magnet as a DF converter in generating a large pressing force, in contrast to its existing application mechanisms that regard the IB magnet only as an attraction device. The enhanced performance of the grippers implies that replacing conventional grippers with them can contribute to the extension of the operation time of robots with limited power supply and to the reduction of electricity costs of robotic arms in production lines. Furthermore, the idea of the width-adjustment mechanism is

valuable for other compensation mechanisms to let them exert the change of the internal state externally while sustaining the compensation precision. The applications of force amplification mechanisms will be further expanded to the studies of other energy-efficient robotic components and labor-saving tools.

Part IV

Development of the DF converter with a stroke-shortened spring, and its application to an electromagnetic brake

Part IV　Development of the DF converter with a stroke-shortened spring, and its application to an electromagnetic brake

Chapter IV.1　Abstract of Part IV

In this part, contrary to the bi-sided IBM gripper with a variable clamping width discussed in Chapter III.5 for various objects with different widths, an application example of the one-sided IBM gripper with a fixed clamping width for a known and designated object was presented to show the applicability of the simplest configuration of the IBM gripper illustrated in Fig. 64.

Equipping the fingers with brake pads to clamp a rotor turns the IBM gripper into a brake mechanism. An electropermanent configuration made the brake capable of exerting more energy-efficient braking torque for both short and long-span braking, compared to an existing electromagnetic brake. The prototype of the proposed mechanism was developed with a newly devised compensation spring comprising two linear springs that shorten the pad-detaching stroke. The maximum static and average dynamic friction torques increased to 161.0 % and 192.9 % , respectively, when identical pads of an EM brake were used for comparison.

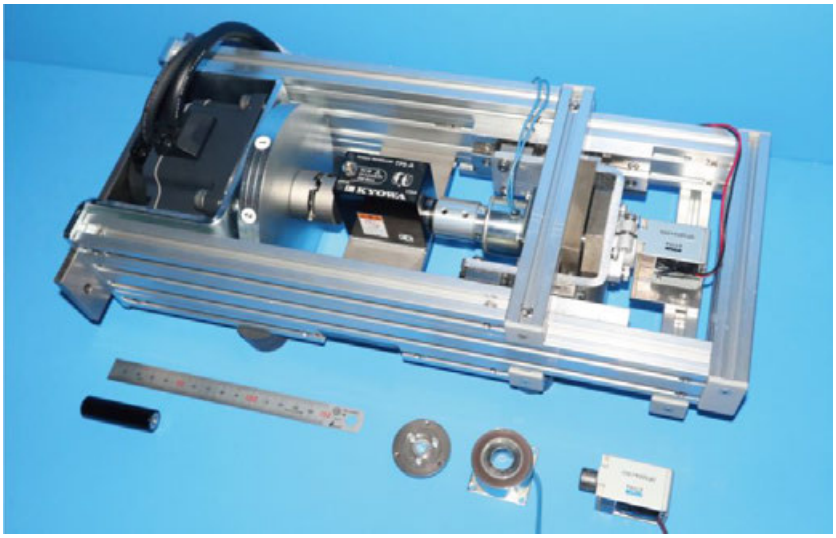

Fig. 121　Appearance of the POC model of the proposed electromagnetic brake using the IB magnet.

Power saving was also achieved when braking for longer than 0.43 s; the torque–energy efficiency multiplied by 4.5 when measured for 1.0 s, successfully revealing the effectiveness of the proposed principle. Further, based on the force – displacement characteristic of the compensated magnet, the theoretical response time was numerically analyzed as 13.6 ms, comparable to the contrasted EM brake, validating the measured value of 14.0 ms.

Chapter IV.2 Application example of the DF converter #3: spontaneous force amplifier for an electromagnetic brake

Electric brakes are used in various mechanisms to control the speed of motion. Because they do not require large and heavy external power sources such as hydraulic or pneumatic pumps, EM brakes are favored for machines with strict limitations of volume and mass [89].

An electromagnetic brake (EM brake) is a typical example of an electric brake that engages the braking system by applying a current on the coil in the field to magnetically attract the facing ferromagnetic armature. A braking force is generated due to friction between the brake pads in these fields and the armature, although there are some different implementations: an EM track brake is used in rail vehicles that considers the rail as the armature [90]; an electric trailer brake employs rounded brake shoes pressed outwards at the drum (rotating cylinder) attached to the output axle [91]. Other EM brakes such as magnetic powder brakes and magnetorheological fluid brakes use the magnetic flux generated by the coil to bind ferromagnetic particles so that the braking torque is transmitted via shear stress from the fixed field to the output shaft [92], [93].

The EM brakes, while being compact, highly responsive, and versatile as they can be activated independent of the speed unlike dynamic brakes (which require a relative speed of the target object to be braked, and therefore, a main brake to hold it [94]), these EM brakes consume electricity to drive their coils. A long-time application of current generates an unignorable amount of Joule heat, which increases the coil resistance and thus degrades braking performance [95]. Active cooling by fans or thermoelectric coolers requires even extra power.

The abovementioned issue implies that energy-efficient EM brakes contribute to the extension of the milage of robots and vehicles with an independent power supply that has a limited capacity. This can be realized by saving energy both for sudden braking and continuous idling. Such brakes also establish the reduction of cumulative electricity cost required for robotic arms in production lines to lock their joints intermittently. To achieve these objectives, the advantages of a permanent magnet (PM) is utilized, i.e., permanent exertion of force, and thereby, the elimination of the volume and mass of the power supply. Similarly, a few existing EM brakes adopt an "electropermanent magnet (EPM)" structure that reverses the engaging state relative to the current input. The magnetic flux of a PM maintains the excitation of the brake, and a counter EM cancels this flux to release the brake [96]. However, because they also consume electricity to keep the brake released, both EM and EPM brakes exhibit limitations in terms of holding either the enabled or disabled state continuously.

Therefore, the study aims to develop a braking system that allows a more energy-efficient actuation of the brake pads via force amplification to verify the effectiveness of the proposed system. In contrast to previous latching EPM brakes and valves that regulate the magnetic circuit passing through the yoke [97]–[99], the magnet itself gets actuated to switch between attached and detached states for directly generating a pressing force, as an application of a compensated magnetic mechanisms [81], [82], [100]. This method is advantageous in that its output is not digital (on and off) when continuously regulating the distance between the magnets and unique in that it would ultimately contribute to braking in any machine and tool because its means of latching include, but are not limited to, electric current in a coil, solenoid, and motor; even mechanical force and human power can be used.

Chapter IV.3 Proposed principle: brake mechanism using the IB magnet (IBM brake)

Most machines use powerful actuators and large gearboxes to exert a large force. On the contrary, the idea of force compensation to avoid affecting the compactness property of the EM brake was adopted; the operating force of an actuator is compensated by maintaining the actuated part (connected to the brake pad) at an equilibrium point of the force regardless of its displacement or orientation by applying an equal load in the opposite direction.

Regarding the IB magnet as a reduction mechanism, a concept of the IBM brake mechanism illustrated in Fig. 122 is proposed. The outer frame of the IB magnet is identified as the active brake pad driven indirectly by an actuator via the compensation spring. The ferromagnetic surface fixed on the mechanism structure (here, a magnet that faces its pole to the unlike pole of the active magnet on the control rod) attracts the control rod such that the active pad approaches the counterpart pad installed on the rotation axle to be braked. This mechanism can be considered topologically equivalent to a nonmagnetic parallel gripper reinforced by IB magnet with a fixed clamping width illustrated in Fig. 64, which extends the outer frame as an active finger to grasp an object between a pair of IB magnets.

The spring for compensation has two roles: 1) It is a method for storing the attraction work of a magnet as elastic energy and minimizing the load on the actuator by assisting it with repulsion work when the control rod is pulled out to detach the magnet. 2) It works as a variable stiffness material for the internal rigidity of the brake pad by adjusting its compression width from the free length.

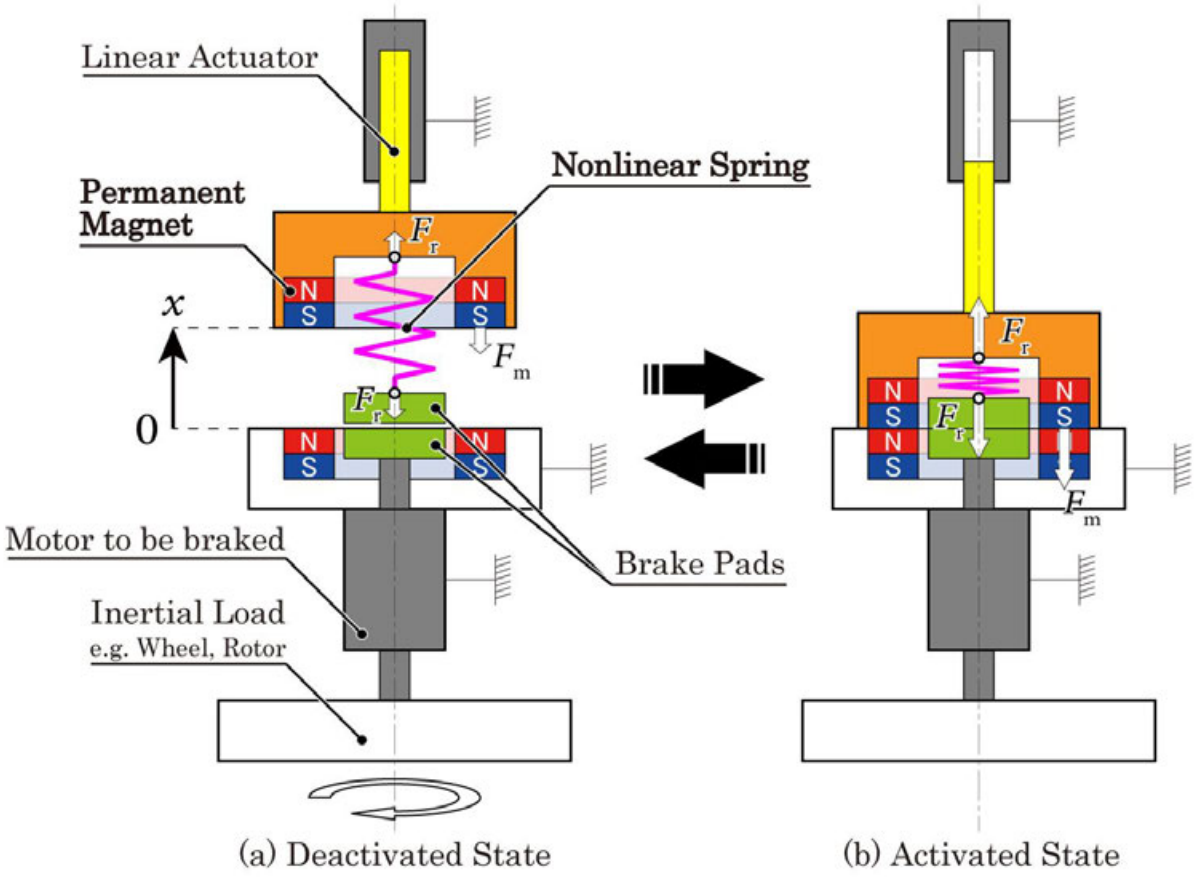

Fig. 122 Principle diagram of IBM brake. Gaps between the brake pads are exaggerated.

Chapter IV.4 Embodiment of the IBM brake

Section IV.4.1 Embodiment of the 1st prototype of the IBM brake with a single conical coil spring

Subsection IV.4.1.1 Design and development of the 1st prototype of the IBM brake with a single conical coil spring

Fig. 123 shows the dimensions of the 1st prototype of the proposed IBM brake for the proof of principle (POC), embedded in a measurement system specified in the Japanese Industrial Standard for EM brakes [101]. The brake pads of an EM brake (Ogura Clutch, AMB2.5) are diverted to those of the IBM brake such that the translational contact force between these pads becomes the single variable that affect the performance comparison of their friction torques. This measurement system can test the EM brake by screwing its field to the mechanism structure. The specifications of the contrasted brakes are listed in TABLE IX.

As shown in Fig. 62, a conventional nonlinear spring for the IB magnet comprises multiple linear springs that activate stepwise. However, springs with different spring constants are required to duplicate the nonlinear characteristic of the magnetic attraction more precisely, which results in a bulky and heavy constitution [28]. Therefore, the nature of a conical coil spring with a varying diameter and pitch was utilized to achieve miniaturization such that its part with a smaller spring constant becomes compressed first, followed by the part with a larger spring constant [77], [102]; this nonlinearly increases its displacement–force characteristic similar to a like-pole pair of magnets by only a single elastic body.

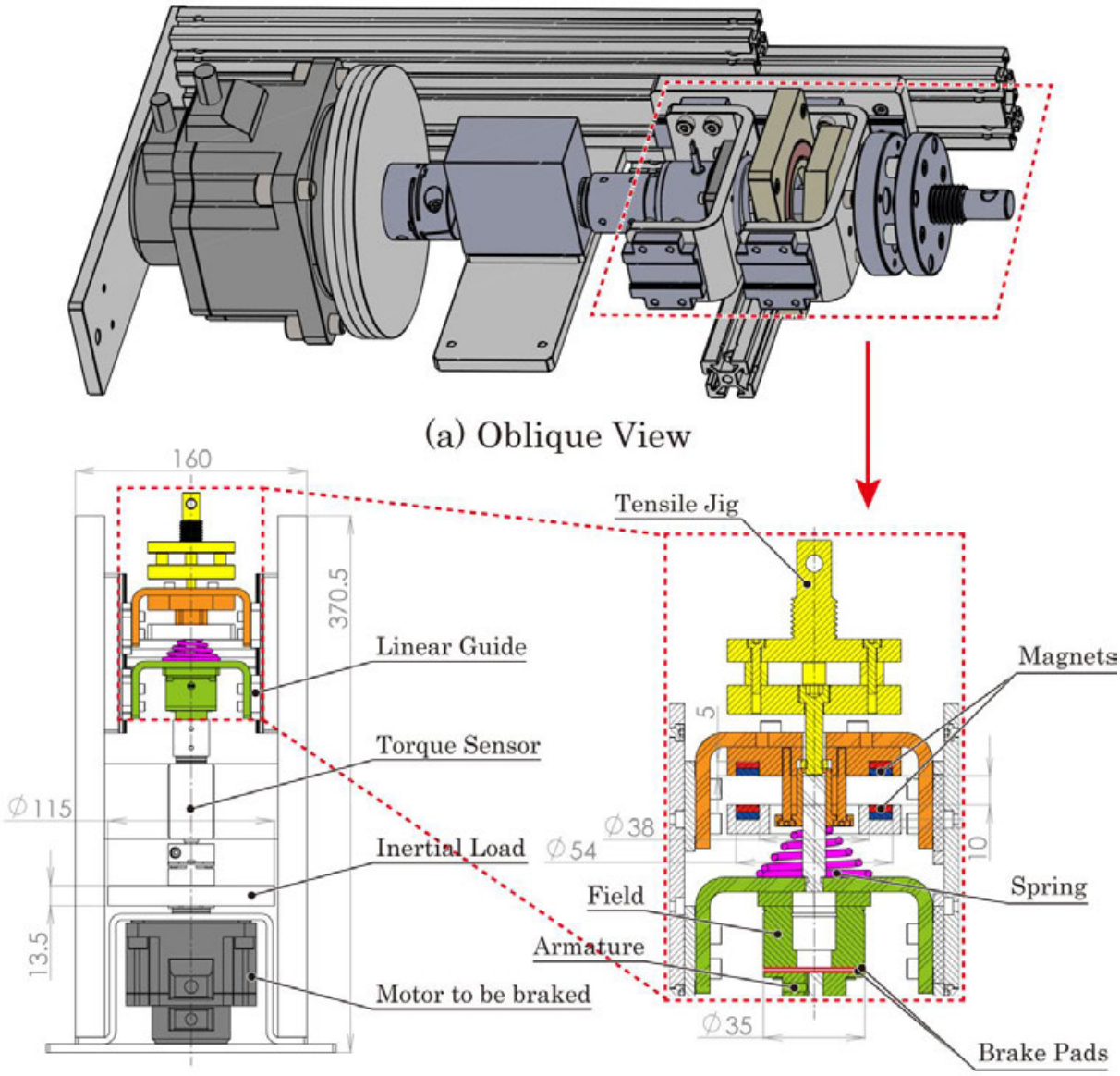

Fig. 123 Design sketch of the 1st prototype of the IBM brake. Some parts and details are omitted for better visibility. The colors of the components correspond to those of the elements in the principle diagram shown in Fig. 122.

TABLE IX

SPECIFICATIONS OF THE 1ST PROTOTYPE OF THE IBM BRAKE, EM BRAKE FOR COMPARISON, AND MOTOR FOR DRIVING THE LOAD

	Components	Mass
IBM Brake with **Conical Coil Spring**	*Mass of Magnet*	40.8 [g]
	Spring	11.1 [g]
	Control Rod	405.0 [g]
	Active Brake Pad	291.7 [g]

EM Brake **AMB2.5**	*Power Rating*	3 [W] at 24 [V]
	Responsiveness	10 [ms]
Motor **BXM5120-A2**	*Rotor Inertia*	2.15 e-3 [kg·m²]
	Rated Torque	0.4 [N·mm] (continuous)
		0.8 [N·mm] (continuous)

Subsection IV.4.1.2 Performance evaluation experiment of the 1st prototype of the IBM brake with a single conical coil spring

Using the 1st prototype, an experiment to measure the forces exerted by each component of the brake is conducted to verify the proposed principle whether a control force F_c required to detach the magnets (and the brake pads) can be reduced by the compensation provided via the nonlinear spring. The system constituents and experimental procedure are shown in Fig. 124, wherein a material testing machine (Instron 3343) actuates the control rod of the IB magnet with both the magnets and the spring; the magnets only; and the spring only.

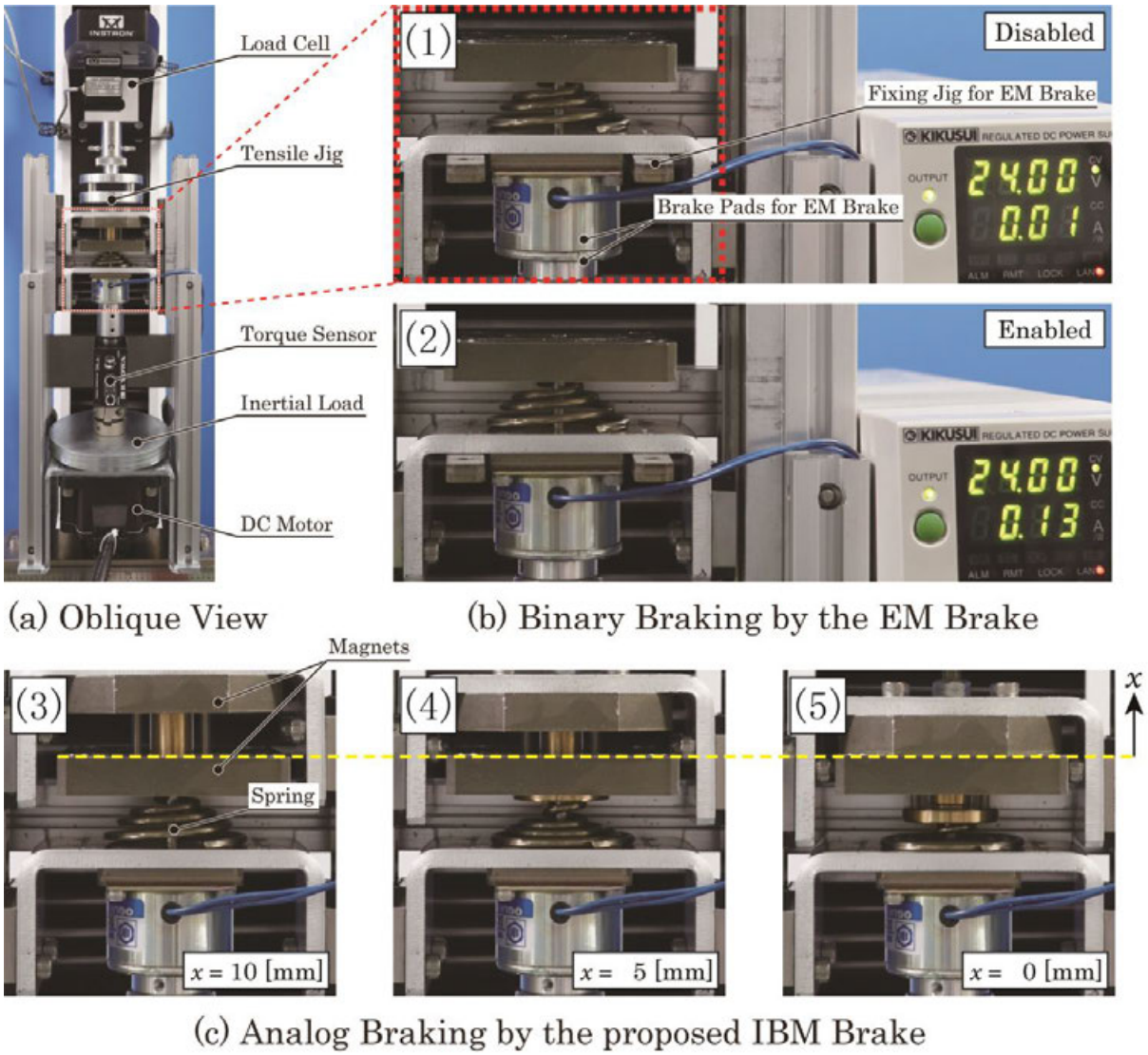

Fig. 124 Experimental system of 1st prototype of IBM brake and its operation procedure. (b) Field of EM brake pulls armature on the axle of the motor by electromagnetic attraction. (c) Pad on the field is pressed on the armature directly by the spring and indirectly by the control rod connected to the tensile jig of the material testing machine.

The respective control force F_c, single attractive force F_m, and single repulsive force F_r are recorded as shown in the graph in Fig. 125. Likewise, the attractive force between the armature and field of the excited EM brake is measured after fixing the field on the mechanism body of the experimental system.

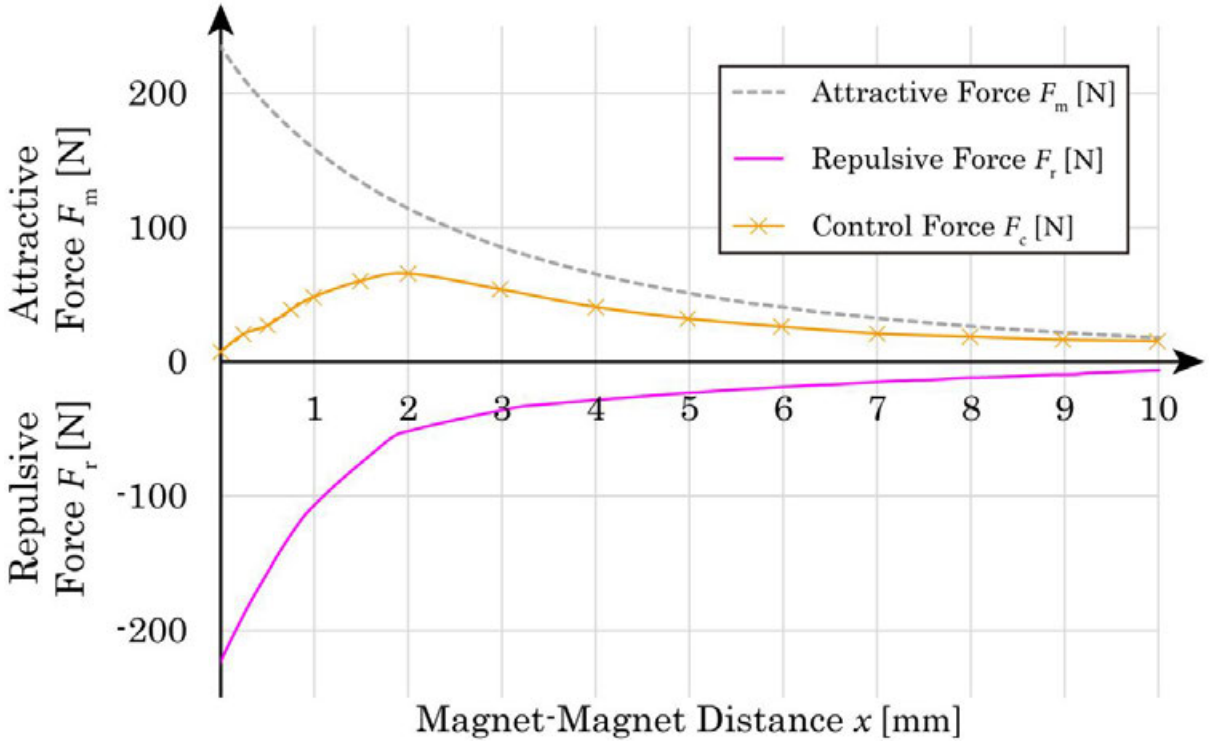

Fig. 125 Five-time average forces exerted on the control rod of the IBM brake.

Meanwhile, another measurement using a torque sensor (Kyowa Electronic Instruments, TPS-A-2 NM) is conducted to evaluate the relationship between the previously recorded forces and the friction torques of the proposed IBM brake and EM brake for comparison. While the position x of the control rod (distance between magnets) is kept by the material testing machine, the command value of the velocity to a brushless motor (Oriental motor, BXM5120-A2) is gradually increased so that the maximum static friction torque, i.e., the spike torque observed when the motor-driven axle starts to slip against the brake, can be measured as shown in Fig. 126.

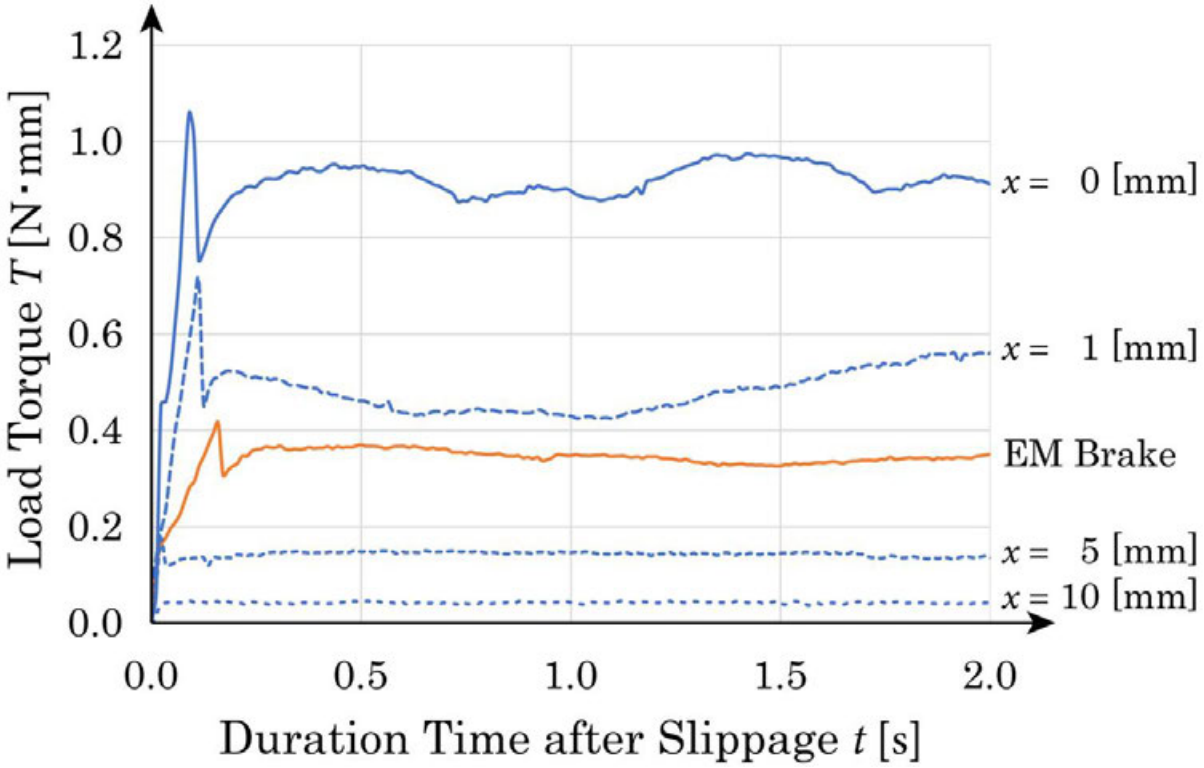

Fig. 126 Typical transitions of the friction torque of the IBM brake vary with the magnet–magnet distance (or compression distance of spring) when the axle driven by the motor begins to slip.

Fig. 127 shows the results of the measurement of the maximum static friction torque, stacked in Fig. 125. As the magnets approach each other, the repulsive force of the spring steplessly increases and so does the pressing force (counterforce of spring force) between the brake pads. This leads to a continuous increase in the friction torque between the brake pads, whereas the control force remains smaller than the pressing force. Comparing the integration of F_c and F_m in range $0 \leq x \leq 10$ reveals that the spring compensation lessened the control work required to disable the brake by 53.9 % (further analyzed in Subsection IV.4.2.4).

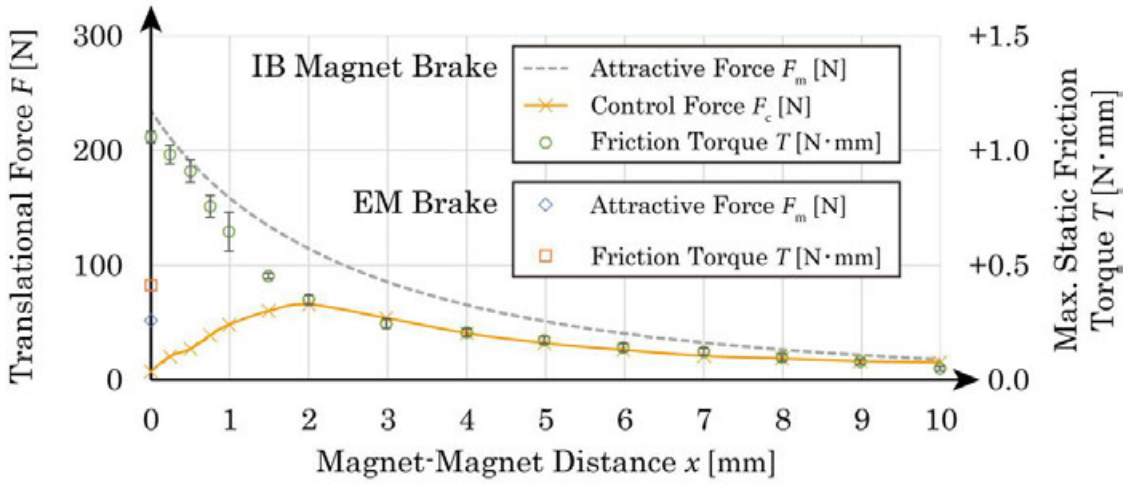

Fig. 127 Ten-time average maximum static friction torques exerted between the brake pads appended to the upper half part of Fig. 125. The values of the EM brake are depicted on the *F*-axis for convenience because they do not have a controllable pad–pad distance.

The ratio of the friction torque to the control force (required to maintain the current position of the control rod) is compared in Fig. 128. The value of the proposed IBM brake is comparable to but less than that of the EM brake in the range of 1.5 mm < x; however, it increases steeply as x approaches zero, where the torque–force ratio is more than 18.1 times that of the EM brake. This occurs because the positive correlation of the torque is established not with F_c but with the magnetic attractive force.

These results successfully prove the continuous force amplification effect by the compensation on the control force, and it indicates that a considerably weaker, smaller, and less power-consuming actuator can be chosen to drive the strong PM of the proposed IBM brake.

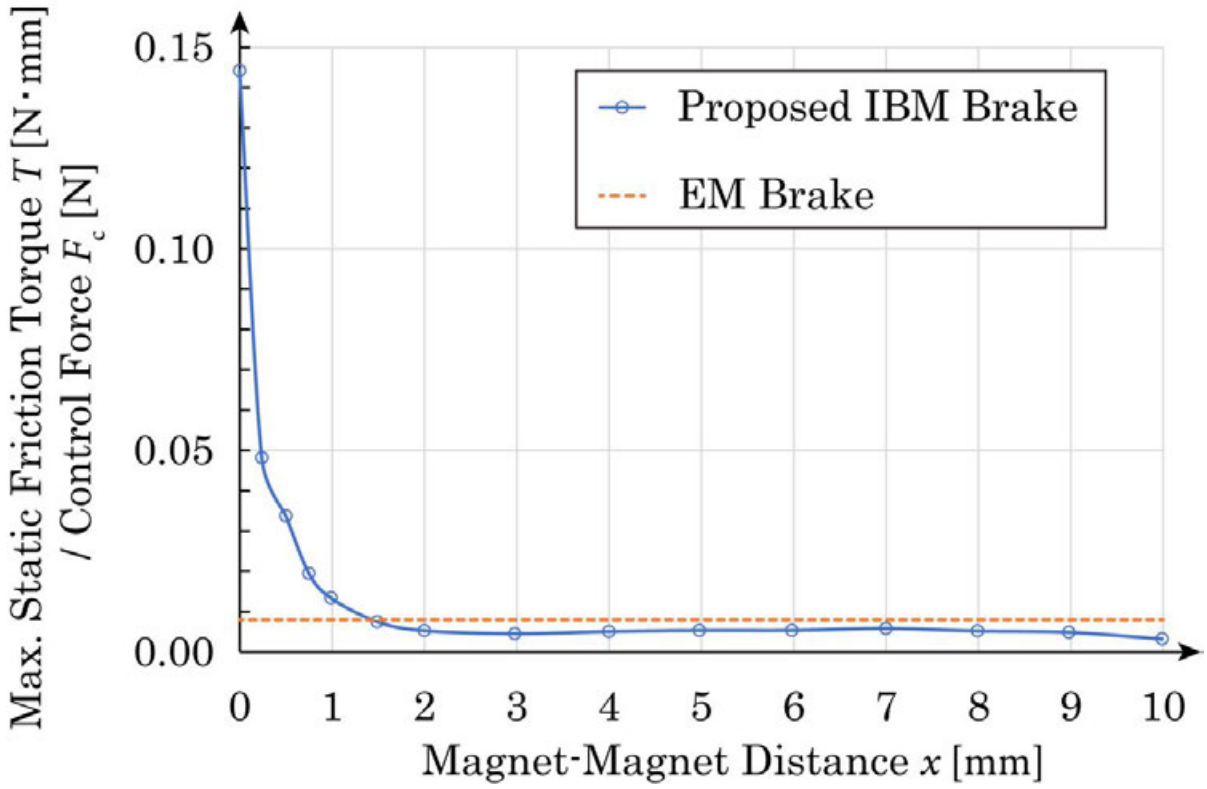

Fig. 128 Ratio of the maximum static friction torque to the control force required to sustain the current magnet–magnet distance x. The value of the EM brake is depicted as a dotted line for the same reason as in Fig. 127.

Section IV.4.2 Embodiment of the 2nd prototype of the IBM brake with a multistage nonlinear spring

Subsection IV.4.2.1 Problems of the 1st prototype of the IBM brake with a single conical coil spring

While proven to be effective in reducing the control force, the IBM brake has a peculiar inconvenience: the control rod needs to be pulled out for a large distance to sufficiently weaken the pressing force (more than 10 mm in the current constitution), although the brake pads that actually matter must be just slightly separated to deactivate braking. This side effect of compensation with an apparent reduction rate emerged because the spring transmits the attractive force of the magnets to the brake pads as long as the spring is in contact with both the control rod and the outer frame.

Further, the conical coil spring itself has a problem in production; its characteristic was adjusted to follow that of the magnetic attraction on every millimeter by rectifying the pitch and diameter, which results in a long lead time. Its size and shape are uncontrollable if the compensation precision is prioritized; therefore, the structural design of the brake is strongly limited by the spring. These features are unfavorable for ensuring the flexibility of the mechanism design for mass production, where each pair of magnets has its own attractive characteristic for the spring to follow. Even magnets of identical models and lot numbers have differences in their magnetization quality, as seen when comparing Fig. 127 and Fig. 130.

Subsection IV.4.2.2 Proposed principle: shortening of the stroke by a multistage nonlinear spring

The brake pads should be separated in an actuation stroke as short as possible to solve the travel distance problem of the control rod. However, simply inserting a suspension spring between them affects the characteristics of the compensation spring, and this results in an excess repulsive force that hinders the activation motion of the brake.

Therefore, the 2nd prototype adopts a newly devised nonlinear spring composed of two linear springs that realizes both the early separation of the brake pads and the simplicity of design by exploiting the existence of that suspension spring.

As illustrated in Fig. 129, the compensation spring K_a and suspension spring K_b are combined in series such that (a) around the free length, they work as a single elastic body with a smaller spring constant k_{12} represented by

$$k_{12} = \left(\frac{1}{K_a} + \frac{1}{K_b}\right)^{-1} = \frac{K_a K_b}{K_a + K_b} \tag{40}$$

As the combined spring k_{12} is compressed, (b) the stopper located at the switching point P_1 touches the connection point of the springs and inhibits further movement of K_b. (c) The multistage spring then has $k_{01} = K_a$ as the only deformable body, which results in increased spring constant. This functionality is similar to a top-out spring for a vehicle, supplementarily added to the main suspension spring in series to react to both large bumps and small vibrations by changing its spring constant based on the compressed length [103].

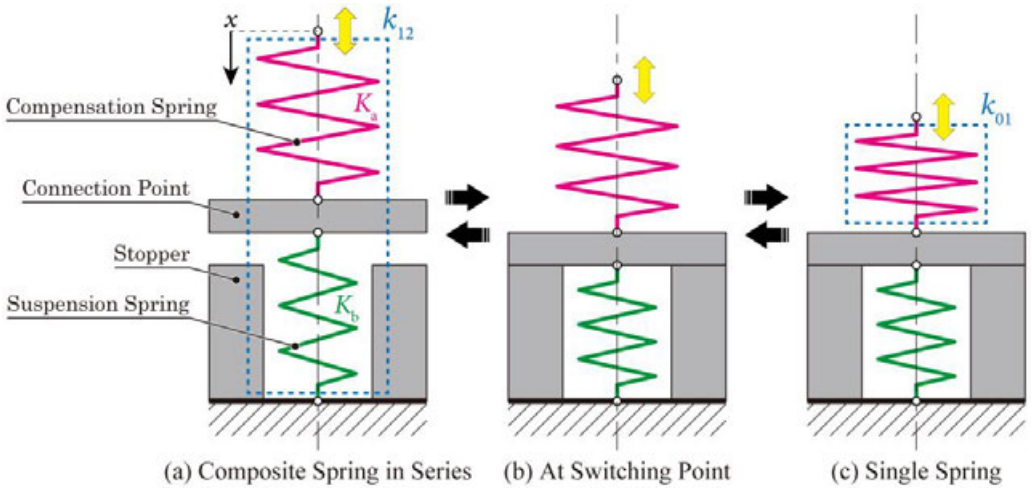

Fig. 129 Multistage nonlinear spring composed of two linear springs.

In this way, the brake pads can be separated in a stroke that is considerably smaller than a single conical coil spring. In exchange, the pressing force applied on the pads by K_a is predicted to be weakened by the internal force generated by K_b, which results in a decrease in the friction torque to some extent. Therefore, an apparent reduction rate emerges, which results in a trade-off relationship between the actuation distance and force.

The spring characteristic illustrated in Fig. 130 was designed, and the linear springs to be combined were selected in the following procedure. First, three temporal points $P_0(0, F_0)$, $P_1(x_1, F_1)$, and $P_0(x_2, 0)$ defined a compensation curve F_{01} with inclination k_{01} and a suspension curve F_{12} with k_{12} as

$$F_{01_{(x)}} = -k_{01}x + b_{01} = \frac{F_1 - F_0}{x_1}x + F_0 \tag{41}$$

$$F_{12_{(x)}} = -k_{12}x + b_{12} = \frac{-F_1}{x_2 - x_1}(x - x_1)x \tag{42}$$

Once the separation point x_1 was fixed according to the mechanism design requirement, the remaining parameters F_0, F_1, and x_2 were optimized by a numerical analysis: minimizing the integral of the control force F_c (difference between F_m and F_s) for the range of compensation, i.e., control work E_c, yields the appropriate coordinates. Then, an actuator with an output force sufficient to pull out and push in the control rod for its stroke $x_s > x_1$ was selected.

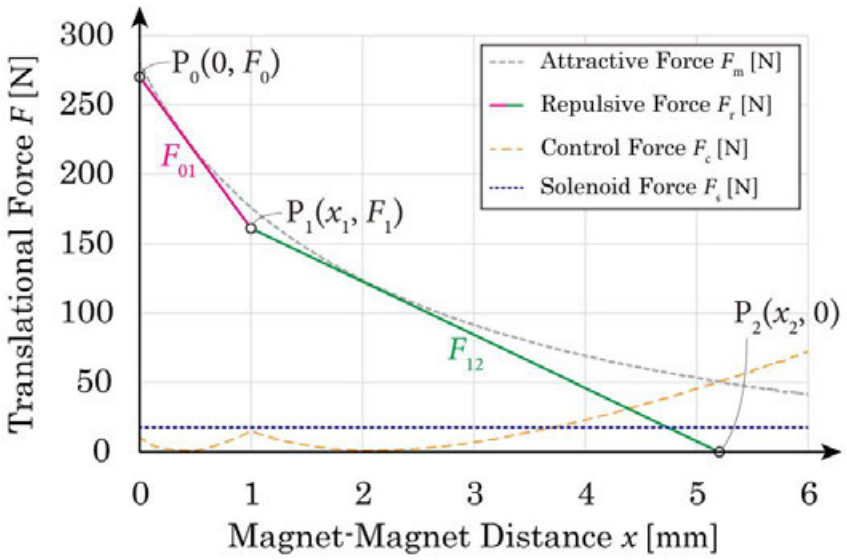

Fig. 130 Characteristic design of devised multistage nonlinear spring ($x_s = 1.5$ mm) is composed of two linear springs for the 2nd prototype of the proposed IBM brake.

An example of how the multistage spring is implemented in the IBM brake is illustrated in Fig. 131. The suspension spring K_b is inserted between the active brake pad (driven indirectly by the control rod via the compensation spring K_a) and the rotation axle so that its own height can be ignored when fully compressed; the brake pads can contact each other. A thrust bearing is installed in-between to isolate the rotation and avoid friction between the axle and the spring.

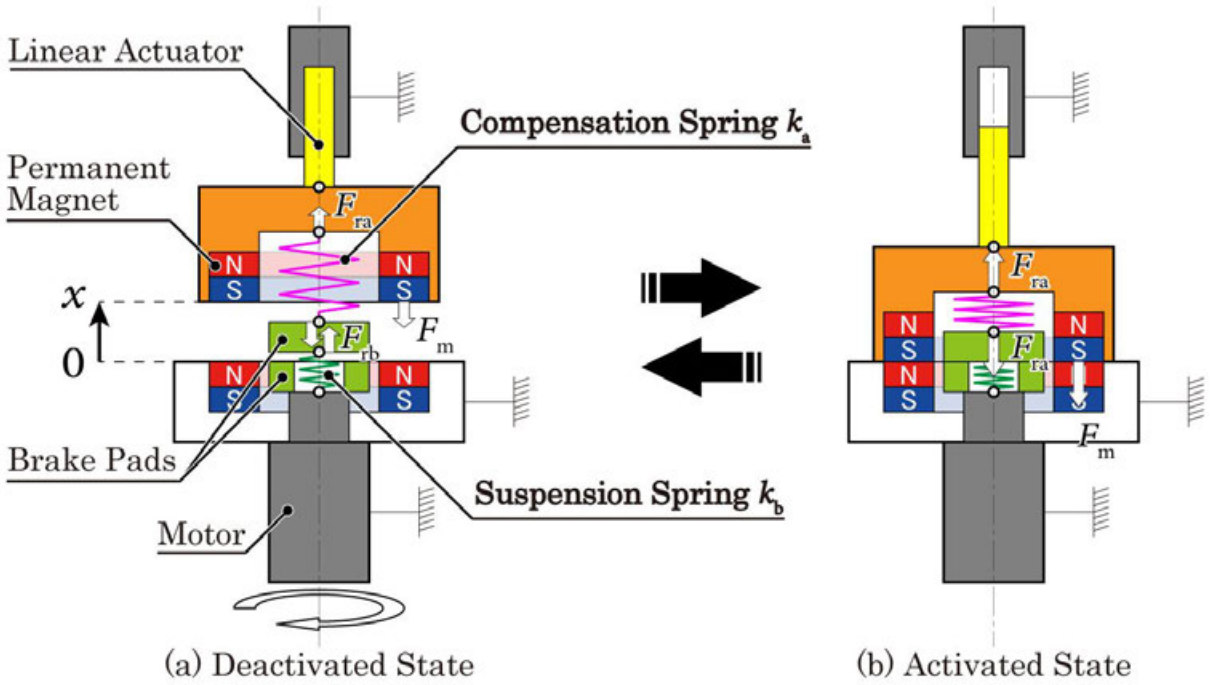

Fig. 131 Principle diagram of the 2nd prototype of the IBM brake using devised multistage spring composed of two linear springs.

Subsection IV.4.2.3 Design and development of the 2nd prototype of the IBM brake with a multistage nonlinear spring

Fig. 132 and TABLE X show the dimensions and specifications of the 2nd prototype of the proposed IBM brake with a multistage spring displayed in Fig. 1 built by replacing the nonlinear spring and some parts for height adjustment on the control rod from the 1st prototype.

In this study, a self-holding pull solenoid (Takaha Kiko, CD12400100) is selected to regulate the control rod as an example of a weak, short-stroke actuator (half in power and one third in mass and volume of CA16620040, for example, a pull solenoid strong enough to actuate the 1st prototype but without self-holding feature). It has the same voltage rating as the EM brake, and therefore, the difference in the current directly represents the difference in power consumption, which simplifies the performance comparison. Meanwhile, any translational actuator can replace the role if they have sufficient capability to shift the rod for the designed stroke.

This self-holding solenoid operates in the following manner. Initially, when the brake is disabled, its internal PM holds keeps the control rod pulled out even without applying a current. The current is applied to the electromagnet to cancel out the flux of the internal magnet and enable the brake. The solenoid does not have a return spring to push the rod, and therefore, the control force of the IB magnet is adjusted to be weakly biased such that the attractive force is still left after compensation and pulls in the rod automatically when the self-holding is deactivated; this results in the activation of the brake. A current in the opposite direction is applied to pull out the rod to release the brake. Brake pads are in contact as soon as the magnet on the mechanism structure and the other on the control rod are attracted to each other; therefore, the solenoid must be excited just for a moment for activation.

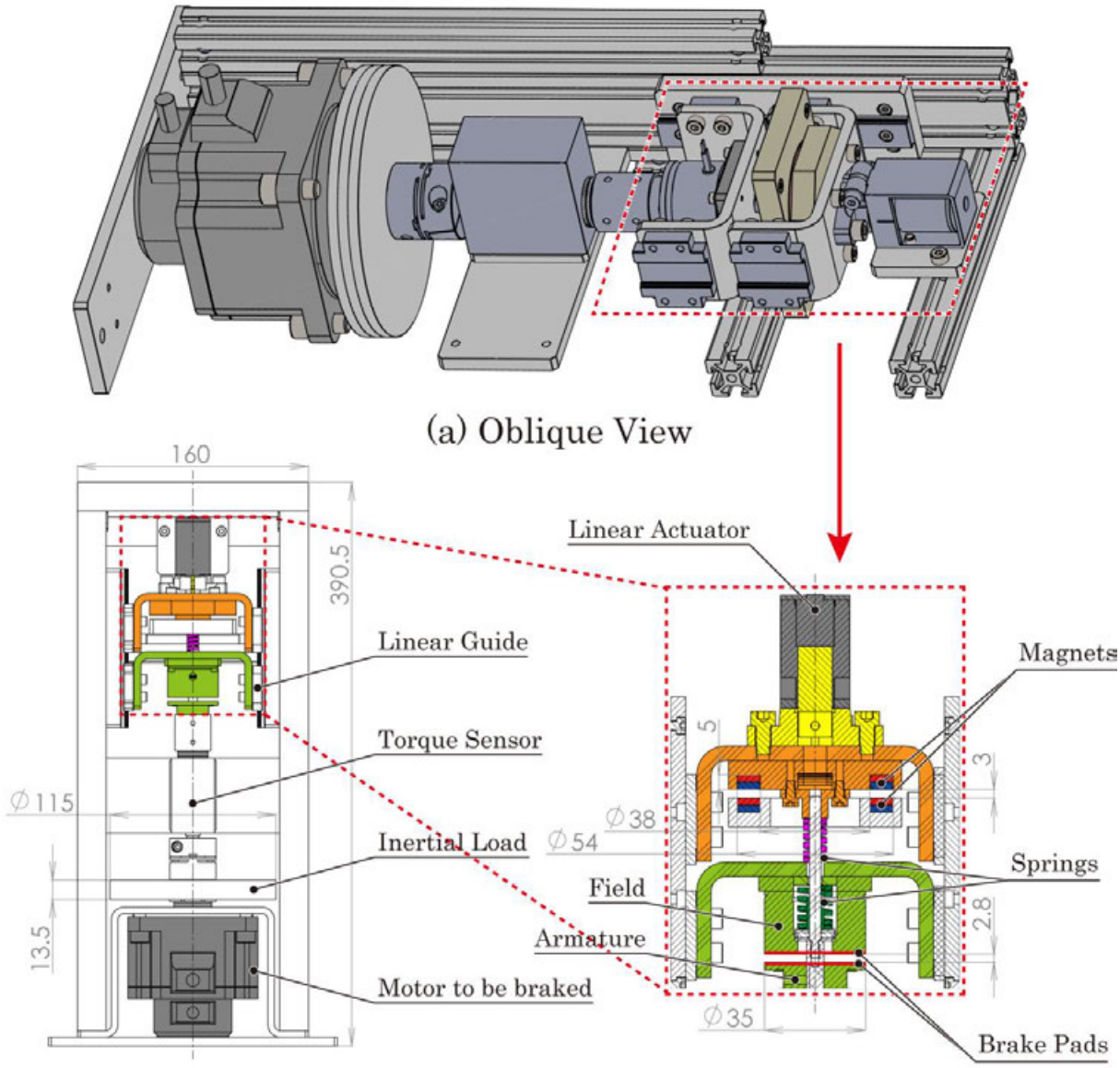

Fig. 132 Design sketch of the 2nd prototype of the IBM brake.

TABLE X

SPECIFICATIONS OF THE 2ND PROTOTYPE OF THE IBM BRAKE AND SOLENOID FOR ACTUATION

	Components	Mass			
IBM Brake with **Multistage Spring**	*Spring K_a*	2.4 [g]	Solenoid **CD12400100**	*Power Rating*	57 [W] at 24 [V]
	Spring K_b	5.0 [g]		*Duty Cycle*	6 [%]
	Control Rod	441.7 [g]		*Mass*	140.6 [g]
	Active Brake Pad	303.0 [g]		*Mass of Plunger*	26.7 [g]
				Self-Hold Force	10.5 [N]

Fig. 133 shows the appearance of the 2nd prototype and Fig. 134 shows its magnified cross-sectional view. As designed, the multistage action of the springs was observed as indicated in the pictures (1)–(3) corresponding to the states of springs in the principle diagram shown in Fig. 129 (a)–(c) respectively: Two springs form a composite spring, while the field (active brake pad) is suspended in stage (1), and the suspension spring stops further compression as the brake pads meet at (2), which results in the activation of the single action of the compensation spring as seen in (3).

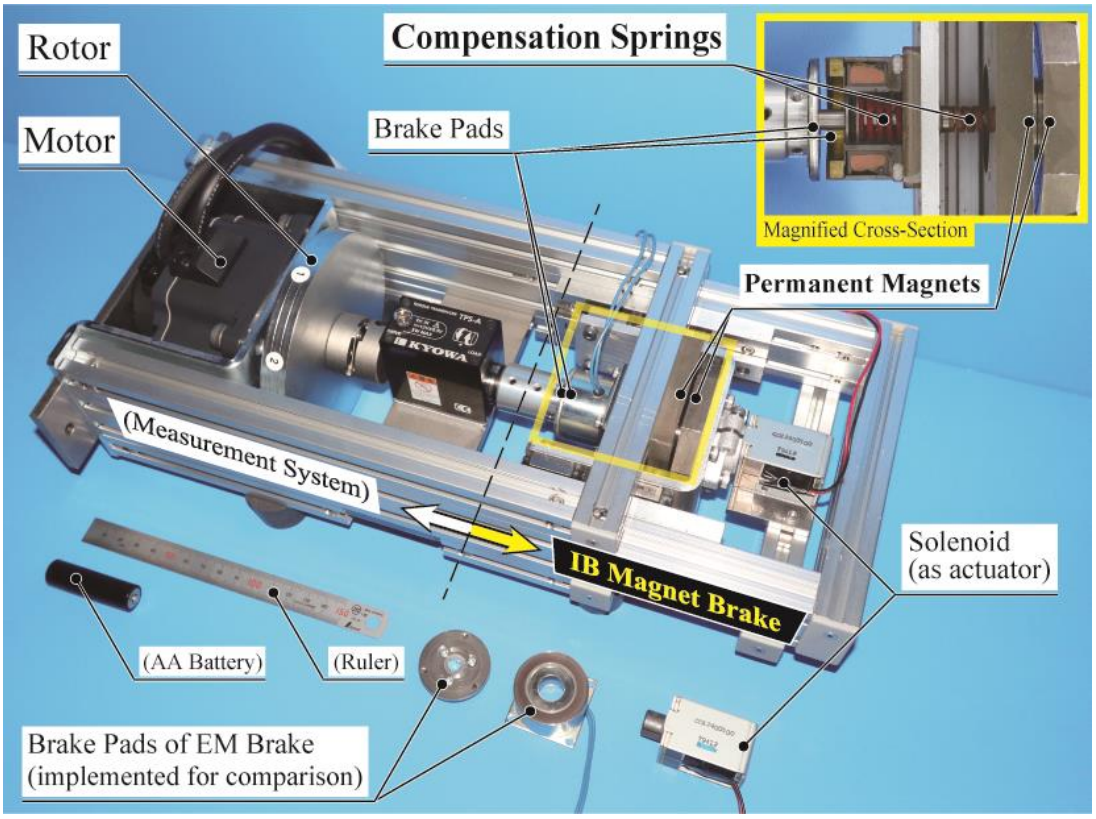

Fig. 133 Appearance and cross-sectional view of the 2nd prototype of the IBM brake.

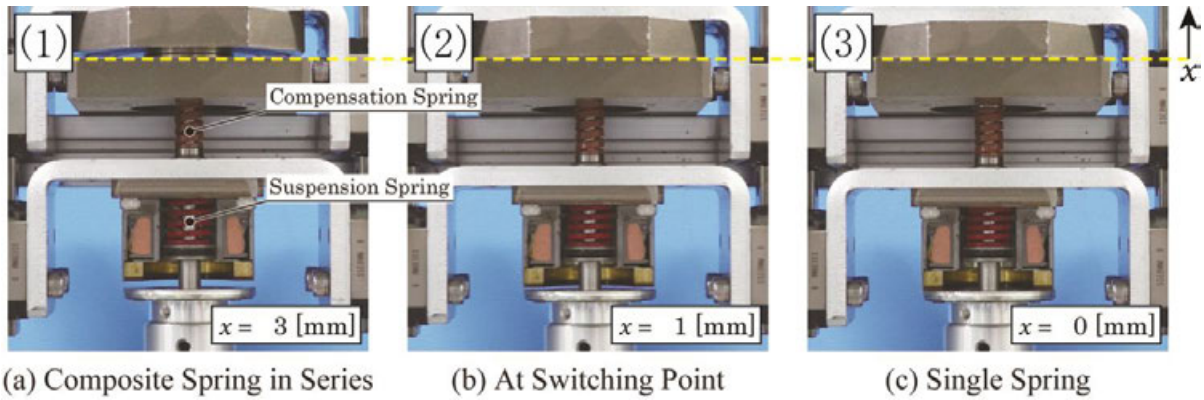

Fig. 134 Magnified cross-sectional view of the brake system of the 2nd prototype of IBM brake.

Subsection IV.4.2.4 Performance evaluation experiment of the 2nd prototype of the IBM brake with a multistage nonlinear spring

To investigate the property of the 2nd prototype in the same way as the experiments in Subsection IV.4.1.2, its maximum static friction torque at magnet–magnet (pad–pad for EM brake) distance $x = 0$ and control force in the range of $0 \leq x \leq 1.5$ mm were measured and integrated with respect to x to derive the control work required for disabling the brake.

The results are shown in Fig. 135 with the values of the 1st prototype, indicating that the multistage spring is also valid for nonlinear compensation. Although the attractive force of PMs in the 2nd prototype is so strong that its control work E_{m} required for an actuator to fully pull out the control rod is 796.8 % of that of the EM brake E_{EM}, the compensation reduced it to 27.4 % of E_{EM}. Meanwhile, the maximum static friction torque is increased to 161.0 % of that of the EM brake, which makes the torque–energy ratio 5.87 times.

Comparing the results of two prototypes clarifies effects of shortening x_{s}: E_{m} gets halved even without compensation, and the rate of reduction of E_{IBM} to E_{EM} improved from 53.9 % to 96.6 %. As a trade-off, the friction torque at $x = 0$ decreased by 38.1 % as the contact force between the pads is hampered by the repulsive force of the suspension spring.

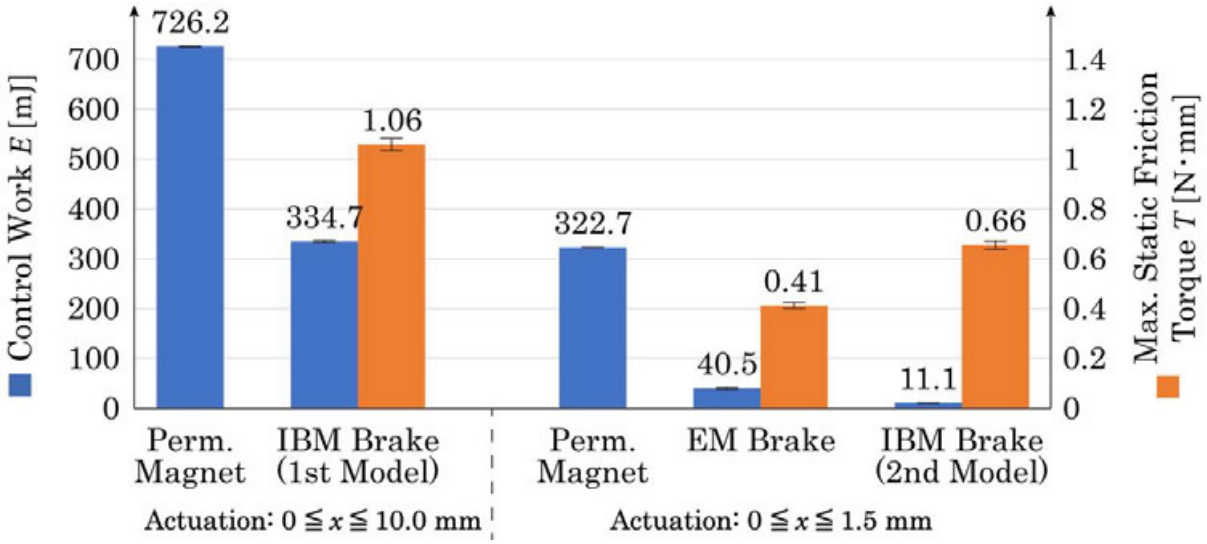

Fig. 135 Ten-time average maximum static friction torques exerted between the brake pads and the five-time average control works required to actuate the brakes for their designed maximum strokes.

To derive a performance index during braking of a rotating object, the dynamic characteristics of the IBM brake were inspected. The experimental system was laid horizontally so that the responsiveness is independent of the weight of the moving parts. While a constant command value was input to the motor to ensure that the motor attempts to maintain its rotation speed, the brake was activated for 1.0 s to exert its dynamic friction torque.

The examples of transitions of power consumption, dynamic friction torque, and rotation speed of the IBM brake and EM brake are compared as shown in Fig. 137. The graph clarifies the difference in the timing of the brakes to consume electricity: the EM brake requires constant consumption, and the IBM brake consumption shows spikes at the beginning and end of braking. The IBM brake generated an apparently larger dynamic torque than the EM brake while using identical brake pads, which resulted in a larger deviation of the motor speed that emerges when activated and deactivated.

Fig. 136 contrasts the results of the dynamic experiment. The dynamic friction torque increased to 192.9 % of the EM brake; however, it required only 42.8 % power consumption. The torque–energy ratio is then increased to be 4.51 times, indicating that the proposed brake accomplished high performance in both braking torque and energy efficiency, for both holding an idling object and braking a rotating object.

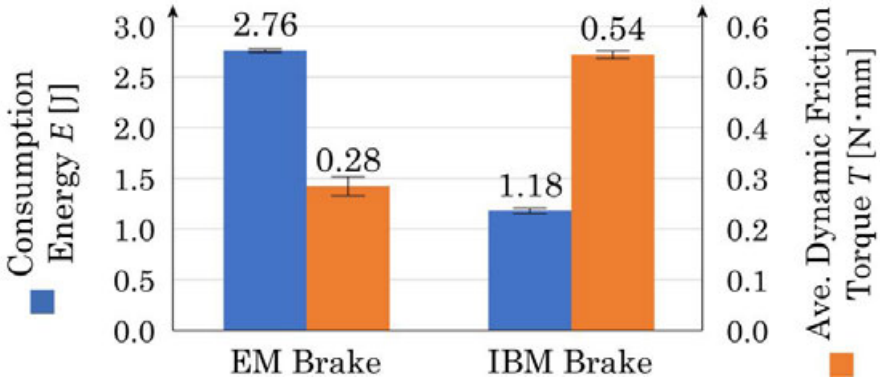

Fig. 136 Ten-time average dynamic friction torques exerted between the brake pads and consumption energy required to apply the brake pads for 1.0 s.

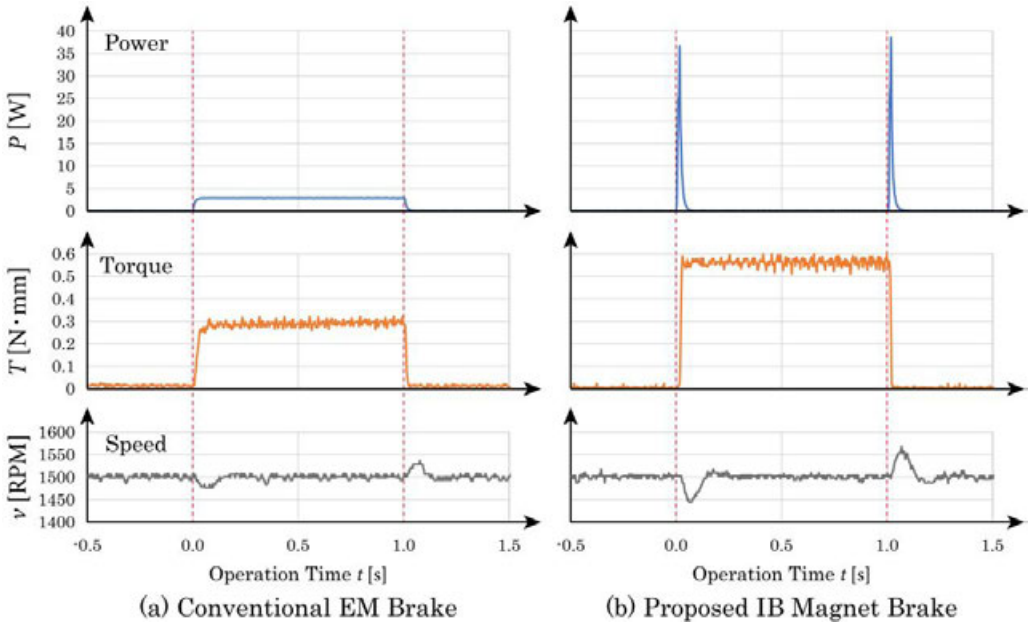

Fig. 137 Typical transitions of power consumption, friction torque, and rotation speed of the EM brake and proposed IBM brake when they braked a motor, regulated to rotate at 1500 RPM, for 1.0 s. The solenoid was excited for 14.0 ms each time the IBM brake was activated and deactivated.

The comparisons were made under the condition of applying brakes for 1.0 s. However, they can be expanded to any braking duration t; The theoretical energy consumption of the EM brake E_{EM} and IBM brake E_{IBM} are calculated as

$$E_{\mathrm{EM}_{(t)}} = 24.0[\mathrm{V}] \times 0.115[\mathrm{A}] \times t[\mathrm{s}] = 2.76t[\mathrm{J}] \tag{43}$$

$$E_{\mathrm{IBM}} = 0.59[\mathrm{J}] \times 2 = 1.18[\mathrm{J}] \tag{44}$$

Solving $E_{\mathrm{EM}_{(t)}} \geq E_{\mathrm{IBM}}$ gives $t \geq 0.43$ s, which means that the proposed IBM brake with current constitution exceeds the energy performance of the EM brake with identical brake pads under any condition of continuous braking time longer than this t (or less frequent than $1/t = 2.3$ Hz); further, it surpasses in the generation of braking torque because of the pressing force amplification effect caused by the compensation. This implies that the IBM brake would not generate a tremendous amount of heat even when braking for a long time. Therefore, the IBM brake can be used in a variety of applications, to which the use of conventional EM brakes has been inadequate owing to the duty cycle. For example, 72 % of cars in Japan wait for the signal crossing for 5 s on average [104], sufficiently long for the EM brake to heat up.

Chapter IV.5 Discussion of the characteristics of the IBM brake

Section IV.5.1 Responsiveness of braking

For the 2nd prototype of the IBM brake, the excitation time of the solenoid was empirically set to 14.0 ms, which is the shortest duration for a stable behavior in any posture wherein the rotation axle of the system lies horizontally; the maximum duty cycle becomes 35.7 Hz. If the current was applied for less than this duration, the control rod could not be fully pushed in and the magnets did not meet, which resulted in a forced deactivation of the brake. A numerical analysis was conducted to evaluate the reasonability of this responsiveness.

Let time T required for the self-holding solenoid to maintain its permanent magnetic flux cancelled out by the EM equal the time required for the control rod to reach a stroke X (distance from x_s); the integration of the control force F_c on the control rod with a mass $m = 400$ g gives its speed v as calculated below, where $x_{(t=0)} = v_{(t=0)} = 0$.

$$\int_0^X F_{\mathrm{c}(x)}\,\mathrm{d}x = \int_0^T m\ddot{x}\frac{\mathrm{d}x}{\mathrm{d}t}\,\mathrm{d}t = \int_0^T m\dot{v}v\,\mathrm{d}t = \frac{1}{2}m\left(v_{(T)}^2 - v_{(0)}^2\right) \tag{45}$$

$$\Rightarrow v_{(t)} = \sqrt{\frac{2}{m}\int_0^{X_{(t)}} F_\mathrm{c}\,\mathrm{d}x} \tag{46}$$

Given the speed of the rod at time moment $\mathrm{n}\Delta t$ $(\mathrm{n} = 1, 2, \dots)$, an iterative calculation yields the required n for the x to reach x_s at the end of the stroke.

$$x_{(\mathrm{n})} \cong x_{(\mathrm{n}-1)} + v_{(\mathrm{n})}\Delta t \tag{47}$$

As plotted in Fig. 138, the transition of the displacement and speed of the control rod were numerically derived with $\Delta t = 50$ μs (defined considering the significant digits), and the duration T to reach x_s was 13.6 ms. The delay in the empirical value may have resulted from friction in the translational movement of the control rod. The inertias of the springs and their connection point (active brake pad in this mechanism) also could have affected the responsiveness because the multistage spring was designed using the synthesis of springs in series assuming they are

negligible, whereas they do have mass in reality, as listed in TABLE X. Now that the performance comparison is done, the massive brake pad (of the EM brake, currently) can be replaced with a specifically dedicated design without unneeded structures such as a coil, both to improve the responsiveness and to reduce the gravitational disturbance on compensation, as discussed in the next subsection.

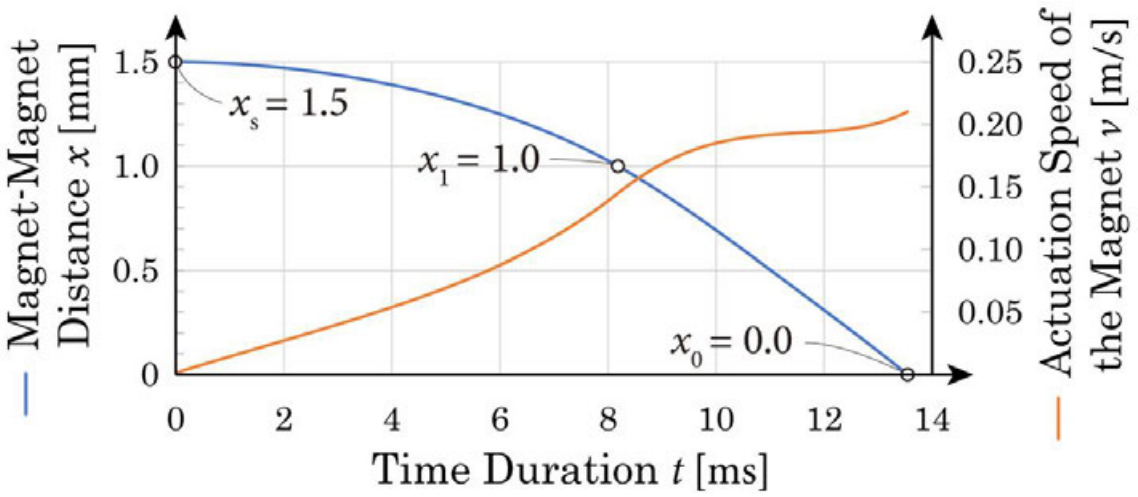

Fig. 138 Numerically analyzed transitions of the distance between the magnets and the actuation speed of the control rod of the proposed IBM brake.

Section IV.5.2 Effect of gravity

The control force and friction torque were measured in a controlled situation such that the effect of the mass of moving parts on the translational pressing force between the pads could be ignored; the compensation spring was designed such that the minimization of the difference between the magnetic attractive force and spring repulsive force was the priority.

Although the experiments sufficiently proved the concept of the IBM brake, brakes can be installed in any orientation in practical applications, and the posture of the belonging mechanism can vary when applied to locomotive machines such as vehicles, robots, and robotic arms. Therefore, not only weight saving by the miniaturization of the structure but also selecting an actuator with a margin to obtain the weight of the control rod, designing the compensation spring with force bias against the known gravity direction, and combining a weight compensation mechanism should be considered for use in the actual environment.

Section IV.5.3 Selection of actuators

A simple self-hold solenoid was selected as an actuator to drive the brake, and experiments with dynamic performance were conducted only in a binary state of braking: activated and deactivated. However, as shown in Fig. 124, the intervention of the spring allows the pair of magnets to be separated from each other at an arbitrary distance. Therefore, other actuators with weak and short-stroke output but with more detailed positioning ability, such as artificial muscles made of shape-memory alloy, make it possible for the IBM brake to adjust the output torque in a more analog (or stepless) manner.

The constitution using an electromagnet (that contains a PM for self-holding feature) to shift the position of a PM may affect the compensation precision if they are aligned closely enough for their magnetic fluxes to interfere with each other. Therefore, if considering miniaturization, it shall be more simplified and evolved into an EPM relation. Hints for further improvement may lie in solenoid actuators with internal force compensation; there are solenoid valves with an embedded PM that use two-staged return springs to provide two flow rates or states of open and close using one degree of freedom selectively [105], [106].

Still, while they are specified as EPM actuators, the way an IB magnet is used in the proposed brake mechanism is categorized as a reduction mechanism that does not restrict the actuator to drive. Therefore, it can be activated even without electricity by human power as a tool or by an external mechanical force in the environment as a passive (load-sensitive) mechanism.

Section IV.5.4 Design of the multistage spring

In addition to the attractive force of the pair of PMs, linear springs also have their own deviation of spring constants and free lengths from their catalog values. The 2nd prototype of the IBM brake in this research absorbed by these errors insert a few shim rings; however, it took an unreasonably long time to determine the best adjustment as it required partial disassembly every time.

For the easier adjustment of the spring independent of its individual difference considering a mass production in the future, another multistage spring made of a single coil spring split in two by a connector can be composed, as shown in Fig. 139. A spiral slit is engraved on the connector so that it can slide up and down on the wire of the spring, while re-defining the spring constants (numbers of active coils) of the two split springs. Weakening the suspension spring also allows the brake pads to be realigned for reduced pad wear.

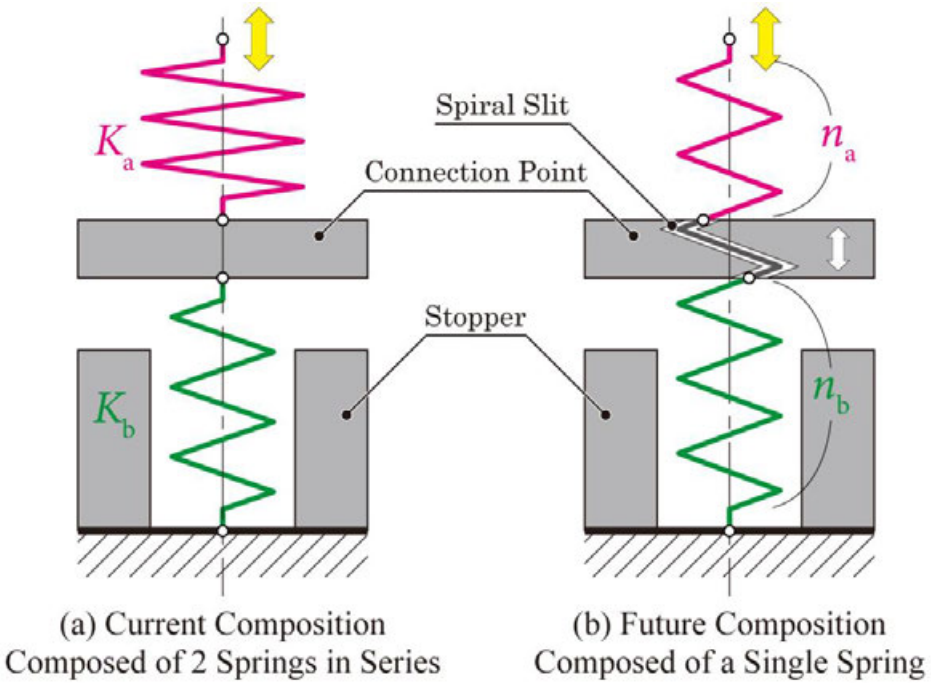

Fig. 139 Concept of the multistage springs composed of (a) two linear springs proposed in this research and (b) a single coil spring split in two by a connector.

Section IV.5.5 Effect of pad wear

Changes in the magnetic attractive and spring repulsive forces are dependent on the translational actuation of the control rod. However, for the brake pads, the contact surfaces of the outer frame and attraction target surface of the IB magnet, wear with each use. This results in the incomplete compression of the spring relative to the approaching surface of the pair of magnets.

Fig. 140 shows the predicted change in the displacement–force characteristics of the multistage spring for the 2nd prototype of the IBM brake after wear. The wear resulted in an increased gap between the pads measuring 0.4 mm, which is the value at which new replacement pads are required for the implemented EM brake. The point P_1, where the spring changes its spring constant, shifts to the left because the pads make contact at a later time than before wear. This results in a delay in the increase of the repulsive force of the spring after the change to the larger spring constant. The estimated maximum repulsive force decreases by 10.0 %. This indicates that the control force required by the actuator becomes larger with the duration of the use, assuming that no mechanical countermeasures are taken to adjust the repulsive force.

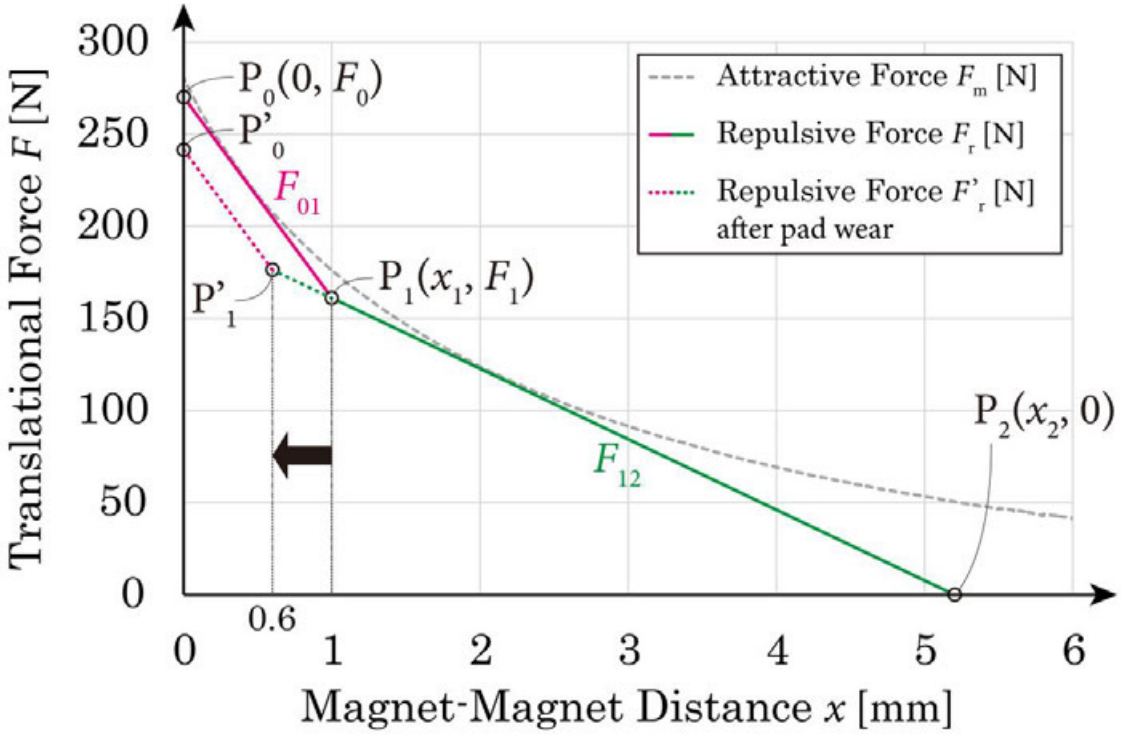

Fig. 140 Predicted change in the characteristic of devised multistage nonlinear spring for the 2nd prototype of the proposed IBM brake owing to pad wear.

Chapter IV.6 Conclusion of Part IV

In this part, the concept of an IBM brake was demonstrated by building the 1st prototype that uses a conical coil spring. Experiments were conducted to verify the amplification feature of its magnets on the braking torque and the compensation feature of its spring on the input control force. The prototype demonstrated that the torque–force ratio was at most 18.1 times that of the contrasted EM brake. Further, the disadvantages of using a conical coil spring, that is, restriction in characteristic design, inconvenience in production, and a long actuation stroke required for pad separation, were analyzed.

Then, to overcome these problems, a novel nonlinear spring comprising two linear springs in series was devised. One spring works for compensation and the other for suspending the brake pads; however, they serve as a single synthesized compensation spring when brake pads are separated; this resulted in switching the spring constant to follow the nonlinearity of the attractive force of magnets. A 2nd prototype using this multistage spring was developed and verified to be effective; the dynamic torque increased to 192.9 % of the EM brake torque while only consuming energy when latching the braking state, resulting in a higher torque–energy efficiency when braking took longer than 0.43 s. The numerical calculation results confirmed that the observed responsiveness of the brake was in line with the theoretical value and comparable to the existing EM brake.

In this manner, the proposed principle of the IBM brake was successfully validated, implying that replacing conventional EM brakes with the IBM brakes would contribute to a significant increase in the mileage of vehicles. Furthermore, the multistage spring would also be effective in shortening the stroke of an IB magnet used as the DF converter and the conventional attraction devices for walls and ceilings.

In future studies, the structural design will be improved and simplified. A multistage single spring will be considered for achieving higher compensation precision with an easier adjustment method, along with a weight compensation mechanism to make the brake orientable to any installation posture. The feedback from the research outcome also contributes to an improvement of the IBM gripper by shortening the actuation distance of the control rod.

Part V

General discussions

Part V General discussions

Chapter V.1 Common features of the mechanisms realized in the study

As described through the paper, the author has developed various compensation mechanisms that use a spring and a "reverse spring." While they ideally cancel out each other's control force for deformation, in most cases the actuator increased its energy consumption, meaning that the control force was required to an unignorable extent. The mechanical advantages, the rate of maximum output to input force expressed as Eq. (1), of the developed robotic components remained realistic as revealed in Fig. 141, which would have been infinitely large if the complete compensation was established.

Summarizing the discussions in the parts and chapters indicates the major causes of difficulties of achieving a high compensation precision. First, forces transmitted via cam–follower, rack–pinion, and lever–follower systems are split into component forces due to the existence of a pressure angle, resulting in a transmission efficiency of less than one. Acquiring proper lubrication is also difficult, as the friction increases the energy consumption of the actuation, and it is necessary for these transmission systems. Second, nonlinearity and individual differences of displacement–force characteristic of linear springs, constant springs, and magnets require the re-measurement of these characteristics and re-calculation in the design procedure of the corresponding compensation spring for each individual machine, leaving a difficulty for mass-production. Third, a lack of sufficient rigidity and assembly precision of the mechanism structure required to endure the large applied internal force results in an unintended deformation that decreases the transmission efficiency and increases the phase difference between the actuations of the spring and reverse spring. This tendency is more notable as the system becomes more complicated mechanically with many components and thus a long transmission route.

Improving the compensation precision of DF converters by solving these problems left unsettled would yield with a much higher mechanical advantage.

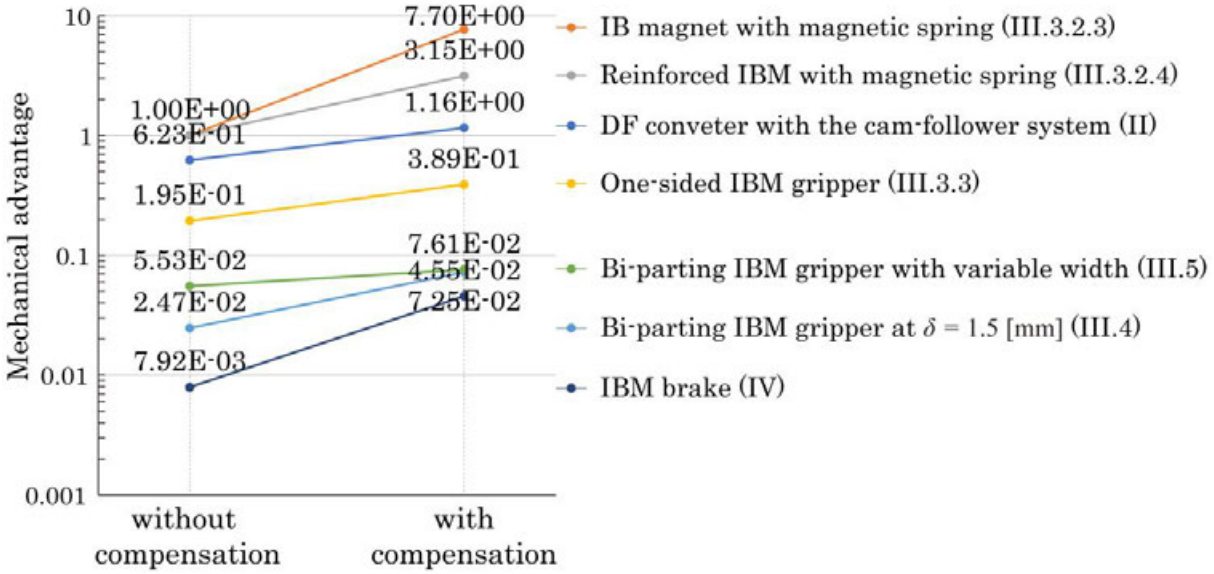

Fig. 141 Mechanical advantages of the prototype models using the DF converter developed in the study. The approximate values of the bi-parting IBM grippers are calculated using a general transmission efficiency 0.6 of the lead screws and the nominal stall torques of the motors found at [38], [80].

Chapter V.2 Further applications of the DF converter

Section V.2.1 Research expansion to "compensation mechanics"

Not limited to the mechanisms that exert attractive and pressing forces, the author has developed various designs that contain an IB magnet as the DF converter inside themselves, as listed in Fig. 142. This includes a repulsive force of the spring and the intensity of magnetic flux, which are briefly introduced in this section. The research team named this comprehensive study "compensation mechanics" and has tried to establish a new systemized academic field on its common design methodology. There many additional ideas implied in the list, such as torque compensation mechanism using diametrically magnetized circular magnets, magnetic variable suspension mechanism, and floating display stand are planned for possible research themes.

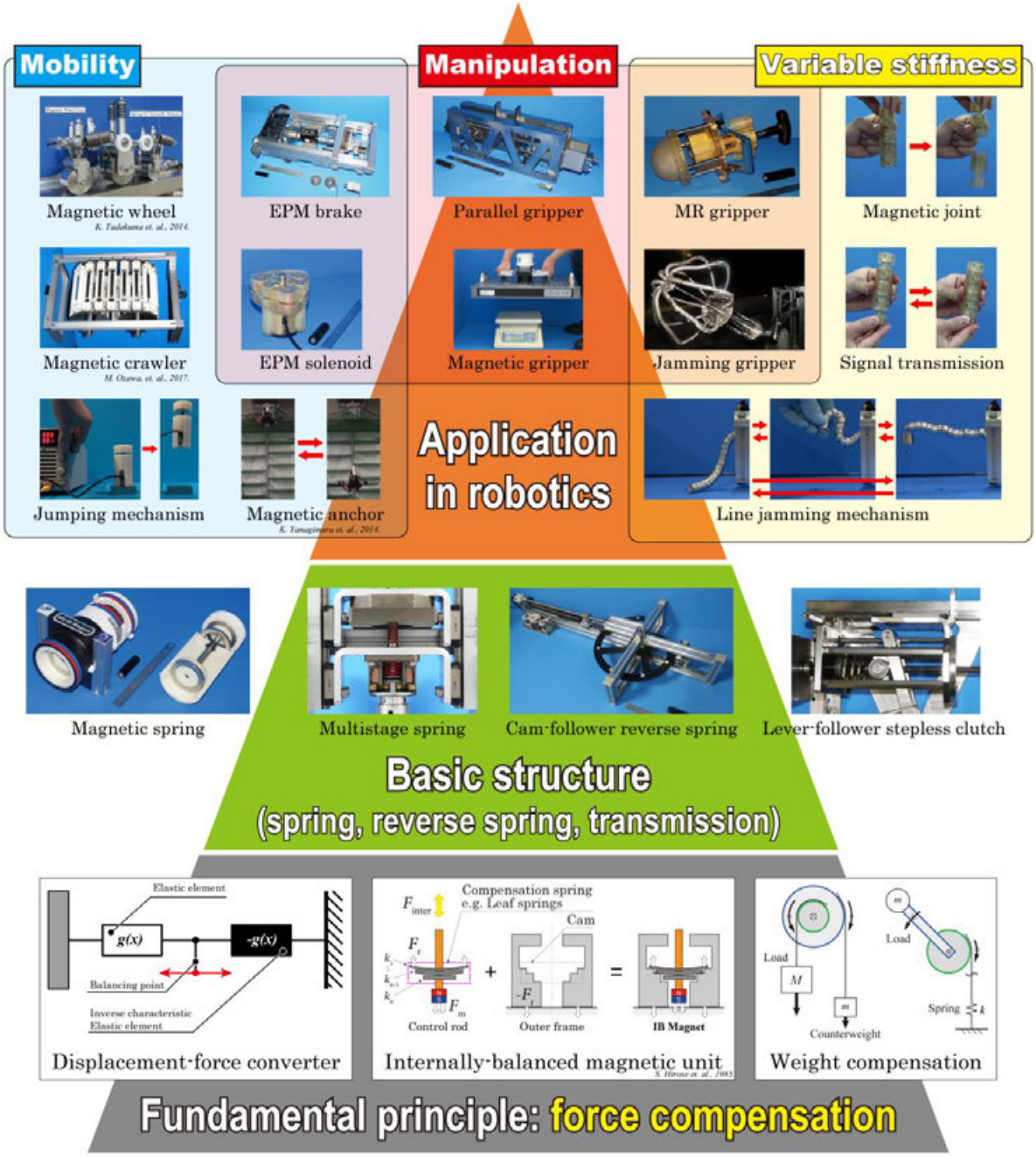

Fig. 142 System diagram of the study on the "compensation mechanics" including fundamental principle, basic structure, and robotics applications of the displacement–force converter (DF converter).

Section V.2.2 Magnetorheological variable stiffness robotic gripper using an IB magnet

Robotic grippers, the most major end effectors for manipulation, have various designs customized to fit each designated shape of target objects to be handled. Therefore, the handling system has to replace its gripper to correspond to items with unique shapes, resulting in the loss of time, such as in the transportation industry and high-mix low-volume production. Moreover, standalone robots with strict limitations on the power source, size, and mass have difficulties in carrying various end effectors to prepare for unexpected tasks, such as in disaster fields and scientific expedition.

Universal soft grippers, whose contact surface deforms to fit an object of any shape and size and then solidifies to hold it firmly have been developed under such demand. They are also advantageous in handling fragile objects, as the grippers do not exert the clamping force actively. This method is accomplished by reversible variable stiffness phenomena such as granular [3]–[5], layer [107], [108], and wire jamming [109], [110]. These grippers are commonly composed of a soft bag- or torus-shaped membrane filled with jamming media such as powder, films, and wires. Moreover, the study team has found that fusible alloy [111] and hot ice (a supercooled solution of supersaturated sodium acetate that does not crystallize under the melting point until a shock is applied) [112], [113] are also applicable. These jamming media in low-rigidity state can move in the membrane fluidly, allowing it to have an indeterminate form, and then fix their relative position in the high-rigidity state once the gap among them is reduced by decompressing the working fluid (typically air or water) inside the membrane. Therefore, contrary to the dexterous advantages, these grippers have inconveniences of equipping a massive and bulky pneumatic or hydraulic source.

To solve the abovementioned problems, two solutions were developed in this study. One is the gripper using the line-jamming mechanism introduced in Chapter II.2, in which wire tension is used to switch the state of rigidity, and the other is a gripper using the magnetorheological (MR) fluid.

Here, the MR fluid is a functional fluid composed of a carrier oil and filler magnetic particles. The particles are distributed in the oil under normal circumstances, while they align along the magnetic flux to form chains to decease fluidity once the magnetic field is applied, resulting in an increase of the apparent viscosity. This feature has been used in electromagnetic brakes [93], dumpers [114], fixtures [115], and variable stiffness grippers [56], [70], [116], [117].

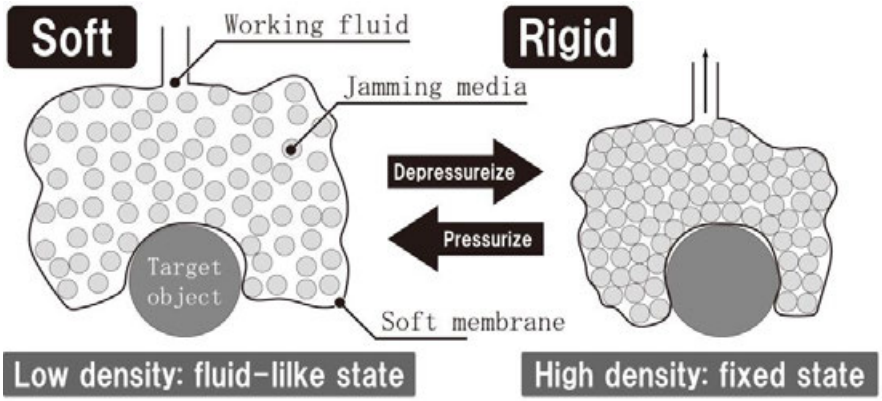

Fig. 143 Principle diagram of variable stiffness robotic gripper using jamming phenomenon.

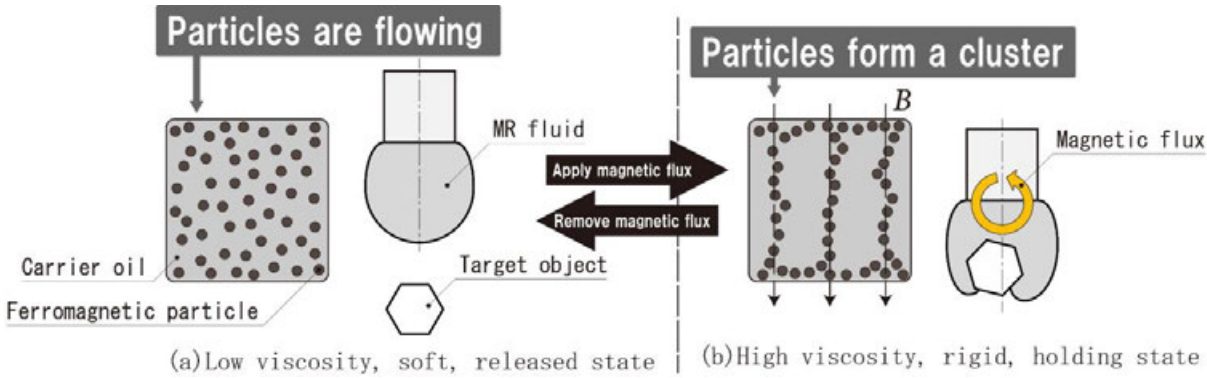

Fig. 144 Principle diagram of an MR variable stiffness robotic gripper.

As illustrated in Fig. 145, there are multiple ways to supply the magnetic field to MR fluid. The fact that they consume electricity to (a) actuate a permanent magnet [116], (b) switch a magnetic yoke [70], (c) excite a solenoid of an electromagnet, and (d) cancel the flux of an electropermanent magnet [56], [115], [118] degrades the profit of the portability of the MR gripper by requiring a large power supply to the robot, which makes it unsuccessful in energy saving or long-time operation.

Therefore, as illustrated in Fig. 146, the study proposes a new method of supplying the flux using the IB magnet such that the permanent magnet can be actuated by a much smaller force than its attraction force. As repeated, while existing applications of IB magnets have been limited to attraction devices, the proposed mechanism is unique in that the IB magnet is used as a magnetic flux supplier that does not any exert force (or perform work) externally, which means that the energy consumption for switching the stiffness can be ideally eliminated if compensation is precisely established.

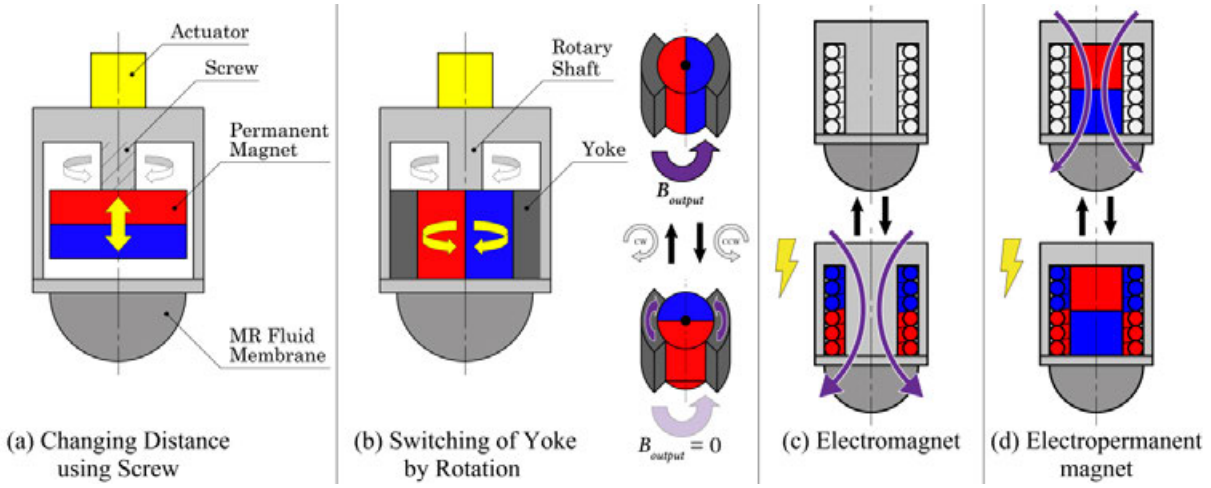

Fig. 145 Conventional methods of providing magnetic flux to the MR variable stiffness robotic gripper.

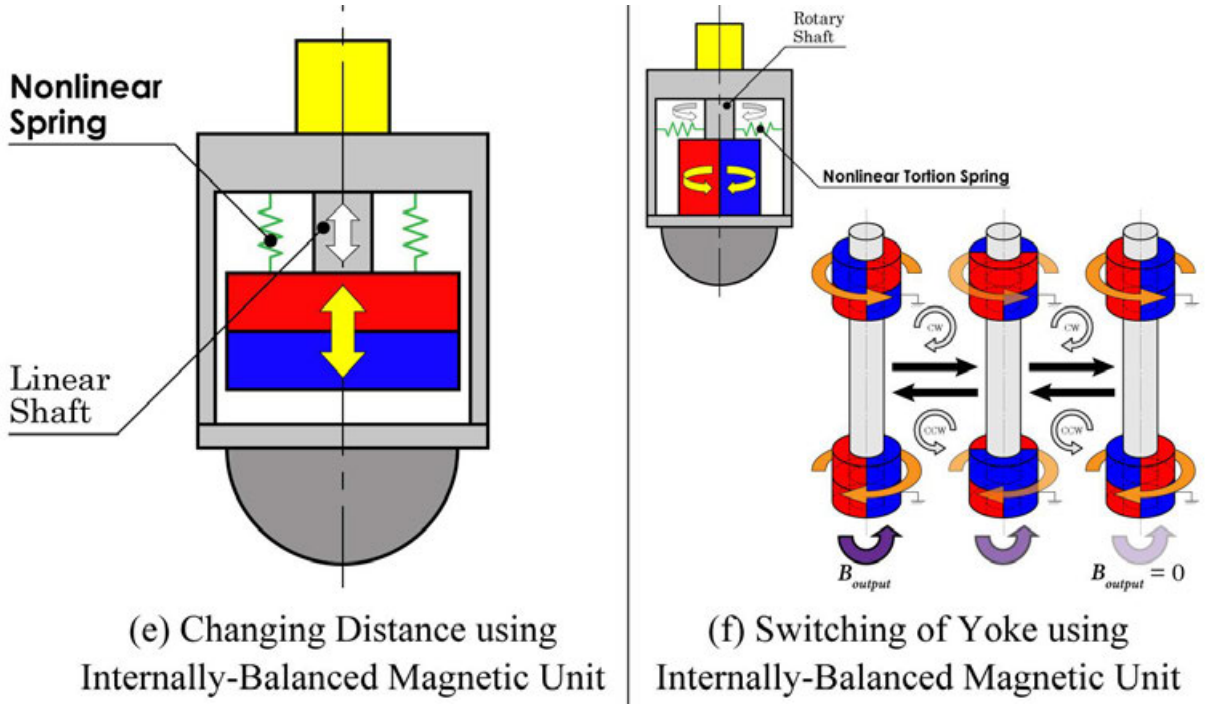

Fig. 146 Principle diagram of the MR variable stiffness robotic gripper using an IB magnet.

Based on the proposed principle, a POC prototype of the MR gripper using an IB magnet was developed, as shown in Fig. 148. To design its nonlinear spring, the attractive force between the magnet and the membrane filled with the MR fluid was measured as recorded in Fig. 147. Observations revealed that countermeasures are required to sustain the diffusion of the ferromagnetic particles in the carrier oil and prevent the attractive force from increasing with time and usage. Without countermeasures, the particles tend to either precipitate owing to gravity or gather near the attraction surface.

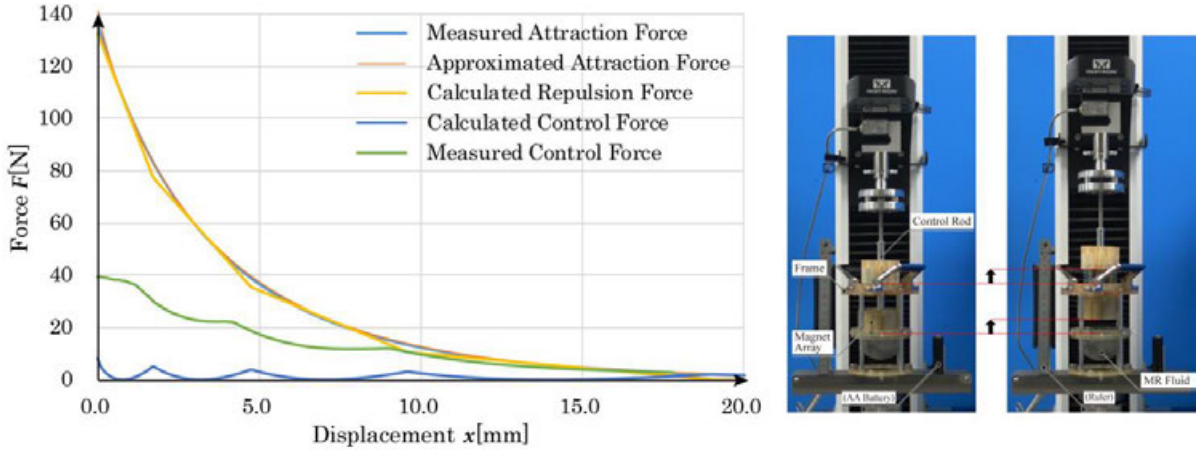

Fig. 147 System constituents and result of the performance evaluation experiment of the prototype of the MR variable stiffness robotic gripper using IB magnet.

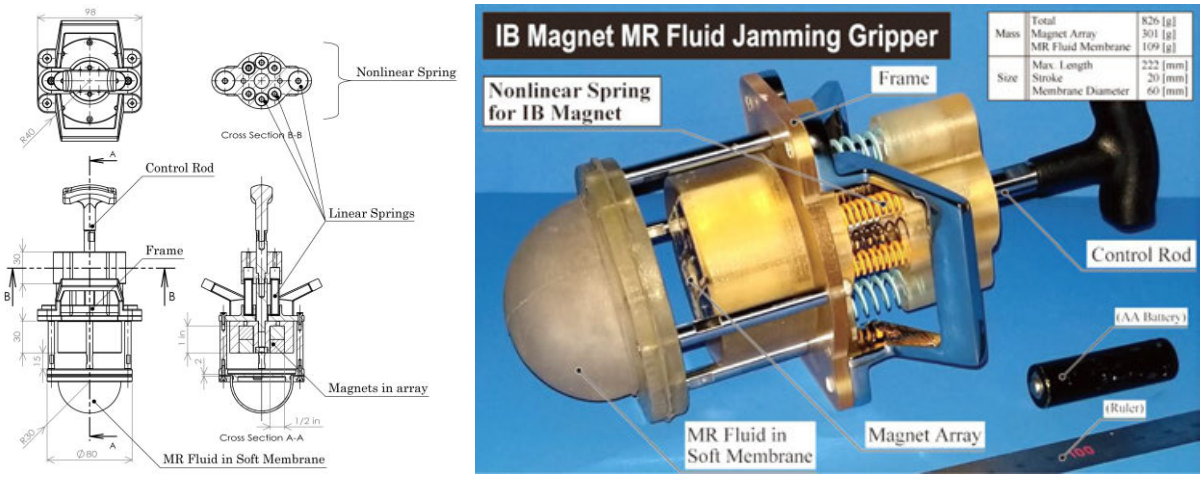

Fig. 148 Design sketch and appearance of the prototype of the MR variable stiffness robotic gripper using an IB magnet.

A basic operation of the MR gripper using an IB magnet to handle a tube fitting (PISCO, PE6, nonmagnetic, 11 g) was conducted as recorded in Fig. 149. (a)–(b) First, the membrane in the low-rigidity state is pressed on the target object. (c) The control rod is pushed down to attach the permanent magnet from the membrane filled with the MR fluid, resulting in a transition to the high-rigidity state. (d) The gripper successfully lifts the object captured on the deformed surface of the membrane. (e)–(g) The membrane is rigid enough to not drop the object even if the gripper is shaken. (h) Last, the control rod is pulled out to re-soften the membrane and thus to release the object. By enabling the operation process with a small hand-driven control force, the gripper successfully validated the applicability of the IB magnet as an energy-saving magnetic flux supplier.

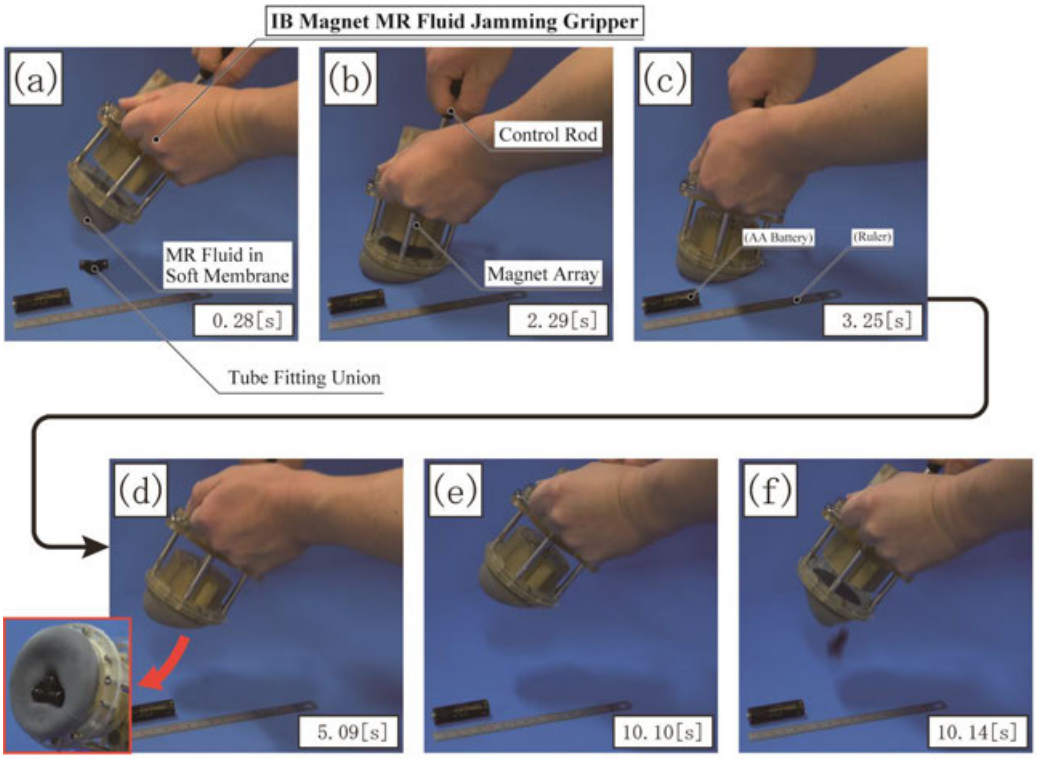

Fig. 149 Experimental operation process of the prototype of the MR variable stiffness robotic gripper using IB magnet.

Section V.2.3 Electropermanent jumping mechanism using the IB magnet

As a method for comprehensively searching a wide area at a disaster site, the effectiveness of a swarm search robot, an operation form in which a many group robots are thrown in has attracted attention [119]–[121]. Dropping from aerial vehicles, throwing from a catapult, and hand throwing [122], [123] have been proposed as the main methods for exploring wide areas efficiently for a rapid disaster response. For this purpose, the platform robot should be small and lightweight to transport objects and enter narrow spaces easily. However, if the height of the step that can be overcome is reduced due to the smaller diameter of the wheel caused by miniaturization, the mobility performance on rough terrains would also decrease.

As a method of improving the mobility performance on rough terrains by wheels, variable-shaped wheels [124], [125] that increase the diameter and jumping mechanisms achieved by elastic bodies or compressed air [126], [127] have been studied. However, these require high-power actuators, which imposes design constraints on downsizing and weight reduction, and causes problems such as a decrease in operating time due to large power consumptions. Therefore, this study proposes a jumping mechanism that solves these problems by implementing the IB magnet as a force amplifier for the actuator to compress the elastic body.

Fig. 150 shows the basic principle of the IB magnet jumping mechanism. (a) First, the nonlinear spring embedded both for compensation and jumping is compressed while relieving the external control force. (b) With the realization of the attached state, the attraction work of the magnet is stored in the spring as elastic energy. (c) Next, momentarily exciting the electromagnet cancels the magnetic field of the permanent magnet, intentionally breaks the balance of the forces, and loses its ability to keep the spring compressed. (d) The control rod now receives only the repulsive force of the spring and thus gets pulled out rapidly. Then, the elastic energy of the spring is converted into the kinetic energy of the control rod. (e) A part of its momentum is transferred to the outer frame when it reaches the maximum stroke point, which leads to the jump of the whole mechanism.

The system requires only a weak force to compress the force and a short-time current input to initiate the jump, providing a desirable energy-saving feature. Furthermore, even the actuator can be omitted if exciting the electromagnet inversely such that both the permanent magnetic and electromagnetic attractive forces work to compress the spring, contributing to miniaturization and weight reduction.

Only attraction mechanisms have been studied according to the IB magnet. The concept of the proposed jumping mechanism is different from conventional research in that the utilization of the repulsive force of the spring in the IB magnet is the main objective. Moreover, the jumping mechanism regards the sudden detachment of the control rod as a positive phenomenon, which has been a serious problem for IB magnets that are precisely balanced, and they are sensitive to external disturbance such as vibration and shock.

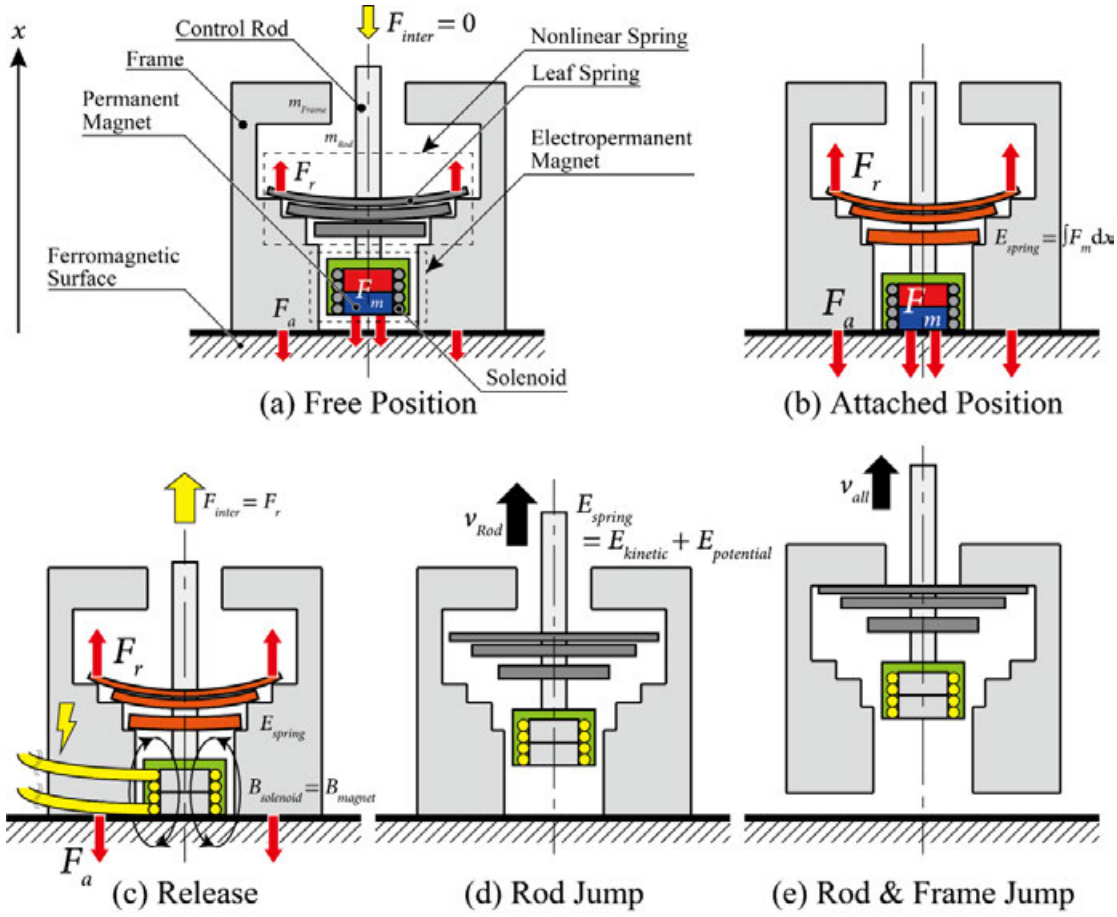

Fig. 150 Principle of the proposed jumping mechanism using an IB magnet.

Based on the proposed principle, a POC prototype of the jumping mechanism using an IB magnet was developed as displayed in Fig. 151. An electropermanent magnet is used as the attraction magnet and magnetic spring composed of a pair of permanent magnets as the compensation spring (at the expense of compensation precision and mass, for a rapid prototyping).

A basic operation using it was conducted as recorded in Fig. 152. (a) First, the mechanism was placed onto an iron block with the dimension of $50 \times 50 \times 15$ mm^3 as the attraction target object. (b) The control rod was pushed in to attach to the target object, as a usual operation for an IB magnet. (c) Soon after the electromagnet was excited, the control rod was released, which led to a jump. In this way, the experiment successfully validated the applicability of the IB magnet as an energy saving generation of a repulsive force.

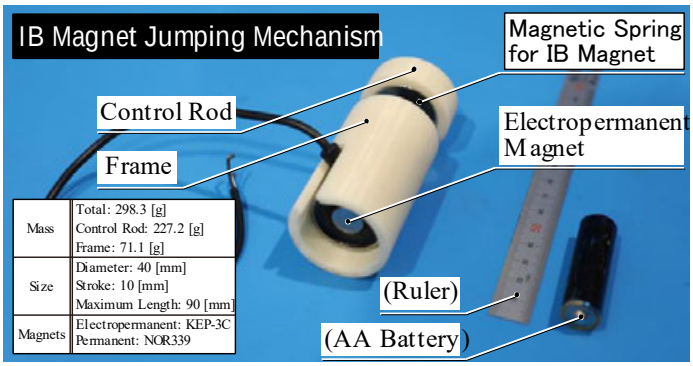

Fig. 151 Appearance of the prototype of the proposed jumping mechanism using an IB magnet.

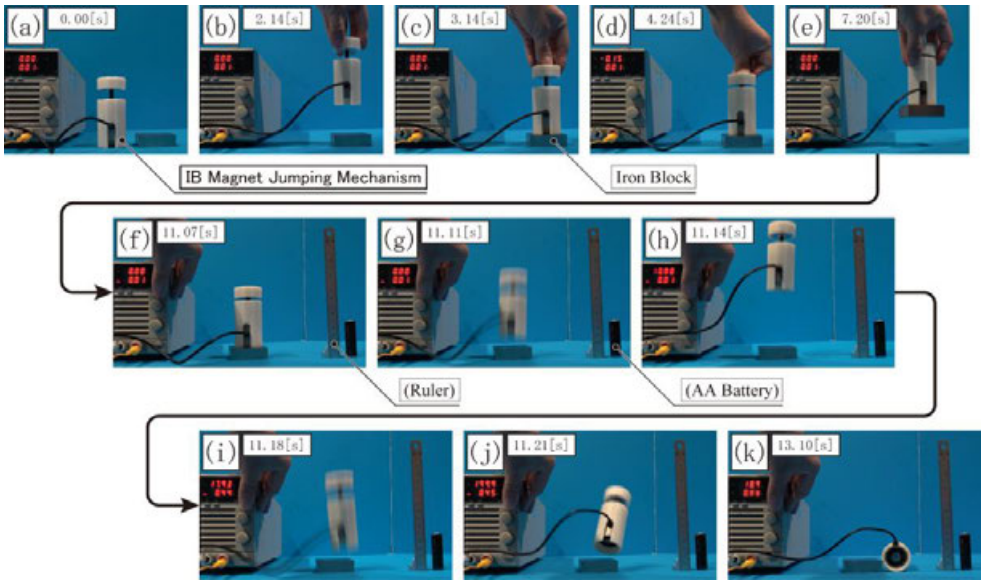

Fig. 152 Experimental operation process of the proposed jumping mechanism using an IB magnet.

Chapter V.3 Significance and novelty of the study: value creation on enhancement of energy efficiency in disaster robotics

Section V.3.1 Applications to mobile robots

Disaster robotics is a study on robotic assistance and replacement of tasks in extreme environments with severe conditions such as temperature, pressure, altitude, vacuum, narrowness, debris, fire, underwater, and radiation. There, remote and autonomous robots are expected to ensure safety, speed up, increase the efficiency, reduce failure, and expand the applicable fields of tasks in areas to which humans cannot enter or stay for a long time. Mobile robots that engage in such disaster responses are mainly powered by an isolated battery or generator, considering the versatility of independence on the target environment and difficulty of handling the power cable. Furthermore, robots penetrating into debris and drones flying for a long time, for example, have more strict restrictions on dimensions, mass, and power source capacity. Therefore, for a robot to perform as efficiently as possible with a limited operation time and number of trials, it has to be equipped with components that have a higher ability per energy consumption, which is expected to be accomplished by the proposed DF converter. This is one of the common motivations of the series of the research developments, which has been conducted to increase performance–energy efficiency of robotic components including but not limited to a parallel gripper. This was done such that they can be driven by small, lightweight, weak, and low-power actuators, which was accomplished by embedding internal force compensation mechanisms inside these components.

Section V.3.2 Applications to machines other than mobile robots

Not limited to disaster response, hardware development on field robotics has tended to focus on mobility mechanism such as omnidirectional locomotion, multi-legged locomotion, and transformable wheels. However, sometimes there occurs a deviation between the technology proposed from the intellectual curiosity and academic interest of robotic researchers and that required by the actual scene of application, as the cost and technological matureness are not the only problem.

In the damage inspections and decommissioning of the Fukushima Daiichi nuclear power plant, triggered by the tsunami in the 2011 Great East Japan earthquake and carried through to the present, there have been situations in which mobile robots were not evaluated as the best solution to apply. Those include: no wide continuing passages to the working place are available for a ground vehicle [128]; robots cannot be salvaged and repaired as they get severely radiated, resulting in a large radioactive waste [129]; Workers wearing protective clothing are more suited, and it is inexpensive to quickly breakthrough infrastructures made for people such as stairs and ladders. In these situations, human workers have not been replaced by robots, or they carry robotic equipment into a designated point and install them at the risk of radiation exposure, which is considered to be more precise and certain than mobile robots.

Other ongoing research and development that choose machinery resembling heavy-duty construction equipment rather than mobile robots: ten-meter class robotic arms are going to be adopted to a debris-collection task in the melted-down reactor containment vessel that can skip over any terrain obstacles and be relatively easily withdrawn by pulling out the base located far from the working place in the worst case [130], [131]; long horizontal booms and platforms loading cranes are going to be inserted from outside the reactor building into the spent fuel pool to remove the fuel rods [132]. However, there is a negative loop of the mass increase of equipment: for example, a substantially designed robotic arm requires powerful, large, and heavy actuators to cover its large self-weight, resulting in a requirement of even more rigid and massive structure. This also leads to another concern; a long robotic arm tends to bend due to self-weight that may lead to an

unintended contact and damage to the environment. To solve this problem, methods such as self- and tip-weight compensation and outsourcing of actuators by a pulley–wire system have been proposed to increase the liftable mass per self-weight, whose effectiveness is evaluated through experiments [133].

Considering these facts, the idea of labor saving of robotic components by the internal compensation proposed in this study provides one of the important perspectives on the use of low-power and lightweight actuators that were recently found to be necessary for further development of practical disaster response technology.

Chapter V.4 Conclusion of Part V

In this part, the features common in the mechanisms built in the entire study and their possible impact in disaster robotics were discussed. Further application instances of the IB magnet such as jumping mechanisms and MR gripper were also introduced, which indicate the unlimited expandability of the proposed DF converter in wider situations.

Part VI

Conclusion and future aspects

Part VI Conclusion and future aspects

Chapter VI.1 Conclusion of the thesis

This study was focused on a method used to gain a large, amplified output force of a robotic component out of a much smaller input force. The idea of the displacement–force converter was invented by embedding an internal force compensation mechanism inside a machine. This is designed to amplify the force continuously and spontaneously by reducing the control force required to convert the actuation displacement to the force amplification state, with the aid of a compensating pair of a spring and reverse spring. By improving their performance–energy efficiency, the DF converter was expected to allow robotic components to select a smaller, weaker, and lighter actuator.

The study was aimed at devising two kinds of reverse springs for the purpose of proving and proposing the concept of the DF converter, and at applying them to three major robotic components for the purpose of demonstrating the usefulness of their force amplification feature in robotics.

First, a preliminary prototype of the DF converter using a pulley–wire system was built, its ability to regulate the elastic tension was proved, and the problem of the deviation angle between the pulley tangent and the vertical direction of the radius was analyzed. As a solution, a DF converter using a cam–follower system was developed, and it successfully decreased the energy consumption and the maximum control force required to extend the spring. The uniformization of the forces for extension and compression implied applicability of an actuator with a smaller maximum output. Moreover, it was incorporated into a variable stiffness mechanism of a fire-resistant gripper as a wire tensioner in place of a conventional massive pneumatic actuator to regulate the rigidity of its finger continuously, indicating the possibility of the efficiency improvement of tasks of a disaster robot.

Next, another DF converter using an internally balanced magnetic unit was developed to realize a parallel gripper with an ability to continuously adjust the amplified clamping force from zero to the maximum by regulating the attraction distance, unlike existing load-sensitive grippers with binary toggles and clutches. By developing methods of parameter optimization, simplification of design

procedure, and downsizing while maintaining precision of the nonlinear springs, the IBM gripper successfully increased the maximum clamping force while suppressing the increase in energy consumption, resulting in the multiplication of the force–energy efficiency ratio, compared to the constitution directly driven by a single actuator without compensation. Furthermore, a width adjustment mechanism using a lever was also devised to achieve a more steady and predictable clamping force independent of the target object width, by splitting the actuation of the finger and the compensation mechanism. This realized the linearization of the width–force characteristic to be sufficiently insignificant on the major value of the output.

Furthermore, as another configuration of the IBM gripper, an electromagnetic brake was developed by equipping the fingers with brake pads. To solve the problem of the pad having to be actuated for a long compensation stroke to fully disable braking, a novel multistage spring comprising two linear springs in series, which detaches the pad in accordance with a small displacement in addition to decreasing its spring constant to compensation, was devised. The prototype verified to be superior to the contrasted EM brake in both static and dynamic friction torque while keeping the responsiveness comparable.

Lastly, general discussions on the common features of the mechanisms observed throughout the entire study, problems on compensation precision and miniaturization left unsettled, and their possible solutions were made.

In these ways, it can be concluded that the research outcomes successfully verified the effectiveness of the DF converter for stepless force amplification and demonstrated its applicability to robotic components, achieving all of the objectives. By introducing even further application instances of the expanding research field named “compensation mechanics,” the study implied an impactful contribution of the DF converter to the performance improvement of machines in extreme environments with strict restrictions on design and operation.

Chapter VI.2 Future aspects

For further development of the mechanisms using the DF converter, methodology of designing a sophisticated structure with a more accurate

compensation precision, reduced friction, and rigid structure shall be established with the aid of the finite element method to achieve a higher amplification rate and transmission efficiency. This will lead to investigating the implementation-oriented version of the robotic components with a more practical and practicable size and mass for integration in robotic systems. An electromagnetic analysis is expected to be effective to shield the magnetic flux such that the magnetic circuit flows into the target surface without leaking out to the environment or interfering with the component, such as its sensors and ferromagnetic structure. Moreover, unlike developed prototypes assuming static movement of the point of equilibrium of force, applications with rapid actuation shall be designed considering its dynamic model with mechanical impedance of its spring and reverse spring.

Moreover, for a higher versatility, adding a weight compensation feature is preferred to make the mechanism orientable to any installation posture. An adjustable feature of the compensation force that realigns to changes of the compensated force (e.g., mechanical fatigue of spring, demagnetization of permanent magnet due to heat and radiation exposure) referencing methods such as [19]–[21] may be integrated.

The feedback from the research outcome of application examples such as the magnetic, conical coil, and multistage linear springs is expected to contribute to the improvement of the IB magnet for realizing miniaturization, low-cost mass production, and shortening the actuation distance of the control rod.

For software development, a numerical model for estimating the exerted clamping force according to the elasticity of the mechanism and clamped object will be established to develop a control law.

Evaluation methods with quantitative indices of performance per input force, energy consumption, volume, and mass, would reveal the replaceability of the conventional products by the proposed robotic components using a DF converter.

Then, the application will be expanded to the studies of hand-driven labor-saving tools and powerless sensors to amplify the change in the environment used for biologging and environmental observation.

ACKNOWLEDGEMENT

First and foremost, I am extremely grateful to my esteemed supervisor and chief inspector, Prof. Tadakuma for his invaluable advice and continuous guidance during my PhD study. His immense knowledge, suggestive ideas and plentiful experience have encouraged throughout the duration of my academic research. I thank Prof. Hashimoto, Prof. Hirata, and Prof. Tadokoro for their insightful feedback that drastically improved my doctoral thesis.

I thank Prof. Watanabe, Prof. Abe, and all the members of the mechanism team of Tadokoro Human–Robot Informatics Laboratory. Their assistance and support made me enjoy my research and academic life in Tohoku University. Furthermore, I am grateful to the laboratory secretaries and dormitory administrators of the University House. Without their support for the eight-years, I would not have completed my research. I would really appreciate if these people kept cheering for me as I am eager to continue giving my best to invent and widespread robotic technology valuable for human society and progress of science as a responsible researcher.

This work was mainly supported by JSPS KAKENHI Grant Number JP20J20184. Moreover, I sincerely thank Nakamura-sekizen Scholarship Foundation, JGC-S Scholarship Foundation, and the Morinokuni Scholarship Foundation for their financial support for my daily life.

Finally, I would like to conclude the acknowledgement by expressing my best gratitude to my parents, my sister Himari, and my grandparents for their tremendous understanding and encouragement.

REFERENCES

[1] K. Tadakuma and T. Tanaka, "Load-Sensitive Screw Clamping Mechanism to Realize Self High Speed & High Torque Mode Change," *Proc. JSME Annu. Conf. Robot. Mechatronics*, pp. 1P2-P09, 2015, doi: 10.1299/jsmermd.2015._1p2-p09_1.

[2] T. Takaki and T. Omata, "Grasp force magnifying mechanism for parallel jaw grippers," in *Proceedings - IEEE International Conference on Robotics and Automation*, 2007, pp. 199–204. doi: 10.1109/ROBOT.2007.363787.

[3] S. Hirose and Y. Umetani, "The development of soft gripper for the versatile robot hand," *Mech. Mach. Theory*, vol. 13, no. 3, pp. 351–359, 1978, doi: 10.1016/0094-114X(78)90059-9.

[4] G. Banconand and B. Huber, "Depression and Grippers with Their Possible Applications," in *12th ISIR*, 1982, pp. 321–329.

[5] J. R. Amend, E. Brown, N. Rodenberg, H. M. Jaeger, and H. Lipson, "A positive pressure universal gripper based on the jamming of granular material," *IEEE Trans. Robot.*, vol. 28, no. 2, pp. 341–350, Apr. 2012, doi: 10.1109/TRO.2011.2171093.

[6] M. L. Visinsky, J. R. Cavallaro, and I. D. Walker, "Robotic fault detection and fault tolerance: A survey," *Reliab. Eng. Syst. Saf.*, vol. 46, no. 2, pp. 139–158, Jan. 1994, doi: 10.1016/0951-8320(94)90132-5.

[7] A. Iborra, J. A. Pastor, B. Álvarez, C. Fernández, and J. M. Fernández Meroño, "Robots in Radioactive Environments," *IEEE Robot. Autom. Mag.*, vol. 10, no. 4, pp. 12–22, Dec. 2003, doi: 10.1109/MRA.2003.1256294.

[8] J. Trevelyan, W. R. Hamel, and S. C. Kang, "Robotics in Hazardous Applications," *Springer Handbooks*, pp. 1521–1548, 2016, doi: 10.1007/978-3-319-32552-1_58/COVER.

[9] V. Arakelian, M. Dahan, and M. Smith, "A Historical Review of the Evolution of the Theory on Balancing of Mechanisms," in *International Symposium on History of Machines and Mechanisms Proceedings HMM 2000*, 2000, pp. 291–300. doi: 10.1007/978-94-015-9554-4_33.

[10] G. Endo, H. Yamada, A. Yajima, M. Ogata, and S. Hirose, "A Weight Compensation Mechanism with a Non-Circular Pulley and a Spring: Application to a Parallel Four-bar Linkage Arm," *J. Robot. Soc. Japan*, vol. 28, no. 1, pp. 77–84, 2010, doi: 10.7210/jrsj.28.77.

[11] N. Takesue, T. Ikematsu, H. Murayama, and H. Fujimoto, "Design and Prototype of Variable Gravity Compensation Mechanism (VGCM)," *J. Robot. Mechatronics*, vol. 23, no. 2, pp. 249–257, Apr. 2011, doi: 10.20965/jrm.2011.p0249.

[12] B. A. Salamon and A. Midha, "An introduction to mechanical advantage in compliant mechanisms," *J. Mech. Des. Trans. ASME*, vol. 120, no. 2, pp. 311–315, 1998, doi: 10.1115/1.2826974.

[13] V. Arakelian, "Gravity compensation in robotics," *http://dx.doi.org/10.1080/01691864.2015.1090334*, vol. 30, no. 2, pp. 79–96, Jan. 2015, doi: 10.1080/01691864.2015.1090334.

[14] C. Baradat, V. Arakelian, S. Briot, and S. Guegan, "Design and prototyping of a new balancing mechanism for spatial parallel manipulators," *J. Mech. Des. Trans. ASME*, vol. 130, no. 7, pp. 0723051–07230513, Jul. 2008, doi: 10.1115/1.2901057/418130.

[15] M. J. French and M. B. Widden, "The spring-and-lever balancing mechanism, George Carwardine and the Anglepoise lamp," *Proc. Inst. Mech. Eng. Part C J. Mech. Eng. Sci.*, vol. 214, no. 3, pp. 501–508, Mar. 2000, doi: 10.1243/0954406001523137.

[16] Thomas R. Zaro, Scott D. Jones, and len F. Seng, "Crossing gate counterweight adjustment," U.S. Patent US6142426A, Oct. 15, 1998

[17] T. Aibara *et al.*, "Development of a Portable Field Arm with Gravity Compensation," *Proc. JSME Annu. Conf. Robot. Mechatronics*, pp. 1A1-H01, Jun. 2008, doi: 10.1299/jsmermd.2008._1a1-h01_1.

[18] R. Dzhavakhyan and N. Dzhavakhyan, "Balanced manipulator," SU Patent SU1521579, Nov. 15, 1989

[19] N. Lauzier, C. Gosselin, T. Laliberté, and P. Tremblay, "Adaptive gravity compensation of decoupled parallel and serial manipulators using a passive hydraulic transmission," *http://dx.doi.org/10.1243/09544062JMES1653*, vol. 223, no. 12, pp. 2871–2879, Sep. 2009, doi: 10.1243/09544062JMES1653.

[20] J. Woo, J. T. Seo, and B. J. Yi, “A Static Balancing Method for Variable Payloads by Combination of a Counterweight and Spring and Its Application as a Surgical Platform,” *Appl. Sci. 2019, Vol. 9, Page 3955*, vol. 9, no. 19, p. 3955, Sep. 2019, doi: 10.3390/APP9193955.
[21] Y. Yoshimoto *et al.*, “Principle Verification Study of Load-Sensitive Gravity Compensation Mechanism - Experimental Considerations from Motion Observationof Prototype Mechanismwith Fixed Angle underVarious Load,” in *Proceedings of the 2022 JSME Conference on Robotics and Mechatronics*, 2022, pp. 2P1-E08.
[22] Y. Tojo, P. Debenest, E. F. Fukushima, and S. Hirose, “Robotic system for humanitarian demining,” Sep. 2004, pp. 2025-2030 Vol.2. doi: 10.1109/robot.2004.1308121.
[23] S. Hirose, K. Ikuta, and K. Sato, “Development of shape memory alloy actuator. (Improvement of output performance by the introduction of a .SIGMA.-mechanism),” *J. Robot. Soc. Japan*, vol. 4, no. 6, pp. 618–628, Dec. 1986, doi: 10.7210/jrsj.4.618.
[24] N. Ulrich and V. Kumar, “Passive mechanical gravity compensation for robot manipulators,” in *IEEE International Conference on Robotics and Automation*, 1991, vol. 2, pp. 1536–1541. doi: 10.1109/robot.1991.131834.
[25] K. Nagata and T. Kawachi, “Fatigue reduction wear,” JP Patent JP2016169444A, Mar. 11, 2015
[26] L. Daiya Industry Co., “Flexible and lightweight support to reduce the burden of half-sitting posture DARWING SATT | Product Details | Daiya Industry Co., Ltd.” https://en.daiyak.co.jp/product/detail/?id=2375 (accessed Nov. 24, 2022).
[27] S. Hirose, M. Imazato, Y. Kudo, and Y. Umetani, “Internally balanced magnetic unit.,” *J. Robot. Soc. Japan*, vol. 3, no. 1, pp. 10–19, Feb. 1985, doi: 10.7210/jrsj.3.10.
[28] M. Suzuki, K. Tsuru, and S. Hirose, “Design of Nonlinear Spring and Mechanism for Internally-balanced Magnetic Unit,” *J. Robot. Soc. Japan*, vol. 27, no. 4, pp. 460–469, 2009, doi: 10.7210/jrsj.27.460.
[29] K. Tadakuma and T. Tanaka, “IBM Wheel：Mechanism of Internal Balanced Magnetic Wheel：Basic Concept and the First Prototype Model,” *Proc. JSME Annu. Conf. Robot. Mechatronics*, pp. 1P2-O01, May 2014, doi: 10.1299/jsmermd.2014._1p2-o01_1.
[30] M. Ozawa, K. Tadakuma, Y. Okada, and S. Tadokoro, “Internally Balanced Magnetic Crawler,” in *the 19th Annual Conference of System Integration Division of Society of Instrument and Control Engineers*, 2017, pp. 1D5-08.
[31] Paul Scirica and Cathy Aranyi, “Surgical instrument,” U.S. Patent 6565508B2, May 20, 2003
[32] K. Tadakuma *et al.*, “Floating Displacement-Force Conversion Mechanism as a Robotic Mechanism,” *arXiv:1907.09955*, Jul. 2019.
[33] T. Okada, “Design of pantograph mechanisms for force generation.,” *J. Robot. Soc. Japan*, vol. 4, no. 2, pp. 109–118, Apr. 1986, doi: 10.7210/jrsj.4.109.
[34] K. Koser, “A cam mechanism for gravity-balancing,” *Mech. Res. Commun.*, vol. 36, no. 4, pp. 523–530, Jun. 2009, doi: 10.1016/j.mechrescom.2008.12.005.
[35] J. Kim, J. Moon, J. Kim, and G. Lee, “Design of Compact Variable Gravity Compensator (CVGC) Based on Cam and Variable Pivot of a Lever Mechanism,” in *IEEE International Conference on Intelligent Robots and Systems*, Nov. 2019, pp. 3583–3588. doi: 10.1109/IROS40897.2019.8967609.
[36] V. L. Nguyen, C. Y. Lin, and C. H. Kuo, “Gravity compensation design of planar articulated robotic arms using the gear-spring modules,” *J. Mech. Robot.*, vol. 12, no. 3, Jun. 2020, doi: 10.1115/1.4045650.
[37] Japan Cam Industry, *Cam mechanism handbook*. Nikkan Kogyo Shimbun, 2001.
[38] “Pololu Items #3046, #3057 (1000:1 Micro Metal Gearmotor HPCB 12V) Performance at 12V,” *Pololu - Micro Metal Gearmotors*. https://www.pololu.com/file/0J1487/pololu-micro-metal-gearmotors.pdf (accessed Oct. 15, 2020).
[39] H. Chiu, H. Ozaki, E. Sato, T. Suzuki, A. Oho, and Y. Ariura, “An Analysis Using Offset Curves for Profiles, Manufacturing and Errors of Plane Cams,” *JSME Int. journal. Ser. C, Dyn. Control. Robot. Des. Manuf.*, vol. 36, no. 1, pp. 110–118, Feb. 1993, doi: 10.1299/jsmec1993.36.110.
[40] T. Takayama, S. Makita, and T. Omata, “Development of a Parallel Jaw Gripper with Bidirectional Force Magnification Mechanism,” *Trans. Japan Soc. Mech. Eng. Ser. C*, vol. 76, no. 772, pp. 3542–3548, 2010, doi: 10.1299/kikaic.76.3542.

[41] T. Takaki and T. Omata, “Load-Sensitive Continuously Variable Transmission for Robot Hands,” *J. Robot. Soc. Japan*, vol. 23, no. 2, pp. 238–244, 2005, doi: 10.7210/jrsj.23.238.
[42] T. Uchida, R. Sato, A. Ming, and M. Shimojo, “Development of leg mechanism using a knee joint with continuously variable reduction ratio adaptive to load,” *2015 IEEE Int. Conf. Mechatronics Autom. ICMA 2015*, pp. 1199–1203, Sep. 2015, doi: 10.1109/ICMA.2015.7237656.
[43] T. Takaki, Y. Yamasaki, and I. Ishii, “Load-sensitive continuously variable transmission using an oblique feed screw for parallel-jaw grippers,” *2011 Int. Symp. Micro-NanoMechatronics Hum. Sci. Symp. “COE Educ. Res. Micro-Nano Mechatronics”, Symp. "Hyper Bio Assem. 3D Cell. Syst. Innov.*, pp. 507–510, 2011, doi: 10.1109/MHS.2011.6102243.
[44] S. Hirose, C. Tibbetts, and T. Hagiwara, “Development of X-screw: a load-sensitive actuator incorporating a variable transmission,” *Proc. - IEEE Int. Conf. Robot. Autom.*, vol. 1, pp. 193–199, 1999, doi: 10.1109/ROBOT.1999.769965.
[45] J. Berengueres, M. Urago, S. Saito, K. Tadakuma, and H. Meguro, “Gecko inspired electrostatic chuck,” *2006 IEEE Int. Conf. Robot. Biomimetics, ROBIO 2006*, pp. 1018–1023, 2006, doi: 10.1109/ROBIO.2006.340368.
[46] A. H. Slocum, S. Awtar, and J. Hart, “Magnebots – A Magnetic Wheels Based Overhead Transportation Concept,” *IFAC Proc. Vol.*, vol. 35, no. 2, pp. 761–766, Dec. 2002, doi: 10.1016/S1474-6670(17)34031-4.
[47] Weimin Shen, J. Gu, and Yanjun Shen, “Proposed wall climbing robot with permanent magnetic tracks for inspecting oil tanks,” in *IEEE International Conference Mechatronics and Automation, 2005*, 2005, vol. 4, pp. 2072–2077. doi: 10.1109/ICMA.2005.1626882.
[48] L. P. Kalra, J. Gu, and M. Meng, “A Wall Climbing Robot for Oil Tank Inspection,” in *2006 IEEE International Conference on Robotics and Biomimetics*, 2006, pp. 1523–1528. doi: 10.1109/ROBIO.2006.340155.
[49] S. HIROSE, H. TSUTSUMITAKE, R. TOYAMA, and K. KOBAYASHI, “Development of Disk Rover, Wall-Climbing Robot using Permanent Magnet Disk.,” *J. Robot. Soc. Japan*, vol. 10, no. 7, pp. 992–997, Nov. 1992, doi: 10.7210/jrsj.10.992.
[50] K. Tsuru and S. Hirose, “Development of Vmax III: Magnetic Wall Climbing Robot with Holonomic and Omni-directional Mobility,” *J. Robot. Soc. Japan*, vol. 30, no. 6, pp. 639–647, 2012, doi: 10.7210/jrsj.30.639.
[51] K. Fondahl, M. Eich, J. Wollenberg, and F. Kirchner, “A magnetic climbing robot for marine inspection services,” *Sci. Eng. Fac.*, 2012.
[52] German Research Center for Artificial Intelligence GmbH, “MINOAS - Projects - Robotics Innovation Center - DFKI GmbH.” https://robotik.dfki-bremen.de/en/research/projects/minoas.html (accessed Feb. 24, 2018).
[53] “Development results: bridge maintenance robots, etc. | Technology Development Laboratory Co., Ltd.” http://www.rdi-japan.com/works.html#works03 (accessed Nov. 28, 2022).
[54] A. F. M. Jacobs, “Magnetic vacuum gripper including inflatable bellows,” U.S. Patent 7086675B2, Dec. 08, 2004
[55] M. Ito, “Magnet chuck type substrate holder,” JP Patent JP2541339B2, Mar. 29, 1990
[56] Y. Tsugami, T. Fukuzaki, and T. Nishida, “Consideration on the components of universal gripper using reformed MR fluid,” in *Proceedings of 35th SICE Kyushu Chapter Annual Conference*, 2016, pp. 208–211.
[57] H. Hayashi, S. Naka, J. Sutani, and T. Dozaki, “Bar magnet and magnetic material removing device,” JP Patent JP2003303714A, Apr. 09, 2002
[58] A. Kamiya, “Empty can separation box,” JP Patent JP5792881B1, Dec. 08, 2014
[59] S. Lee, “Moving robot using magnetic-force and cleaning robot for window having the same,” KR Patent 20160090711A, Jan. 22, 2015
[60] R. E. Meyer, “Magnetic gripper device,” U.S. Patent 5192155A, Apr. 20, 1992
[61] “Product Features | Window Cleaning Robot Window Mate WM Series .” https://windowmate-jp.translate.goog/pro/feature/?_x_tr_sl=auto&_x_tr_tl=ja&_x_tr_hl=ja&_x_tr_pto=wapp (accessed Nov. 28, 2022).

[62] K. Koura, Y. Okada, K. Ohono, and S. Tadokoro, “Unit performance evaluation of adhesion mechanism using electro and permanent magnets for UAVs,” *Proc. JSME Annu. Conf. Robot. Mechatronics*, vol. 2015, no. 0, pp. 2A1-G06, May 2015, doi: 10.1299/jsmermd.2015._2A1-G06_1.
[63] T. Fujinaka, K. Nagaya, N. Sakamoto, and K. Kasima, “Two-Dimensional Position Control Mechanism using Spring Actuator Stacked with Iron Particle Layers,” *Trans. Japan Soc. Spring Eng.*, vol. 2008, no. 53, pp. 37–43, May 2008, doi: 10.5346/trbane.2008.37.
[64] H. Yaguchi, S. Sakuma, and T. Kato, “A New Type of Magnetic Actuator Capable of Wall-Climbing Movement Using Inertia Force,” *J. Eng.*, vol. 2014, pp. 1–6, Oct. 2014, doi: 10.1155/2014/903178.
[65] K. Nagaya, M. Ishikawa, and N. Fujisawa, “Actuators for a Noncontact Magnetic Levitation Table and Its Application to Vibration Isolation Control.,” *Trans. Japan Soc. Mech. Eng. Ser. C*, vol. 61, no. 584, pp. 1381–1388, Apr. 1995, doi: 10.1299/kikaic.61.1381.
[66] K. NAGAYA, M. NAKATA, Y. MASUO, and S. IKAI, “On a new type torque-controllable electromagnetic disk brake.,” *Trans. Japan Soc. Mech. Eng. Ser. C*, vol. 54, no. 497, pp. 247–253, Jan. 1988, doi: 10.1299/kikaic.54.247.
[67] T. Go, T. Osawa, T. Ogawa, and T. Nakamura, “Development of Traveling Wave Type Omni-directional Wall Climbing Robot Using an Adhesion Device with Permanent Magnet,” *Trans. Soc. Instrum. Control Eng.*, vol. 51, no. 5, pp. 282–289, 2015, doi: 10.9746/sicetr.51.282.
[68] F. L. Simmons, “Permanent magnet chuck,” U.S. Patent 2700744A, May 24, 1951
[69] C. D. Briggs, “Magnetic chuck,” U.S. Patent 2918610A, Jan. 16, 1956
[70] T. Fukusaki, Y. Tsugami, and K. Nishida, “Development of universal gripper using modified MR fluid for gripping small objects,” in *18th SICE System Integration Division Annual Conference*, 2017, pp. 2446–2451.
[71] F. Kocijan, “Switchable magnetic device,” EP Patent 1425763B1, Aug. 26, 2002
[72] Y. Suzuki and K. Ohhata, “Permanent electromagnetic holder and conveyance device,” WO2021206074A1, Apr. 06, 2021
[73] “Magswitch Tools | Aichi Sangyo Co., Ltd.” https://www.aichi-sangyo.co.jp/products/magswitch/index.html (accessed Nov. 28, 2022).
[74] K. Tsuru and S. Hirose, “The omni directional vehicle moved on the wall,” *Proc. JSME Annu. Conf. Robot. Mechatronics*, vol. 2002, no. 0, p. 51, 2002, doi: 10.1299/jsmermd.2002.51_6.
[75] M. Suzuki and S. Hirose, “Proposal of Swarm Type Wall Climbing Robot System Anchor Climber and Development of Adhering Mobile Units,” *J. Robot. Soc. Japan*, vol. 28, no. 5, pp. 614–623, 2010, doi: 10.7210/jrsj.28.614.
[76] K. Yanagimura, K. Ohno, Y. Okada, E. Takeuchi, and S. Tadokoro, “Hovering of MAV by using magnetic adhesion and winch mechanisms,” in *Proceedings - IEEE International Conference on Robotics and Automation*, Sep. 2014, pp. 6250–6257. doi: 10.1109/ICRA.2014.6907781.
[77] S. Murata, E. Yoshida, A. Kamimura, H. Kurokawa, K. Tomita, and S. Kokaji, “M-TRAN: self-reconfigurable modular robotic system,” *IEEE/ASME Trans. Mechatronics*, vol. 7, no. 4, pp. 431–441, Dec. 2002, doi: 10.1109/TMECH.2002.806220.
[78] T. Goto, M. Uchida, and H. Onogaki, “External Environment Sensing by a Module on Self-reconfiguration Robot,” *IEEJ Trans. Fundam. Mater.*, vol. 131, no. 4, pp. 239–245, Apr. 2011, doi: 10.1541/ieejfms.131.239.
[79] M. Suzuki and S. Hirose, “Adjust Mechanism of Balance Force for Internally-Balanced Magnetic Unit,” 2007.
[80] “Pololu Items #3042, #3053 (150:1 Micro Metal Gearmotor HPCB 12V) Performance at 12V,” *Pololu - Micro Metal Gearmotors*. https://www.pololu.com/file/0J1487/pololu-micro-metal-gearmotors.pdf (accessed Feb. 24, 2021).
[81] T. Shimizu *et al.*, “Small Swarm Search Robot System with Rigid-Bone Parachute Rapidly Deployable from Aerial Vehicles,” in *2019 IEEE International Symposium on Safety, Security, and Rescue Robotics, SSRR 2019*, Sep. 2019, pp. 88–93. doi: 10.1109/SSRR.2019.8848955.
[82] T. Shimizu *et al.*, “MR Fluid Jamming Gripper Applying Internally-Balanced Magnetic Unit Controllable by Small Control Force,” *Proc. JSME Annu. Conf. Robot. Mechatronics*, pp. 2A2-G03, 2019, doi: 10.1299/jsmermd.2019.2A2-G03.
[83] H. Arakawa, “One-way chuck ,” S58-051470, Nov. 24, 1983

[84] K. Yamamoto, “Linear clutch,” JP Patent 2006132712A, May 25, 2006
[85] I. Onda *et al.*, “Force Diode Mechanism,” *Proc. JSME Annu. Conf. Robot. Mechatronics*, vol. 2021, no. 0, pp. 2P1-F06, 2021, doi: 10.1299/JSMERMD.2021.2P1-F06.
[86] K. Ito, “Linear clutch,” JP Patent 2895509B2, May 24, 1999
[87] M. Kawai, “The basic principle and example of Torque Diodes,” *JSME Ref. Collect. Annu. Meet.*, vol. 2006.8, no. 0, pp. 186–187, Sep. 2006, doi: 10.1299/JSMEMECJSM.2006.8.0_186.
[88] “About Arakawagrip,” *Arakawa & Co., Ltd.* https://www.arakawagrip-global.com/products/about-arakawagrip/ (accessed Nov. 25, 2022).
[89] F. Flemming, “The Basics of Electromagnetic Clutches and Brakes,” *MACHINE DESIGN*, pp. 55–58, Jul. 09, 2009.
[90] C. Xiang, J. C. Wang, Y. F. Gu, S. J. Zhang, and S. A. Chen, “Experiment, Optimization, and Design of Electromagnetic Track Brake for High-Speed Railways System,” *Math. Probl. Eng.*, vol. 2020, p. 6957963, 2020, doi: 10.1155/2020/6957963.
[91] M. Zhileykin and G. Skotnikov, “The method of increasing the stability of trailer-trucks in case of emergency braking in a turn and emergency failure of the trailer brake system,” *IOP Conf. Ser. Mater. Sci. Eng.*, vol. 820, no. 1, p. 012017, Apr. 2020, doi: 10.1088/1757-899X/820/1/012017.
[92] J. L. Liu, S. K. Wang, and J. Z. Wang, “The Experimental Research of Magnetic Powder Brake Loading Characteristic in Rotary System,” *Appl. Mech. Mater.*, vol. 130–134, pp. 3237–3241, 2012, doi: 10.4028/WWW.SCIENTIFIC.NET/AMM.130-134.3237.
[93] W. H. Li and H. Du, “Design and Experimental Evaluation of a Magnetorheological Brake,” *Int. J. Adv. Manuf. Technol. 2003 217*, vol. 21, no. 7, pp. 508–515, 2003, doi: 10.1007/S001700300060.
[94] J. Nadeau, M. Boisvert, and P. Micheau, “Implementation of a cooperative strategy between a vehicle’s mechanical and regenerative brake system,” Oct. 2014. doi: 10.1109/VPPC.2014.7007086.
[95] T. Zalud, “Getting A Grip On Clutch And Brake Selection,” *MACHINE DESIGN*, pp. 83–86, Sep. 09, 1999.
[96] Zeyaullah Ansari, Mohd Khalid Ahmed, Asif Ahmed, Shahid Husain, and Shadab Raza, “Design and development of Electro Magnetic Braking System,” *Int. J. Eng. Res.*, vol. 6, no. 04, Apr. 2017, doi: 10.17577/IJERTV6IS040373.
[97] J. Kim and J. Chang, “A new electromagnetic linear actuator for quick latching,” *IEEE Trans. Magn.*, vol. 43, no. 4, pp. 1849–1852, Apr. 2007, doi: 10.1109/TMAG.2006.892289.
[98] Y. P. Yang, J. J. Liu, P. H. Lu, Y. R. Cheng, and D. H. Ye, “Multifunctional optimal design of an electromagnetic valve actuator with hybrid magnetomotive force for a camless engine,” *2011 Int. Conf. Electr. Mach. Syst. ICEMS 2011*, 2011, doi: 10.1109/ICEMS.2011.6073321.
[99] B. V. Ravi Kumar, K. Sivakumar, Y. Srinivas Rao, and S. Karunanidhi, “Design of a New Electromagnetic Brake for Actuator Locking Mechanism in Aerospace Vehcile,” *IEEE Trans. Magn.*, vol. 53, no. 11, Nov. 2017, doi: 10.1109/TMAG.2017.2707242.
[100] T. Shimizu, K. Tadakuma, M. Watanabe, E. Takane, M. Konyo, and S. Tadokoro, “Internally-Balanced Magnetic Mechanisms Using a Magnetic Spring for Producing a Large Amplified Clamping Force,” in *2020 IEEE International Conference on Robotics and Automation*, Sep. 2020, pp. 1840–1846. doi: 10.1109/icra40945.2020.9197151.
[101] Japanese Industrial Standards, *B1404-2-2005 Electromagnetic clutches and electromagnetic brakes-Part 2:Test methods*. 2005.
[102] K. Nagaya, K. Kobayashi, M. Nenoi, Y. Hosokawa, and I. Murakami, “Low driving energy engine valve mechanism using permanent-electromagnet and conical spring,” *Int. J. Appl. Electromagn. Mech.*, vol. 28, no. 1–2, pp. 267–273, Jan. 2008, doi: 10.3233/JAE-2008-984.
[103] R. C. Redfield, “Design Parameter Sensitivity for a Mountain Bike Rear Shock,” *Am. Soc. Mech. Eng. Dyn. Syst. Control Div. DSC*, pp. 1167–1174, Dec. 2007, doi: 10.1115/IMECE2006-14761.
[104] K. MORI and M. TANIGUCHI, “A Study on the Influence of the idling stop at signals on the traffic smoothness,” *Infrastruct. Plan. Rev.*, vol. 24, pp. 775–780, 2007, doi: 10.2208/JOURNALIP.24.775.
[105] Kenneth E. Beyer and Wilhelm H. Horlacher, “Two-stage solenoid valve,” U.S. Patent 4546955A, Oct. 14, 1982

[106] Franz Fuchs, “Solenoid valve,” U.S. Patent 5029807A, Apr. 30, 1990
[107] Y. J. Kim, S. Cheng, S. Kim, and K. Iagnemma, “A novel layer jamming mechanism with tunable stiffness capability for minimally invasive surgery,” *IEEE Trans. Robot.*, vol. 29, no. 4, pp. 1031–1042, 2013, doi: 10.1109/TRO.2013.2256313.
[108] R. Mukaide *et al.*, “Radial-Layer Jamming Mechanism for String Configuration,” *IEEE Robot. Autom. Lett.*, vol. 5, no. 4, pp. 5221–5228, Oct. 2020, doi: 10.1109/LRA.2020.2983679.
[109] K. Tadakuma *et al.*, “Fire-Resistant Deformable Soft Gripper Based on Wire Jamming Mechanism,” in *2020 3rd IEEE International Conference on Soft Robotics, RoboSoft 2020*, May 2020, pp. 740–747. doi: 10.1109/RoboSoft48309.2020.9116036.
[110] I. Onda *et al.*, “Highly Articulated Tube Mechanism with Variable Stiffness and Shape Restoration Using a Pneumatic Actuator,” *IEEE Robot. Autom. Lett.*, vol. 7, no. 2, pp. 3664–3671, Apr. 2022, doi: 10.1109/LRA.2022.3147246.
[111] K. Tadakuma *et al.*, “Morphing Omnidirectional Gripper: ‘Morphing Omni-Gripper’ with Function of Phase-Change Grasping : The Methods to Make the Performance of the Grasping Speed Higher,” *Proc. 2009 JSME Annu. Conf. Robot. Mechatronics*, vol. 2009, pp. 2A2-B02, May 2009, doi: 10.1299/JSMERMD.2009._2A2-B02_1.
[112] K. Tadakuma *et al.*, “Liquid-Solid State Changing Omnidirectional Gripper Mechanism with the Performance of the ‘Hot-Ice’ Phenomenon,” *Proc. JSME Annu. Conf. Robot. Mechatronics*, vol. 2010, no. 0, p. _2A2-D08_1, 2010, doi: 10.1299/JSMERMD.2010._2A2-D08_1.
[113] T. SHIMIZU, S. HAYASHI, M. WATANABE, K. TADAKUMA, M. KONYO, and S. TADOKORO, “Omnidirectional Gripper Mechanism using Hot-Ice Phenomenon - 4th Report: Effect of Adding Fine Particles in the Solution on Crystallization-,” *Proc. 2019 JSME Annu. Conf. Robot. Mechatronics*, vol. 2019, no. 0, pp. 1P2-C05, 2019, doi: 10.1299/JSMERMD.2019.1P2-C05.
[114] X. Zhu, X. Jing, and L. Cheng, “Magnetorheological fluid dampers: A review on structure design and analysis,” *J. Intell. Mater. Syst. Struct.*, vol. 23, no. 8, pp. 839–873, May 2012, doi: 10.1177/1045389X12436735/ASSET/IMAGES/LARGE/10.1177_1045389X12436735-FIG2.JPEG.
[115] Y. Rong, R. Tao, and X. Tang, “Flexible fixturing with phase-change materials. Part 1. Experimental study on magnetorheological fluids,” *Int. J. Adv. Manuf. Technol.*, vol. 16, no. 11, pp. 822–829, 2000, doi: 10.1007/s001700070016.
[116] Y. Tsugami and K. Nishida, “Development of Parallel Gripper Using Modified MR Fluid - Google Scholar,” in *Proceedings of The 34th Annual Conference of the Robotics Society of Japan*, 2016, pp. 3A3-03.
[117] Y. Okaya and K. Nishida, “Development of universal robot gripper using MRα fluid,” in *The 32nd Annual Conference of the Robotics Society of Japan*, 2014, p. 3N3.
[118] Y. Okatani, T. Nishida, and K. Tadakuma, “Development of universal robot gripper using MRα fluid,” *2014 Jt. 7th Int. Conf. Soft Comput. Intell. Syst. SCIS 2014 15th Int. Symp. Adv. Intell. Syst. ISIS 2014*, pp. 231–235, Feb. 2014, doi: 10.1109/SCIS-ISIS.2014.7044707.
[119] S. Tadokoro, “Earthquake disaster and expectation for robotics,” *Rescue Robot. DDT Proj. Robot. Syst. Urban Search Rescue*, pp. 1–16, 2009, doi: 10.1007/978-1-84882-474-4_1/COVER.
[120] D. P. Stormont, “Autonomous rescue robot swarms for first responders,” *Proc. 2005 IEEE Int. Conf. Comput. Intell. Homel. Secur. Pers. Safety, CIHSPS 2005*, vol. 2005, pp. 151–157, 2005, doi: 10.1109/CIHSPS.2005.1500631.
[121] M. Micire and R. Murphy, “Analysis of the robotic-assisted search and rescue response to the World Trade Center disaster,” 2002.
[122] Y. Qu, R. Liu, R. Chen, S. Cheng, and L. Wang, “Development of a reconfigurable miniature throwable robot for indoor surveillance,” *Proc. 2012 7th IEEE Conf. Ind. Electron. Appl. ICIEA 2012*, pp. 502–506, 2012, doi: 10.1109/ICIEA.2012.6360780.
[123] T. J. Mathew, G. Knox, W. K. Fong, and T. Booysen, “The Design of a Rugged, Low-Cost, Man-Packable Urban Search and Rescue Robotic System,” *Proc. 2014 IEEE Robot. Mechatronics Conf. South Africa*, 2014.
[124] J. A. Jones, “Inflatable Robotics for Planetary Applications.”
[125] T. Aoki, Y. Murayama, and S. Hirose, “Development of a Transformable Three-wheeled Lunar Rover: Tri-Star IV,” *J. F. Robot.*, vol. 31, no. 1, pp. 206–223, Jan. 2014, doi: 10.1002/ROB.21482.

[126] H. TSUKAGOSHI, Y. MORI, M. SASAKI, T. TANAKA, and A. KITAGAWA, “Development of a Jumping & Rolling Inspector to Improve the Debris-Traverse Ability,” *Trans. Japan Soc. Mech. Eng. Ser. C*, vol. 70, no. 692, pp. 1068–1076, 2004, doi: 10.1299/kikaic.70.1068.
[127] Thomas Barse, “Spring arming/disarming mechanism and jumping toy including the latter,” US20150352454A1, 2015
[128] A. R. Jones *et al.*, “On the design of a remotely-deployed detection system for reactor assessment at fukushima daiichi,” *2016 IEEE Nucl. Sci. Symp. Med. Imaging Conf. Room-Temperature Semicond. Detect. Work. NSS/MIC/RTSD 2016*, vol. 2017-January, Oct. 2017, doi: 10.1109/NSSMIC.2016.8069713.
[129] T. Yoshida, K. Nagatani, S. Tadokoro, T. Nishimura, and E. Koyanagi, “Improvements to the rescue robot quince toward future indoor surveillance missions in the Fukushima Daiichi nuclear power plant,” *Springer Tracts Adv. Robot.*, vol. 92, pp. 19–32, 2014, doi: 10.1007/978-3-642-40686-7_2/COVER.
[130] T. Mitsui *et al.*, “Long Reach Manipulator for PCV Repair at Fukushima Daiichi - 17082,” 2017.
[131] Agency for Natural Resources and Energy, “Fukushima Daiichi Nuclear Power Station, The challenge of retrieving fuel debris Article No.3: The frontier of technological development,” Jul. 27, 2020.
[132] T. Mitsui, M. Kishimoto, H. Maekawa, M. Cole, S. Martin, and M. Rood, “Conceptual Study of Fuel Debris Retrieval System for Fukushima Daiichi Reactors ,” Jul. 2016.
[133] A. Takata, H. Nabae, K. Suzumori, and G. Endo, “Tension Control Method Utilizing Antagonistic Tension to Enlarge the Workspace of Coupled Tendon-Driven Articulated Manipulator,” *IEEE Robot. Autom. Lett.*, vol. 6, no. 4, pp. 6647–6653, Oct. 2021, doi: 10.1109/LRA.2021.3094489.

RESEARCH ACHIEVEMENTS

I. Peer-reviewed journals: 3 main-authored

1) **Tori Shimizu**, Kenjiro Tadakuma, Masahiro Watanabe, Eri Takane, Masashi Konyo, Satoshi Tadokoro, “Internally-Balanced Displacement–Force Converter for Stepless Control of Spring Deformation Compensated by Cam With Variable Pressure Angle”, in *IEEE Robotics and Automation Letters*, vol. 6, no. 3, pp. 4576-4583, Feb. 2021.
2) **Tori Shimizu**, Kenjiro Tadakuma, Masahiro Watanabe, Kazuki Abe, Masashi Konyo, Satoshi Tadokoro, “Permanent-magnetically Amplified Brake Mechanism Compensated and Stroke-Shortened by a Multistage Nonlinear Spring”, in *IEEE Robotics and Automation Letters*, vol. 7, no. 3, pp. 6266-6273, Jul. 2022.
3) **Tori Shimizu**, Kenjiro Tadakuma, Masahiro Watanabe, Kazuki Abe, Masashi Konyo, Satoshi Tadokoro, “Permanent-magnetically Amplified Robotic Gripper with Less Clamping Width Influence on Compensation Realized by a Stepless Width Adjustment Mechanism”, in *IEEE Robotics and Automation Letters*, vol. 8, no. 2, pp. 736-743, Feb. 2023.

II. Peer-reviewed international conferences: 5 main-authored, 3 co-authored

1) Eri Takane, Kenjiro Tadakuma, **Tori Shimizu**, Sosuke Hayashi, Masahiro Watanabe, Shingo Kagami, Keiji Nagatani, Masashi Konyo, Satoshi Tadokoro, "Basic Performance of Planar Omnidirectional Crawler during Direction Switching using Disturbance Degree of Ground Evaluation Method", in *Proceedings of the IEEE/RSJ International Conference on Intelligent Robots and Systems*, 2019, pp.2732-2739.
2) ○**Tori Shimizu**, Sosuke Hayashi, Toshiki Midorikawa, Takumi Fujikawa, Eri Takane, Masahiro Watanabe, Kenjiro Tadakuma, Masashi Konyo, Satoshi Tadokoro, “Small Swarm Search Robot System with Rigid-Bone Parachute Rapidly Deployable from Aerial Vehicles”, in *Proceedings of 2019 IEEE International Symposium on Safety, Security, and Rescue Robotics*, 2019, pp. 88-93.
3) Kenjiro Tadakuma, ○Tomoya Takayashi, Natsumi Hookabe, Masahiro Watanabe,Yu Ozawa, **Tori Shimizu**, Eri Takane, Hiroshi Kajihara, Takeshi Yamazaki, Masashi Konyo, Satoshi Tadokoro, “Nemertea Proboscis Inspired Extendable Mechanism”, in *Proceedings of the 30th 2019 International Symposium on Micro-NanoMechatronics and Human Science*, 2019, pp.MP2-1-8.
4) Kenjiro Tadakuma, Toshiaki Fujimoto, Masahiro Watanabe, **Tori Shimizu**, Eri Takane, Masashi Konyo, Satoshi Tadokoro, “Fire Resistance Deformable Soft Gripper Based on Wire Jamming Mechanism”, in *Proceedings of 2020 3rd IEEE International Conference on Soft Robotics*, 2020, pp.740-747.
5) ○**Tori Shimizu**, Kenjiro Tadakuma, Masahiro Watanabe, Eri Takane, Masashi Konyo, Satoshi Tadokoro, “Internally-Balanced Magnetic Mechanisms Using Magnetic Spring for Producing Large Amplified Clamping Force”, in *Proceedings of 2020 IEEE International Conference on Robotics and Automation*, 2020, pp. 1840-1846.
6) ○**Tori Shimizu**, Kenjiro Tadakuma, Masahiro Watanabe, Eri Takane, Masashi Konyo, Satoshi Tadokoro, “Amplification of Clamping Mechanism Using Internally-Balanced Magnetic Unit”, in *Proceedings of 2021 IEEE/RSJ International Conference on Intelligent Robots and Systems*, 2021, pp. 2765-2771.
7) ○**Tori Shimizu**, Kenjiro Tadakuma, Masahiro Watanabe, Eri Takane, Masashi Konyo, Satoshi Tadokoro, “Internally-Balanced Displacement–Force Converter for Stepless Control of Spring Deformation Compensated by Cam With Variable Pressure Angle”, in *Proceedings of 2021 IEEE International Conference on Robotics and Automation*, 2021, pp.TuBT9.3.
8) ○**Tori Shimizu**, Kenjiro Tadakuma, Masahiro Watanabe, Kazuki Abe, Masashi Konyo, Satoshi Tadokoro, “Permanent-magnetically Amplified Brake Mechanism Compensated and Stroke-Shortened by a Multistage Nonlinear Spring”, in *Proceedings of 2022 IEEE International Conference on Robotics and Automation*, 2022, pp.TuB12.08.

III. International conferences: 1 main-authored

1) ○**Tori Shimizu**, “Research Expansion of the Internally Balanced Magnetic Unit - Principle of Balancing Method using Magnetic Spring and Application Mechanisms -”, Fukushima Research Conference “Radiation Hardness and Smartness in Remote Technology for Nuclear Decommissioning”, No. 8, 2018/11/27.

IV. Awards: 12

1) 計測自動制御学会東北支部優秀発表奨励賞, “磁気復元力生成により内部補償を実現するマグネット機構”, 2017/12/19.
2) 日本機械学会畠山賞, 2018/3/27.
3) 第 14 回競基弘賞 2018 年レスキュー工学奨励賞 最終候補者, “飛行輸送体から投入可能な探査用小型群ロボット - 第 1 報:基本概念と本体・跳躍機構の具体的構成 -”, 2018/12/14.
4) 2018 年度計測自動制御学会学術奨励賞技術奨励賞, “磁気復元力生成により内部補償を実現するマグネット機構”, 2019/2/19.
5) 2018 年度日本機械学会若手優秀講演フェロー賞, “磁気復元力生成により内部補償を実現するマグネット機構 - 第 2 報 各種応用 要素例の考案と第一次具現化 -”, 2019/6/6.
6) 第 34 回日本ロボット学会研究奨励賞, “1 次元柔剛切替メカニズムを活用したトーラスグリッパ機構 - 線状ジャミング転移機構を基軸とした構造例 -”, 2019/9/5.
7) Best Paper Award in 2019 International Symposium on Micro-NanoMechatronics and Human Science, “Nemertea Proboscis Inspired Extendable Mechanism”, 2019/12/4.
8) 計測自動制御学会ｼｽﾃﾑｲﾝﾃｸﾞﾚｰｼｮﾝ部門講演会（SI2019）優秀講演賞, “微小操作力での把持状態切替を可能とするＩＢマグネット式万力機構”, 2019/12/19.
9) 令和元年度 東北大学 総長賞, 2020/3/25.
10) 令和元年度 東北大学情報科学研究科 研究科長賞, 2020/3/25.
11) 日本機械学会ﾛﾎﾞﾃｨｸｽ･ﾒｶﾄﾛﾆｸｽ部門 ROBOMECH 表彰（学術研究分野）, “1 次元柔剛切替メカニズムを活用した耐火性トーラスグリッパ機構”, 2020/5/28.
12) 2020 IEEE Robotics and Automation Society Japan Joint Chapter Young Award (ICRA2020), “Internally-Balanced Magnetic Mechanisms Using a Magnetic Spring for Producing a Large Amplified Clamping Force”, 2020/6/5.

V. Review articles: 1 main-authored

1) **清水　杜織**, “磁気復元力生成式内部力補償型磁気吸着機構とその応用構造”, 計測と制御, vol. 58, no. 9, pp. 725, 2019.

VI. Invited presentations: 1 main-authored

1) **○清水 杜織**, “1 次元柔剛切替メカニズムを活用した耐火性トーラスグリッパ機構”, 第 26 回ロボティクスシンポジア, 2021.

VII. Patents: 1 main-authored, 2 co-authored

1) 小澤悠, **清水　杜織**, “無線給電システム”, 特願 2018-75045, 2018/3/23 特許出願.
2) **清水　杜織**, 多田隈 建二郎, 昆陽雅司, 田所諭, “ジャミンググリッパ”, 特願 2018-106056, 2022/9/6 特許査定.
3) 渡辺将広, **清水　杜織**, 多田隈建二郎, 昆陽雅司, 田所諭, “アクチュエータ”, 特願 2019-093376, 2019/5/17 特許出願.

VIII. Media appearances: 5

1) 仙台放送, “ロボットの知能競うコンテスト”, 仙台放送 NEWS, 2017/6/10.
2) 日経産業新聞, “磁石, 電気使わず簡単脱着”, 2018/3/26.
3) テレビ東京, “ものづくりファンディング 「磁石で人命救助」”, ニュースモーニングサテライト, 2018/7/4.
4) heise online, “Robotikkonferenz SSRR: Cyberhunde, Kabelkrabbler und Roboter am Fallschirm”, https://www.heise.de/newsticker/meldung/Robotikkonferenz-SSRR-Cyberhunde-Kabelkrabbler-und-Roboter-am-Fallschirm-4512285.html, 2019/9/3.
5) 東北大学情報科学研究科ニュースレター, “学生の声”, vol. 19, 2021/1.

IX. Degree programs: 2

1) 東北大学原子炉廃止措置工学プログラム, 2020/03 修了.
2) 東北大学変動地球共生学卓越大学院, 2023/03 修了.

X. National conferences: 10 main-authored, 47 co-authored (10 as the presenter)

1) ○鉄井 光, 西村 礼貴, 藤本 敏彰, **清水 杜織**, 多田隈 建二郎, 昆陽 雅司, 田所 諭, “2 層トーラス型グリッパ機構”, 日本機械学会ﾛﾎﾞﾃｨｸｽ・ﾒｶﾄﾛﾆｸｽ講演会 2018, 1P1-I14, 2018.
2) ○藤本 敏彰, **清水 杜織**, 藤田 政宏, 髙根 英里, 小松 洋音, 多田隈 建二郎, 昆陽 雅司, 田所 諭, “1 次元柔剛切替メカニズムを活用したトーラスグリッパ機構 - 線状ジャミング転移機構を基軸とした構造例 -”, 日本機械学会ﾛﾎﾞﾃｨｸｽ・ﾒｶﾄﾛﾆｸｽ講演会 2018, 1P2-I12, 2018.
3) ○西村 礼貴, 藤本 敏彰, **清水 杜織**, 小松 洋音, 多田隈 建二郎, 昆陽 雅司, 田所 諭, “軸方向推進の観点からの全方向駆動メカニズム”, 日本機械学会ﾛﾎﾞﾃｨｸｽ・ﾒｶﾄﾛﾆｸｽ講演会 2018, 1P2-K03, 2018.
4) 藤本 敏彰, **○清水 杜織**, 小松 洋音, 髙根 英里, 藤田 政宏, 野村 陽人, 多田隈 建二郎, 多田隈 理一郎, 昆陽 雅司, 田所 諭, “双リング式全方向車輪機構 - 交差型ヘリカル歯車機構によるリング状車輪の能動化 -”, 日本機械学会ﾛﾎﾞﾃｨｸｽ・ﾒｶﾄﾛﾆｸｽ講演会 2018, 2A1-H05, 2018.
5) **○清水 杜織**, 藤本 敏彰, 小松 洋音, 多田隈 建二郎, 昆陽 雅司, 田所 諭, “磁気復元力生成により内部補償を実現するマグネット機構 - 第 2 報 各種応用要素例の考案と第一次具現化 - ”, 日本機械学会ﾛﾎﾞﾃｨｸｽ・ﾒｶﾄﾛﾆｸｽ講演会 2018, 2A2-I15, 2018.
6) ○髙根 英里, 藤本 敏彰, **清水 杜織**, 藤田 政宏, 小松 洋音, 多田隈 建二郎, 昆陽 雅司, 田所 諭, “面状全方向クローラ機構 - 第 8 報:テーパ状履帯版における段差・雪上走行実験 および左右 2 ユニット履帯構成 -”, 日本機械学会ﾛﾎﾞﾃｨｸｽ・ﾒｶﾄﾛﾆｸｽ講演会 2018, 2A2-L04, 2018.
7) ○藤本 敏彰, **清水 杜織**, 藤田 政宏, 髙根 英里, 小松 洋音, 多田隈 建二郎, 昆陽 雅司, 田所 諭, “浮遊式変位・力変換メカニズム - 平衡点の移動を活用した増力機構 -”, 日本機械学会ﾛﾎﾞﾃｨｸｽ・ﾒｶﾄﾛﾆｸｽ講演会 2018, 2P1-G14, 2018.
8) ○藤田 政宏, 藤本 敏彰, **清水 杜織**, 髙根 英里, 小松 洋音, 多田隈 建二郎, 昆陽 雅司, 田所 諭, “房状ジャミング膜グリッパ機構”, 日本機械学会ﾛﾎﾞﾃｨｸｽ・ﾒｶﾄﾛﾆｸｽ講演会 2018, 2P1-J06, 2018.
9) 藤本 敏彰, **○清水 杜織**, 小松 洋音, 多田隈 建二郎, 昆陽 雅司, 田所 諭, “可食無限回転メカニズム”, 日本機械学会ﾛﾎﾞﾃｨｸｽ・ﾒｶﾄﾛﾆｸｽ講演会 2018, 2P1-J10, 2018.
10) **○清水 杜織**, 藤本 敏彰, 林 聡輔, 渡辺 将広, 多田隈 建二郎, 昆陽 雅司, 田所 諭, “磁気復元力生成により内部補償を実現するマグネット機構, - 第 3 報:大型強力化と平行指グリッパ機構の実機具現化 -”, 第 36 回日本ロボット学会学術講演会, 1G1-02, 2018.
11) ○林 聡輔, 多田隈 建二郎 , 岡田 佳都, **清水 杜織**, 藤本 敏彰 , 田所 諭, “柔剛切替式膨縮パッド循環移動体 - 大型ボイラ内壁検査のための壁面移動ロボット機構 -”, 第 36 回日本ロボット学会学術講演会, 1D2-01, 2018.
12) 藤本 敏彰, **○清水 杜織**, 藤田 政宏, 髙根 英里, 林 聡輔, 渡辺 将広, 多田隈 建二郎, 昆陽 雅司, 田所 諭, “1 次元柔剛切替メカニズムを活用したトーラスグリッパ機構 - 線状ジャミング転移機構を基軸とした構造例 -”, 第 36 回日本ロボット学会学術講演会, 3K1-01, 2018.
13) ○渡辺 将広, 林 聡輔 , 藤本 敏彰, **清水 杜織**, 多田隈 建二郎 , 昆陽 雅司, 田所 諭, “加圧すると“縮む”ベローズ機構 - ポリゴナル折紙駆動体 -”, 第 36 回日本ロボット学会学術講演会, 3K3-04, 2018.
14) **○清水 杜織**, 藤川 匠, 緑川 俊貴, 林 聡輔, 髙根 英里, 渡辺 将広, 多田隈 建二郎, 昆陽 雅司, 田所 諭, “飛行輸送体から投入可能な探査用小型群ロボット - 第 1 報:基本概念と本体・跳躍機構の具体的構成 -”, 第 19 回計測自動制御学会ｼｽﾃﾑｲﾝﾃｸﾞﾚｰｼｮﾝ部門講演会, 1C2-09, 2018.
15) ○西村 礼貴, 藤本 敏彰, 林 聡輔, **清水 杜織**, 渡辺 将広, 多田隈 建二郎, 昆陽 雅司, 田所 諭, “軸方向波動伝播ホイール機構 - 第 4 報:駆動基礎部の高剛性化および車両構成 -”, 第 19 回計測自動制御学会ｼｽﾃﾑｲﾝﾃｸﾞﾚｰｼｮﾝ部門講演会, 2C3-12, 2018.
16) ○林 聡輔, 緑川 俊貴, 藤川 匠, **清水 杜織**, 髙根 英里, 渡辺 将広, 多田隈 建二郎, 昆陽 雅司, 田所 諭, “小型移動体投入のための高剛性骨格パラシュート機構”, 第 19 回計測自動制御学会ｼｽﾃﾑｲﾝﾃｸﾞﾚｰｼｮﾝ部門講演会, 3B1-01, 2018.
17) ○野村 陽人, 藤本 敏彰, 林 聡輔, **清水 杜織**, 渡辺 将広, 多田隈 理一郎, 多田隈 建二郎, 昆陽 雅司, 田所 諭, “スクリュー式差動回転機構 - 全方向サスペンション・クローラ化による不整地踏破性の向上 -”, 第 19 回計測自動制御学会ｼｽﾃﾑｲﾝﾃｸﾞﾚｰｼｮﾝ部門講演会, 3C4-04, 2018.
18) 髙根 英里, 藤本 敏彰, **清水 杜織**, 藤田 政宏, 小松 洋音, 多田隈 建二郎, 多田隈 理一郎, 昆陽 雅司, 田所 諭, “スクリュー式差動回転機構を活用した関節・腕メカニズム —２入力２出力の伝達構造の観点からの駆動方法—”, 第 62 回システム制御情報学会研究発表講演会（SCI’18）, 115-7, 京都, 26-28 May.2018.
19) ○林 聡輔, **清水 杜織**, 渡辺 将広, 緑川 俊貴, 髙根 英里, 多田隈 建二郎, 昆陽 雅司, 田所 諭, “伸展分岐可能な柔軟トーラス駆動機構”, 日本機械学会ﾛﾎﾞﾃｨｸｽ・ﾒｶﾄﾛﾆｸｽ講演会 2019, 1P1-H04, 2019.

20) ○林 聡輔, **清水 杜織**, 郡司 芽久, 渡辺 将広, 多田隈 建二郎, 昆陽 雅司, 田所 諭, “アリクイ舌構造を生物抽能する連続吐出メカニズム”, 日本機械学会ﾛﾎﾞﾃｨｸｽ・ﾒｶﾄﾛﾆｸｽ講演会 2019, 1P1-H05, 2019.
21) **○清水 杜織**, 林 聡輔, 髙根 英里, 渡辺 将広, 多田隈 建二郎, 昆陽 雅司, 田所 諭, “微小操作力での弾性体圧縮が可能な 永電ＩＢマグネット跳躍機構 - 第 1 報:基本構成と動作モデルの検証 -”, 日本機械学会ﾛﾎﾞﾃｨｸｽ・ﾒｶﾄﾛﾆｸｽ講演会 2019, 1P1-K07, 2019.
22) **○清水 杜織**, 林 聡輔, 渡辺 将広, 多田隈 建二郎, 昆陽 雅司, 田所 諭, “Hot-Ice 現象を活用した全方向包み込み式なじみグリッパ機構 - 第４報：微小粒子の添加による結晶化時の剛性向上 -”, 日本機械学会ﾛﾎﾞﾃｨｸｽ・ﾒｶﾄﾛﾆｸｽ講演会 2019, 1P2-C05, 2019.
23) ○渡辺 将広, 林 聡輔, **清水 杜織**, 郡司 芽久, 多田隈 建二郎, 昆陽 雅司, 田所 諭, “組織を三次元曲面に切離可能な能動湾曲式超薄型メス機構”, 日本機械学会ﾛﾎﾞﾃｨｸｽ・ﾒｶﾄﾛﾆｸｽ講演会 2019, 1P2-G01, 2019.
24) 鉄井 光, ○猪股 翔平, 林 聡輔, **清水 杜織**, 渡辺 将広, 多田隈 建二郎, 昆陽 雅司, 田所 諭, “軸方向伸展拘束型トーラスバルーン機構”, 日本機械学会ﾛﾎﾞﾃｨｸｽ・ﾒｶﾄﾛﾆｸｽ講演会 2019, 1P2-G03, 2019.
25) ○緑川 俊貴, 林 聡輔, **清水 杜織**, 髙根 英里, 渡辺 将広, 多田隈 理一郎, 多田隈 建二郎, 昆陽 雅司, 田所 諭, “交差型ヘリカル歯車機構に基づく能動双リング式全方向駆動車輪 - 斜め方向移動の高円滑化 -”, 日本機械学会ﾛﾎﾞﾃｨｸｽ・ﾒｶﾄﾛﾆｸｽ講演会 2019, 1P2-L03, 2019.
26) ○林 聡輔, **清水 杜織**, 野村, 西村, 緑川 俊貴, 髙根 英里, 渡辺 将広, 多田隈 建二郎, 多田隈 理一郎, 昆陽 雅司, 田所 諭, “軸方向推進の観点からの全方向駆動メカニズム - 第 2 報 軸方向波動伝播ホイール機構およびスクリュー式差動回転機構の車両化 -”, 日本機械学会ﾛﾎﾞﾃｨｸｽ・ﾒｶﾄﾛﾆｸｽ講演会 2019, 1P2-M03, 2019.
27) **○清水 杜織**, 林 聡輔, 渡辺 将広, 多田隈 建二郎, 昆陽 雅司, 田所 諭, “可食柔剛切替メカニズム”, 日本機械学会ﾛﾎﾞﾃｨｸｽ・ﾒｶﾄﾛﾆｸｽ講演会 2019, 2A1-C03, 2019.
28) ○渡辺 将広, 林 聡輔, **清水 杜織**, 多田隈 建二郎, 昆陽 雅司, 田所 諭, “ポリゴナル折り紙駆動体:収縮動作が可能な剛体ベローズ機構 - 基本変形特性の導出 -”, 日本機械学会ﾛﾎﾞﾃｨｸｽ・ﾒｶﾄﾛﾆｸｽ講演会 2019, 2A1-C14, 2019.
29) ○髙根 英里, **清水 杜織**, 林 聡輔, 渡辺 将広, 多田隈 建二郎, 鏡 慎吾, 永谷 圭司, 昆陽 雅司, 田所 諭, “面状全方向クローラ機構 - 第 9 報:方向切替進行時の路面乱動抑制効果 - ”, 日本機械学会ﾛﾎﾞﾃｨｸｽ・ﾒｶﾄﾛﾆｸｽ講演会 2019, 2A2-D09, 2019.
30) **○清水 杜織**, 林 聡輔, 鉄井 光, 猪股 翔平, 向出 陸央, 渡辺 将広, 多田隈 建二郎, 昆陽 雅司, 田所 諭, “微小操作力での柔剛切替を可能とする ＭＲ流体ジャミンググリッパ機構 - 第 1 報:基本構成と磁石配列によるＩＢマグネットの小型強力化 -”, 日本機械学会ﾛﾎﾞﾃｨｸｽ・ﾒｶﾄﾛﾆｸｽ講演会 2019, 2A2-G03, 2019.
31) ○林 聡輔, **清水 杜織**, 髙根 英里, 渡辺 将広, 郡司 芽久, 多田隈 建二郎, 昆陽 雅司, 田所 諭, “吸引捕食を生物抽能した劣駆動グリッパ機構 - 負圧生成式引寄せ機能の実現-”, 日本機械学会ﾛﾎﾞﾃｨｸｽ・ﾒｶﾄﾛﾆｸｽ講演会 2019, 2A2-Q05, 2019.
32) ○猪股 翔平, 鉄井 光, 林 聡輔, **清水 杜織**, 渡辺 将広, 多田隈 建二郎, 清水 達也, 関根 秀一, 本間 順, 清水 将伍, 佐野 和紀, 昆陽 雅司, 田所 諭, “細胞シート貼付を可能にする軸方向伸展拘束型トーラスグリッパ機構”, 日本機械学会ﾛﾎﾞﾃｨｸｽ・ﾒｶﾄﾛﾆｸｽ講演会 2019, 2A2-T05, 2019.
33) ○林 聡輔, **清水 杜織**, 緑川 俊貴, 髙根 英里, 渡辺 将広, 多田隈 建二郎, 昆陽 雅司, 田所 諭, “2 次元ファスナ機構”, 日本機械学会ﾛﾎﾞﾃｨｸｽ・ﾒｶﾄﾛﾆｸｽ講演会 2019, 2P1-B08, 2019.
34) ○多田隈 建二郎, 林 聡輔, **清水 杜織**, 鉄井 光, 髙根 英里, 渡辺 将広, 昆陽 雅司, 田所 諭, “柔剛切替えが可能なジャミング膜グリッパ機構 - 構造の洗練化の過程とこれまでの取り組みの総括 -”, 日本機械学会ﾛﾎﾞﾃｨｸｽ・ﾒｶﾄﾛﾆｸｽ講演会 2019, 2P1-E07, 2019.
35) **○清水 杜織**, 林 聡輔, 藤本, 向出 陸央, 猪股 翔平, 緑川 俊貴, 鉄井 光, 髙根 英里, 渡辺 将広, 多田隈 建二郎, 昆陽 雅司, 田所 諭, “1 次元柔剛切替メカニズムを活用した耐火性トーラスグリッパ機構”, 日本機械学会ﾛﾎﾞﾃｨｸｽ・ﾒｶﾄﾛﾆｸｽ講演会 2019, 2P1-E08, 2019.
36) ○渡辺 将広, 林 聡輔, **清水 杜織**, 髙根 英里, 多田隈 理一郎, 多田隈 建二郎, 昆陽 雅司, 田所 諭, “履帯上での進行波生成により全方向移動可能なクローラ機構”, 日本機械学会ﾛﾎﾞﾃｨｸｽ・ﾒｶﾄﾛﾆｸｽ講演会 2019, 2P2-A14, 2019.
37) ○恩田 一生, 小澤 悠, 髙橋 知也, **清水 杜織**, 渡辺 将広, 多田隈 建二郎, 昆陽 雅司, 田所 諭, “膜破損時にも柔剛切替機能を維持可能な被覆式ジャミング機構”, 第 37 回日本ロボット学会学術講演会, 1D1-04, 2019.
38) ○向出 陸央, **清水 杜織**, 小澤 悠, 髙橋 知也, 渡辺 将広, 多田隈 建二郎, 昆陽 雅司, 田所 諭, “径方向層状ジャミング機構”, 第 37 回日本ロボット学会学術講演会, 1I1-06, 2019.
39) 小澤 悠, **清水 杜織**, 髙橋 知也, 恩田 一生, 渡辺 将広, ○多田隈 建二郎, 昆陽 雅司, 田所 諭, “可食バネ要素”, 第 37 回日本ロボット学会学術講演会, 2D1-07, 2019.

40) 猪股 翔平, ○高橋 知也, 小澤 悠, **清水 杜織**, 髙根 英里, 渡辺 将広, 多田隈 建二郎, 昆陽 雅司, 田所 諭, “軸柔軟式流体貯蔵タンク機構”, 第 20 回計測自動制御学会ｼｽﾃﾑｲﾝﾃｸﾞﾚｰｼｮﾝ部門講演会, 1B5-05, 2019.
41) **○清水 杜織**, 小澤 悠, 渡辺 将広, 多田隈 建二郎, 昆陽 雅司, 田所 諭, “微小操作力での把持状態切替を可能とするＩＢマグネット式万力機構”, 第 20 回計測自動制御学会ｼｽﾃﾑｲﾝﾃｸﾞﾚｰｼｮﾝ部門講演会, 2B1-16, 2019.
42) ○小澤 悠, **清水 杜織**, 恩田 一生, 向出 陸央, 猪股 翔平, 山田 健斗, 矢内 智大, 渡辺 将広, 多田隈 建二郎, 昆陽 雅司, 田所 諭, “飛行輸送体から投入可能な探査用小型群ロボット”, 第 20 回計測自動制御学会ｼｽﾃﾑｲﾝﾃｸﾞﾚｰｼｮﾝ部門講演会, 2D1-03, 2019.
43) ○鉄井 光, **清水 杜織**, 小澤 悠, 髙橋 知也, 恩田 一生, 髙根 英里, 渡辺 将広, 多田隈 建二郎, 昆陽 雅司, 田所 諭, “極小剛を網羅配置した保護外皮メカニズム”, 第 20 回計測自動制御学会ｼｽﾃﾑｲﾝﾃｸﾞﾚｰｼｮﾝ部門講演会, 3D2-08, 2019.
44) ○西城 直人, **清水 杜織**, 小澤 悠, 髙橋 知也, 恩田 一生, 髙根 英里, 渡辺 将広, 多田隈 理一郎, 多田隈 建二郎, 昆陽 雅司, 田所 諭, “ピッチ軸型ラックチェーン機構”, 第 20 回計測自動制御学会ｼｽﾃﾑｲﾝﾃｸﾞﾚｰｼｮﾝ部門講演会, 3C3-08, 2019.
45) ○小澤 悠, 髙橋 知也, **清水 杜織**, 髙根 英里, 渡辺 将広, 多田隈 建二郎, 昆陽 雅司, 田所 諭, “可食反射型駆動メカニズム”, 第 20 回計測自動制御学会ｼｽﾃﾑｲﾝﾃｸﾞﾚｰｼｮﾝ部門講演会, 3D4-12, 2019.
46) ○藤本 敏彰, **清水 杜織**, 西村 礼貴, 野村 陽人, 鉄井 光, 髙根 英里, 藤田 政宏, 小松 洋音, 多田隈 建二郎, 昆陽 雅司, 田所 諭, “1 次元ジャミング転移機構の原理考案と具現化”, 第 312 回計測自動制御学会東北支部研究集会, 312-5, 2017.
47) **○清水 杜織**, 藤本 敏彰, 西村 礼貴, 野村 陽人, 鉄井 光, 藤田 政宏, 髙根 英里, 小松 洋音, 多田隈 建二郎, 昆陽 雅司, 田所 諭, “磁気復元力生成により内部補償を実現するマグネット機構”, 第 313 回計測自動制御学会東北支部研究集会, 313-5, 2017.
48) ○渡辺 将広, 藤本 敏彰, **清水 杜織**, 多田隈 建二郎, 昆陽 雅司, 田所 諭, “先端伸展式トーラス型投入メカニズム”, 第 315 回計測自動制御学会東北支部研究集会, 315-4, 2018.
49) ○林 聡輔, **清水 杜織**, 藤本 敏彰, 髙根 英里, 藤田 政宏, 緑川 俊貴, 渡辺 将広, 多田隈 建二郎, 昆陽 雅司, 田所 諭, “ラックチェーン機構 - 無限回転体を履帯上で循環駆動可能なメカニズム -”, 第 320 回計測自動制御学会東北支部研究集会, 320-4, 2018.
50) ○林 聡輔, **清水 杜織**, 藤本 敏彰, 藤田 政宏, 髙根 英里, 渡辺 将広, 郡司 芽久(国立科学博物館), 多田隈 建二郎, 昆陽 雅司, 田所 諭 , “生体解剖の観点からのロボット機構研究の展開”, 第 320 回計測自動制御学会東北支部研究集会, 320-6, 2018.
51) ○林 聡輔, **清水 杜織**, 髙根 英里, 渡辺 将広, 郡司 芽久, 多田隈 建二郎, 昆陽 雅司, 田所 諭 , “吸引捕食を生物抽能した負圧生成式引寄せ機能を実現する劣駆動グリッパ機構”, 第 321 回計測自動制御学会東北支部研究集会, 321-2, 2019.
52) ○林 聡輔, **清水 杜織**, 渡辺 将広, 多田隈 建二郎, 昆陽 雅司, 田所 諭, “伸展分岐可能なトーラス駆動機構 - ヒモムシ吻構造を生物抽能した柔軟メカニズム -”, 第 321 回計測自動制御学会東北支部研究集会, 321-4, 2019.
53) 小澤 悠, **○清水 杜織**, 鉄井 光, 髙橋 知也, 恩田 一生, 髙根 英里, 渡辺 将広, 多田隈 建二郎, 昆陽 雅司, 田所 諭, “柔剛兼備な保護外皮用ウロコ状機構”, 第 324 回計測自動制御学会東北支部研究集会, 324-8, 2019.
54) 恩田 一生, 高橋 知也, 小澤 悠, **清水 杜織**, 髙根 英里, 渡辺 将広, 多田隈 建二郎, 多田隈 理一郎, 昆陽 雅司, 田所 諭, "軸方向推進の観点からの全方向駆動メカニズム　－繊毛振動体の実機具現化と交差型ヘリカル歯車機構による移動体化－", 日本機械学会ﾛﾎﾞﾃｨｸｽ・ﾒｶﾄﾛﾆｸｽ講演会 2020, 1A1-H14, 2020.
55) 髙橋 昌己, **清水 杜織**, 岡田 佳都, 高橋 知也, 藤倉 大貴, 髙根 英里, 大野 和則, 渡辺 将広, 多田隈 建二郎, 昆陽 雅司, 田所 諭, "磁力鍵トリガ式連結分離機構", 第 38 回日本ロボット学会学術講演会, 1K1-04, 2020.
56) 吉本 悠人, 西城 直人, 佐野 峻輔, **清水 杜織**, 渡辺 将広, 阿部 一樹, 多田隈 建二郎, 昆陽 雅司, 田所 諭, "負荷感応式重力補償機構の原理検証的研究", 第２２回計測自動制御学会ｼｽﾃﾑｲﾝﾃｸﾞﾚｰｼｮﾝ部門講演会, 3H4-07, pp. 3484-3488, 2021.
57) 吉本 悠人, 釼持 優人, 髙橋 景虎, 西城 直人, **清水 杜織**, 佐野 峻輔, 渡辺 将広, 阿部 一樹, 多田隈 建二郎, 昆陽 雅司, 田所 諭, "負荷感応式重力補償機構の原理検証的研究　－荷重変化時角度固定型の動作観察機による実験的考察－", 日本機械学会ﾛﾎﾞﾃｨｸｽ・ﾒｶﾄﾛﾆｸｽ講演会 2022, 2P1-E08, 2022.